TECHNICAL REPORT STANDARD TITLE PAGE

1. Report No.	2. Government Accession No.	3. Recipient's Catalog No.
FAA-72-32		

4. Title and Subtitle	5. Report Date
Investigation of Parastic Loop Counterpoise Antennas and Their Application to VOR Systems	December 1972
	6. Performing Organization Code

7. Author(s)	8. Performing Organization Report No.
DIPAK L. SENGUPTA JOSEPH E. FERRIS	

9. Performing Organization Name and Address	10. Work Unit No.
The University of Michigan Radiation Laboratory Department of Electrical and Computer Engineering Ann Arbor, Michigan 48105	330-001-03N
	11. Contract or Grant No. FA-69WA-2085
	13. Type of Report and Period Covered Final Report for Period Aug. 1969 - October 1972
12. Sponsoring Agency Name and Address Federal Aviation Administration; Systems Research and Development Service, Washington, D. C. 20591	14. Sponsoring Agency Code

15. Supplementary Notes

16. Abstract

The radiation fields produced by conventional VOR and parastic loop counterpoise antennas have been investigated both theoretically and experimentally. Theoretical expressions for the side band mode radiation fields produced by conventional VOR antennas have been obtained by applying the concepts of geometrical theory of diffraction. Using similar techniques expressions have been obtained for both carrier and side band mode radiation fields produced by single parastic loop counterpoise antennas. It has been found that for large separation distance between the parastic loops, the mutual coupling effects may be neglected during the evaluation of double parastic loop counterpoise antennas.

All the above theoretical results have been compared with the experimental results obtained from model measurements. Within the ranges of approximations made in the theoretical analysis and the experimental errors, the agreement between theory and experiment has been found to be satisfactory.

On the basis of the parametric studies of the radiation patterns, optimum double parastic loop counterpoise antennas have been developed so that the side band mode patterns have maximum field gradients at the horizon. Full scale flight testing of a conventional VOR system using the above optimum antenna indicated that the new antenna system reduces the scalloping errors by a ratio of six to one.

Large polarization errors have been observed with the conventional VOR system using the double parasitic loop counterpoise antennas. More work should be done to reduce this undesirable polarization error.

17. Key Words	18. Distribution Statement
Parastic Loop Counterpoise Antennas VOR Antennas Geometrical theory of diffraction Improved VOR systems Optimum VOR antennas	Availability is unlimited. Document may be released to the National Technical Information Service, Springfield, Va. 22151, for sale to the public.

19. Security Classif. (of this report)	20. Security Classif. (of this page)	21. No. of Pages	22. Price
UNCLAS	UNCLAS	192	$3 PC .95 MF

Form DOT F 1700.7 (8-69)

3051-1-F

INVESTIGATION OF PARASITIC LOOP COUNTERPOISE ANTENNAS AND THEIR APPLICATION TO VOR SYSTEMS

Final Report
(August 11, 1969 — October 22, 1972)

December 1972

Contract No. FA69WA-2085
Project No. 330-001-03N
SRDS Report No. RD-72-

This report has been prepared by The University of Michigan Radiation Laboratory of the Department of Electrical and Computer Engineering for the Systems Research and Development Service, Federal Aviation Administration, under Contract FA69WA-2085. The contents of this report reflect the views of the contractor, who is responsible for the facts and the accuracy of the data presented herein, and do not necessarily reflect the official views or policy of the FAA.

Prepared by

Dipak L. Sengupta and Joseph E. Ferris
The University of Michigan Radiation Laboratory
Department of Electrical and Computer Engineering
Ann Arbor, Michigan 48105

for

Systems Research and Development Service
Federal Aviation Administration, Washington, DC 20590

TABLE OF CONTENTS

I	INTRODUCTION	1
	1.1 Preliminary Remarks	1
	1.2 Discussion on Conventional VOR System Performance	1
	1.3 Conventional VOR Performance in Non-Ideal Location	3
	1.4 The Parasitic Loop Counterpoise Antenna	3
	1.5 Previous Work Accomplished	4
	1.6 Outline of the Report	4
	1.7 Summary of Results Obtained	7
	Table I	9
	Table II	10
	Scalloping Error Amplitudes	11
	Polarization Errors	11
	Table III	12
II	FREE SPACE RADIATION CHARACTERISTICS OF CONVENTIONAL VOR ANTENNAS	13
	2.1 Introduction	13
	2.2 Carrier Mode Pattern	13
	2.3 Side Band Mode Pattern	18
	2.3.2 Description of the Experimental Arrangement	21
	2.3.3 Comparison Between Theory and Experiment	22
	2.3.4 More Information About the Side Band Pattern	22
	2.4 Discussion	28
III	INVESTIGATION OF SINGLE PARASITIC LOOP COUNTERPOISE ANTENNA	31
	3.1 Introduction	31
	3.2 Carrier Mode Pattern	31
	3.3 Numerical Investigation of the Parasitic Current for the Carrier Mode Case	34
	3.4 Side Band Mode Pattern	38
	3.4.1 Theoretical Expressions	38
	3.4.2 Comparison Between Theory and Experiment	44
	3.5 Discussion	46

TABLE OF CONTENTS
(continued)

IV	INVESTIGATION OF A DOUBLE PARASITIC LOOP COUNTERPOISE ANTENNA	47
	4.1 Introduction	47
	4.2 Theoretical Expressions for the Radiation Field	47
	4.3 Description of the Experimental Arrangement	49
	4.4 Comparison Between Theory and Experiment	51
	4.5 Optimum Double Parasitic Loop Counterpoise Antenna	51
	4.6 Optimum Antenna Patterns	53
	4.7 Full Scale Parameters of the Optimum Antenna	58
	4.8 Discussion	58
V	FABRICATION OF THE FULL SCALE DOUBLE PARASITIC LOOP COUNTERPOISE ANTENNA	60
	5.1 Introduction	60
	5.2 Standard VOR Antenna at NAFEC	60
	5.3 Full Scale Parasitic Loop Assembly	60
	5.4 Discussion	61
VI	NAFEC FACILITIES AND INITIAL GROUND TESTS	67
	6.1 Introduction	67
	6.2 Standard VOR Experimental Station Terrain	67
	6.3 Ground Test Facility	67
	6.4 Introduction of Known Scattering Sources	68
VII	GROUND TEST RESULTS FOR STANDARD VOR AND DOUBLE PARASITIC LOOP COUNTERPOISE ANTENNAS	71
	7.1 Introduction	71
	7.2 Field Expressions	71
	7.3 Full Scale Ground Test Results	74
	7.4 Discussion	75
VIII	FLIGHT TESTS OF DOUBLE PARASITIC LOOP COUNTERPOISE AND STANDARD VOR ANTENNAS	81
	8.1 Introduction	81
	8.2 Test Antennas	81
	8.3 Field Strength Results	82
	8.4 Scalloping Effects	83
	8.5 Distance Range	85
	8.6 Discussion	85

TABLE OF CONTENTS
(continued)

IX	EXPERIMENTAL STUDY OF THE POLARIZATION ERROR	94
	9.1 Introduction	94
	9.2 Polarization Errors in Standard VOR System	94
	9.3 Polarization Error Study with the Passive Polarizer	95
	9.4 The Active Polarizer	104
	9.5 Parasitic Loop Counterpoise Antenna System II with Active Polarizer	106
	9.6 Discussion	112
X	APPLICATION OF PARASITIC LOOP COUNTERPOISE ANTENNA TO VOR SYSTEM	116
	10.1 Introduction	116
	10.2 Limitations of Conventional VOR Systems	116
	10.3 Application of Parasitic Loop Counterpoise Antennas	117
	10.4 Discussion	118
XI	CONCLUSIONS AND RECOMMENDATIONS	120
	11.1 Conclusions	120
	11.2 Recommendations for Further Work	122
	ACKNOWLEDGMENT	123
	REFERENCES	124
	APPENDIX A (The Radiation Field of a Circular Loop Carrying a Non-Uniform Harmonic Current	126
	A.1 Introduction	126
	A.2 Nature of Excitation	126
	A.3 Far Field Expressions	128
	A.4 Discussion	131
	APPENDIX B (Mutual Coupling Effects in Parasitic Loop Counterpoise Antennas	133
	B.1 Introduction	133
	B.2 Parasitic Currents	133
	B.3 Far Field Expressions	137
	B.4 Numerical Results	140
	B.5 Discussion	141

TABLE OF CONTENTS
(continued)

APPENDIX C (Double Parasitic Loop Counterpoise Antenna Patterns) 144
C.1 Introduction 144
C.2 Preliminary Experiment 144
C.3 Optimization of the Lower Parasitic Loop Parameters 145
C.4 Optimization of the Upper Parasitic Loop Parameters 150
C.5 Maximum Obtainable Field Gradient 150
C.6 Discussion 158
APPENDIX D (Numerical Values for Parasitic Currents in Single Parasitic Loop Counterpoise Antennas 161
D.1 Introduction 161
APPENDIX E (Computer Programs for IBM 360, Model-67) 166
C.1 Program for evaluating the far field elevation plane side band mode pattern of a conventional VOR antenna ($S^A(\theta)$ versus θ). The subroutines given in this section are also used in all the subsequent programs 166
E.2 Program for evaluating the far field elevation plane carrier mode patterns of conventional VOR and single parasitic loop counterpoise antennas ($S^A(\theta)$, $S(\theta)$). 174
E.3 Program for evaluating the far field elevation plane carrier mode pattern of a double parasitic loop counterpoise antenna (mutual effects neglected) 176
E.4 Program for evaluating the far field elevation plane side band mode pattern of a double parasitic loop counterpoise antenna (mutual effects neglected). 179
E.5 Program for evaluating the mutual coupling coefficients K_{12}, K_{21} and also the far field elevation plane carrier mode pattern of a double parasitic loop counterpoise antenna taking into account the effects of mutual coupling 182

TABLE OF CONTENTS
(continued)

E.6 Program for evaluating the far field elevation plane side band mode pattern of a conventional VOR antenna above ground 185
E.7 Program for evaluating the far field elevation plane carrier mode pattern of a double parasitic loop counterpoise antenna above ground 188
E.8 Program for evaluating the far field elevation plane side band mode pattern of a double parasitic loop counterpoise antenna 191
E.9 Program for evaluating the quasi far zone elevation plane side band mode field of conventional VOR antenna above ground 194
E.10 Program for evaluating the quasi far zone elevation plane carrier mode field of a double parasitic loop counterpoise antenna above ground 196
E.11 Program for evaluating the quasi far zone elevation plane side band mode field of a double parasitic loop counterpoise antenna above ground 199
APPENDIX F (Theoretical Elevation Patterns of Conventional VOR and Double Parasitic Loop Counterpoise Antennas 202

LIST OF ILLUSTRATIONS

Figure No.	Caption	Page No.
2-1	Theoretical model for the conventional VOR antenna.	14
2-2	Carrier mode elevation plane far field pattern of a conventional VOR antenna.	17
2-3	Photograph of the Alford loop model.	23
2-4	Photograph of the two Alford loops mounted above the 15' diameter counterpoise.	24
2-5	Side band mode elevation plane far field pattern of a conventional VOR antenna.	25
2-6	Side band mode elevation plane far field pattern of a conventional VOR antenna.	26
2-7	Side band mode elevation plane far field pattern of a conventional VOR antenna.	27
2-8	Measured side band mode elevation plane far field pattern of a conventional VOR antenna.	29
2-9	Measured side band mode azimuthal plane far field pattern of a conventional VOR antenna.	30
3-1	Schematic representation of single parasitic loop counterpoise antenna and the coordinate system used.	32
3-2	Theoretical field gradient (α_g) as a function of H for a single parasitic loop counterpoise antenna operating in the carrier mode.	35
3-3	Carrier mode elevation plane far field pattern of a single parasitic loop counterpoise antenna.	36
3-4	Theoretical model for a single parasitic loop counterpoise antenna.	39
3-5	Dominant rays contributing to the parasitic current.	40
3-6	Side band mode elevation plane far field pattern of a single parasitic loop counterpoise antenna.	45

LIST OF ILLUSTRATIONS
(continued)

4-1	Theoretical model for the double parasitic loop counterpoise antenna.	48
4-2	Side view of the double parasitic loop counterpoise antenna.	50
4-2a	A close-up view of the double parasitic loop counterpoise antenna model.	50
4-3	Carrier mode elevation plane far field pattern of a double parasitic loop counterpoise antenna.	52
4-4	Side band mode elevation plane far field pattern of a double parasitic loop counterpoise antenna.	54
4-5	Theoretical maximization of the horizon field gradient of a double parasitic loop counterpoise antenna operating in the side band mode.	55
4-6	Theoretical carrier and side band mode elevation plane pattern of the optimized double parasitic loop counterpoise antenna.	56
4-7	Measured side band mode elevation plane far field pattern of the optimum double parasitic loop counterpoise antenna.	57
5-1	150' diameter counterpoise conventional VOR antenna mounted on a 75' tower at NAFEC.	62
5-2	The details of the mechanical fabrication of the full scale parasitic elements.	63
5-3	A section of the two full scale parasitic loops mounted on the counterpoise.	64
5-4	The details of the tension adjuster used for the installed parasitic loops.	65
5-5	Two full scale parasitic loops mounted on the 150' diameter counterpoise.	66
6-1	The terrain surrounding the VOR station at NAFEC.	69
6-2	Standard VOR Experimental Station terrain.	70

LIST OF ILLUSTRATIONS
(continued)

7-1	Geometrical representation of a double parasitic loop counterpoise VOR antenna above ground.	72
7-2	Carrier mode field strength variation as a function of θ at a distance 300' away from a conventional VOR antenna located 75' above ground.	76
7-3	Carrier mode field strength variation as a function of θ at a distance 300' away from the (Systems-II) optimum double parasitic loop counterpoise VOR antenna located 75' above ground.	77
7-4	Side band mode field strength variation as a function θ at a distance 300' away from the optimum double parasitic loop counterpoise VOR antenna (Systems-II) located 75' above ground.	78
7-5	Measured carrier mode field strength variation in a vertical plane located 300' away from a non-optimum double parasitic loop counterpoise VOR antenna.	79
7-6	Measured side band mode field strength variation in a vertical plane located 300' away from a non-optimum double parasitic loop counterpoise VOR antenna (Systems-I).	80
8-1	Radiation field produced by a standard VOR antenna above ground.	87
8-2	Radiation field produced by the double parasitic loop counterpoise system II above ground.	88
8-3	Radiation field produced by a double parasitic loop counterpoise antenna system II above ground.	89
8-4	Location of the wire grid reflector with respect to the VOR station.	90
8-5	Scalloping results obtained with a conventional VOR system using a conventional antenna.	91

LIST OF ILLUSTRATIONS
(continued)

8-6	Scalloping results obtained with a conventional VOR system using a double parasitic loop counterpoise antenna (System-I).	92
8-7	Scalloping results obtained with a conventional VOR system using the optimum double parasitic loop counterpoise antenna (System-II).	93
9-1	Conventional 4 loop VOR (Mannheim, No Polarizer)Results.	96
9-2	Conventional 4 loop VOR (Mannheim, with Polarizer) Results.	97
9-3	Double parasitic loop counterpoise antenna system II results (Mannheim, no Polarizer).	98
9-4	Double parasitic loop counterpoise antenna system II results (Mannheim, with polarizer).	99
9-5	Double parasitic loop counterpoise antenna system II results (Mannheim, with polarizer).	102
9-6	Active Polarizer No. 1.	103
9-7	Active Polarizer No. 2.	105
9-8	Active polarizer installation.	107
9-9	Field Strength for active polarizer No. 2.	109
9-10	Field strength for double parasitic loop counterpoise antenna system II.	110
9-11	Polarization error for double parasitic loop counterpoise antenna system II.	111
9-12	Polarization error versus angle for double parasitic loop counterpoise antenna system II.	113

LIST OF ILLUSTRATIONS
(continued)

9-12c, d.	Polarization error versus angle for double parasitic loop counterpoise antenna system II.	114
A-1	Coordinate system used.	127
A-2	Orientation of the circular loop.	129
B-1	Double parasitic loop counterpoise antenna.	133
B-2	Rays contributing to K_{12}.	135
B-3	Theoretical carrier mode pattern of a double parasitic loop counterpoise antenna with and without mutual coupling effects.	142
B-4	Theoretical and experimental carrier mode patterns of a double parasitic loop counterpoise antenna.	143
C-1a	Measured elevation plane side band mode pattern of a double parasitic loop counterpoise antenna.	147
C-1b	Measured elevation plane side band mode pattern of a double parasitic loop counterpoise antenna.	148
C-1c	Measured elevation plane side band mode pattern of a double parasitic loop counterpoise antenna.	149
C-2	Measured elevation plane side band mode pattern of a double parasitic loop counterpoise antenna.	151
C-3	Measured elevation plane side band mode pattern of a double parasitic loop counterpoise antenna.	152
C-4	Measured elevation plane side band mode pattern of double parasitic loop counterpoise antenna.	153
C-5a	Measured elevation plane side band mode pattern of double parasitic loop counterpoise antenna.	154
C-5b	Measured elevation plane side band mode pattern of double parasitic loop counterpoise antenna.	155
C-6a	Measured elevation plane side band mode pattern of double parasitic loop counterpoise antenna.	156
C-6b	Measured elevation plane side band mode pattern of double parasitic loop counterpoise antenna.	157

LIST OF ILLUSTRATIONS
(continued)

C-7a	Measured elevation plane side band mode pattern of very large gradient double parasitic loop counterpoise antenna.	159
C-7b	Measured elevation plane side band mode pattern of very large gradient double parasitic loop counterpoise antenna.	160

I

INTRODUCTION

1.1 Preliminary Remarks

This is the Final Report on Contract FA69WA-2085, Project 330-001-03N, "VOR Parasitic Loop Counterpoise Systems-II", and covers the period from 11 August 1969 to 22 October 1972. The main objectives of the research reported here have been: (i) to investigate the radiation characteristics of parasitic loop counterpoise antennas and to evolve an optimum antenna configuration so that it may be incorporated into an existing conventional (or standard) VOR (V HF Omni Range) system, (ii) to evaluate the improvement in the performance of a conventional VOR system brought about by the above new antenna system.

A major part of the present investigation has been devoted to the development of satisfactory theories of radiation patterns of parasitic loop counterpoise antennas and also for the radiation patterns of conventional VOR antennas. The performance of a conventional VOR system using an optimum double parasitic loop counterpoise antenna, developed during the present contract, has been evaluated by ground as well as flight tests.

In the following sections of this chapter we at first give some of the relevant background information and discuss briefly the previous work done on this problem. A brief outline of the report is then given. Finally, the main results accomplished during the contract period are summarized in the last section.

1.2 Discussion on Conventional VOR System Performance

It is appropriate here to give a short discussion on the performance of a conventional VOR system. This will put into proper perspective the need for the use of parasitic loop counterpoise antennas to VOR systems.

The operation of conventional VHF Omnirange systems is described in detail by Hurley, et al (1951). In this section we discuss certain aspects of the conventional VOR system performance and its antenna system which are appropriate for our purpose. A detailed description of conventional VOR antenna systems was given by Anderson, et al (1953) and Anderson (1965) and will not be repeated here. The antenna system of a standard VOR system consists of four Alford loops located at the same height above a 52' diameter circular and conducting ground plane or

counterpoise. These four loops are mounted at the corners of a square symmetrically around the axis of the system and they lie in a plane parallel to the counterpoise. The antenna is oriented with the ground plane lying in the horizontal plane. The entire antenna assembly is usually mounted such that the counterpoise is at a height 15' above ground. Depending on the local terrain conditions, the entire antenna assembly may be located at different heights. Henceforth this antenna will be referred to as the conventional VOR or 4-Alford loop counterpoise antenna. The standard VOR system operates at a single frequency within the band 108 - 118 MHz.

The requirements of the VOR system are such that the antenna operates in two distinct modes. In the first mode, called the carrier mode, all four loops are simultaneously driven in phase with carrier frequency currents. The carrier mode pattern of the antenna is omnidirectional in azimuth. In the second mode, called the side band mode, at any instant of time each diagonal pair of loops is excited such that the horizontal plane pattern of each pair of loops above the counterpoise is a figure-of-eight. Each figure-of-eight pattern is then rotated about the vertical axis at 30 revolutions per second. The relative phase between the pairs of loops is such that the combined effects of these in space is to produce a single figure-of-eight azimuthal pattern rotating at 30 revolutions per second. The free space elevation plane patterns of the antenna in both modes are symmetrical bout the vertical axis and have principal maxima at 30^{o}-35^{o} above the horizon and have minima in the axial direction (Sengupta et al, 1968; Sengupta, 1971). Thus when the carrier field is combined with the total side band field at each instant of time throughout the goniometer cycle, a rotating limacon field pattern results. The free space patterns of such antennas show considerable response in directions below the plane of the counterpoise. It is known that the field gradient at the horizon (defined to be the rate of decrease of field just below the horizon) is about $3dB/6^{o}$ in both modes of operation. As we shall see later, this field gradient value has significant influence on the accuracy obtainable from a conventional VOR system.

In the ideal situation the conventional VHF omnirange produces two 30 Hz signals for reception by a flying aircraft: one is constant in phase and independent of the aircraft position, and the other varies in relative phase directly in accordance with the magnetic bearing of the aircraft from the VOR station. The former is referred to as the reference phase signal and the latter as the variable phase signal. The reference phase signal is obtained by frequency modulating at 30 Hz a 9.96KHz subcarrier signal which in turn amplitude modulates the rf carrier signal. The reference phase signal is radiated by the antenna in the carrier mode of operation having an omnidirectional pattern discussed earlier. The variable phase signal is

produced by space amplitude modulating the rf carrier signal with 30 Hz side-band radiated energy. This signal is radiated in the form of a figure-of-eight pattern in azimuth, by effectively rotating it at 30 revolutions per second thereby providing the desired variable signal under this condition. In this case the antenna operates in the side band mode. A phase measuring device in the receiver enables the pilot to determine his bearing with respect to the station by comparing the phase difference between these signals. In the ideal situation when there exists no disturbing object between the VOR station and the flying aircraft the bearing indications obtained by the aircraft in the above manner are found to be quite accurate.

1.3 Conventional VOR Performance in Non-Ideal Location

In an actual situation whenever there exists a multipath between the VOR ground station and the flying aircraft, the multipath signals combine with the desired signals at the aircraft. The source of these multipath signals may be trees, buildings, etc., or any other scattering object. The strengths of the multipath signals at the aircraft is directly proportional to the free space response of the antenna in directions below the plane of the counterpoise, if it is assumed that the scattering objects are located below the counterpoise plane. The overall effects of the multipath signals combine to produce siting errors and scalloping in the bearing indications of a conventional VOR (Anderson, 1965).

To avoid the errors in the bearing indications of the standard VOR systems the ideal requirements on the free space antenna radiation pattern are such that in the upper half plane of the counterpoise the elevation field pattern should resemble the Alford loop connterpoise pattern and in directions below the counterpoise plane should be zero or negligible. In other words the field gradient at the horizon should be infinite or very large. Such a pattern is possible only with an infinitely large counterpoise. However, to increase the counterpoise diameters well beyond the values used in the existing systems is impractical and expensive.

From the discussion given above it is evident that any antenna system having overall free space radiation pattern characteristics mentioned above but which produces little field in directions below the horizontal plane is potentially capable of reducing the VOR siting errors. The parasitic loop counterpoise antenna is such an antenna.

1.4 The Parasitic Loop Counterpoise Antenna

The parasitic loop counterpoise antenna, as originally defined (Sengupta et al, 1968), consists of a small excited circular loop (or Alford loop) placed above and parallel to a circular and conducting ground plane along with one or more suitably

placed large parasitic loops oriented coaxially and parallel to the counterpoise. Parasitic loop counterpoise systems, defined this way, can be used only in the carrier mode operation described in the previous sections. We generalize the definition of the parasitic loop counterpoise antenna to include the case where the excitation consists of more than one Alford loop so that it can operate also in the side band mode. As we shall see later, the chief advantage of the parasitic loop concept is that it makes it possible to increase the field gradient of the VOR antenna without increasing the counterpoise size; an additional advantage of the parasitic system is that it is relatively simple to convert the existing conventional VOR antennas to the new systems by inserting parasitic loops at appropriate heights.

1.5 Previous Work Accomplished

Theoretical and experimental investigation of parasitic loop counterpoise antennas operating in the carrier mode have been reported in our Final Report under a previous contract (Sengupta, et al, 1968). Theoretical analysis of the carrier mode patterns of single parasitic loop counterpoise and of conventional VOR antennas have been discussed by Sengupta and Weston (1969). Detailed parametric studies of the radiation patterns of such antennas may be found in Sengupta and Ferris (1970). All these studies have shown that with the help of parasitic loop concepts it is possible to reduce considerably the free space field produced in directions below the counterpoise by conventional VOR antennas operating in the carrier mode. In particular with an optimum double parasitic loop counterpoise antenna operating in the carrier mode, it has been found that in the elevation plane the rate of decrease of the far electric field just below the horizon is 21dB/5.5^{o} (Sengupta et al, 1968). Possible application of parasitic loop counterpoise antennas operating in the carrier mode has been reported by Sengupta and Weston (1968). On the basis of the research reported in Sengupta et al (1968) there evolved three specific parasitic loop counterpoise antenna configurations having possible application to a VOR system.

As mentioned, all the previous work discussed above has been devoted only to the carrier mode type of operation for the antenna. However, from the viewpoint of VOR system operation, it is the side band mode elevation plane pattern of the antenna which is of importance (Hurley et al, 1951). A major part of the present research has thus been devoted to the investigation of the side band mode patterns of conventional VOR and parasitic loop counterpoise antennas.

1.6 Outline of the Report

The theories of radiation from conventional VOR and parasitic loop counterpoise antennas operating in the side band mode have been hitherto unknown. For this

reason a substantial portion of our investigation has been devoted to the development of satisfactory theories for these antennas. This study led to an optimum configuration for a double parasitic loop counterpoise antenna and subsequently to its application to a conventional VOR system. The outline of the report follows.

The free space carrier and side band mode radiation properties of the conventional VOR antennas are discussed in Chapter II. Theoretical expressions are derived for the side band radiation patterns of a conventional VOR antenna. The theory is verified by experimental results obtained from model measurements done at 1.09 GHz.

The free space carrier and side band mode radiation properties of single parasitic loop counterpoise antennas are both investigated theoretically in Chapter III. The theoretical results derived in this chapter are of fundamental importance in the development of double parasitic loop counterpoise antenna theory. The theory is then confirmed by results obtained from model measurements. The nature and values of the parasitic currents in the case of carrier mode operation of single parasitic loop counterpoise antennas are also discussed theoretically and numerically. These results included therein may be found useful in analyzing the measured parasitic currents, if such an investigation is carried out in the future.

Chapter IV discusses theories of both carrier and side band mode patterns produced by double parasitic loop counterpoise antennas. The theories are confirmed by results obtained from model measurements. On the basis of the parametric study of the side band mode patterns, an optimum double parasitic loop counterpoise antenna configuration is obtained. The antenna is optimized in the sense that the horizon field gradient in the elevation plane side band pattern is maximum. Design parameters are obtained for an optimum antenna with a 150' diameter counterpoise operating at the full scale frequency of 109 MHz.

Mechanical fabrication and assembly of the full scale optimum double parasitic loop counterpoise antenna are discussed in Chapter V. The conversion of the experimental conventional VOR antenna, located at Mannheim Avenue Experimental VOR Facility at NAFEC (National Aviation Facility Experimental Center) into an optimum double parasitic loop counterpoise antenna is also described in detail.

Chapter VI describes briefly the test facilities available at National Aviation Facility Experimental Center where the full scale testing of the double parasitic loop counterpoise antenna has been carried out.

Chapter VII describes the results obtained from ground tests conducted to evaluate the performance of the conventional VOR and the double parasitic loop counterpoise antennas.

Results obtained from flight tests conducted with conventional VOR systems using standard 4-Alford loop counterpoise and double parasitic loop counterpoise antennas are discussed in Chapter VIII. The results discussed in this chapter indicate the following: (i) verify at the full scale frequency and for practical systems the horizontally polarized elevation plane pattern information obtained earlier for such antennas from theoretical and model measurements considerations. (ii) in the presence of a known multipath signal, the use of optimum double parasitic loop counterpoise antenna reduces the scalloping errors associated with a conventional VOR system by a factor of 6 to 1.

Large polarization errors were observed during the flight tests of the conventional VOR systems using double parasitic loop counterpoise antennas. Chapter IX discusses the results of our experimental investigation of polarization errors associated with such antennas. Due to the shortage of time this phase of our investigation remains incomplete. The results of our limited investigation indicate that the polarization errors in the parasitic system can be reduced to acceptable values for $\theta < 80^{o}$; however, for $\theta > 80^{o}$ the maximum value of the total polarization error has been found to be about 12^{o}.

The application of parasitic loop counterpoise antennas to a conventional VOR system is discussed critically in Chapter X.

Chapter XI gives our general conclusions and recommendations for future work.

The radiation field of a circular loop carrying a non-uniform harmonic current is discussed theoretically in Appendix A. The results given here may have implications in the analysis of polarization errors associated with the parasitic loop counterpoise VOR antenna systems.

The significance of mutual interaction between parasitic currents in the evaluation of patterns of a double parasitic loop counterpoise antenna is discussed in Appendix B.

Appendix C supplies the investigation which gave rise to an optimum double parasitic loop counterpoise antenna using a 52' diameter counterpoise at the full scale frequency of 108 MHz.

Appendix D gives the numerical values of the parasitic currents for a single parasitic loop counterpoise antenna operating in the carrier mode.

Appendix E gives Fortran IV computer programs used for various numerical computations.

Appendix F gives some selected numerical results.

1.7 Summary of Results Obtained

As mentioned in Section 1.1, the main objectives of the present research program have been to develop an optimum double parasitic loop counterpoise antenna configuration and to investigate its application to a conventional VOR system. In this section we summarize the significant results that have been obtained to this end.

The principal results accomplished in the present contract period are:

(i) Development of satisfactory theories for the carrier and side band mode far field patterns of 4-Alford loop counterpoise standard VOR antennas.

(ii) Development of satisfactory theories for the carrier and side band mode far field patterns of parasitic loop counterpoise standard VOR antennas.

(iii) Design and development of an optimum double parasitic loop counterpoise antenna compatible with a conventional VOR system.

(iv) Verification of the theories developed in (i) - (iii) by model measurements at 1.09 GHz and by ground and flight tests conducted at the full scale frequency of 109 MHz.

(v) Flight test results giving the course scalloping errors produced in the VOR bearing indications of a flying aircraft when there exists a known multipath signal source between the standard VOR ground station and the flying aircraft. Results have been obtained for the standard VOR ground station with and without parasitic antenna system.

(vi) Polarization error results associated with a standard VOR system with and without parasitic loop antenna system. Development of an active polarizer for correcting the polarization errors. This phase of our study remains incomplete due to lack of time.

For ready reference, we give in tabular form below some selected results of interest. The following list of symbols may be found useful in reading the tables of results.

$2A$ = diameter of the counterpoise.

h = height of the Alford loops above the counterpoise.

$2d$ = separation distance between a diagonal pair of Alford loops,

w = width of the conducting strips comprising the parasitic loops,

H_1, H_2 = the heights of the first and second parasitic loops above the counterpoise,

$2B_1$, $2B_2$ = diameters of the first and second parasitic loops,

θ_{max} = direction of the principal maximum in the elevation plane ($\phi = 0^o$) far field pattern. $\theta = 0^o$ is the vertical direction,

$\alpha_g = -20 \log_{10} \dfrac{E_\phi(96^o)}{E_\phi(90^o)}$ = the far field gradient at the horizon in the elevation plane $\phi = 0^o$,

$\alpha_f = -20 \log_{10} \dfrac{E_\phi(90^o)}{E_\phi(\theta_{max})}$ = the far field reduction factor in the direction of the horizon.

For all the test results given below, the operating frequency is 109 MHz and the corresponding wavelength $\lambda = 9.02'$.

TABLE I

RESULTS FOR 150' DIAMETER COUNTERPOISE SYSTEM

Standard 4-Alford Loop Counterpoise VOR Antenna Design Parameters:

2A = 150', h = 4', d = 1'4" and 4 Standard Alford Loops.

Optimum Double Parasitic Loop Counterpoise Antenna Design Parameters:

The above 4-Alford loop counterpoise VOR antenna design parameters plus the following; w = 10", H_1 = 5', $2B_1$ = 46'10", H_2 = 18'8" and $2B_2$ = 32'10".

Elevation Plane ($\phi = 0^o$) Pattern Characteristics

	Standard VOR Antenna	
	Carrier Mode	Side Band Mode
θ_{max}	62^o	65^o
α_g	5.56dB/6^o	5.54dB/6^o
α_f	14.82dB	14.7dB

	Optimum Double Parasitic Loop Counterpoise Antennas	
	Carrier Mode	Side Band Mode
θ_{max}	62^o	66^o
α_g	5.66dB/6^o	23.71dB/6^o
α_f	10.3dB	23.18dB

TABLE II

RESULTS FOR 52' DIAMETER COUNTERPOISE SYSTEM

Standard 4-Alford Loop Counterpoise VOR Antenna Design Parameters:

$2A = 52'$, $h = 4'$, $d = 1'4''$.

Optiumm Double Parasitic Loop Counterpoise Antenna Design Parameters:
The above 4-Alford loop counterpoise antenna design parameters plus the following: $w = 10''$, $H_1 = 5'2''$, $2B_1 = 48'8''$, $H_2 = 15'8''$ and $2B_2 = 34'10''$.

Elevation Plane ($\phi = 0^o$) Pattern Characteristics

	Standard VOR Antenna	
	Carrier Mode	Side Band Mode
θ_{max}	58^o	60^o
α_g	$3.11dB/6^o$	$3.05dB/6^o$
α_f	10.44dB	9.47dB

	Double Parasitic Loop Counterpoise Antenna	
	Carrier Mode	Side Band Mode
θ_{max}	58^o	60^o
α_g	$3.11dB/6^o$	$21.22dB/6^o$
α_f	7.4dB	16.5dB

Only the 150' diameter antenna systems have been tested at the full scale frequency 109 MHz.

Scalloping Error Amplitudes

Course scalloping errors in the standard VOR bearing indications of a flying aircraft have been measured with the conventional VOR ground station using standard 4-Alford loop and optimum double parasitic loop antenna systems along with a 150' diameter counterpoise located 75' above ground. In each case the aircraft was flying on a 20 mile orbit, around the VOR station, at an altitude of 6575' (which corresponds to a minimum in the vertical plane pattern nearest to the horizon); there existed a multipath signal source in the direction $\phi = 52'$ and at a distance 1000' away from the VOR ground station. In each case the scalloping errors were observed to be maximum in the $\phi \simeq 140^{o}$ direction and are given as follows:

maximum scalloping error for the conventional VOR system using standard 4-Alford loop antenna = 12.5^{o}

maximum scalloping error for the conventional VOR system using the optimum double parasitic loop counterpoise antenna = 2^{o}

In addition to the above scalloping errors have been measued for the case of a conventional VOR system using a non-optimum double parasitic loop counterpoise antenna. The details may be found in Chapter VIII:

Polarization Errors

Polarization errors associated with a conventional VOR system with and without parasitic loop antennas have been measured in the range $62^{o} \leq \theta \leq 90^{o}$. The measurements were carried out with the help of an aircraft flying at an altitude of 3220 feet along selected radials with respect to the VOR ground station. In each case errors have been measured for VOR ground station antennas with and without passive polarizers.

TABLE III

MEASURED TOTAL POLARIZATION ERRORS

Standard VOR Using 4-Alford Loop Antenna		
θ	NO Polarizer	With Passive Polarizer
	Total Polarization Error	Total Polarization Error
$62^{o} \leq \theta \leq 82^{o}$	$11^{o}.5$	$1^{o}.9$
$82^{o} \leq \theta \leq 90^{o}$	$13^{o}.5$ (maximum)	5^{o} (maximum)
Standard VOR Using Optimum Double Parasitic Loop Antenna		
	NO Polarizer	With Passive Polarizer
$62^{o} \leq \theta \leq 80^{o}$	8^{o}	3^{o}
$80^{o} < \theta < 90^{o}$	14^{o}	12^{o} (maximum)

We have developed an active polarizer for the purpose of reducing the polarization errors associated with conventional VOR systems. The details may be found in Chapter IX. From the results given here, it appears that the polarization errors associated with the parasitic system are large in directions $\theta > 80^{o}$. As mentioned before our polarization error study is incomplete. However, we believe that this error can be reduced further by improving the existing passive polarizers.

II

FREE SPACE RADIATION CHARACTERISTICS OF CONVENTIONAL VOR ANTENNAS

2.1 Introduction

In this chapter, both theoretical and experimental free space radiation patterns produced by a conventional VOR antenna are discussed. The conventional VOR antenna system consists of four Alford loops placed about 4'· above a conducting ground plane or counterpoise. As mentioned earlier the antenna operates in two distinct modes characterized by the method of excitation of these four loops. In the carrier mode, the four loops are excited with equal amplitude and phase all the time. The pattern of the antenna in this mode is omnidirectional in the horizontal plane. The elevation plane pattern is symmetrical about the axial direction; it has a maximum in the direction 30^{o} - 40^{o} above the horizon and has a minimum (ideally a null) in the axial direction. The carrier mode radiation pattern of a conventional VOR antenna has been discussed in detail previously (Sengupta, et al, 1968; Sengupta and Weston, 1969) and will not be repeated here. The theoretical expression for the carrier mode pattern along with some relevant pattern details for a specific antenna configuration are given here for future reference.

In the side band mode, at any instant of time, each diagonal pair of Alford loops are excited with equal amplitude but opposite phase. The pattern of each pair of loops above the counterpoise is a figure-of-eight in the horizontal plane; in the elevation plane the pattern is similar to that of the carrier mode. Although these facts about the side band mode patterns are well documented experimentally, there has been no satisfactory theory until we developed it recently (Sengupta and Ferris 1970a; Sengupta 1971). In the following sections, we discuss the theory of the side band mode radiation pattern produced by a conventional VOR antenna. The theory is then compared with experimentally measured patterns.

2.2 Carrier Mode Pattern

For the purpose of theoretical analysis of the radiation pattern, the conventional VOR antenna operating in the carrier mode is approximated by a small circular loop carrying a constant amplitude current and located above a circular ground plane. Thus the VOR loop counterpoise antenna can be replaced by a point source with appropriate far field variation and placed above the counterpoise as shown in Fig. 2-1. The free space far-zone electric field of the point source (in the absence of the counterpoise) is represented by the following:

$$E_{\phi}^{i} = \eta_{o} I_{o} \left(\frac{ka}{2}\right)^{2} \sin\theta \frac{e^{ikr}}{r} \quad , \tag{2.1}$$

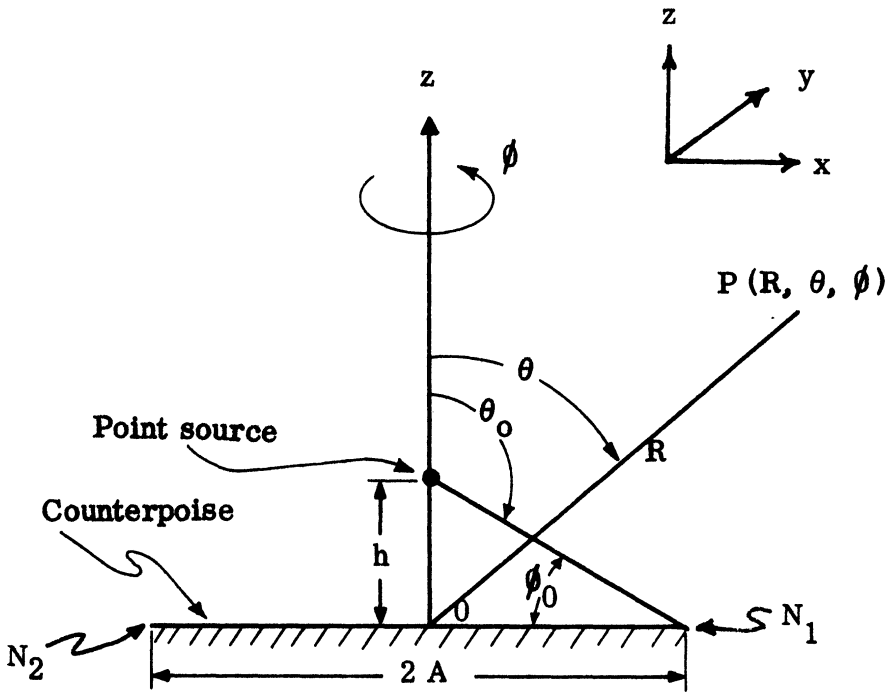

FIG. 2-1: Theoretical model for the conventional VOR antenna.

where

r, θ, ϕ are the spherical coordinates of the far field point with origin located at the point source,

η_o is the intrinsic impedance of free space,

$k = 2\pi/\lambda$ is the free space propagation constant,

a is the radius of the circular loop,

I_o is the amplitude of the loop current given by:

$$\bar{I} = \hat{\phi}\, I_o\, e^{-i\omega t}, \tag{2.2}$$

$\hat{\phi}$ is the unit vector in the ϕ-direction,

ω is the angular frequency,

assumed time dependence is $e^{-i\omega t}$.

Note that the field in eq. (2.1) is polarized in the ϕ-direction and is omnidirectional in the $\theta = \pi/2$ plane. The symmetry of the system dictates that the far field produced by the antenna shown in Fig. 2-1 will also be polarized in the ϕ-direction and that the far-field pattern will be omnidirectional in the horizontal or $\theta = \pi/2$ plane. It can be shown (Sengupta and Weston, 1969) that the complete expression for the far zone elevation plane (x-z plane) electric field produced at a point $P(R, \theta)$ and valid in the range $0 < \theta < \pi$ is given by:

$$E_\phi^A \simeq \eta_o I_o \left(\frac{ka}{2}\right)^2 \frac{e^{i(kR-\pi/4)}}{R}\, S^A(\theta), \tag{2.3}$$

where

$$S^A(\theta) = \left\{ \frac{F^o(\theta)\sin\theta}{\sqrt{2}}\, e^{-ikA\sin\theta} + \frac{|\cos\theta|\, \sin\left(\frac{\phi_o}{2}\right)}{\sqrt{\pi k r_o \sin\theta}}\, e^{ikr_o}\, L^o(\theta) \right\}, \tag{2.4}$$

$$L^o(\theta) = \frac{e^{i\left(\frac{\pi}{2} - kA\sin\theta\right)}}{\sqrt{1-\sin\theta}} \left(\frac{\cos^{3/2}\phi_o - \sin^{3/2}\theta}{\cos\phi_o - \sin\theta} \right) - \frac{e^{ikA\sin\theta}}{\sqrt{1+\sin\theta}} \frac{\cos^{3/2}\phi_o}{\cos\phi_o + \sin\theta}, \tag{2.5}$$

$$F^o(\theta) = e^{ikr_o\sin(\theta-\phi_o)} \int_{-\infty}^{p_1} e^{i\pi t^2/2}\, dt - e^{ikr_o\sin(\theta+\phi_o)} \int_{-\infty}^{p_2} e^{i\pi t^2/2}\, dt, \tag{2.6}$$

$$p_1 = 2\left(\frac{kr_o}{\pi}\right)^{1/2} \cos\left(\frac{\phi_o - \theta - \pi/2}{2}\right), \tag{2.7}$$

$$p_2 = 2\left(\frac{kr_o}{\pi}\right)^{1/2} \cos\left(\frac{\phi_o + \theta + \pi/2}{2}\right), \tag{2.8}$$

$$r_o^2 = A^2 + h^2, \tag{2.9}$$

$$\tan \phi_o = \frac{h}{A} \tag{2.10}$$

and the other parameters are as explained in Fig. 2-1. The term $S^A(\theta)$ in eq. (2.3) may be looked upon as the complex far field pattern of the conventional VOR antenna operating in the carrier mode. Thus $|S^A(\theta)|$ is the conventional far field radiation pattern.

Detailed discussions of eq. (2.3) and its comparison with experimentally measured patterns have been given elsewhere (Sengupta et al, 1968). The measured free space far field elevation pattern of the conventional VOR antenna with a 15' diameter counterpoise is shown in Fig. 2-2. The theoretical pattern of the same antenna, obtained by numerically computing the far field expressions given above, is superposed on Fig. 2-2 for comparison. The agreement between theory and experiment may be considered to be excellent over most of the regions in space. The slight kink in the experimental pattern near the region $\theta = 95^o$ is attributed to a reflecting object lying near the outside pattern range.

Since the model antenna considered in Fig. 2-2 corresponds to the full scale VOR antenna located at NAFEC, the theoretical values of the important parameters characterizing the free space elevation pattern of the antenna in the carrier mode at 1080 MHz are given below:

Direction of principal maximum $\theta_{max} = 65^o$.

Far field gradient at the horizon $\alpha_g = -20 \log_{10}\left|\frac{E(96^o)}{E(90^o)}\right| = 5.56$ dB/6°.

Field reduction factor $\alpha_f = -20 \log_{10}\left|\frac{E(90^o)}{E(\theta_{max})}\right| = 14.85$ dB .

The normalized parameters of the antenna are kh = 2.75, kA = 51.69 at the frequency f = 1080 MHz. These correspond to a full scale antenna having 150' diameter counterpoise and the Alford loops located 4' above the counterpoise. Parametric study of the carrier mode radiation pattern for the same antenna under various situations may be found elsewhere (Sengupta et al, 1968).

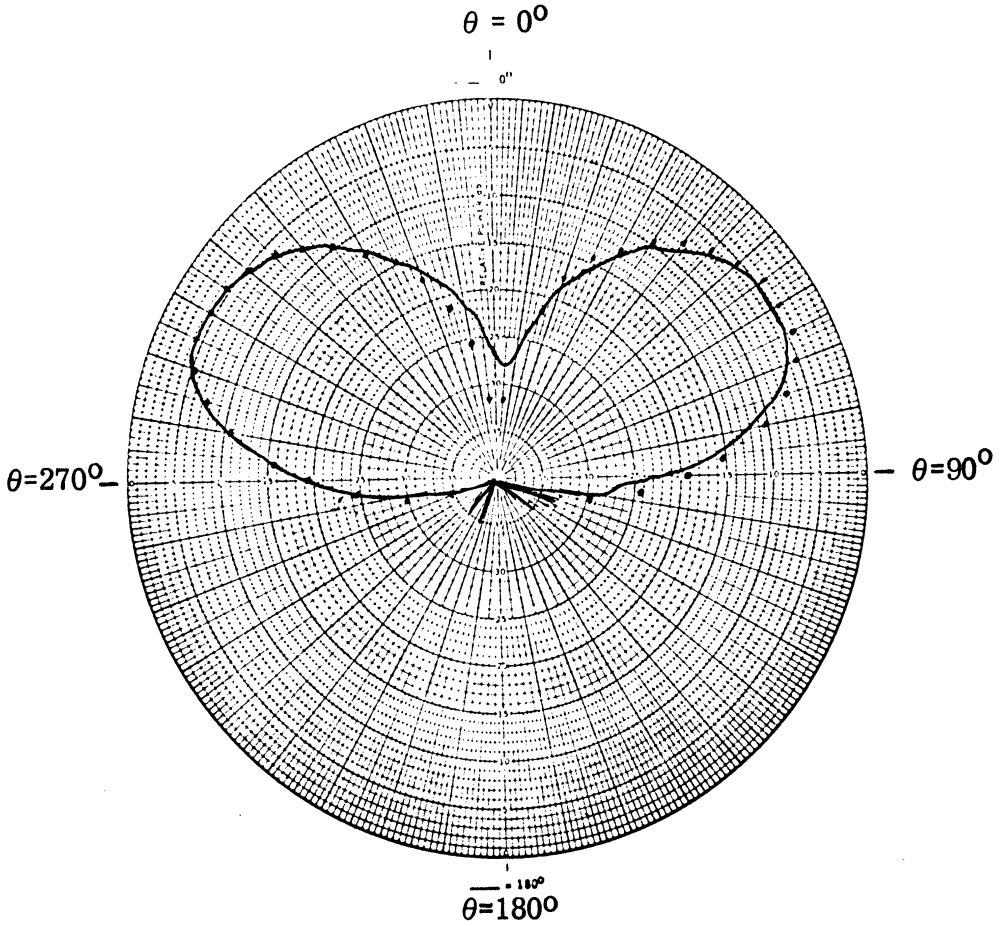

FIG. 2-2: Carrier mode elevation plane far field pattern of a conventional VOR antenna. kh = 2.75, kA= 51.69, f = 1080 MHz. —— Experimental; . . . . Theoretical

2.3 Side Band Mode Pattern

In this section we develop and discuss the theoretical expressions for the radiation field produced by a conventional VOR antenna operating in the side band mode. The theory is then compared with measured results at 1080 MHz. From the point of view of the side band mode radiation pattern, the antenna consists of a pair of Alford loops suitable excited and placed at the proper height above a counterpoise. The two Alford loops lie in the same plane which is parallel to the plane of the counterpoise. The Alford loops are separated by a distance, 2d, small compared to a wavelength and are excited with signals having equal amplitude but opposite phase. Thus the free space azimuthal pattern of the antenna would be a figure-of-eight.

2.3.1 Theoretical Expression for the Elevation Plane Pattern.

For the purpose of theoretical analysis the conventional VOR antenna operating in the side band mode is replaced by a point source with appropriate far field variation placed above the counterpoise as shown in Fig. 2-1. The free space far-zone electric field of the point source (in the absence of the counterpoise) can be represented by:

$$E_{\phi}^{i} = \eta I_o \left(\frac{ka}{2}\right)^2 f(\theta,\phi)\sin\theta \frac{e^{ikr}}{r} , \qquad (2.11)$$

where all the parameters are as explained in Section 2.2 and $f(\theta,\phi)$ is the source pattern function which is determined by the method of excitation and orientation of the two loops. Note that the field in eq. (2.11) is polarized in the ϕ-direction. In the present case, the two Alford loops are excited with equal amplitude but opposite phase so that $f(\theta,\phi)$ can be written explicitly as follows:

$$f(\theta,\phi) = 2i \sin(kd \sin\theta \cos \phi) . \qquad (2.12)$$

Equation (2.12) means that in the azimuthal plane $\theta = \pi/2$, the pattern is a figure-of-eight having a maximum along the x-axis. In the following we discuss the vertical pattern produced by the antenna.

The exact analysis of the radiation field produced by the above antenna is an extremely complicated problem, if not impossible. We apply the concepts of geometrical theory of diffraction (Keller, 1962) and the results of Sommerfeld's half-plane diffraction theory (Sommerfeld, 1954) to investigate the problem.

In obtaining the far field in the high frequency limit (which implies in the present case that $kA \gg 1$), it is convenient to separate the entire space into three distinct regions. Region I, defined as $0 \leq \theta \leq \pi/2 - \phi_o$, is the illuminated region, where the total field at the far field point $P(R,\theta,\phi)$ can be formally written as,

$$E_\phi(P) = E_\phi^i(P) + E_\phi^r(P) + E_\phi^d(P) \quad , \tag{2.13}$$

where

$E_\phi^i(P)$ is the incident field at P,

$E_\phi^r(P)$ is the reflected field at P,

$E_\phi^d(P)$ is the diffracted field at P.

The diffracted field $E_\phi^d(P)$ consists mainly of the fields diffracted by the near and far edges, respectively, of the counterpoise (N_1, N_2 in Fig. 2-1). Of the two diffracted fields, the near edge contribution dominates in this region. In Region II, defined as

$$(\frac{\pi}{2} - \phi_o) \leq \theta \leq (\frac{\pi}{2} + \phi_o)$$

and known as the transition region, $E_\phi^r(P) = 0$ and $E_\phi^d(P)$ is essentially due to that diffracted by the near edge. In Region III, defined as

$$(\frac{\pi}{2} - \phi_o) \leq \theta \leq \pi \ ,$$

and known as the shadow region, the field consists of the near- and far-edge diffracted components only.

The incident and reflected field components $E_\phi^i(P)$ and $E_\phi^r(P)$ can be obtained very easily. The problem thus reduces to the determination of the correct components for $E_\phi^d(P)$ and the combination of them in proper phase. Geometrical theory of diffraction and the results of Sommerfeld's theory of half-plane diffraction are used in developing the correct expressions for $E_\phi^d(P)$. We do not go into the details of the method here, since it has been discussed elsewhere (Sengupta and Weston, 1969) for the case $f(\theta, \phi = 1$ in eq. (2.11). In the following we give the final expression for the far field along with the key expressions necessary in obtaining it.

It can be shown that the far field expression valid in the transition region

$$\frac{\pi}{2} - \phi_o \leq \theta \leq \frac{\pi}{2} + \phi_o \ ,$$

is given by (Sengupta and Weston, 1969; Sengupta et al, 1968):

$$E_\phi \sim \eta_o I_o (\frac{ka}{2})^2 f(\theta_o, \phi) \frac{e^{ik(R - A\sin\theta)}}{R\sqrt{\sin\theta}} \cdot \left[U(r_o, \psi_1) - U(r_o, \psi_2)\right] \quad , \tag{2.14}$$

where

$$U(r, \psi) = e^{-ikr\cos\psi} \frac{(1-i)}{2} \int_{-\infty}^{p} e^{i\pi t^2/2} \, dt \ , \tag{2.15}$$

$$\psi_1 = \phi_o - \frac{\pi}{2} - \theta, \qquad \psi_2 = \phi_o + \frac{\pi}{2} + \theta, \qquad \tan\phi_o = \frac{h}{A} \tag{2.16}$$

$$p = 2\left(\frac{kr}{\pi}\right)^{1/2} \cos\frac{\psi}{2} . \tag{2.17}$$

Equation (2.14) neglects the effect of far edge diffraction which is a reasonable approximation in the transition region. If necessary, the incident field $E_\phi^i(P)$ in this region can be separated out from eq.(2.14) by asymptotically evaluating the integral given by (2.15). Proceeding the same way, it is now possible to separate the near edge diffracted field component from eq. (2.14) valid in the shadow region.

The near edge diffracted field component valid in the illuminated region,

$$0 < \theta < \frac{\pi}{2} - \phi_o ,$$

is given by:

$$E_{\phi_{N_1}} \sim \eta_o I_o \left(\frac{ka}{2}\right)^2 f(\theta_o, \phi) \frac{\cos\theta \sin\frac{\phi_o}{2}}{\cos\phi_o - \sin\theta} \times \left[\frac{\cos^3\phi_o}{\pi k r_o \sin\theta(1-\sin\theta)}\right]^{1/2} \times$$

$$\times \frac{e^{i\frac{\pi}{4}} \cdot e^{ik(R - A\sin\theta + r_o)}}{R} . \tag{2.18}$$

The far edge diffracted field component valid in the illuminated region,

$$0 < \theta < \frac{\pi}{2} - \phi_o$$

is given by the following expression:

$$E_{\phi_{N_2}} \sim -\eta_o I_o \left(\frac{ka}{2}\right)^2 f(\theta_o, \phi) \frac{\cos^{3/2}\phi_o}{\cos\phi_o + \sin\theta} \times \frac{\cos\theta \sin\frac{\phi_o}{2}}{\sqrt{1+\sin\theta}} \times$$

$$\times \frac{e^{-i\left(\frac{\pi}{4} - kA\sin\theta\right)}}{\sqrt{\pi k r_o \sin\theta}} \cdot \frac{e^{ikR}}{R} . \tag{2.19}$$

With the help of the above expressions along with the incident and reflected components of the field, it is possible to develop the complete expression for the field at any point in space. It is clear from the above that different field expressions would be obtained for a field point in different regions of space. For computational purposes it is convenient to derive a single expression for the field which would be valid in all the three regions of space. With the field expressions given in eqs. (2.14) through (2.19), it is possible to asymptotically develop a single expression for the far field valid in the region $0 < \theta < \pi$. This can be done

by starting with the transition region field given by eq. (2.14) and modifying it asymptotically to account for the different contributions in the various regions of space. The details of asymptotic development of such an expression has been discussed in Sengupta and Weston (1969) and will not be repeated here. The complete expression for the far field thus obtained and valid in the region $0<\theta<\pi$ can be expressed as

$$E_{\phi} \sim \eta_o I_o \left(\frac{ka}{2}\right)^2 \frac{e^{i(kR-\frac{\pi}{4})}}{R} S^A(\theta) \ , \tag{2.20}$$

where

$$S^A(\theta)=\left\{ \frac{F^o(\theta)f(\theta,\phi)\sin\theta}{\sqrt{2}} e^{-ikA\sin\theta} + \frac{|\cos\theta| \sin\frac{\phi_o}{2}}{\sqrt{\pi kr_o \sin\theta}} e^{ikr_o} L^o(\theta) \right\} , \tag{2.21}$$

$$F^o(\theta)=e^{ikr_o\sin(\theta-\phi_o)} \int_{-\infty}^{p_1} e^{i\pi\frac{t^2}{2}} dt - e^{ikr_o\sin(\theta+\phi_o)} \int_{-\infty}^{p_1} e^{i\pi\frac{t^2}{2}} dt \ , \tag{2.22}$$

$$L^o(\theta)= \frac{e^{i(\frac{\pi}{2}-kA\sin\theta)}}{\sqrt{1-\sin\theta}} \cdot \frac{f(\theta_o,\phi)\cos^{3/2}\phi_o - f(\theta,\phi)\sin^{3/2}\theta}{\cos\phi_o-\sin\theta} - \frac{e^{ikA\sin\theta}}{\sqrt{1+\sin\theta}} \frac{f(\theta_o,\phi)\cos^{3/2}\phi_o}{\cos\phi_o+\sin\theta} \ . \tag{2.23}$$

It should be remembered that in obtaining the above expressions the basic assumptions of geometrical theory of diffraction have been used. In the present case it mainly implies that eq. (2.20) is valid for $kA \gg 1$. Equations (2.20) through (2.23) give the far field produced by a loop counterpoise antenna that is being used in the existing VOR system. To the best of our knowledge the expressions given above are new and appeared for the first time in one of the Interim Reports under this contract (Sengupta and Ferris, 1970a). In the next section we make a comparison between the results obtained by numerical computation of (2.21) for the case $\phi = 0^o$ and the corresponding measured results.

2.3.2 Description of the Experimental Arrangement

Experimental investigations have been carried out at the frequency 1080 MHz with the help of an outside antenna pattern range. Each of the Alford loops used is a tenth scale model of a typical loop used in the existing VOR antenna system, the design of which is discussed by Anderson (1965). A photograph of the Alford loop

model is shown in Fig. 2-3. Each loop is made of brass strips and fed by a coaxial line with the help of a balance-to-unbalance transformer. Each loop is square-shaped with each side equal to 2.1", which is about $\lambda/5$ at the frequency 1080 MHz. The excited element here consists of two such Alford loops fed 180° out of phase and placed in the same plane which is parallel to the 15' diameter counterpoise. The 15' diameter counterpoise was fabricated on a wooden framework. The central portion of the counterpoise consists of a solid aluminum disc mounted on the frame. This was done to mount the Alford loops conveniently. The rest of the counterpoise consists of household aluminum screen stapled to the wooden framework. The two loops are placed at a height of 4.8" above the counterpoise. They are displaced on either side of the axis of the counterpoise by 1.6" so that the two Alford loops are 3.2" apart. Figure 2-4 shows a photograph of the double Alford loop counterpoise model used during the experiment. In all the measurements to be discussed below, the above model has been used as a receiving antenna in conjunction with an antenna pattern range.

2.3.3 Comparison Between Theory and Experiment

The measured free space elevation patterns of conventional VOR antennas operating in the side band mode are shown in Figs. 2-5, 2-6 and 2-7 for three selected values of the counterpoise diameter. All the patterns have been measured in the x-z plane (Fig. 2-1) and at the frequency 1080 MHz. The corresponding theoretical patterns obtained by numerical computation of eqs. (2.20) through (2.23) are shown in Figs. 2-5 through 2-7 for comparison. The normalized dimensions of the antennas given in Figs. 2-6 and 2-7 correspond at 108 MHz to those of conventional VOR antennas with 52' and 150' diameter counterpoises respectively.

The agreement between theory and experiment for the cases kA = 17.92 (2A = 5.2') and kA = 51.69 (2A = 15') may be considered to be very good. The minor lobes in the pattern in directions $\theta > \pi/2$ as well as the kink in the pattern just below the $\theta = \pi/2$ for the case kA = 51.69 are attributed to the outside pattern range and the feed system of the antenna. The measured results shown in Figs. 2-5 and 2-6 were taken with an antenna pattern range inside a large anechoic chamber. The agreement between theory and experiment for the case kA = 6.32 (2A = 22") is not so good, although it may be considered to be fair over most of the region (see Fig. 2-5). The reason for this is attributed to the fact that due to the small size of the counterpoise, the geometrical diffraction theory approximation made in obtaining the far field expressions becomes poor.

2.3.4 More Information About the Side Band Pattern

Because of the fundamental importance of the 15' diameter antenna, its patterns were studied in more detail. Figure 2-8 shows measured far field elevation pattern of the antenna at 1080 MHz. Figure 2-8 is the same as 2-7 except for the fact that the pattern here is shown as a rectangular plot for obtaining

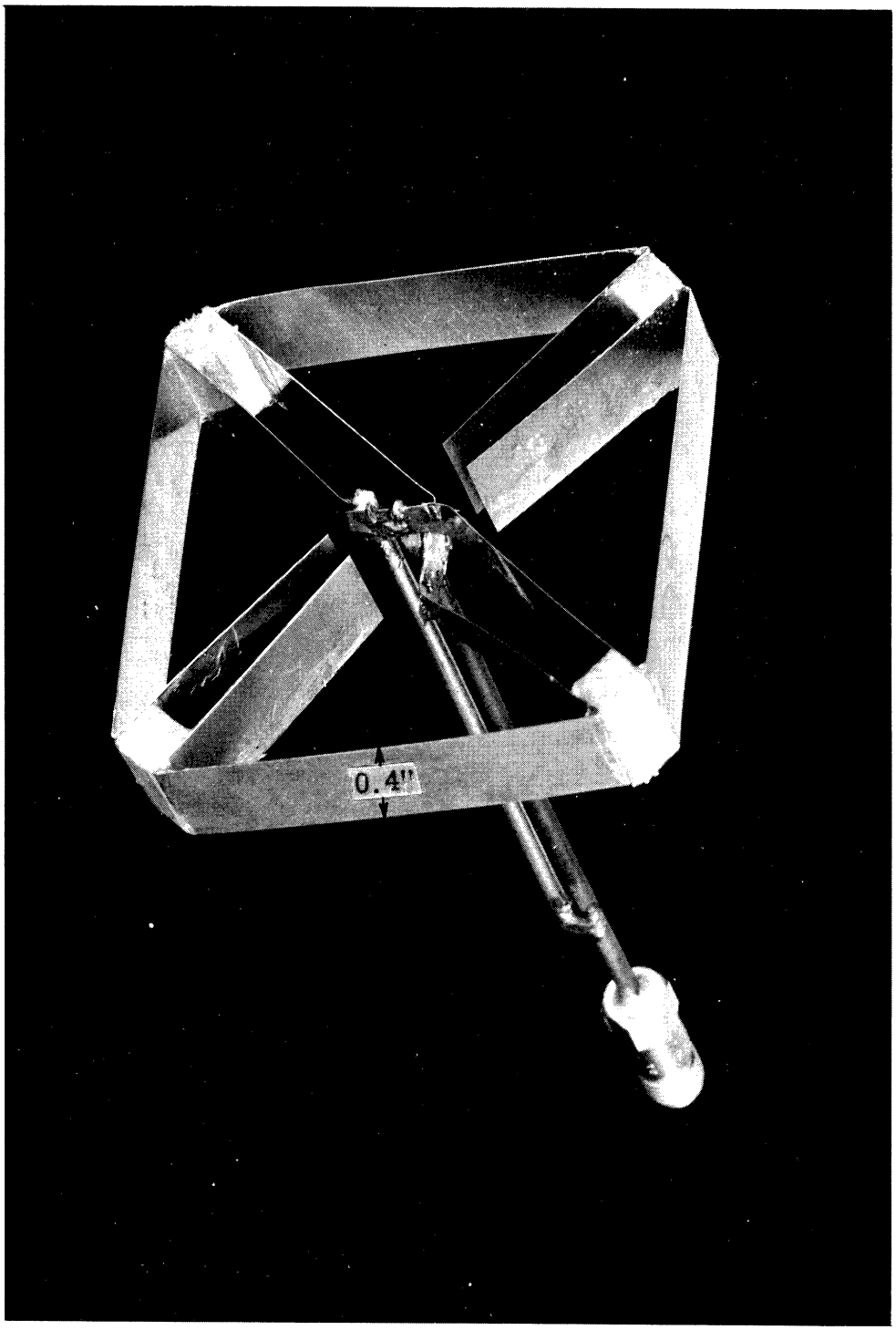

FIG. 2-3: Photograph of the Alford loop model.

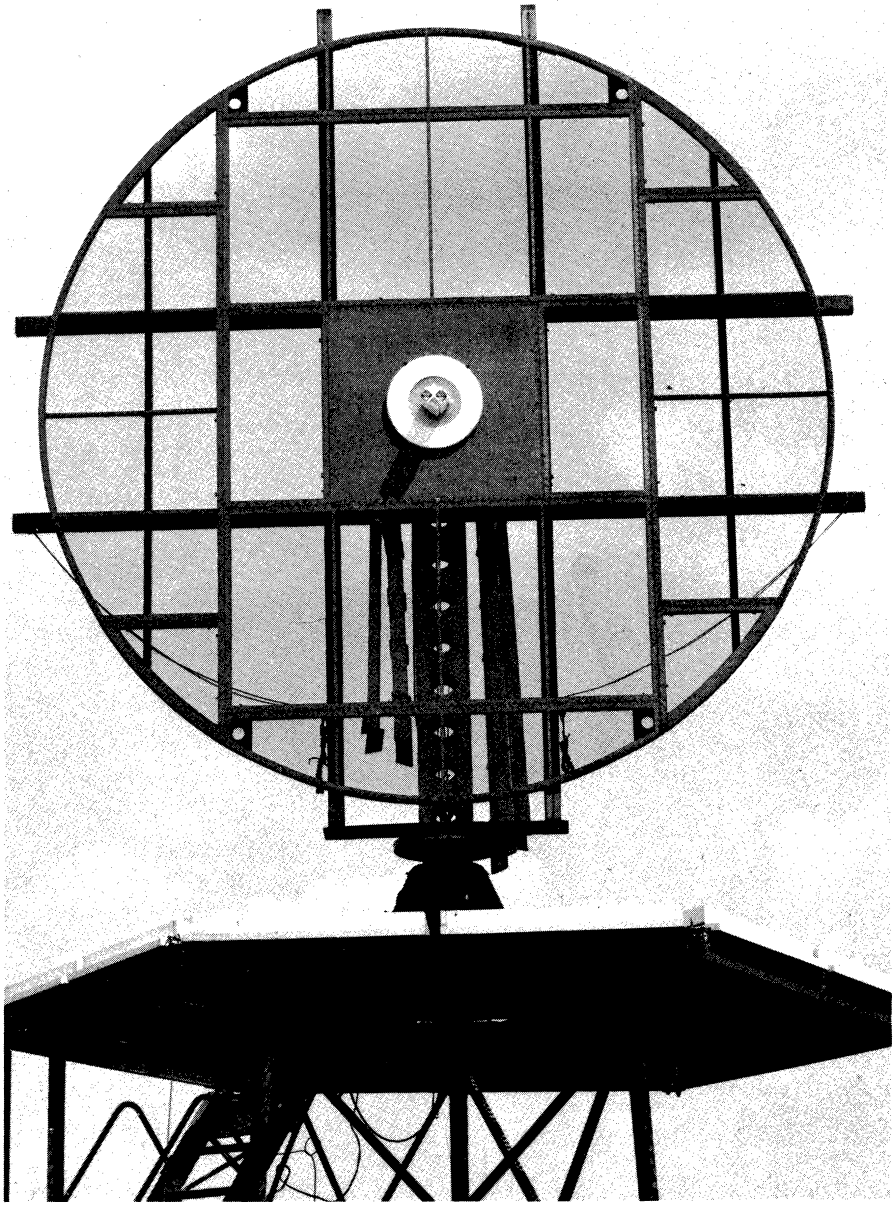

FIG. 2-4: Photograph of the two Alford loops mounted above the 15' diameter counterpoise.

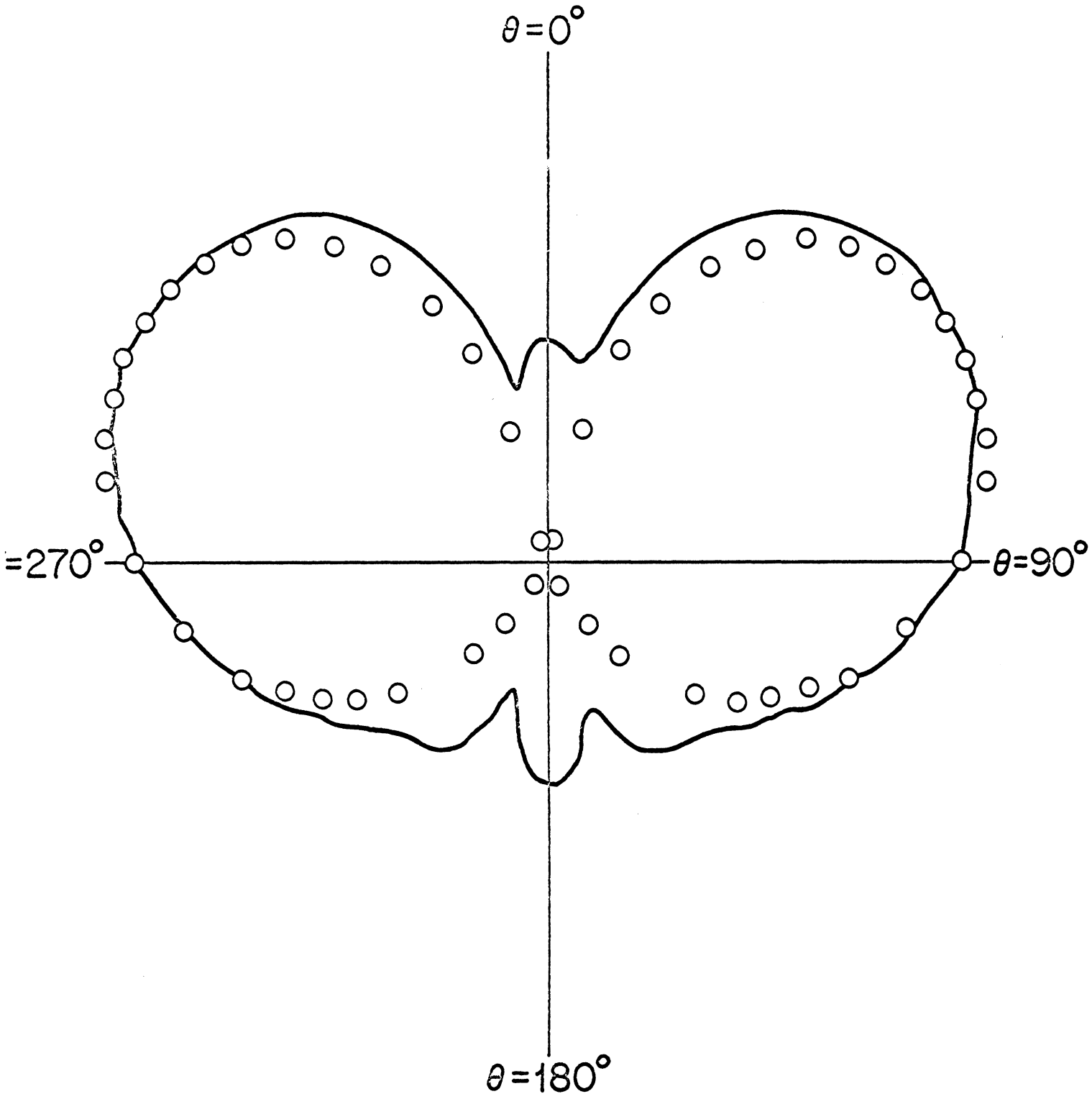

FIG. 2-5: Side band mode elevation plane far field pattern of a conventional VOR antenna. kh = 2.75, kd = 0.92, kA = 6.32, f = 1080 MHz. —— Experimental, ooo Theoretical

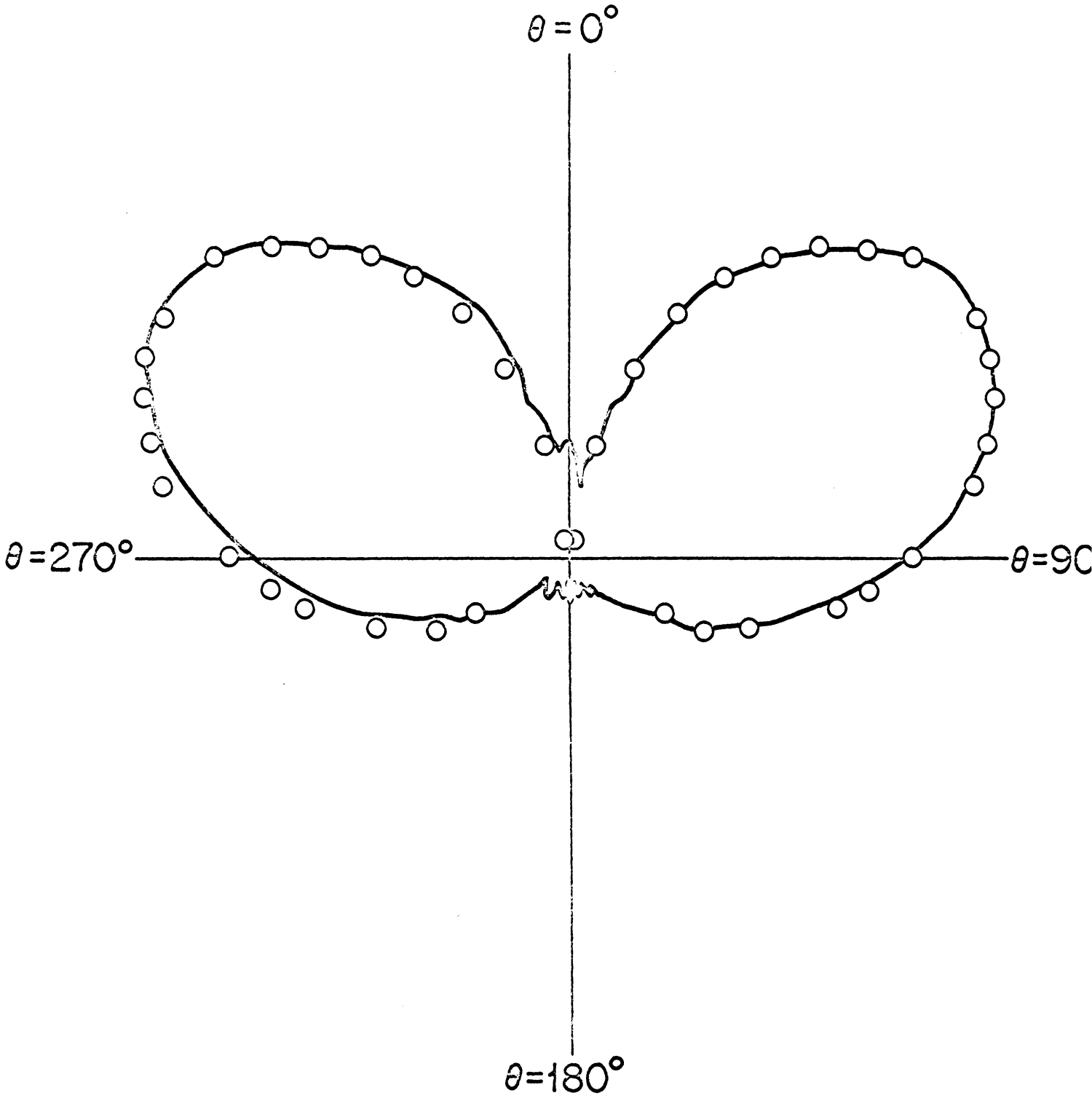

FIG. 2-6: Side band mode elevation plane far field pattern of a conventional VOR antenna. kh = 2.75, kd = 0.92, kA = 17.92, f = 1080 MHz —— Experimental, o o o o Theoretical.

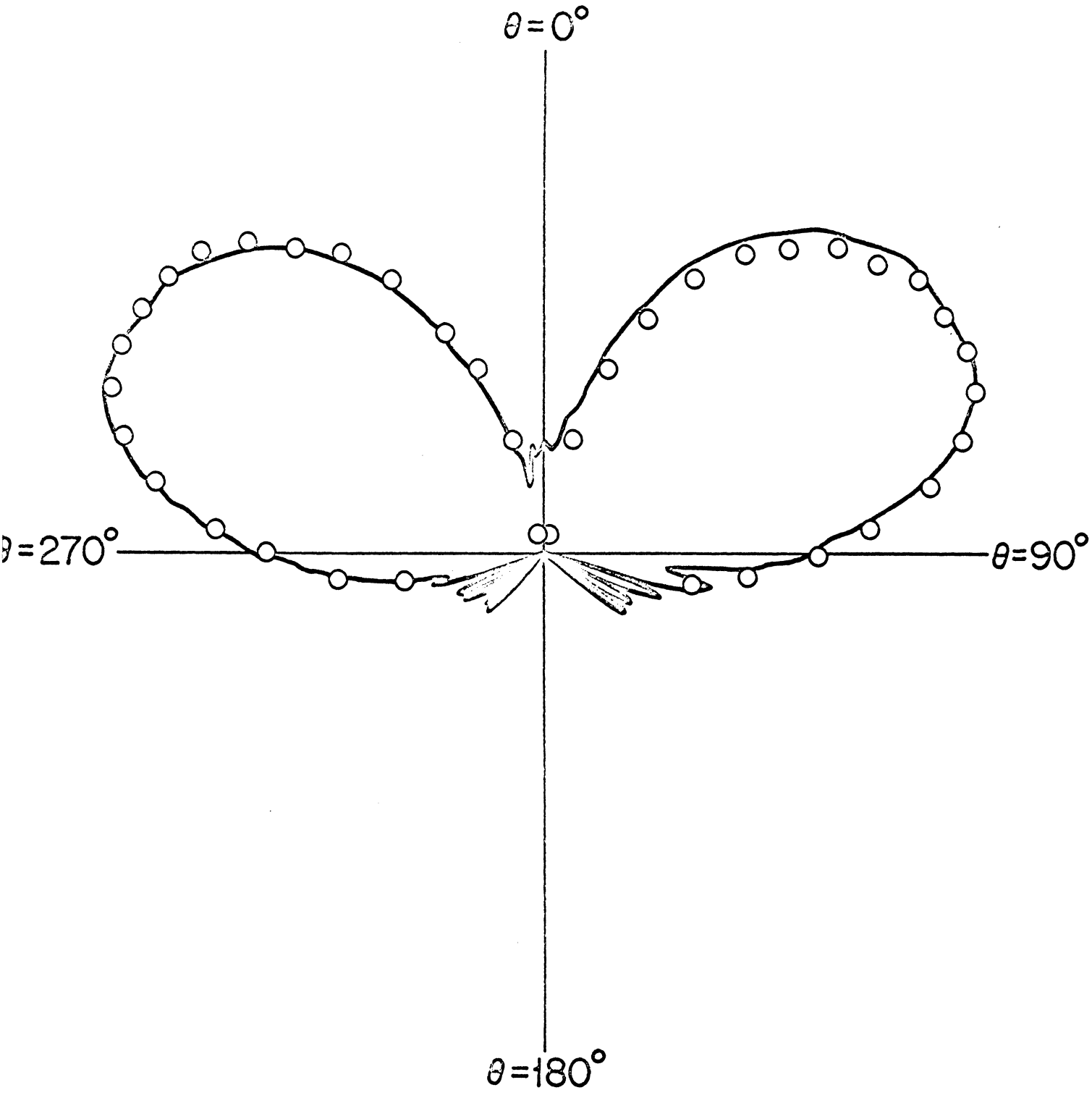

FIG. 2-7: Side band mode elevation plane far field pattern of a conventional VOR antenna. kh = 2.75, kd = 0.92, kA=51.69, f = 1080 MHz. —— Experimental, o o o o o Theoretical.

better pattern details. Figure 2-9 shows the azimuthal pattern of the same antenna. The shape of Fig. 2-9 indicates that the feed system used has been satisfactory for the side band mode of operation of the antenna.

The theoretical values of the other important parameters of the free space elevation pattern of the antenna operating at 1080 MHz and in the side band mode are given below.

Direction of the principal maximum $\theta_{max} = 65^{o}$
Far field gradient at the horizon $\alpha_{g} = 5.54$ dB/6^{o}
Field reduction factor $\alpha_{F} = 14.7$ dB .

The above parameters are not appreciably different from those for the case of carrier mode operation as given in Section 2.2. Numerical values for the free space elevation plane side band mode far field pattern of the above antenna are given in Table F-1a. Numerical values for the side band mode elevation plane pattern of a similar antenna with 5.2' diameter counterpoise (i.e. 52' diameter at 108 MHz) are also given in Table F-1b.

2.4 Discussion

Both the theoretical and experimental free space radiation characteristics of conventional VOR antennas operating in the carrier and side band modes have been discussed here. Theoretical expressions for the side band mode given here are new and have been developed during the present contract period. The results given in the present chapter will be used later in evaluating the performance of the parasitic loop counterpoise systems.

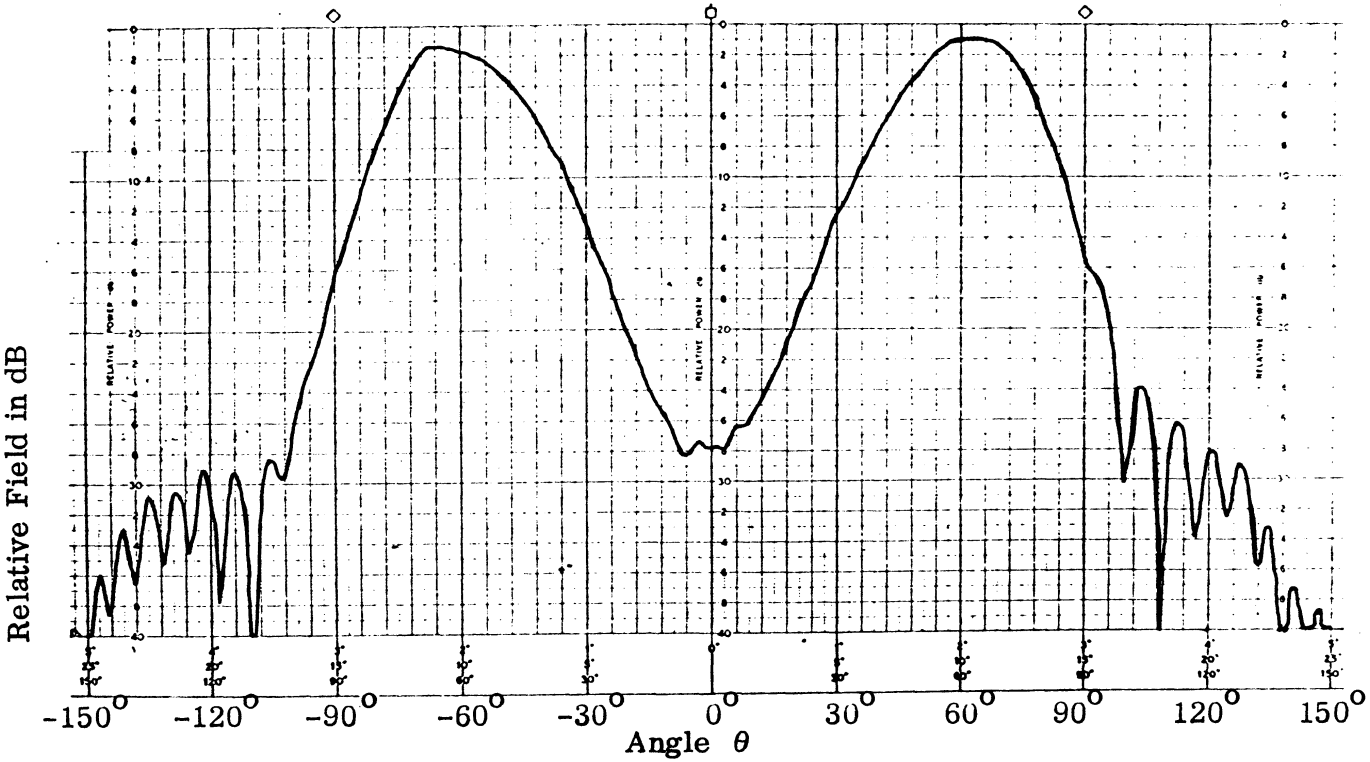

FIG. 2-8: Measured side band mode elevation plane far field pattern of a conventional VOR antenna. kh = 2.75, kd = 0.92, kA = 51.69, f = 1080 MHz.

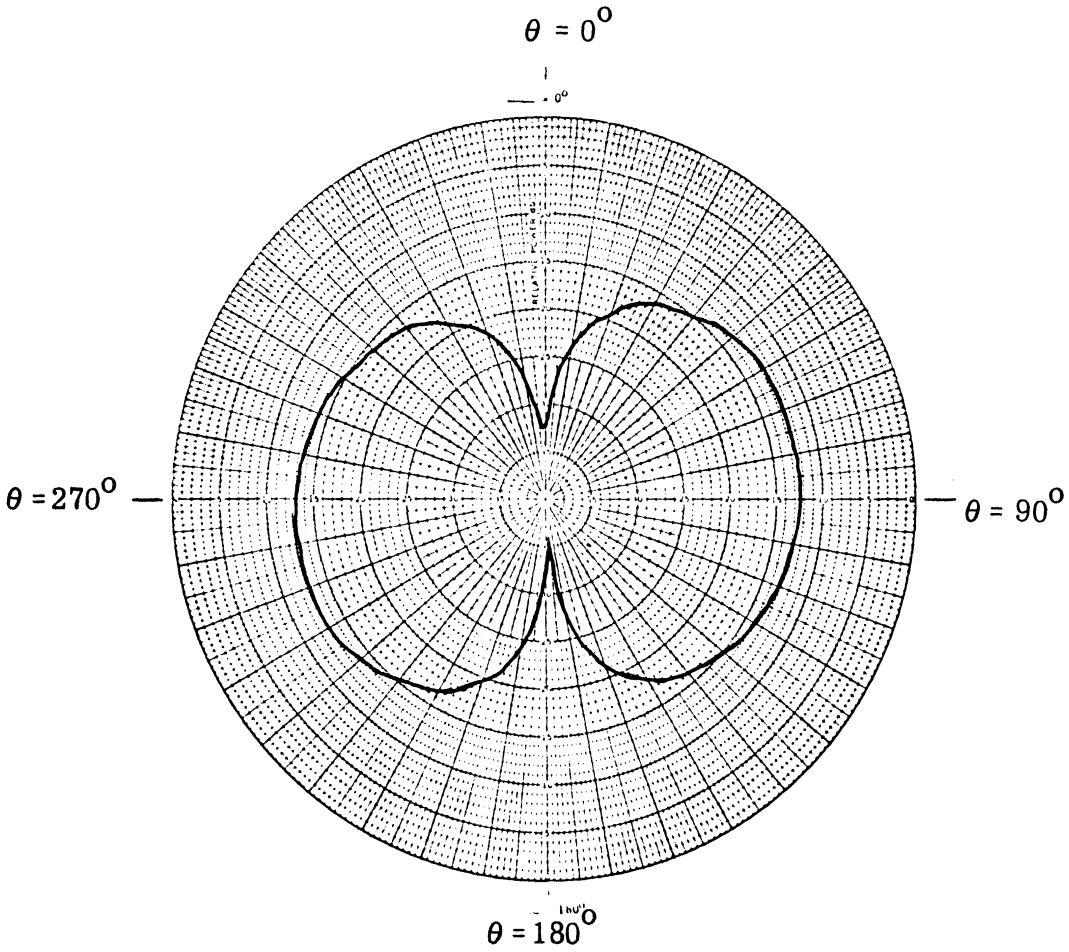

FIG. 2-9: Measured side band mode azimuthal plane far field pattern of a conventional VOR antenna. kh = 2.75, kd = 0.92, kA = 51.69, f = 1080 MHz.

III

INVESTIGATION OF SINGLE PARASITIC LOOP COUNTERPOISE ANTENNA

3.1 Introduction

In this chapter we discuss the theory of radiation from a single parasitic loop counterpoise antenna. The theory of such an antenna is of fundamental importance for the investigation of the radiation from double parasitic loop counterpoise antennas to be considered later. As we shall see, the theory developed here can be generalized directly for the latter antenna operating under some constraints of practical interest. The study of the single parasitic loop counterpoise antenna is also quite important on its own merit. In some applications where the required field gradients in the pattern are not very large, this type of antenna may be found to be more advantageous to use.

The single parasitic loop counterpoise antenna is obtained by placing coaxially a large parasitic loop at a convenient height above and parallel to the counterpoise of a conventional VOR antenna. Figure 3-1 shows a schematic diagram of such an antenna. The parasitic loop has a radius B and is placed at a height H above the counterpoise; it is assumed to be made of a conducting wire of radius b (or equivalently, of a conducting strip of width $w = 4b$).

Theory and performance of single parasitic loop counterpoise antennas operating in the carrier mode have been discussed in detail elsewhere (Sengupta et al, 1968; Sengupta and Weston 1969; Sengupta and Ferris, 1970) and will not be repeated here.

In the following sections we first give some of the important pattern characteristics for such an antenna with a 15' diameter counterpoise and operating in the carrier mode at the frequency 1080 MHz. These pattern characteristics will correspond to those of a full scale parasitic loop counterpoise VOR antenna with a 150' diameter counterpoise operating at the frequency 108 MHz. For the carrier mode operation, the nature of the induced current in the parasitic loop and its dependence on the antenna parameters are then studied numerically. Finally, we develop the theory for the side band mode radiation pattern produced by a single parasitic loop counterpoise antenna. The theory is then compared with results obtained from model measurements.

3.2 Carrier Mode Pattern

Theoretical expressions for the carrier mode pattern are given here for future reference. It can be shown (Sengupta and Weston, 1969) that the far zone electric field produced by a single parasitic loop counterpoise antenna shown in Fig. 3-1 is given by the following:

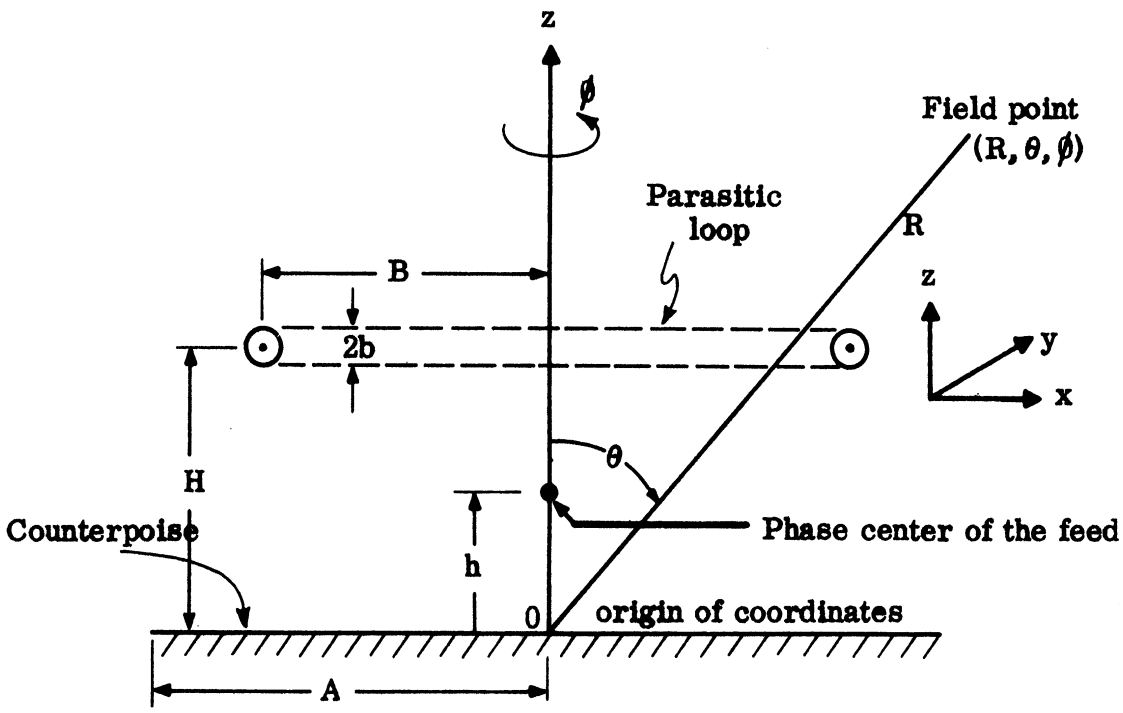

FIG. 3-1: Schematic representation of single parasitic loop counterpoise antenna and the coordinate system used.

$$E_\phi \sim \eta_o I_o \left(\frac{ka}{2}\right)^2 \frac{e^{i(kR-\pi/4)}}{R} S(\theta), \quad 0 < \theta < \pi \ . \tag{3.1}$$

where $S(\theta)$ is identified as the complex far field pattern and can be written formally as

$$S(\theta) = S^A(\theta) + S^P_{12}(\theta) + S^P_{56}(\theta) \ . \tag{3.2}$$

In eq. (3.2), $S^A(\theta)$ is the free space complex far field pattern of the antenna in the absence of the parasitic loop and is given by eqs. (2.4) - (2.10). The last two terms in eq. (3.2) constitute the complex far field pattern produced by the parasitic loop only in the presence of the counterpoise. The conventional radiation pattern of the antenna is given by $|S(\theta)|$. Explicit expressions for $S^P_{12}(\theta)$ and $S^P_{56}(\theta)$ are given by the following

$$S^P_{12}(\theta) = \frac{\pi (kB)^2}{iM} \left[\frac{e^{ikr_1}}{(kr_1)^2} - \frac{e^{ikr_2}}{(kr_2)^2} \right] F(\theta) \ , \tag{3.3}$$

$$S^P_{56}(\theta) = \frac{\pi^2 (kB)^2}{2M^2} \frac{e^{ikr_1}}{(kr_1)^2} \left[\left(\frac{1}{\pi kB}\right)^{1/2} e^{i(2kB + \frac{\pi}{4})} - \left(\frac{1}{\pi kH}\right)^{1/2} e^{i(2kH - \frac{\pi}{4})} \right] F(\theta) \tag{3.4}$$

$$r_1^2 = B^2 + (H-h)^2 \ , \quad r_2^2 = B^2 + (H+h)^2$$

$$M = 0.577 + \ell n \left(\frac{kb}{2}\right) - i\frac{\pi}{2}$$

$$F(\theta) = \frac{J_1(kB \sin\theta)}{\sqrt{2}} F^P(\theta) e^{-ikA \sin\theta} + \frac{|\cos\theta| \sin\left(\frac{\phi_P}{2}\right)}{\sqrt{\pi k r_P \sin\theta}} e^{ikr_P} L^P(\theta) \ , \tag{3.5}$$

$$L^P(\theta) = \frac{e^{i(\frac{\pi}{2} - kA\sin\theta)}}{\sqrt{1-\sin\theta}} \left[\frac{\cos^{1/2}\phi_P J_1(kB\cos\phi_P) - \sin^{1/2}\theta J_1(kB\sin\theta)}{\cos\phi_P - \sin\theta} \right] - \frac{e^{ikA\sin\theta}}{\sqrt{1+\sin\theta}} \left[\frac{J_1(kB\cos\phi_P)\cos^{1/2}\phi_P}{\cos\phi_p + \sin\theta} \right], \tag{3.6}$$

$$F^P(\theta) = e^{ikr_P \sin(\theta - \phi_P)} \int_{-\infty}^{p_5} e^{i\pi \frac{t^2}{2}} dt \quad - \quad \text{(continued)}$$

$$-e^{ikr_P \sin(\theta+\phi_P)} \int_{-\infty}^{p_6} e^{i\pi \frac{t^2}{2}} dt \,, \tag{3.7}$$

$$p_5 = 2\left(\frac{kr_P}{\pi}\right)^{1/2} \cos\left(\frac{\phi_P - \theta - \frac{\pi}{2}}{2}\right) \,, \tag{3.8}$$

$$p_6 = 2\left(\frac{kr_P}{\pi}\right)^{1/2} \cos\left(\frac{\phi_P + \theta + \frac{\pi}{2}}{2}\right) \,, \tag{3.9}$$

$$r_P^2 = A^2 + H^2 \,, \tag{3.10}$$

$$\tan \phi_P = \frac{H}{A} \,, \tag{3.11}$$

and J_1 is the usual notation for the Bessel function of the first kind and first order. The far field expressions given by eqs. (3.1) - (3.11) are valid under the following approximation:

$$kA \gg 1,\ kB \gg 1,\ kH \gg 1,\ kb \ll 1 \text{ and } kA > kB \,. \tag{3.12}$$

From a numerical investigation carried out with the help of the above expressions, it appeared that a parasitic loop having a radius B such that $kB = 3\pi$ (i.e. $2B = 3\lambda$) would produce a good field gradient when placed at a proper height H above the counterpoise having the normalized dimension $kA = 51.69$. The parasitic loop was assumed to be made of 1" wide conducting strip (i.e. $b = 0.25''$). The theoretical field gradient as a function of the height H of the parasitic loop above the counterpoise is shown in Fig. 3-2. It can be seen from this figure that a parasitic loop counterpoise antenna having $kH = 13$ and $kB = 3\pi$ produces a maximum field gradient of 9.6 dB/6°. It should be mentioned here, for comparison, that the carrier mode pattern of a conventional VOR antenna with the same counterpoise ($kA = 51.69$) has a field gradient of 5.56 dB/6° . The measured far field elevation pattern of the above parasitic loop counterpoise antenna is shown in Fig. 3-3. The corresponding theoretical pattern of the antenna is also superimposed on Fig. 3-3 for comparison

3.3 Numerical Investigation of the Parasitic Current for the Carrier Mode Case

In this section we give the results of a numerical investigation carried out to study the nature of the induced current in the parasitic loop and its dependence on the antenna parameters for the case of carrier mode operation. Detailed discussions of the theoretical expressions for the induced current in the parasitic loop have been given in the Final Report under our previous Contract (Sengupta et al, 1968). Here, we only quote the final expressions without derivation. The normalized induced current in the parasitic loop can be formally written as follows:

$$\frac{I_{P_o}}{I_o} = I_{P_o}^{12} + I_{P_o}^{34} + I_{P_o}^{56} \,, \tag{3.13}$$

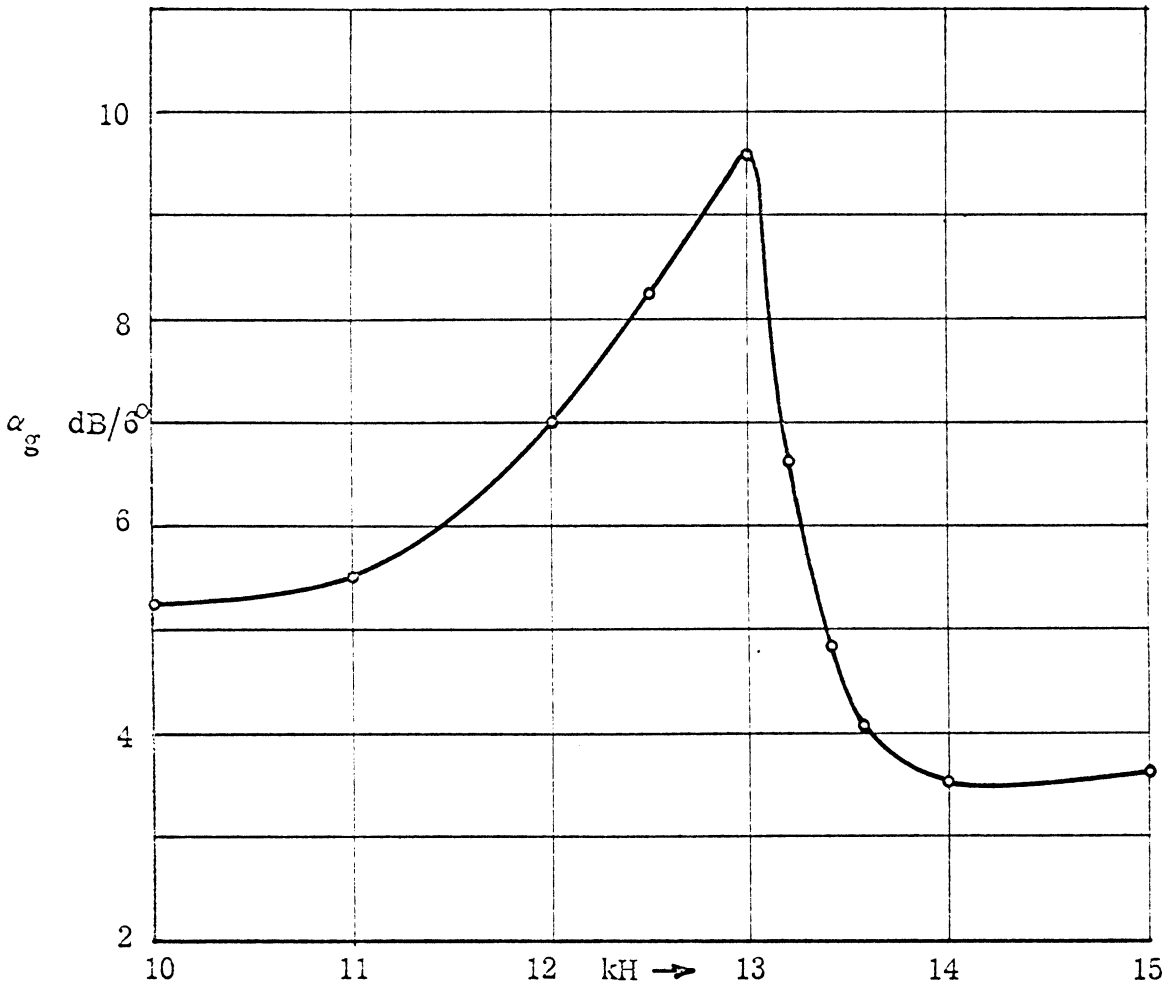

FIG. 3-2: Theoretical field gradient (α_g) as a function of H for a single parasitic loop counterpoise antenna operating in the carrier mode. kh = 2.75, kA = 51.69, kB = 3π, f = 1080 MHz, kH is variable.

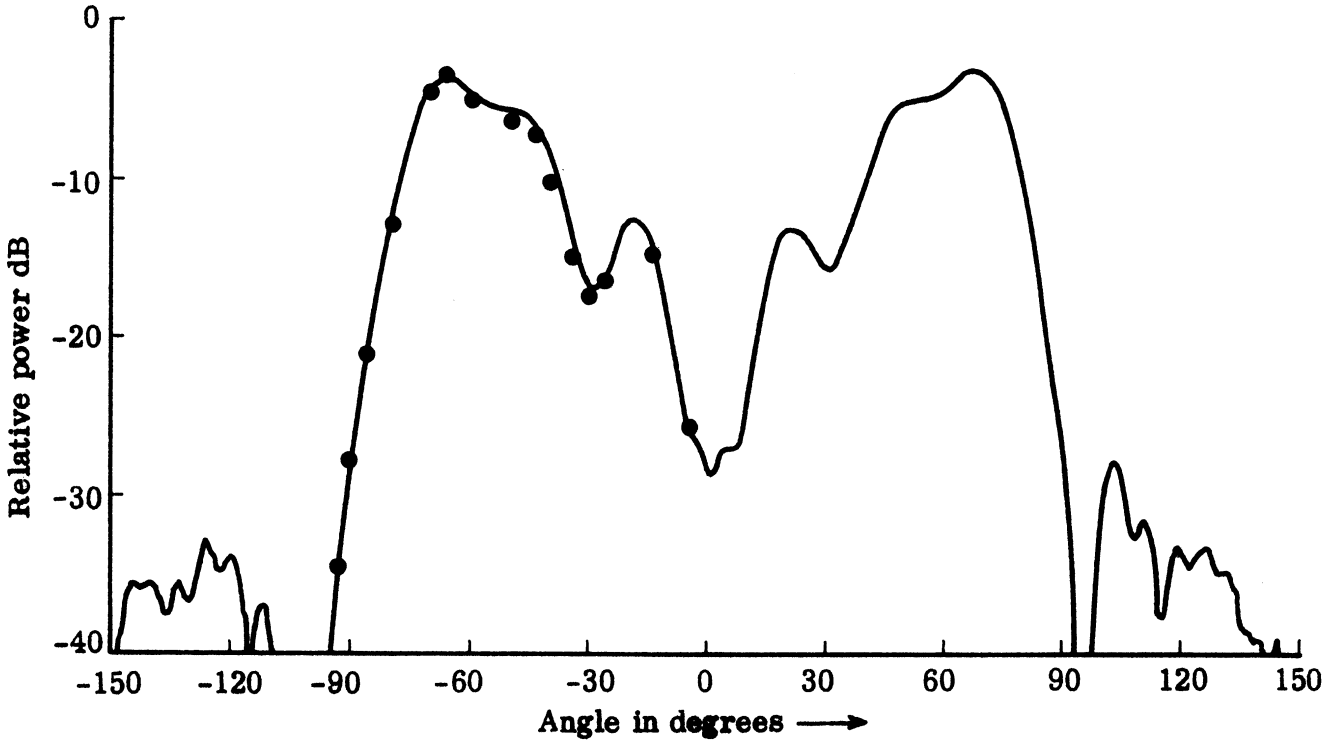

FIG. 3-3: Carrier mode elevation plane far field pattern of a single parasitic loop counterpoise antenna, kh = 2.75, kA = 51.69, kB = 3π, kH = 13, f = 1080 MHz.

. . . . . Theoretical, ——— Experimental

where I_o is the current in the excited loop and I_{P_o} is the current in the parasitic loop. The first term on the right hand side of (3.13) represents the current induced due to the direct wave from the driven element and due to the wave singly reflected from the counterpoise. The other two terms, $I_{P_o}^{34}$ and $I_{P_o}^{56}$ in (3.13) represent the currents due to the waves diffracted by the counterpoise edges. The reason for splitting the current expression into three terms is to study the order of magnitude of the different contributions so that the information obtained can be used for proper approximation in the far field analysis. It can be shown that the three terms on the right hand side of eq. (3.13) are given by (Sengupta et al, 1968):

$$I_{P_o}^{12} = \frac{2\pi B}{ikM}\left[\frac{e^{ikr_1}}{r_1^2} - \frac{e^{ikr_2}}{r_2^2}\right], \tag{3.14}$$

$$r_1^2=B^2+(H-h)^2,\quad r_2^2=B^2+(H+h)^2,\quad M=0.577+\ell n\left(\frac{kb}{2}\right)-i\frac{\pi}{2}, \tag{3.15}$$

$$I_{P_o}^{34} = \frac{\pi}{ikM}\frac{A}{r_0^2}e^{ikr_0}\frac{e^{-i3\frac{\pi}{4}}}{\sqrt{2}}\left(\frac{A}{B}\right)^{1/2} \times$$

$$\times\left[\left(\frac{1}{\pi kr_3}\right)^{1/2} e^{ikr_3}\left\{\sec\left(\frac{\phi_0-\phi_3}{2}\right)-\sec\left(\frac{\phi_0+\phi_3}{2}\right)\right\}\right.$$

$$\left.+i\left(\frac{1}{\pi kr_4}\right)^{1/2} e^{ikr_4}\left\{\sec\left(\frac{\phi_0-\phi_4}{2}\right)-\sec\left(\frac{\phi_0+\phi_4}{2}\right)\right\}\right], \tag{3.16}$$

$$\left.\begin{aligned} &r_3^2=(A-B)^2+H^2\ ;\ r_4^2=(A+B)^2+H^2\\ &r_0^2=A^2+h^2\\ &\tan\phi_3=\frac{H}{A-B},\ \tan\phi_4=\frac{H}{A+B},\ \tan\phi_0=\frac{h}{A}\end{aligned}\right\}, \tag{3.17}$$

$$I_{P_o}^{56} = \frac{\pi^2(kB)}{M^2}\left[\left(\frac{1}{\pi kB}\right)^{1/2} e^{i\left(2kB+\frac{\pi}{4}\right)} - \left(\frac{1}{\pi kH}\right)^{1/2} e^{i\left(2kH-\frac{\pi}{4}\right)}\right]. \tag{3.18}$$

The various notations used in eqs. (3.14) - (3.18) are as explained in the reference cited.

A computer program has been developed for obtaining the current induced in the parasitic loop with the help of the above expressions. We give here the results obtained for a specific single parasitic loop counterpoise antenna having the following

parameters: kA=17.92, kb=0.15, kh=2.75, kB=3π and kH=11.78. The values obtained for the normalized current are shown in Table III-1.

TABLE III-1: Normalized Value of the Parasitic Current

	Real	Imaginary	Absolute Value	Argument in Radians
$I_{P_o}^{12}$	-0.03893	0.17908	0.18326	1.785
$I_{P_o}^{34}$	-0.00070	0.00035	0.00068	2.678
$I_{P_o}^{56}$	0.02911	-0.00159	0.02915	-0.055
$\frac{I_{P_o}}{I_o}$	-0.01052	0.17784	0.17815	1.630

Parasitic currents induced for other values of the antenna parameters are shown in tabular form in Appendix D.

From the results shown here and in Appendix D, one fact appears to be consistent, namely that the contribution to the parasitic current due to the second term in (3.13) (i.e. $I_{P_o}^{34}$) is negligible compared to the others for the values of B and H considered here. Hence in the analysis of the far field pattern this term may be omitte This observation was made in our previous study (Sengupta et al, 1968) intuitively. The results given in this section justify that approximation quantitatively. The results given here will be found useful if an experimental program is developed to measure the current in the parasitic loop of a single parasitic loop counterpoise antenna

3.4 Side Band Mode Pattern

In this section we develop the theoretical expressions for the radiation field produced by a single parasitic loop counterpoise antenna operating in the side band mode. The accuracy of the expressions are then compared with the measured values. The theory developed here will be used to calculate the patterns produced by double parasitic loop counterpoise antennas with similar excitation.

3.4.1 Theoretical Expressions

The theoretical model of a single parasitic loop counterpoise antenna is shown in Fig. 3-4.

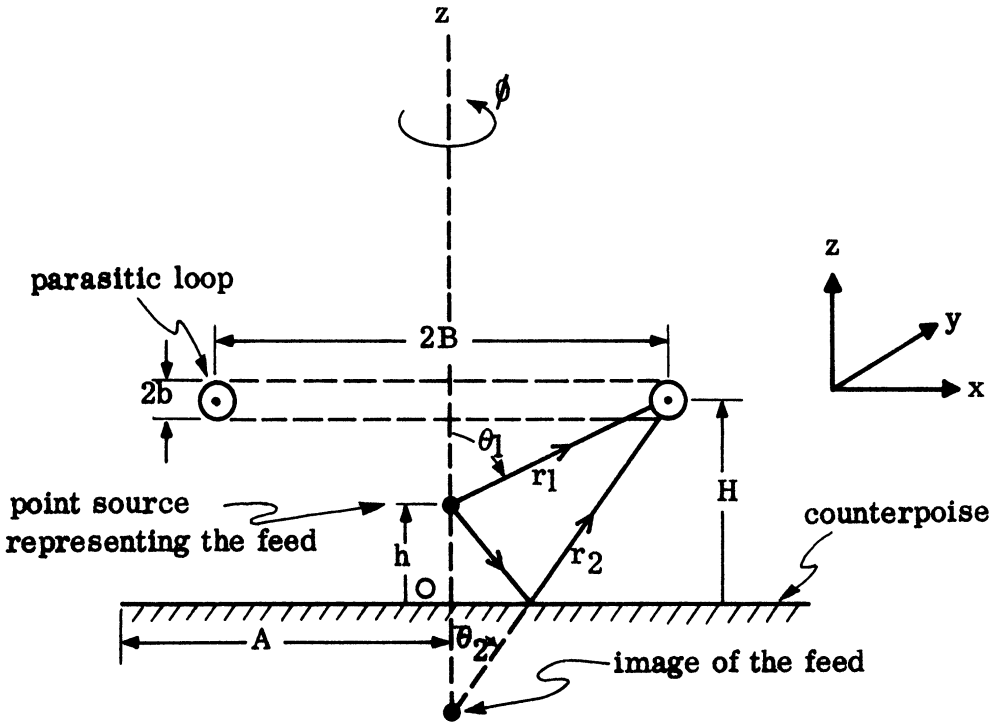

FIG. 3-4: Theoretical model for a single parasitic loop counterpoise antenna.

As before, the free space far field produced by the excited elements elements only (represented by the point source in Fig. 3-4) is:

$$E_{\phi}^{i} = \eta_o I_o \left(\frac{ka}{2}\right)^2 \cdot f(\theta,\phi)\sin\theta \, \frac{e^{ikr}}{r} , \tag{3.19}$$

where

$$f(\theta,\phi) = 2i \sin(kd \sin\theta \cos\phi) . \tag{3.20}$$

The first step in the analysis involves the determination of the current induced in the parasitic element.

Parasitic Current: Let the total field incident at the point P (Fig. 3-5) on the parasitic loop be denoted by $E_{\phi}^{inc}(P)$. Then the parasitic current I_{P_o} is given by

$$I_{P_o} = \frac{2\pi}{i\eta_o kM} E_{\phi}^{inc}(P) \tag{3.21}$$

where

$$M = 0.577 + \ell n \left(\frac{kb}{2}\right) - i\frac{\pi}{2} . \tag{3.22}$$

The basis and nature of approximations involved in (3.21) has been discussed elsewhere (Sengupta and Weston, 1969) and will not be repeated here.

The incident field $E_{\phi}^{inc}(P)$ consists of direct, reflected and diffracted fields.

A representation of the different field components that would be used in obtaining the parasitic current are shown in Fig. 3-5. Thus $E_{\phi}^{inc}(P)$ can be written formally as follows:

$$E_{\phi}^{inc}(P) = E_{\phi}^{12}(P) + E_{\phi}^{56}(P) \quad . \tag{3.23}$$

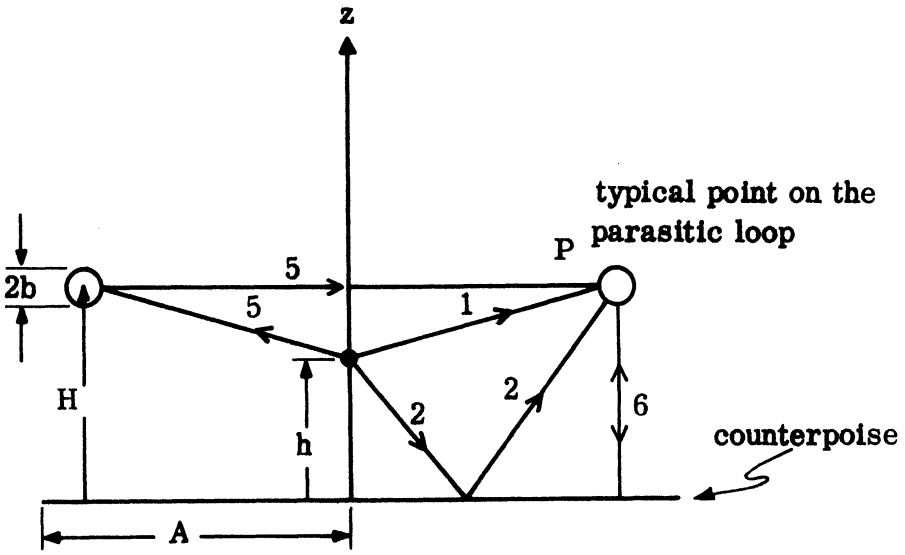

FIG. 3-5: Dominant rays contributing to the parasitic current.

Explicit expressions for the component fields $E_{\phi}^{12}(P)$ and $E_{\phi}^{56}(P)$ can be obtained by following a method similar to that discussed by Sengupta et al (1968) and by Sengupta and Weston (1969). These expressions are:

$$E_{\phi}^{12}(P) = \eta_o I_o \left(\frac{ka}{2}\right)^2 \left[f(\theta_1, \phi) \frac{B}{r_1} \frac{e^{ikr_1}}{r_1} - f(\theta_2, \phi) \frac{B}{r_2} \frac{e^{ikr_2}}{r_2} \right] , \tag{3.24}$$

where

$$r_1^2 = B^2 + (H-h)^2 \quad , \qquad r_2^2 = B^2 + (H+h)^2 \quad , \tag{3.25}$$

$$E_{\phi}^{56}(P) = -\eta_o I_o \left(\frac{ka}{2}\right)^2 \frac{\pi}{2iM} f(\theta_1, \phi) \cdot \frac{B}{r_1} \frac{e^{ikr_1}}{r_1}$$

$$\times \left[\left(\frac{1}{\pi kB}\right)^{1/2} e^{i(2kB+\frac{\pi}{4})} - \left(\frac{1}{\pi kH}\right)^{1/2} e^{i(2kH-\frac{\pi}{4})} \right]. \tag{3.26}$$

Using (3.21) and (3.24) - (3.26) it can be shown that

$$I_{P_o} = I_{P_o}^{12} + I_{P_o}^{56} , \tag{3.27}$$

where

$$I_{P_o}^{12} = I_o \left(\frac{ka}{2}\right)^2 \frac{2\pi B}{ikM} \left[f(\theta_1, \phi) \frac{e^{ikr_1}}{r_1} - f(\theta_2, \phi) \frac{e^{ikr_2}}{r_2} \right] , \tag{3.28}$$

$$I_{P_o}^{56} = I_o \left(\frac{ka}{2}\right)^2 \cdot \frac{\pi^2 (kB)}{M^2} \frac{e^{ikr_1}}{(kr_1)^2} f(\theta_1, \phi)$$

$$\times \left[\left(\frac{1}{\pi kB}\right)^{1/2} e^{i(2kB + \frac{\pi}{4})} - \left(\frac{1}{\pi kH}\right)^{1/2} e^{i(2kH - \frac{\pi}{4})} \right] . \tag{3.29}$$

We now make the following approximation valid for $kd << 1$,

$$f(\theta_1, \phi) = 2i \sin (kd \sin\theta_1 \cos \phi) \simeq f(\theta_1) \cos \phi , \tag{3.30}$$

$$f(\theta_2, \phi) \simeq f_1(\theta_2) \cos \phi , \tag{3.31}$$

where

$$f_1(\theta_1) = 2i\, kd \sin\theta_1 = 2i(kd) \frac{B}{r_1} , \tag{3.32}$$

$$f_1(\theta_2) = 2i\, kd \sin\theta_2 = 2i\,(kd) \frac{B}{r_2} . \tag{3.33}$$

After introducing (3.30) through (3.33) into (3.28) and (3.29) we obtain

$$I_{P_0}^{12} = I_o \left(\frac{ka}{2}\right)^2 \frac{2\pi B}{ikM} \left[f(\theta_1) \frac{e^{ikr_1}}{r_1^2} - f_1(\theta_2) \frac{e^{ikr_2}}{r_2^2} \right] \cos \phi \tag{3.34}$$

$$I_{P_o}^{56} = I_o \left(\frac{ka}{2}\right)^2 \frac{\pi^2 (kB)}{M^2} \frac{e^{ikr_1}}{(kr_1)^2} \cdot f_1(\theta_1)$$

$$\times \left[\left(\frac{1}{\pi kB}\right)^{1/2} e^{i(2kB + \frac{\pi}{4})} - \left(\frac{1}{\pi kH}\right)^{1/2} e^{i(2kH - \frac{\pi}{4})} \right] \cos \phi . \tag{3.35}$$

Thus we can write the parasitic current expression I_{P_o} in the following form.

$$I_{P_o} = I_{P_o}^{12} + I_{P_o}^{56} = I'_{P_o} \cos \phi , \tag{3.36}$$

where explicit expressions for I'_{P_o} may be obtained after introducing eqs. (3.34) and (3.35) into (3.36). It is important to note there that due to the nature of excitation, the parasitic current is not independent of ϕ. This completes the

derivation of the theoretical expressions for the current induced in the parasitic loop in a single parasitic loop counterpoise antenna with figure-of-eight type of excitation.

The Radiation Field: The complete side band mode radiation field produced by a single parasitic loop counterpoise antenna is obtained by vectorially adding the individual fields produced by a pair of Alford loops above the counterpoise and the parasitic loop above the counterpoise. The Alford loop counterpoise side band mode radiation field is given in Section 2.3. The parasitic field expression under this condition is derived below.

The free space radiation field produced by a circular loop carrying a current of the form given by eq. (3.36) is discussed in Appendix A. In general, the far electric fields are given by the following.

$$E_{\phi}^{i} \sim i\eta_o I'_{P_o} \left(\frac{kB}{2}\right) J'_1(kB \sin\theta)\cos\phi \frac{e^{ikR}}{R} , \tag{3.37}$$

$$E_{\theta}^{i} \sim i\eta_o I'_{P_o} \left(\frac{kB}{2}\right) \frac{J_1(kB\sin\theta)}{(kB\sin\theta)} \cos\theta \sin\phi \frac{e^{ikR}}{R} , \tag{3.38}$$

where

R, θ, ϕ are the usual spherical coordinates of the far field point with origin in the center of the parasitic loop which lies in the x-y plane, and J_1 is the first order Bessel function of the first kind and the prime indicates differentiation with respect to the argument.

For obtaining the principal plane field we are interested in the $\phi = 0^o$ plane and thus we have:

$$E_{\phi}^{i} \sim i\eta_o I'_{P_o} \left(\frac{kB}{2}\right) \frac{e^{ikR}}{R} J'_1(kB \sin\theta), \qquad E_{\theta}^{i} = 0 . \tag{3.39}$$

Let us obtain the ϕ - component of the far electric field. With the incident field given by (3.37) it can be shown that the far field produced by the parasitic loop only above the counterpoise is given by the following expression valid in the region $0 < \theta < \pi$,

$$E_{\phi}^{P} \sim \eta_o I'_{P_o} \left(\frac{kB}{2}\right) \frac{e^{i(kR-\frac{\pi}{4})}}{R} i F(\theta) \cos\phi , \tag{3.40}$$

where

$$F(\theta) = \frac{J'_1(kB\sin\theta)}{\sqrt{2}} F^P(\theta) e^{-ikA\sin\theta} + \frac{|\cos\theta| \sin\left(\frac{\phi_P}{2}\right)}{\sqrt{\pi k r_P \sin\theta}} e^{ikr_P} L^P(\theta) , \tag{3.41}$$

$$L^P(\theta)=\frac{e^{i(\frac{\pi}{2}-kA\sin\theta)}}{\sqrt{1-\sin\theta}}\left[\frac{\cos^{1/2}\phi_p J_1'(kB\cos\phi_P)-\sin^{1/2}\theta J_1'(kB\sin\theta)}{\cos\phi_P-\sin\theta}\right]-\frac{e^{-ikA\sin\theta}}{\sqrt{1+\sin\theta}}\times$$

$$\times\left[\frac{\cos^{1/2}\phi_P J_1'(kB\cos\phi_P}{\cos\phi_P+\sin\theta}\right] \quad , \tag{3.42}$$

$$F^P(\theta)=e^{ikr_P\sin(\theta-\phi_P)}\int_{-\infty}^{p_5} e^{i\frac{\pi t^2}{2}}dt-e^{ikr_P\sin(\theta+\phi_P)}\int_{-\infty}^{p_6} e^{i\frac{\pi t^2}{2}}dt \quad , \tag{3.43}$$

$$p_5=2\left(\frac{kr_P}{\pi}\right)^{1/2}\cos\left(\frac{\phi_P-\theta-\frac{\pi}{2}}{2}\right) \quad , \quad p_6=2\left(\frac{kr_P}{\pi}\right)^{1/2}\cos\left(\frac{\phi_P+\theta+\frac{\pi}{2}}{2}\right) \quad , \tag{3.44}$$

$$r_P^2=A^2+H^2 \quad , \quad \text{and} \quad \tan\phi_P=\frac{H}{A} \quad . \tag{3.45}$$

The complete far field is now obtained by combining eqs. (2.20) and (3.40). It can be written formally as

$$E_\phi \sim \eta_o I_o\left(\frac{ka}{2}\right)^2\frac{e^{i(kR-\frac{\pi}{4})}}{R}\,S(\theta) \quad , \tag{3.46}$$

where

$$S(\theta)=S^A(\theta)+S_{12}^P(\theta)+S_{56}^P(\theta) \quad . \tag{3.47}$$

Explicit expressions for $S^A(\theta)$ are given by eqs. (2.20) through (2.23). The last two terms on the right hand side of (3.47) are given by

$$S_{12}^P(\theta)=\frac{\pi(kB)^2}{M}\left[f(\theta_1)\frac{e^{ikr_1}}{(kr_1)^2}-f(\theta_2)\frac{e^{ikr_2}}{(kr_2)^2}\right]F(\theta)\cos\phi \tag{3.48}$$

$$S_{56}^P(\theta)=\frac{i\pi^2(kB)^2}{2M^2}\frac{e^{ikr_1}}{(kr_1)^2}f(\theta_1)$$

$$\times\left[\left(\frac{1}{\pi kB}\right)^{1/2}e^{i(2kB+\frac{\pi}{4})}-\left(\frac{1}{\pi kB}\right)^{1/2}e^{i(2kH-\frac{\pi}{4})}\right]F(\theta)\cos\phi \quad . \tag{3.49}$$

For the purpose of numerical computation, the principal plane pattern ($\phi = 0^o$ plane) is written in the following final form:

$$S^A(\theta) = \frac{F^o(\theta)\, 2i(kd)\sin^2\theta}{\sqrt{2}}\, e^{-ikA\sin\theta} + \frac{|\cos\theta|\sin(\frac{\phi_o}{2})}{\sqrt{\pi k r_o \sin\theta}}\, e^{ikr_o}\, L^o(\theta) \quad , \tag{3.50}$$

$$L^o(\theta) = \frac{e^{i(\frac{\pi}{2} - kA\sin\theta)}}{\sqrt{1-\sin\theta}} \left[\frac{2i(kd)\cos^{5/2}\phi_o - 2ikd\sin^{5/2}\theta}{\cos\phi_o - \sin\theta} \right.$$

$$\left. - \frac{e^{ikA\sin\theta}}{\sqrt{1+\sin\theta}} \frac{2i(kd)\cos^{5/2}\phi_o}{\cos\phi_o + \sin\theta} \right] \quad , \tag{3.51}$$

$$S^P_{12}(\theta) = \frac{\pi(kB)^2}{M} \left[2ikd\frac{B}{r_1} \frac{e^{ikr_1}}{(kr_1)^2} - 2ikd\frac{B}{r_2}\frac{e^{ikr_2}}{(kr_2)^2} \right] F(\theta) \quad , \tag{3.52}$$

$$S^P_{56}(\theta) = \frac{i\pi^2(kB)^2}{2M^2} \frac{e^{ikr_1}}{(kr_1)^2} \frac{(kB)}{(kr_1)} 2ikd \left[(\frac{1}{\pi kB})^{1/2} e^{i(2kB+\frac{\pi}{4})} - (\frac{1}{\pi kH})^{1/2} e^{i(2kH-\frac{\pi}{4})} \right] F(\theta), \tag{3.53}$$

and the other parameters are as defined before. This completes the derivation of the elevation plane pattern (x-z plane) of the single parasitic loop counterpoise antenna for the side-band mode of operation. In this plane (ϕ=0^o) the only component of the field is the E_ϕ component. However in other elevation planes, i.e. for $\phi \neq 0$ there will exist a θ-component of the field as evidenced by eq. (3.38) (see also Appendix A). During the present contract we have not investigated the θ-component of the field produced by the antenna.

3.4.2 Comparison Between Theory and Experiment

A single parasitic loop counterpoise has been fabricated by placing a parasitic loop of diameter 2B = 31.75" at a height H = 22.5" above the double Alford loop counterpoise antenna whose patterns are shown in Figs. 2-8 and 2-9. The measured electric far field pattern produced by this antenna in the $\phi = 0^o$ plane is shown in Fig. 3-6. The computed theoretical points are also shown in one half of the pattern in Fig. 3-6 for comparison. It can be seen that the agreement between the theory and experiment is quite satisfactory.

It should be noted that except for the excitation the parameters of the antennas whose patterns are shown in Figs. 3-3 and 3-6 are kept the same so that the patterns can be compared. From a comparison of Figs. 3-3 and 3-6 the

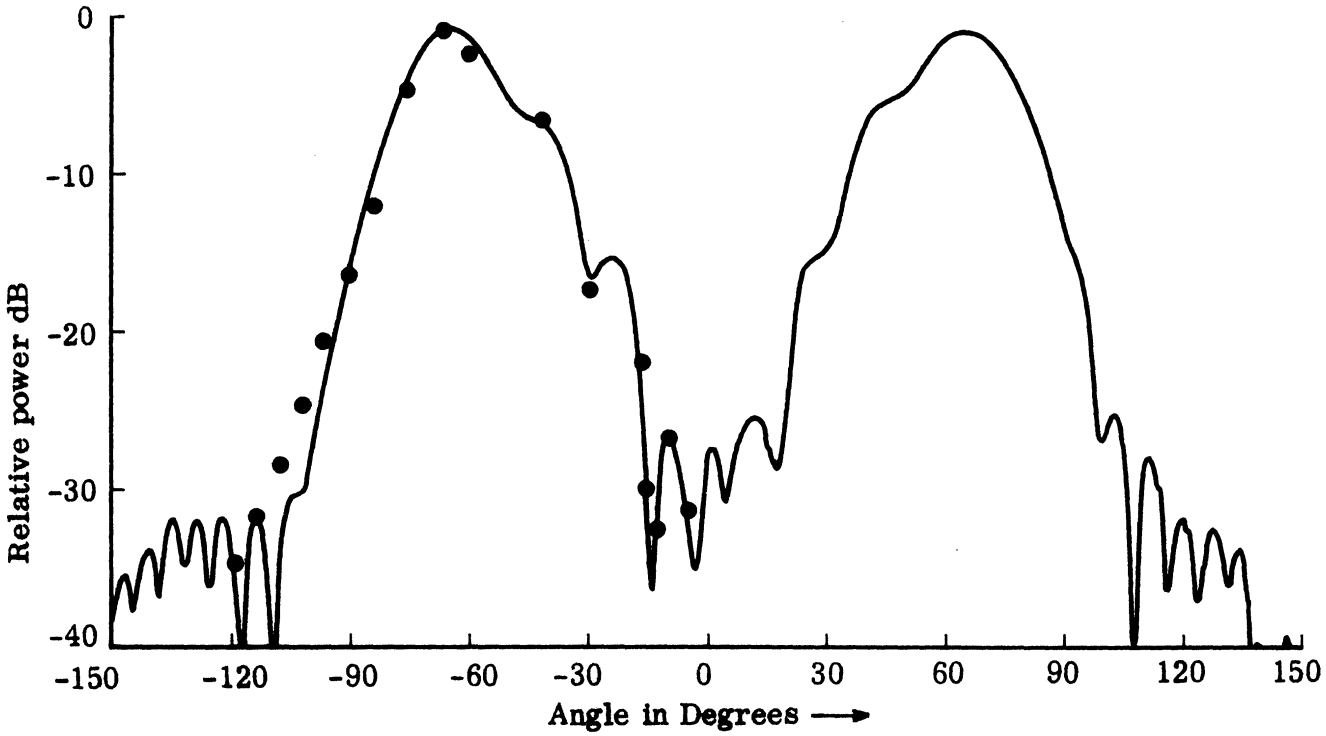

FIG. 3-6: Side band mode elevation plane far field pattern of a single parasitic loop counterpoise antenna, kh = 2.75, kA = 51.69, kd = 0.92, kB = 3π, kH = 13, f = 1080 MHz.

——— Experimental, ... Theoretical

following two observations are made; (i) non-uniform excitation of the parasitic loop gives rise to minor lobes in the pattern near the axial region $\theta = 0^{o}$. However, it is anticipated that with proper choice of height H of the parasitic loop it would be possible to reduce this lobe considerably by utilizing the concept of image. (ii) The result shown in Fig. 3-6 does show some improvement in the field gradient (7.5 dB/6^{o}) compared to that of the corresponding conventional VOR antenna pattern (5.54 dB/6^{o}) but it is less than that obtained in the case of single parasitic loop counterpoise antennas operating in the carrier mode. However, the field gradient in the side band mode case may be improved up to at least the carrier mode value by adjusting the parameters H and B.

3.5 Discussion

The free space radiation patterns of single parasitic loop counterpoise antennas operating both in the carrier and the side band modes have been discussed and theoretical and experimental results are shown. Theoretical expressions for the side band mode given here are new and have been developed during the present Contract. We have also discussed the nature and value of the parasitic current when the antenna operates in the carrier mode. The current information given here may be found useful in developing some future experimental programs. From the pattern information given in this chapter it appears that from the viewpoint of optimum field gradients, the necessary parameters H and B of the antenna will be different for different modes of operation. Thus in an actual case a compromise must be made. On the basis of the results reported above it is found that for a full scale 150' diameter counterpoise the introduction of a parasitic loop in the conventional VOR antenna increases the field gradient by about 4dB/6^{o}. In order to improve the field gradient further, it is necessary to use more than one parasitic loop. Double parasitic loop counterpoise antennas are discussed from this viewpoint in the next chapter.

IV

INVESTIGATION OF A DOUBLE PARASITIC LOOP COUNTERPOISE ANTENNA

4.1 Introduction

The results discussed in Chapter III indicate that a single parasitic loop counterpoise antenna produces a field gradient at the horizon larger than that of a conventional VOR Alford loop counterpoise antenna. However, from the viewpoint of improved VOR system performance it is desirable that the antenna should produce much larger field gradients. Field gradient values larger than those of single parasitic loop counterpoise antennas can be obtained from double parasitic loop antennas. The latter type of antenna is obtained by inserting coaxially another parasitic loop at an appropriate height (Fig. 4-1).

In the present chapter we at first develop an approximate theory for the radiation patterns of double parasitic loop counterpoise antennas operating in both carrier and side band modes. The theory is then compared with measured results. Finally, the parameters for a specific double parasitic loop counterpoise antenna are obtained such that the field gradient produced by the antenna is maximum. Such an antenna will be referred to as the optimum antenna.

4.2 Theoretical Expressions for the Radiation Field

The theoretical model of a double parasitic loop counterpoise antenna is shown schematically in Fig. 4-1. It consists of a conventional VOR antenna with two large parasitic loops placed parallel to each other and to the plane of the counterpoise as shown in Fig. 4-1 with the origin of coordinate system located at the center of the counterpoise which lies in the x-y plane. The point source in Fig. 4-1 represents the excited elements. During the analysis the free space far field variation of this equivalent point source is assumed to correspond to that of the carrier or side band mode operation of the antenna.

If the distance between the two parasitic loops is small compared to a wavelength, then the mutual coupling effects between them may be strong and must be taken into account. Under these circumstances the theoretical analysis of the radiation field becomes complicated. However, from our previous study (Sengupta et al, 1968) it has been found that for the cases of interest the two parasitic loops should be separated by a distance of at least the order of one wavelength or more. The theory of double parasitic loop counterpoise antenna given in this section therefore neglects the effects of mutual interaction between the parasitic loops. The mutual coupling effects and their influence in the far field patterns are discussed in Appendix B.

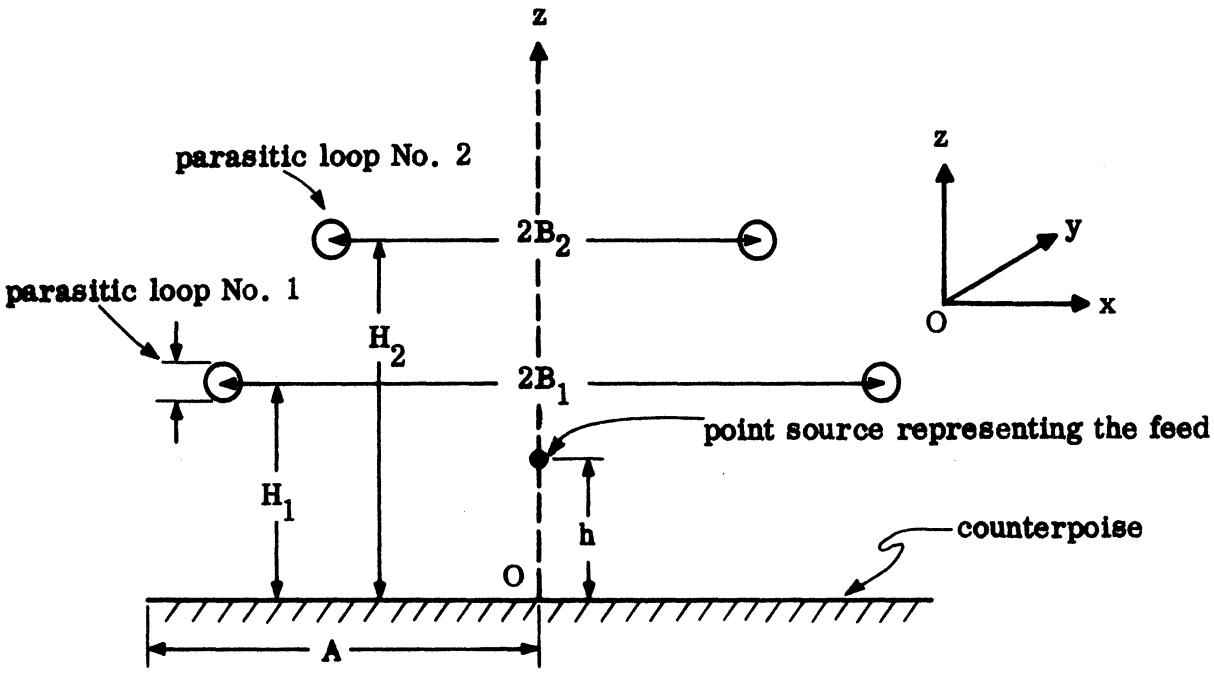

FIG. 4-1: Theoretical model for the double parasitic loop counterpoise antenna.

In the absence of mutual coupling, the theoretical expressions for the radiation field produced by a double parasitic loop counterpoise system can be obtained by simple modification of the theory given in Chapter III.

The far electric field produced at a point $P(R, \theta, \phi)$ by an antenna consisting of the excited Alford loops, parasitic loop No. 1 and the counterpoise can be written as:

$$E_{\phi_1} = \eta_o I_o \left(\frac{ka}{2}\right)^2 \frac{e^{i(kR - \frac{\pi}{4})}}{R} S_1(\theta) , \tag{4.1}$$

where

$$S_1(\theta) = S^A(\theta) + S^P_{12}(\theta) + S^P_{56}(\theta) , \tag{4.2}$$

and all the other notations are as explained in Chapter III. Explicit expressions for the different terms in eq. (4.2) are as shown in the previous chapter and should pertain to those with parasitic loop No. 1.

Similarly, the far electric field produced by the parasitic loop No. 2 only above the counterpoise can be written as

$$E_{\phi_2} = \eta_o I_o \left(\frac{ka}{2}\right)^2 \frac{e^{i(kR-\frac{\pi}{4})}}{} S_2^P(\theta) , \tag{4.3}$$

where

$$S_2^P(\theta) = S_{12}^{P'}(\theta) + S_{56}^{P'}(\theta) . \tag{4.4}$$

Explicit expressions for the different terms in eq. (4.4) may be obtained from Chapter III with the understanding that the different parameters involved pertain to the parasitic loop No. 2. The complete expression for the far field produced by the double parasitic loop counterpoise antenna is obtained by superposition of the above two fields and is given by:

$$E_{\phi} = \eta_o I_o \left(\frac{ka}{2}\right)^2 \frac{e^{i(kR-\frac{\pi}{4})}}{R} \left[S_1(\theta)+S_2^P(\theta)\right] , \tag{4.5}$$

for $0 < \theta < \pi$.

The approximations involved in (4.5) are the same as discussed previously. Thus, $S_1(\theta) + S_2^P(\theta)$ gives the complex far field pattern of the double parasitic loop counterpoise antenna. The patterns of the antenna for the carrier and side band mode operations are obtained by using the appropriate expressions for $S_1(\theta)$ and $S_2^P(\theta)$.

4.3 Description of the Experimental Arrangement

For experimental investigations, the parasitic loops were positioned coaxially on the axis of the basic model of the conventional VOR antenna described in Section 2.3.2. Figure 4-2 shows the side view of the 15' diameter counterpoise along with the installed pair of parasitic loops mounted on a 40' tower. A close-up view of the double parasitic loop counterpoise antenna is shown in Fig. 4-2a. Foam cylinders were used to hold the parasitic loops in place in such a way that the diameters and heights of the parasitic loops above the counterpoise could be easily adjusted during the experiment. The parasitic loops were made of conducting strips rather than conducting wires as assumed in the theory. This has been done for mechanical simplicity. In comparing the experimental results with theory it is assumed that a conducting strip of width w is electrically equivalent to a conducting cylinder of radius b, which is a reasonable assumption provided $w = 4b$ and $w, b \ll \lambda$. The parasitic elements were fabricated from 1" wide brass strips $9.15 \times 10^{-3}\lambda$ thick at 1080 MHz. It should be noted that the height H of the parasitic loop is measured from the top surface of the counterpoise to the center w/2 of the element. All the patterns were measured on the outside range with the antenna under test mounted on the 40' tower (Fig. 4-2) and used as a receiving antenna.

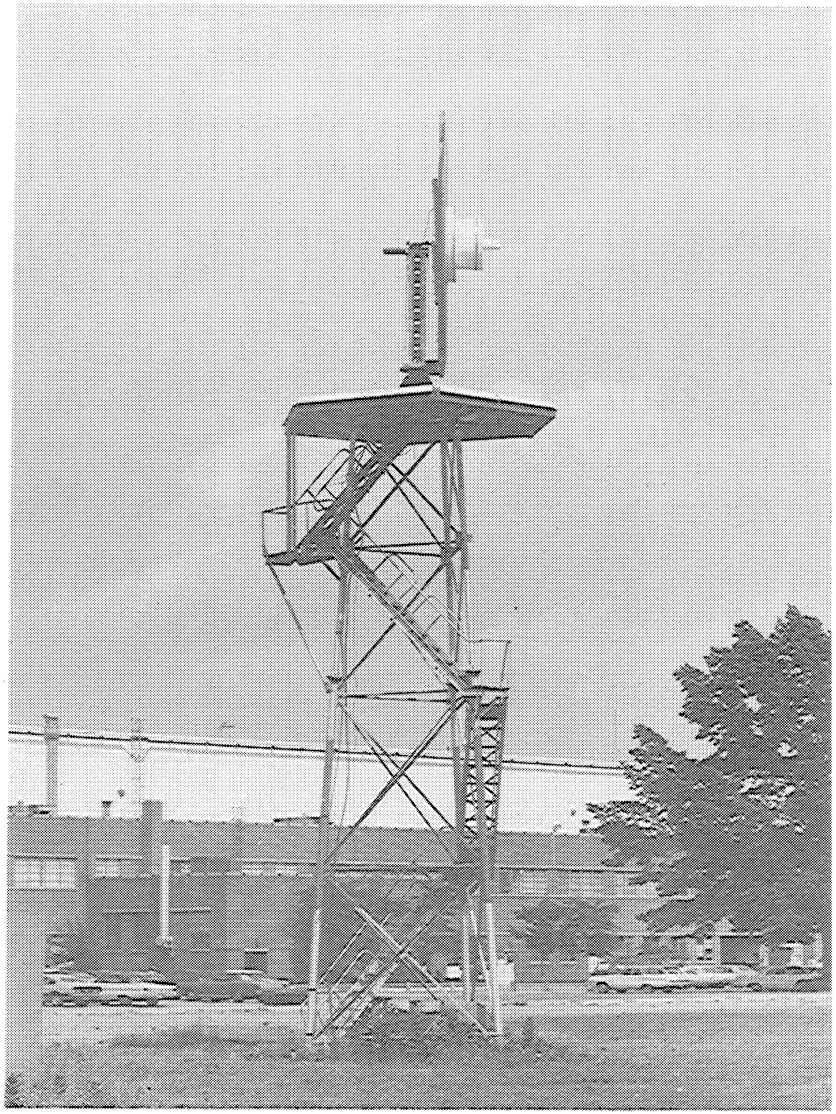

FIG. 4-2: Side view of the double parasitic loop counterpoise antenna.

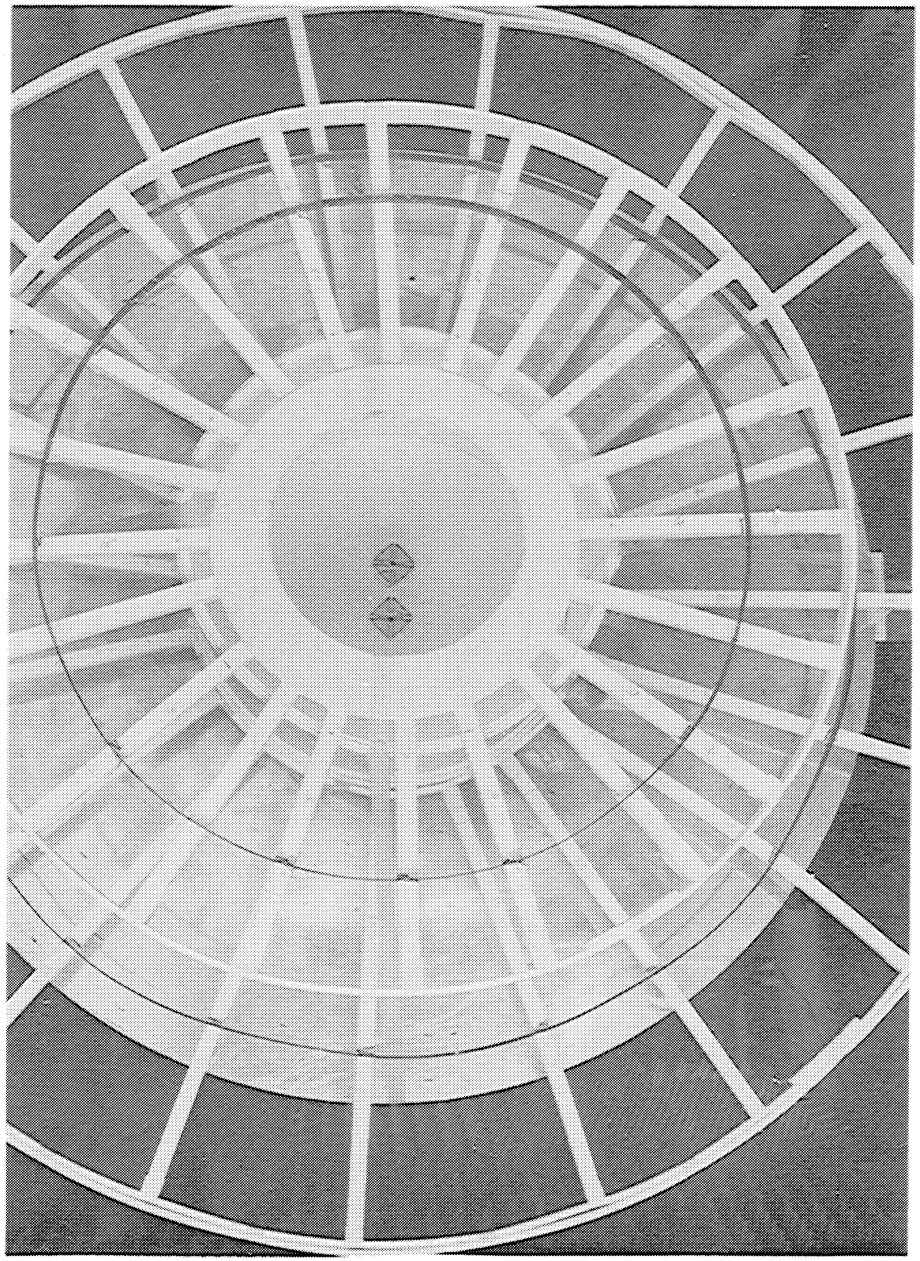

FIG. 4-2a: A close-up view of the double parasitic loop counterpoise antenna model.

4.4 Comparison Between Theory and Experiment

The theoretical electric far field pattern for the elevation plane of a double parasitic loop counterpoise antenna operating in the carrier mode is given in Fig. 4-3. The corresponding measured far field pattern is also shown in Fig. 4-3. A similar set of patterns is given in Fig. 4-4 for such an antenna operating in the side band mode. Notice that the counterpoise size as well as the measurement frequency are different for the results shown in Fig. 4-3. This has been done so that the results may correspond to a full scale 150' diameter counterpoise at the changed full scale frequency of 109 MHz.

Considering the fact that the theory ignores the effects of mutual coupling, the general agreement between theory and experiment as found in Figs. 4-2 and 4-3 may be considered to be fair. Thus for the ranges of parameters used here (particularly $H_2-H_1 > \lambda$), the theory given here can be used with sufficient accuracy to investigate the double parasitic loop counterpoise antenna radiation patterns. It is anticipated, however, that the theory may be improved further by more rigorous analysis (Appendix B).

4.5 Optimum Double Parasitic Loop Counterpoise Antenna

The results given in section 4.4 reveal the fact that double parasitic loop counterpoise antennas produce field gradient values larger than those obtained from single parasitic loop counterpoise or conventional VOR Alford loop counterpoise antennas . Of course, the field gradient produced by the antenna is a function of the antenna parameters. In this section we vary the parameters H_1, B_1, H_2, B_2 while keeping the other parameters fixed and theoretically study their effects on the field gradient. In this manner an optimum set of these parameters is obtained so that the antenna produces maximum field gradient. It is realized that other criteria may also be used for optimizing the antenna (for example, maximum field gradient and minimum side lobe below the horizon). As mentioned in the previous Chapter the field gradient produced by the antenna is different for different modes of operation. Here we optimize the antenna parameters so that the field gradient is maximum in the side band mode of operation of the antenna, since this is the mode which is of most interest from the viewpoint of VOR operation. The optimization is done for an antenna having the normalized parameter, $kA = 52.16860$ for the counterpoise so that it may correspond to the 150' diameter counterpoise at the full scale frequency of 109 MHz.

Figure 4-5 summarizes the results of the optimization procedure. Preliminary studies indicate that large field gradient values may be obtained for the following approximate normalized parameters, $kH_1 = 3.48190$, $kH_2 = 12.76710$, $kB_1 = 3\pi$ and $kB_2 = 5\pi$. The optimization procedure is then initiated by keeping kH_1 and kH_2 fixed at these values and computing the field gradient α_g as functions of kB_1 and kB_2. Curve A in Fig. 4-5 shows α_g as a function of kB_1 for the fixed value of $kB_2 = 3.0\pi$.

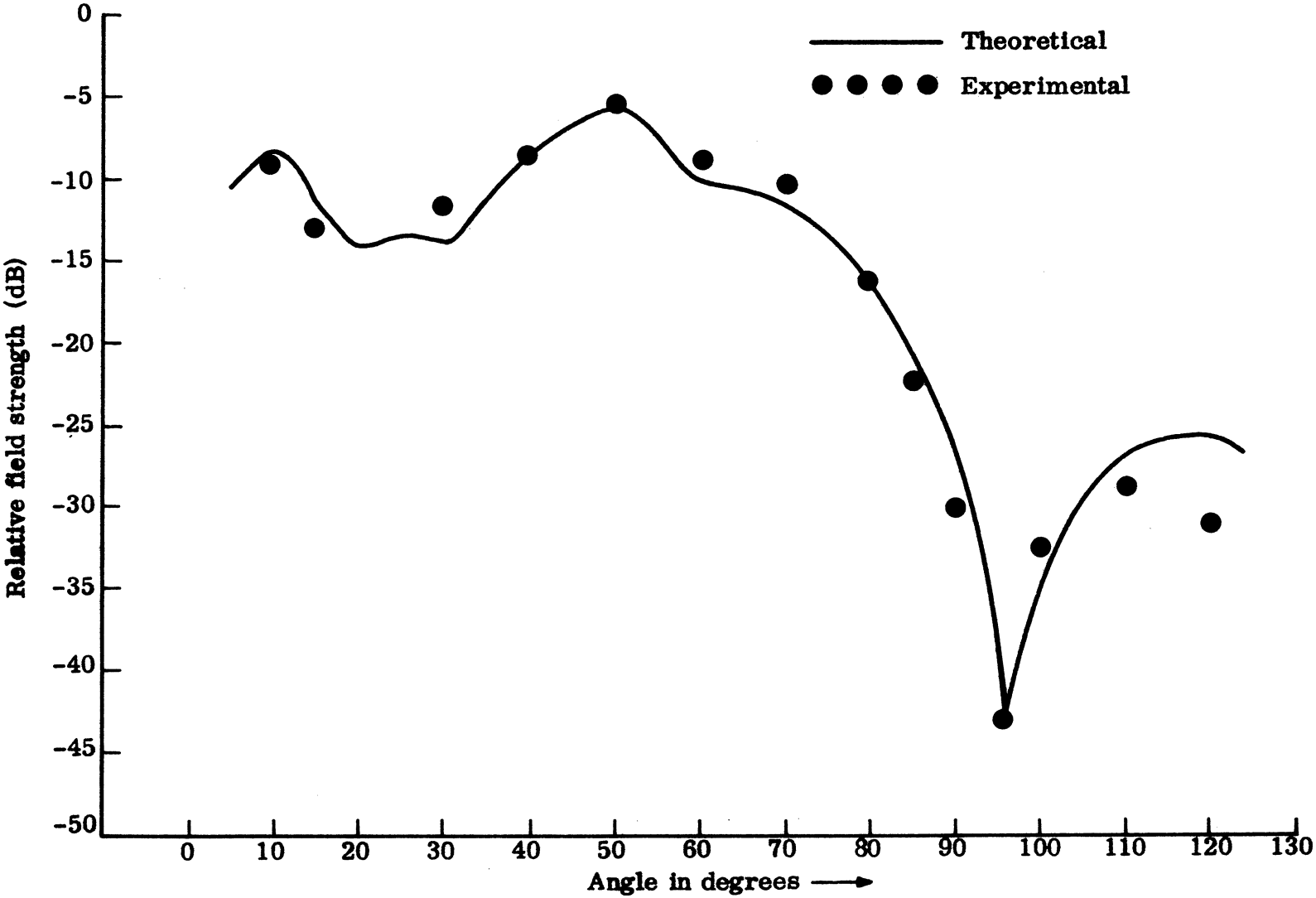

FIG. 4-3: Carrier mode elevation plane far field pattern of a double parasitic loop counterpoise antenna. kh = 2.75, kb = 0.15, kA = 17.92, kH_1 = 3.70, $kB_1 = 4\pi$, kH_2 = 11.78, $kB_2 = 3\pi$, f = 1080 MHz.

It can be seen that α_g appears to be a periodic function of kB_2, i.e. for the range of values shown α_g reaches a maximum for $kB_1 = 5.2\pi$ and $kB_1 = 6.2\pi$. The maximum value of α_g in this case is 4.75 dB/6° which is rather low. The second optimization is now carried out by calculating α_g as a function of kB_2 for $kB_1 = 5.2\pi$. The smaller value of kB_1 is chosen for the reason that it will give rise to a smaller physical size of the antenna. Curve B in Fig. 4-5 shows the results of this computation. A maximum value of $\alpha_g = 23.7$ dB/6° is obtained for $kB_2 = 3.6\pi$. Curve C shows α_g as a function of kB_1 for $kB_2 = 3.6\pi$. It is found from Curve C that the maximum value of $\alpha_g = 23.7$ dB/6° is obtained for $kB_1 = 5.2\pi$. Finally, α_g has been calculated as functions of kH_1 and kH_2, for $kB_1 = 5.2\pi$ and $kB_2 = 3.6\pi$ and it has been found that α_g does reach the maximum value for the values of kH_1 and kH_2 cited above.

On the basis of the results given here we obtain the following normalized parameters for an optimum double parasitic loop counterpoise antenna:

$kh = 2.7755$, $kd = 0.9276$, $kb = 0.1514$, $kA = 52.1686$

$kH_1 = 3.4819$, $kB_1 = 16.3363$,

$kH_2 = 12.7671$, $kB_2 = 11.3097$.

Before closing this section it is appropriate to mention that the physical mechanism by which a large field gradient is obtained in the optimum configuration is the method of cancellation of the Alford loop field in a certain preferred direction by the parasitic fields. It is therefore obvious that the performance of any such optimum antenna will be highly frequency sensitive. Frequency sensitivity of such antennas has been discussed earlier (Sengupta et al, 1968).

4.6 Optimum Antenna Patterns

In this section we discuss the carrier and side band mode elevation plane patterns of a double parasitic loop counterpoise antenna optimized for the side band mode of operation. The elevation plane patterns for the carrier and side band mode of operation have been calculated theoretically for the optimum antenna described in the previous section. The unnormalized results are shown in Fig. 4-6 so that the two patterns can be compared directly. The antenna has $\alpha_g = 23.71$ dB/6° in the side band mode but the carrier mode value of α_g is 5.67 dB/6°. In a practical situation if one wishes to have larger field gradient values in the carrier mode, a compromise must be made.

Figure 4-7 shows the experimentally measured elevation plane pattern of the optimum antenna operating in the side band mode.

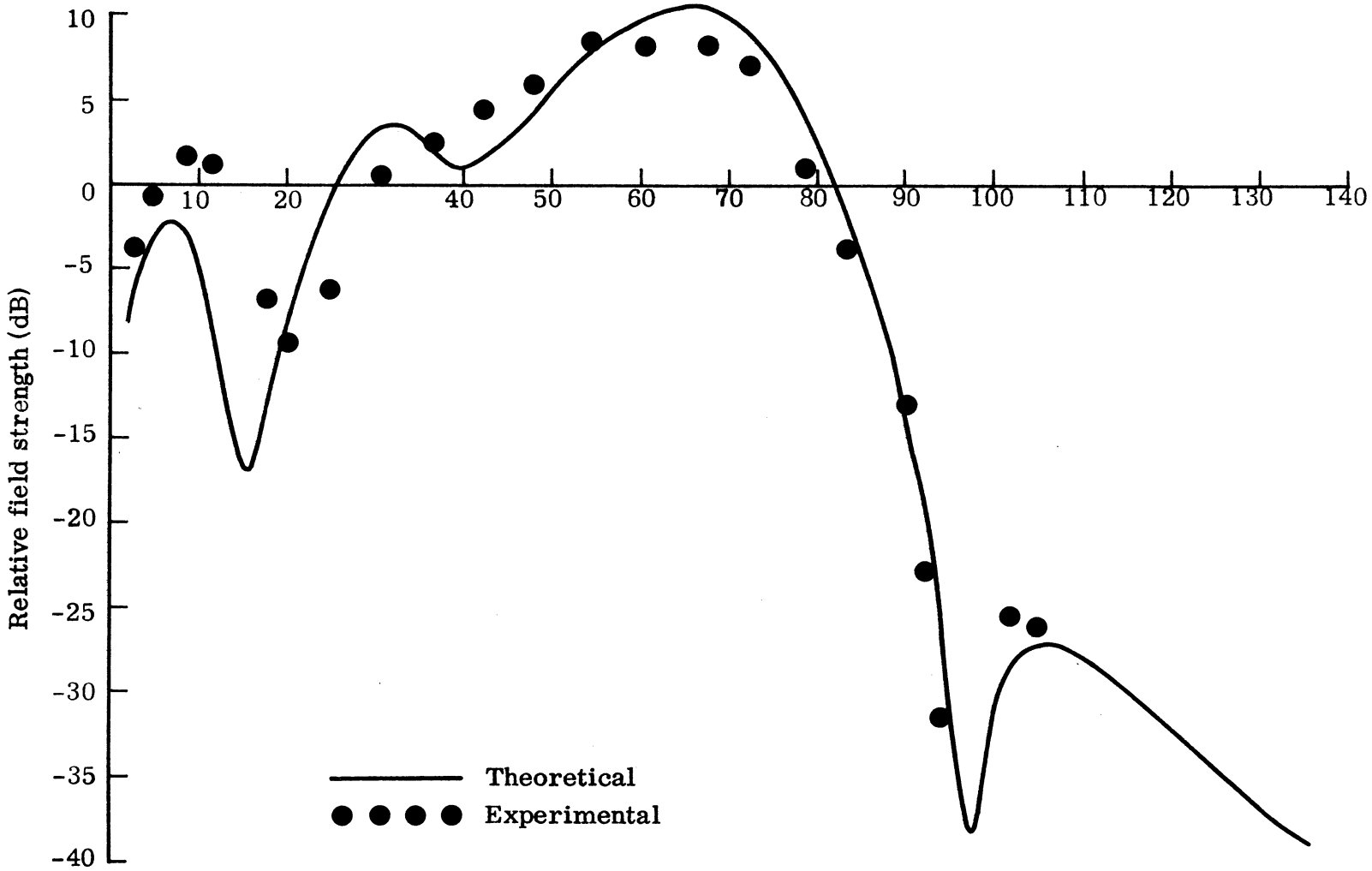

FIG. 4-4: Side band mode elevation plane far field pattern of a double parasitic loop counterpoise antenna. kh = 2.7755, kb = 0.1514, kd = 0.9276, kA = 52.1686, kH_1 = 3.4819, kB_1 = 16.1704, kH_2 = 12.7671, kB_2 = 11.4144, f = 1090 MHz.

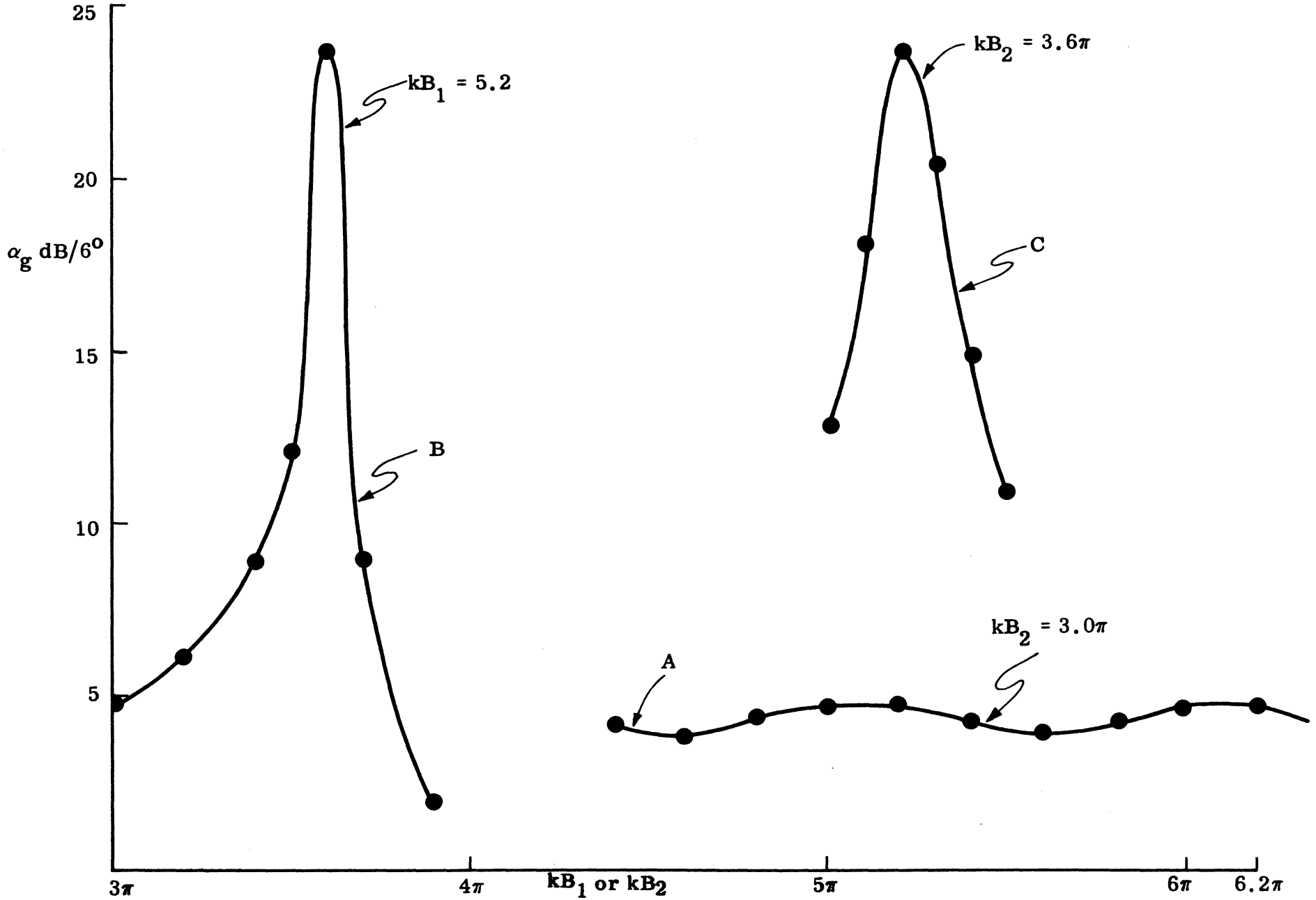

FIG. 4-5: **Theoretical maximization** of the horizon field gradient of a double parasitic loop **counterpoise antenna operating in the side band mode.** **kh = 2.7755, kb = 0.1514, kd = 0.9276, kA = 52.1686, kH_1 = 3.4819, kH_2 = 12.7671, kB_1 and kB_2 are variable.** f = 1090 MHz.

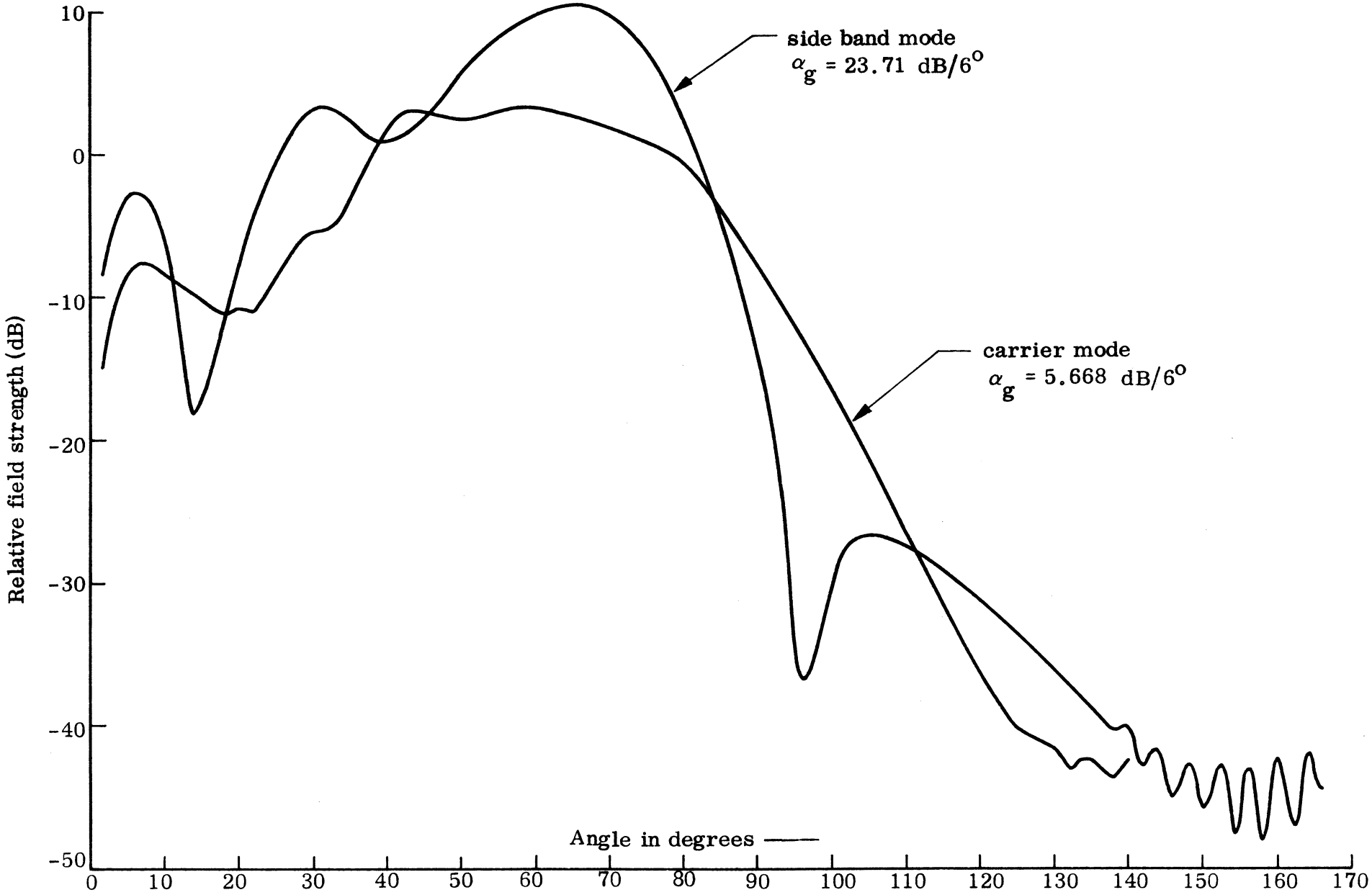

FIG. 4-6: Theoretical carrier and side band mode elevation plane pattern of the optimized double parasitic loop counterpoise antenna. kh = 2.7755, kb = 0.1514, kd = 0.9276, kA = 52.1686, kH_1 = 3.4819, $kB_1 = 3.6\pi$, kH_2 = 12.7671, $kB_2 = 5.2\pi$, f = 1090 MHz.

FIG. 4-71. Measured side lobe gain elevation plane far field pattern of the optimum circle parasitic loop omnidirectional antenna

4.7 Full Scale Parameters of the Optimum Antenna

In this section we give the full scale values of the different parameters of the optimum double parasitic loop counterpoise antenna. Also given are some of the important pattern characteristics of the antenna. This section should serve as a handy reference for the full scale antenna and its expected performance. The antenna is assumed to operate at the frequency f = 109 MHz. The mechanical dimensions of the antenna are:

$h=4'$, $d=1'4''$, $w=10''$, $A=75'$, $2B_1=46.8'$,
$H_1=5'$, $2B_2=32.5'$, $H_2=18'4''$, operating wavelength
$\lambda_{opt} = 9.02'$.

The expected elevation plane pattern characteristics are as follows:

Carrier Mode

Direction of principal maximum $\theta_{max} = 60^o$,
Far field gradient at the horizon $\alpha_g = 5.66$ dB/6^o,
Field reduction factor $\alpha_F = 10.3$ dB.

Side Band Mode

Direction of principal maximum $\theta_{max} = 66^o$,
Far field gradient at the horizon $\alpha_g = 23.71$ dB/6^o,
Field reduction factor $\alpha_F = 23.18$ dB,
Amplitude of the minor lobe below $\theta = 90^o$:
13.63 dB down relative to the field in direction $\theta=90^o$,
Position of the minor lobe below $\theta=90^o$ is 106^o.

For the carrier mode the level of the field immediately below $\theta = 90^o$ is much larger than that in the side band mode (Fig. 4-6). The meaning of all the notations used here are as explained before. The complete numerical values for the theoretical patterns discussed above are given in Appendix F (Tables F-II and F-III).

4.8 Discussion

In the present chapter we have developed approximate theory for the elevation plane radiation patterns produced by double parasitic loop counterpoise antennas operating in both carrier and side band modes. Although the theory neglects the effects of mutual interaction between the parasitic loops, the general agreement between theory and experiment has been found to be satisfactory.

On the basis of the above theory the design parameters have been obtained for an optimum configuration for such an antenna using a 150' diameter counterpoise and operating in the side band mode at the frequency f = 109 MHz. The characteristics of the optimum antenna patterns have also been discussed from both the theoretical and experimental point of view.

During the contract period we have also obtained experimentally the design parameters of an optimum antenna using 52' diameter counterpoise and operating at the frequency 108 MHz. This was done before the theory for such antennas was developed. However, because of the contract priority, the emphasis of both theoretical and experimental investigations have been shifted to the 150' diameter counterpoise case operating at 109 MHz. Since the standard VOR antenna systems use 52' diameter counterpoises, the results of our investigation of such antennas are given in Appendix C. Theroetical optimization of this antenna can be carried out following a similar procedure discussed in this chapter.

V

FABRICATION OF THE FULL SCALE DOUBLE PARASITIC LOOP COUNTERPOISE ANTENNA

5.1 Introduction

On the basis of model measurements, we obtained in Chapter IV the physical dimensions for a double parasitic loop counterpoise antenna designed for optimum side band mode performance at the full scale frequency 109 MHz. The full scale double parasitic loop counterpoise antenna has been obtained by installing two appropriate parasitic loops on the standard VOR Alford loop counterpoise antenna located at the end of Manheim Road outside of the NAFEC (National Aviation Facility Experimental Center). In the present chapter we describe the mechanical fabrication of the parasitic loop assembly and also the method of incorporating it into the standard VOR antenna located at NAFEC.

5.2 Standard VOR Antenna at NAFEC

The experimental standard VOR antenna system at NAFEC uses a counterpoise 150' in diameter and is mounted on a 75' tall tower so that the counterpoise level is 75' above ground level. Figure 5-1 shows a photograph of the tower which supports the counterpoise along with the conical dielectric housing which contains the standard four-Alford loop assembly. The necessary electronics to operate the station as a VOR system is housed in a building on ground. The details of the electronics involved are not discussed here. Interested readers may find the description of the VOR equipment in Hurley, et al (1951).

5.3 Full Scale Parasitic Loop Assembly

As described in section 4.7, the two parasitic loops for the optimum double parasitic loop counterpoise antenna have the following full scale dimension: $2B_1$ = 46'10", H_1 = 5', $2B_2$ = 32'6", H_2 = 18'4". The loops are to be made of 10" wide conducting strips. The other dimensions of the complete antenna are as given in section 4.7.

The parasitic loops were fabricated from expanded aluminum. This material was chosen so as to reduce the surface area exposed to wind forces. The expanded aluminum came in 8' long sections, 10" wide and 0.085" thick. Aluminum tubings , 3/4" in diameter have 0.049" thick walls, were used to hold the expanded aluminum in place. The structure was then cut to the appropriate length and bent to the proper radius of curvature for the appropriate loop. The expanded aluminum was attached to the tubing with rivets. At the junction points additional pieces of expanded aluminum were attached with screws over the junctions in order to ensure good electrical contact between the junctions (see Fig. 5-2).

The loops were held at the appropriate heights with redwood poles. Figure 5-3 is a photograph showing a section of the two parasitic loops installed on the counterpoise. Sixteen redwood poles were used to support each parasitic loop. This number of poles was selected on the basis of the support structure associated with the 150' diameter counterpoise located at NAFEC. To ensure a rigid structure upon which to mount the parasitic loops, each of the wooden poles was mounted over one of the principal spokes of the counterpoise (Fig. 5-2). The set of poles supporting the lower parasitic loop were 6' tall and the set supporting the upper loop were 20' tall. Each of the 6' poles were held in place by three 3/16" Mylar guy ropes; six such guy ropes were used to support each of the 20' poles. The counterpoise ends of the guy ropes were attached to chains such that they would provide some fine adjustment in the tension associated with the ropes (Fig. 5-4). Provisions were made also so that the heights of the parasitic loops could be adjusted slightly if necessary.

Mylar was chosen as the rope material because of its stability and also because of the hostile environment in which the entire antenna assembly is located. The redwood poles were treated with wood preservative and moisture resistant solution so that a minimum amount of moisture would be absorbed by the poles. The bases of the redwood poles were placed on metal supports welded to the 16 spokes that run radially out from the center of the counterpoise (Fig. 5-2). These metal bases were located at the appropriate distances from the geometric center of the four Alford loops mounted above the counterpoise. A plumb line was used to ensure proper orientation of the poles with respect to the counterpoise and its geometric center.

Figure 5-5 shows a photograph of the two parasitic loops mounted on the 150' diameter counterpoise. The central conical structure is a dielectric housing which contains the standard four Alford loop assembly used in a VOR system.

5.4 Discussion

In this chapter we have described the mechanical fabrication and assembly of the full scale double parasitic loop counterpoise VOR antenna. It should be noted that provisions were made so that the heights of the parasitic loops could be adjusted if found necessary during the time of testing.

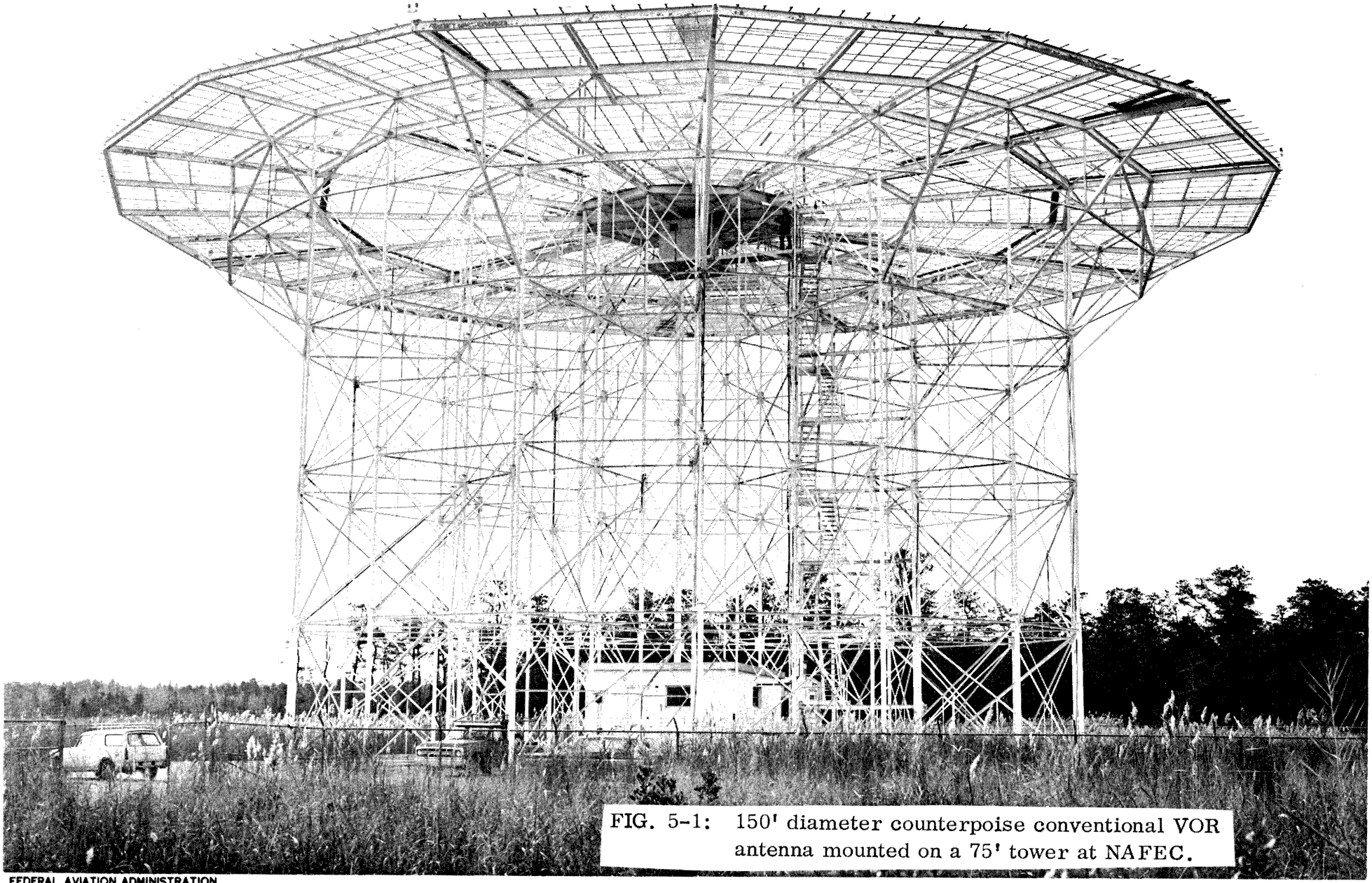

FIG. 5-1: 150' diameter counterpoise conventional VOR antenna mounted on a 75' tower at NAFEC.

FEDERAL AVIATION ADMINISTRATION
ATLANTIC CITY, NEW JERSEY

10-2440

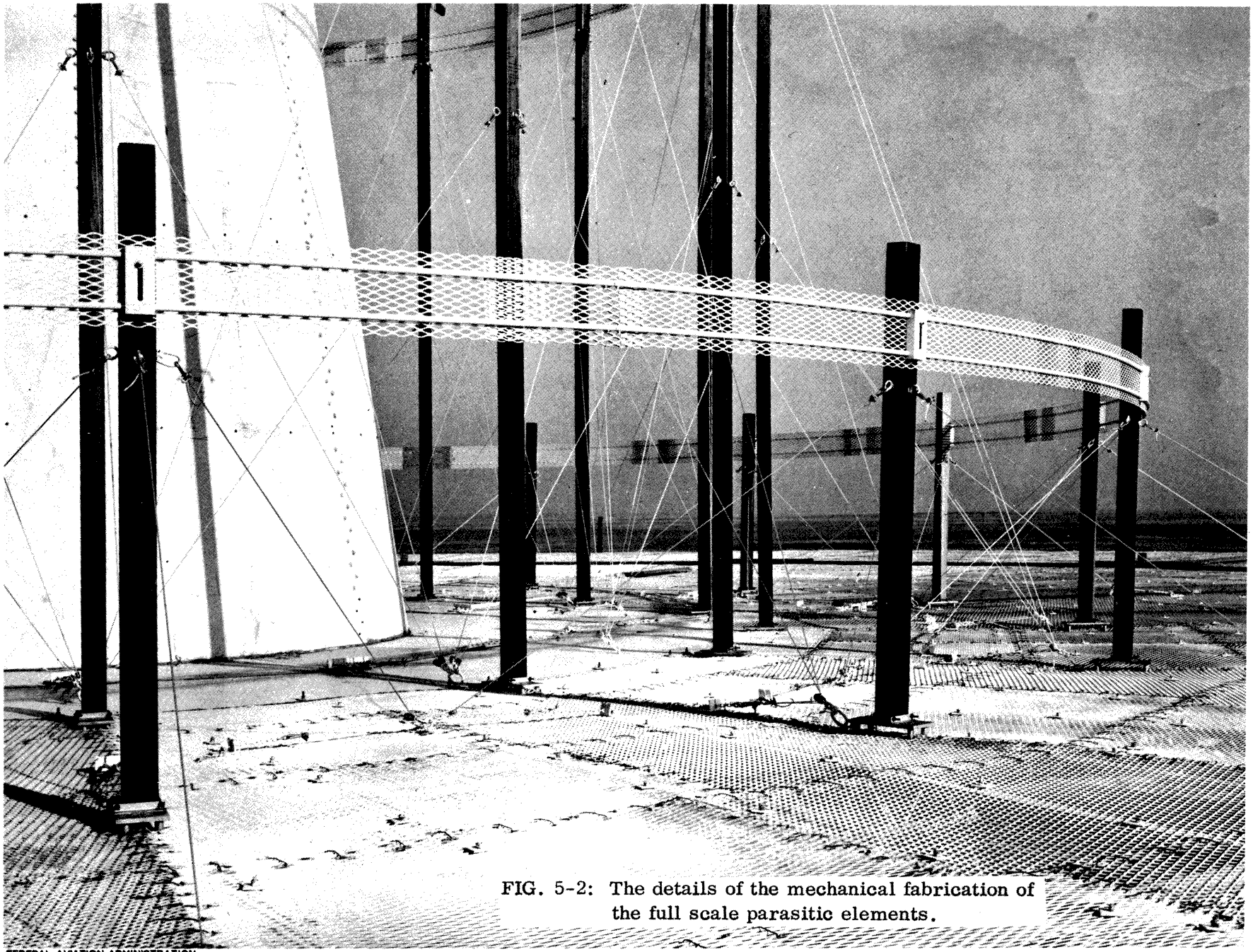

FIG. 5-2: The details of the mechanical fabrication of the full scale parasitic elements.

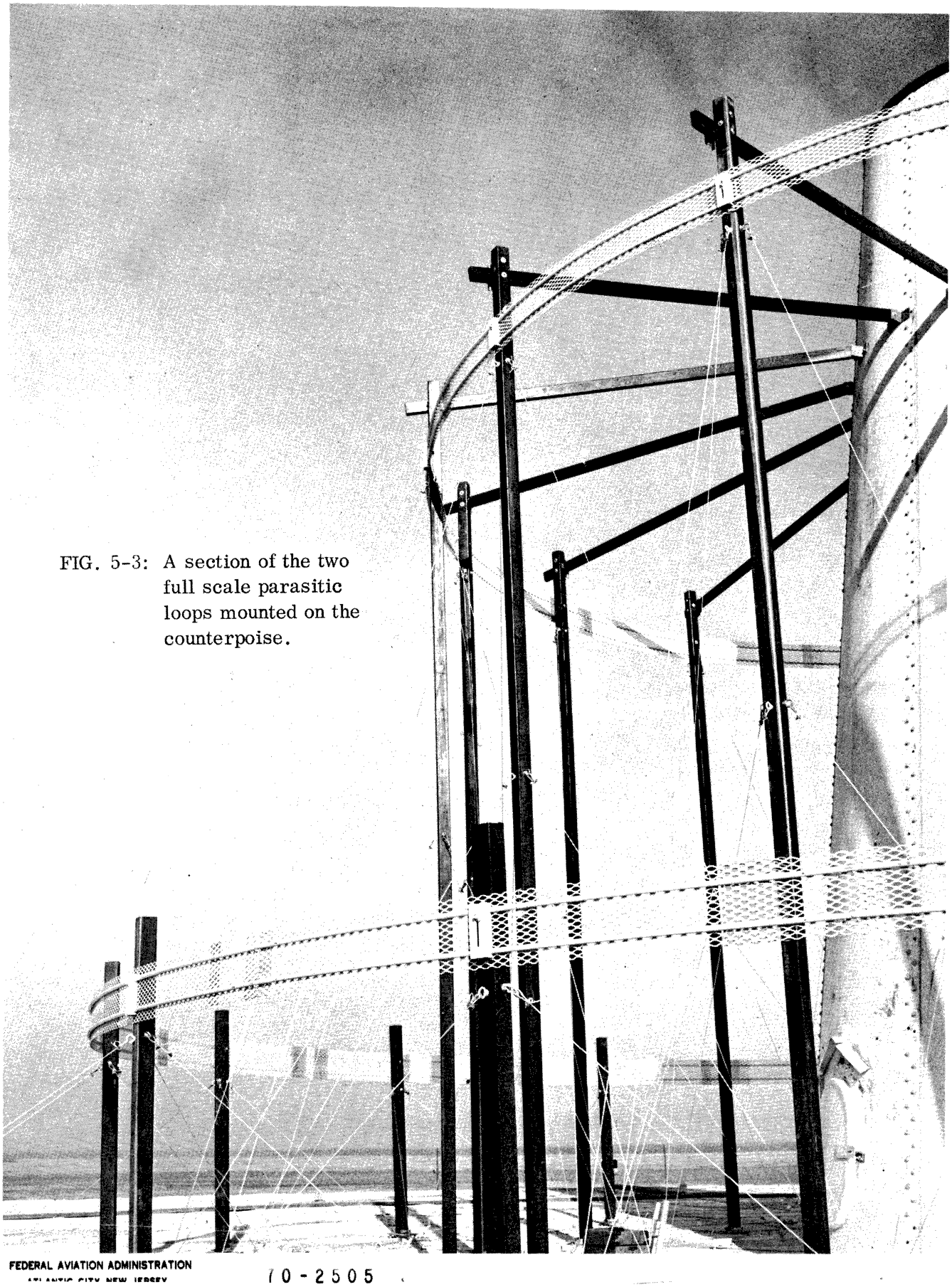

FIG. 5-3: A section of the two full scale parasitic loops mounted on the counterpoise.

FIG. 5-4: The details of the tension adjuster used for the installed parasitic loops.

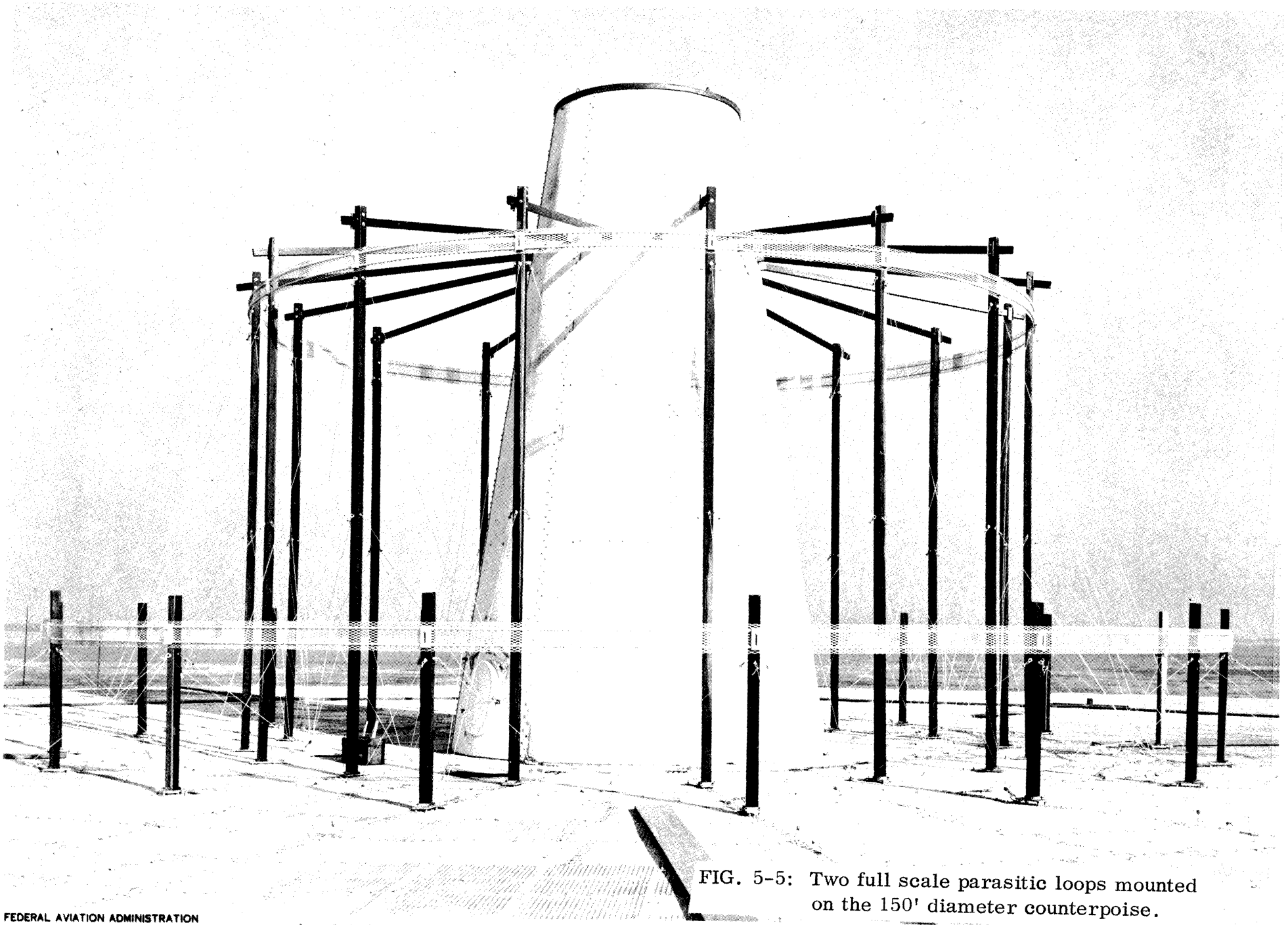

FIG. 5-5: Two full scale parasitic loops mounted on the 150' diameter counterpoise.

FEDERAL AVIATION ADMINISTRATION
ATLANTIC CITY, NEW JERSEY

10-2501

VI

NAFEC FACILITIES AND INITIAL GROUND TESTS

6.1 Introduction

In this chapter we comment briefly on the test facilities available at National Aviation Facility Experimental Center where the full scale testing of the double parasitic loop counterpoise VOR antenna has been carried out. In the following sections we mention only the relevant information about the arrnagement.

6.2 Standard VOR Experimental Station Terrain

The standard VOR antenna at NAFEC has been described in section 5.2. For the purpose of analyzing the data discussed later, it is appropriate to discuss briefly the terrain surrounding the VOR station, parts of which can be seen in Fig. 6-1. The east side of the station (foreground in Fig. 6-1) is relatively clear with no major visible obstructions. On the west side of the station there are a number of trees whose heights range from 65' to 70'. The trees run in a west-northwest to east southeast direction such that there is a fairly straight line of trees starting just to the west of the station. A geometrical representation of the terrain and the coordinate system used are shown in Fig. 6-2.

6.3 Ground Test Facility

Facilities are available to probe the fields along a vertical line above ground and at convenient distances from the VOR antenna. We have made use of a wooden pole 75' tall located 300 feet from the center line of the counterpoise. A vertical track is attached to the front side of this pole and oriented such that a small horizontal detecting dipole antenna can be oriented normal to a radial of the test antenna and can be readily raised and lowered by use of a rope. The height of the detecting antenna above ground can be varied from 0' to 85' in steps of 5'. The output of the detecting dipole feeds a Micro-Tel receiver connected to a Hewlett-Packard model 415 standing wave indicator.

The area between the test antenna and the 75' pole where the field probing is done, consists primarily of marsh grass approximately 5 - 6 feet tall and a 8' fence that encloses the VOR facility. It is estimated that the fence is approximately 125' from the vertical line through the center of the counterpoise.

6.4 Introduction of Known Scattering Sources

Facilities are also available to introduce known scattering sources in the vicinity of the VOR antenna system. These scattering objects act as the known sources of scalloping errors and thereby enable a flying aircraft to be used to evaluate the performance of the VOR antenna system under test.

One such scattering object is in the form of a wire grid reflecting structure mounted between a pair of poles, so that the plane of the structure is vertical. The reflecting grid structure is made of eight conducting wires, each approximately 1/16" in diameter and 200' in length. The eight wires are placed parallel to each other and to the ground. The wires are oriented 18" apart and the topmost wire is located 30' above the ground. The entire structure is positioned approximately 1000' from the VOR station and oriented 45^{o} with respect to the 52^{o} radial from the north of the VOR station. A second pair of poles is located at a distance of 2000' from the VOR antenna and supports a similar reflecting screen. A theodolite mount and a small shelter are located midway between these poles. The theodolite is used when making accurate bearing measurements (with respect to the theodolite position) of an aircraft circling the station at a constant altitude and at a constant distance from the station.

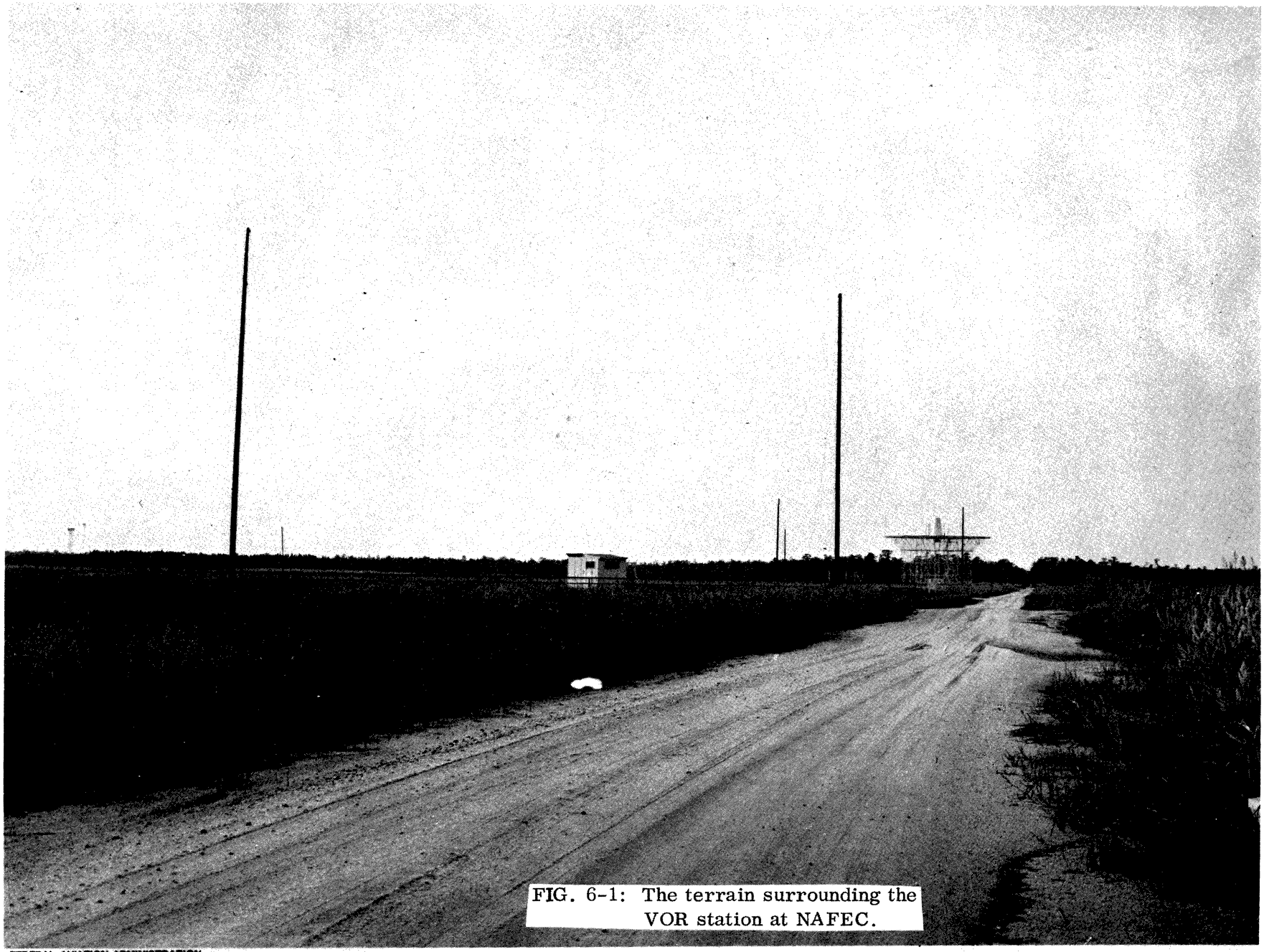

FIG. 6-1: The terrain surrounding the VOR station at NAFEC.

FEDERAL AVIATION ADMINISTRATION
ATLANTIC CITY, NEW JERSEY

70-2439

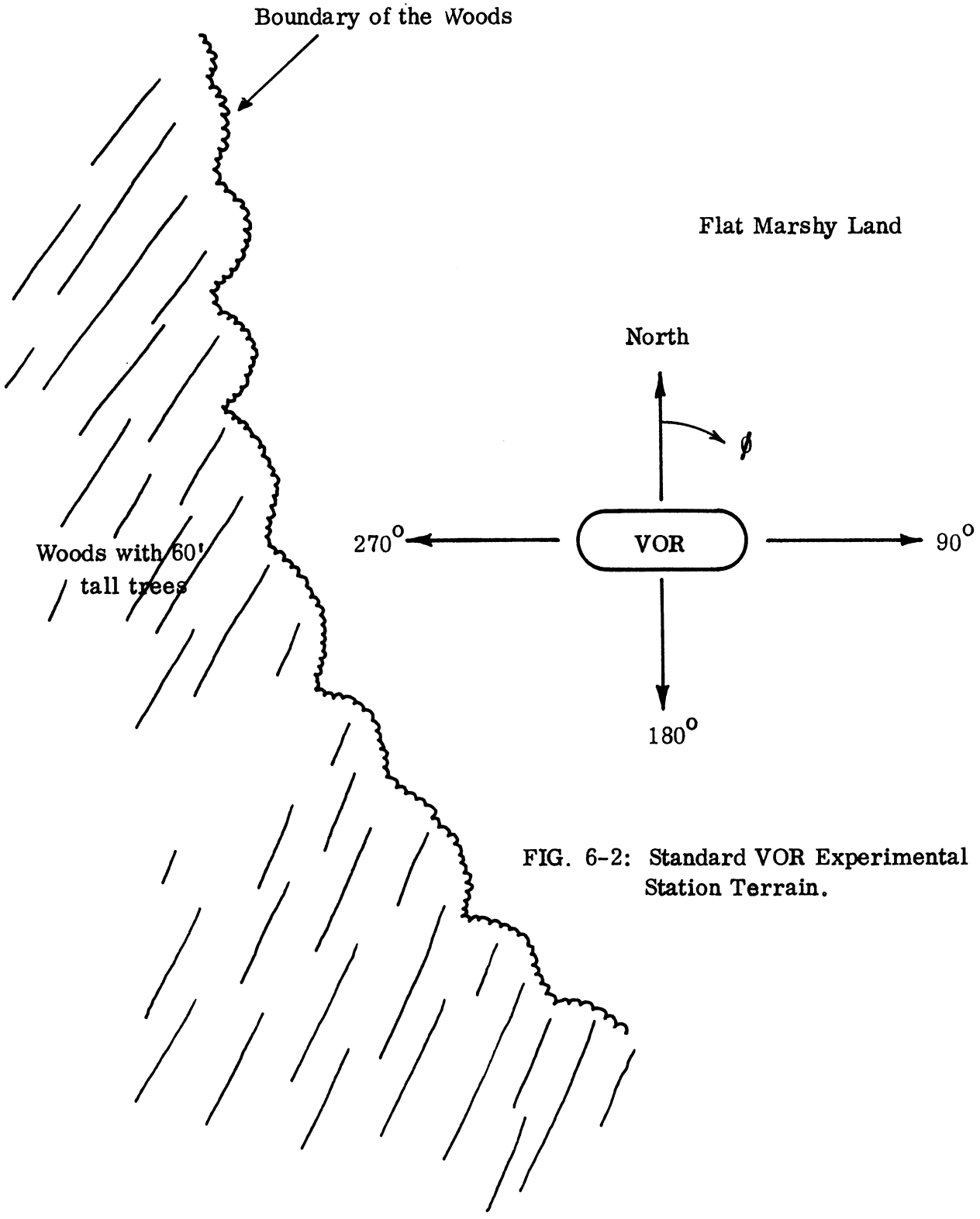

FIG. 6-2: Standard VOR Experimental Station Terrain.

VII

GROUND TEST RESULTS FOR STANDARD VOR AND DOUBLE PARASITIC LOOP COUNTERPOISE ANTENNAS

7.1 Introduction

In this chapter we discuss the results obtained by probing the fields at 109 MHz produced by the full scale standard VOR and double parasitic loop counterpoise antennas located above ground. The probing of the fields is done at a distance 300' from the antenna and along a vertical pole above ground in a manner described in section 6.3. The reduced data obtained from the ground tests are compared with the corresponding theoretical results. Theoretical results given here have been obtained on the assumption that the test antenna is located above a perfectly conducting plane earth. The full scale ground test results discussed here have been obtained at the National Aviation Facilities Experimental Center. Thus the results given in this chapter will also indicate the validity of the design of optimum double parasitic loop counterpoise antennas whose theory and design have been discussed in earlier chapters. Before discussing the test results we give a brief theoretical discussion of the fields produced by the test antennas located above a conducting earth.

7.2 Field Expressions

In view of the fact that during the full scale testing on the ground, the direct and reflected rays reaching the detector at the field point are not parallel to each other, it is clear that the field point in such a case is located in the quasi radiation zone of the antenna under consideration. For this reason we investigate here the case when the field point lies in quasi radiation zone so that the results can be compared directly with the full scale test results.

Figure 7-1 shows the theoretical model used for the analysis. The VOR antenna represented by a point source in this figure is assumed to correspond to the particular antenna configuration under consideration.

In this zone the usual geometrical optics approximations are used. We consider the arrangement sketched in Fig. 7-1 along with the coordinate system used. Let the field point P be located below the x-y plane at (R, θ) from the origin of the coordinate system. The distance of the point P from the center of the antenna is D. It is evident from the figure that the field at P consists of the contributions from a direct and a reflected ray originating from the antenna.

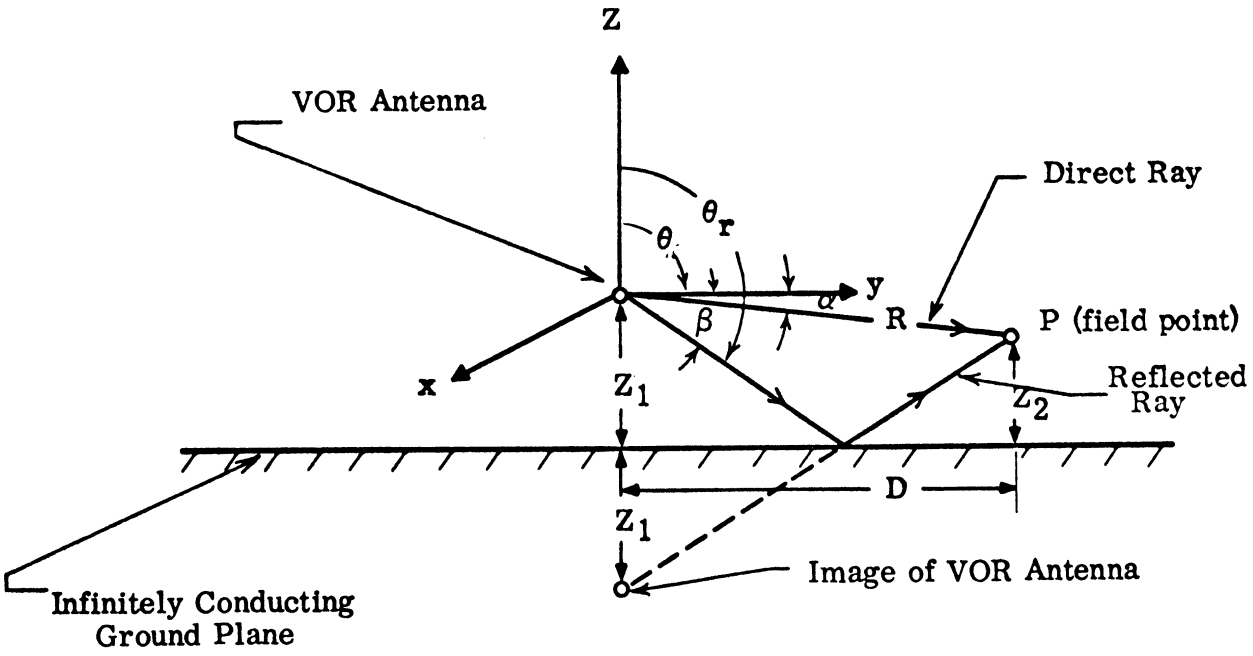

FIG. 7-1: Geometrical representation of a double parasitic loop counterpoise VOR antenna above ground.

Let the free space electric field of the VOR antenna at a point (R, θ) in the radiation zone be given by the following expression:

$$\bar{E} = K \frac{e^{ikR}}{R} S(\theta) \hat{a}_{\phi} \quad , \tag{7.1}$$

where

$S(\theta)$ is the free space complex far field pattern of the antenna,
$\hat{a}_{\phi}$ is the unit vector in the ϕ-direction,
$k = 2\pi/\lambda$ is the free space propagation constant,
R, θ are the coordinates of the field point in spherical system,
and K is a constant.

Note that the field is polarized in the ϕ-direction, i.e. horizontally polarized.

In the present case, it is quite simple to show that the direct and reflected components of the electric field at the point P are given by

$$\bar{E}_D = K \cdot \frac{e^{ikR}}{R} S(\theta) \hat{a}_{\phi} \quad , \tag{7.2}$$

$$\bar{E}_r = -K \cdot \frac{e^{ikR'}}{R'} S(\theta_r)\, \hat{a}_\phi \ , \tag{7.3}$$

where R' is the path length of the reflected ray between the source and field points and the other parameters are as shown in Fig. 7-1. The negative sign in front of (7.3) appears because of the assumption of infinite conductivity for the ground. For a more realistic ground the negative sign in (7.3) should be replaced by a general reflection coefficient

$$\Gamma = |\Gamma| e^{j\delta} \ ,$$

where $|\Gamma|$ is the amplitude and δ the phase of the reflection coefficient.

From Fig. 7-1 it can be shown that

$$\theta = \frac{\pi}{2} + \alpha \ , \qquad \theta_r = \frac{\pi}{2} + \beta \tag{7.4}$$

and

$$\tan\alpha = \frac{Z_1 - Z_2}{D} \ , \quad \tan\beta = \frac{Z_1 + Z_2}{D} \ . \tag{7.5}$$

It can also be seen from Fig. 7-1 that

$$R^2 = D^2 + (Z_1 - Z_2)^2 \ , \quad R'^2 = D^2 + (Z_1 + Z_2) \ . \tag{7.6}$$

Assuming $Z_1, Z_2 \ll D$ it can be shown that

$$R' \simeq R + \frac{2Z_1 Z_2}{D} \ . \tag{7.7}$$

Using eqs. (7.2), (7.3) and (7.7) it can be shown that the total field $\bar{E}_T$ at P is given by

$$\bar{E}_T = \bar{E}_D + \bar{E}_r \simeq K \cdot \frac{e^{ikR}}{R} \left[S(\theta) - e^{ik \frac{2Z_1 Z_2}{D}} S(\theta_r) \right] \hat{a}_\phi \ . \tag{7.8}$$

Thus the complex field pattern $S_T(\theta)$ produced by the antenna configuration shown in Fig. 7-1 can be written as

$$S_T(\theta) = S(\theta) - S(\theta_r) e^{ik \frac{2Z_1 Z_2}{D}} \tag{7.9}$$

where θ and θ_r are given by eqs. (7.4) and (7.5).

If the field point P is taken to be above the x-y plane, then the complex field pattern is again given by (7.9) but with the following modified definitions of θ and θ_r:

$$\tan\theta = \frac{D}{Z_2 - Z_1} \quad , \quad \theta_r = \frac{\pi}{2} + \beta \quad , \qquad \tan\beta = \frac{Z_1 + Z_2}{D} \quad . \tag{7.10}$$

In Eq. (7.9) $S(\theta)$ is the free space elevation plane complex far field pattern of the antenna under test. Analytic expressions for $S(\theta)$ for double parasitic loop counterpoise and standard VOR antennas operating in both carrier and side band modes are discussed in Chapters II - IV. In the following section we compare the theoretical results obtained from Eq. (7.9) with the corresponding ground test results.

7.3 Full Scale Ground Test Results

In this section we compare some of the relevant full scale test results with the appropriate theoretical results discussed earlier. The description of the full scale testing facility and the method of obtaining results have already been discussed. We only mention here that the full scale test facility consists of a conventional or double parasitic loop counterpoise antenna located 75' above ground. The counterpoise has a diameter of 150'. The antenna system is excited at a frequency of 109 MHz, $\lambda = 9.028'$. The field produced by the antenna is detected by a horizontal dipole mounted on a vertical pole located at a distance 300' away from the antenna. The detector height can be varied from the ground level to about 85' above ground in steps of 5'.

Figure 7-2 shows the theoretical field strength variation in a vertical plane located 300' away from the standard VOR antenna operating in the carrier mode. In the same figure we also show the reduced results obtained from the full scale test. In view of the approximations made in the theoretical analysis, the agreement between numerical and experimental results may be considered to be very good. It should be pointed out that the accuracy of the measurement deteriorates as the detector approaches the ground.

Figure 7-3 shows similar results for the optimum double parasitic loop counterpoise antenna operating in the carrier mode. Within the experimental range of accuracy, the agreement between theory and experiment in this case may also be considered to be satisfactory.

Figure 7-4 gives the results obtained for the side band mode operation of the double parasitic loop counterpoise antenna. The agreement between the critical regions of the theoretical and experimental curves may be considered to be good in view of the various approximations made in the analysis and the experimental errors involved.

The parasitic loop dimensions corresponding to the experimental results in Figs. 7-3 and 7-4 are: $2B_1$ = 46'10", H_1 = 4'9", $2B_2$ = 32'6", H_2 = 19'2". The corresponding theoretical values for the same dimensions for the optimum configuration as given in section 4.7 are: $2B_1$ = 46'10", H_1 = 5', $2B_2$ = 32'6", H_2 = 18'4". Comparing these values it may be concluded that the parameters for the optimum antenna obtained on the basis of theretical and model measurements are within the range of full scale measurement accuracy. The slight adjustments of the heights that have been necessary during the full scale testing is not surprising if one considers the effects of terrain and other possible mechnical maladjustments on the performance of the entire system. From now on we shall refer to the antenna considered in Figs. 7-3 and 7-4 as the optimum parasitic loop counterpoise antenna system II.

The optimum double parasitic loop counterpoise antenna system whose quasi radiation field characteristics are shown in Figs. 7-3 and 7-4 has a theoretical field gradient value of about 23dB/6° in the side band mode of operation.

In addition to the above optimum configuration we have chosen another double parasitic loop counterpoise antenna to be flight tested. This antenna is designed to have less than optimum value for the horizontal field gradient. The parasitic loops for this system have the following settings: $2B_1$ = 46'10", H_1 = 3'10", $2B_2$=32'6" H_2 = 18'7". The ground test results obtained from this antenna are shown in Figs. 7-5 and 7-6 for carrier and side band mode operations respectively. The theoretical horizontal field gradient of this antenna is about 15dB/6°. This antenna will be referred to as the parasitic loop counterpoise system I.

7.4 Discussion

The full scale ground test results discussed in this chapter indicate the validity of the theoretical design and the proper mechanical fabrication of the optimum double parasitic loop counterpoise antenna. Considering the various approximations involved, the agreement between the theoretical and actual measured full scale design values may be considered to be satisfactory and within the range of experimental accuracy.

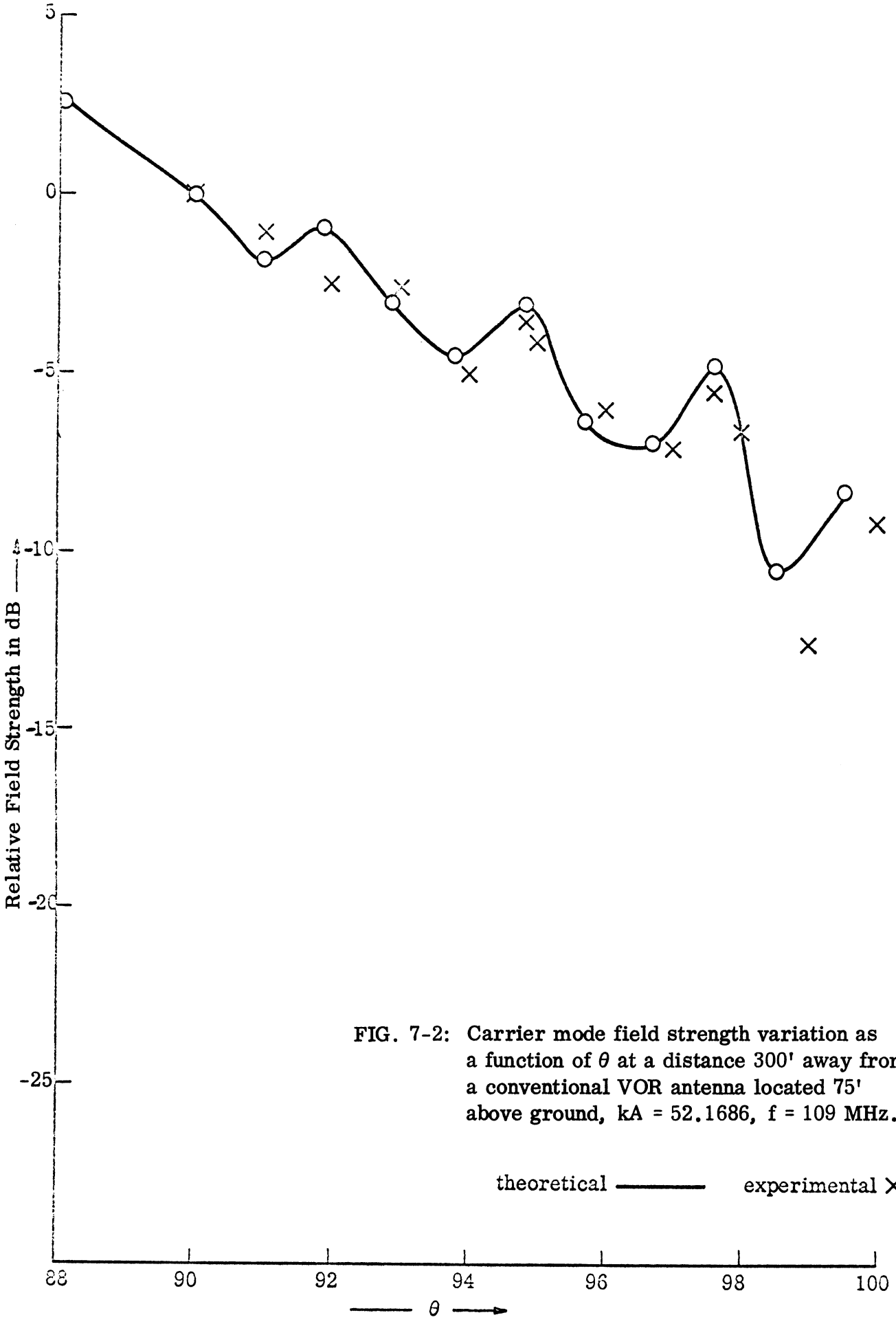

FIG. 7-2: Carrier mode field strength variation as a function of θ at a distance 300' away from a conventional VOR antenna located 75' above ground, kA = 52.1686, f = 109 MHz.

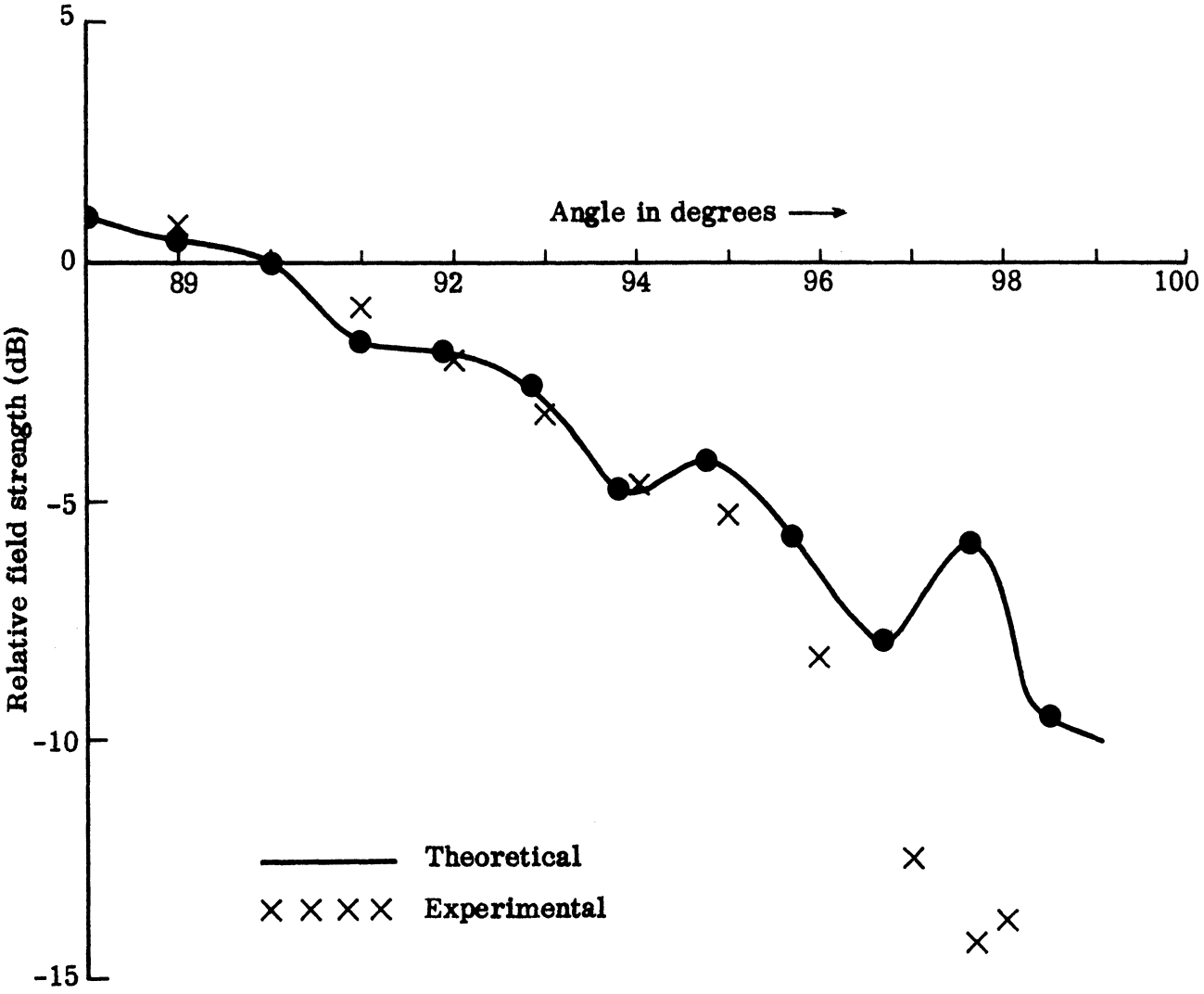

FIG. 7-3: Carrier mode field strength variation as a function of θ at a distance 300' away from the (Systems II) optimum double parasitic loop counterpoise VOR antenna located 75' above ground. f = 109 MHz.

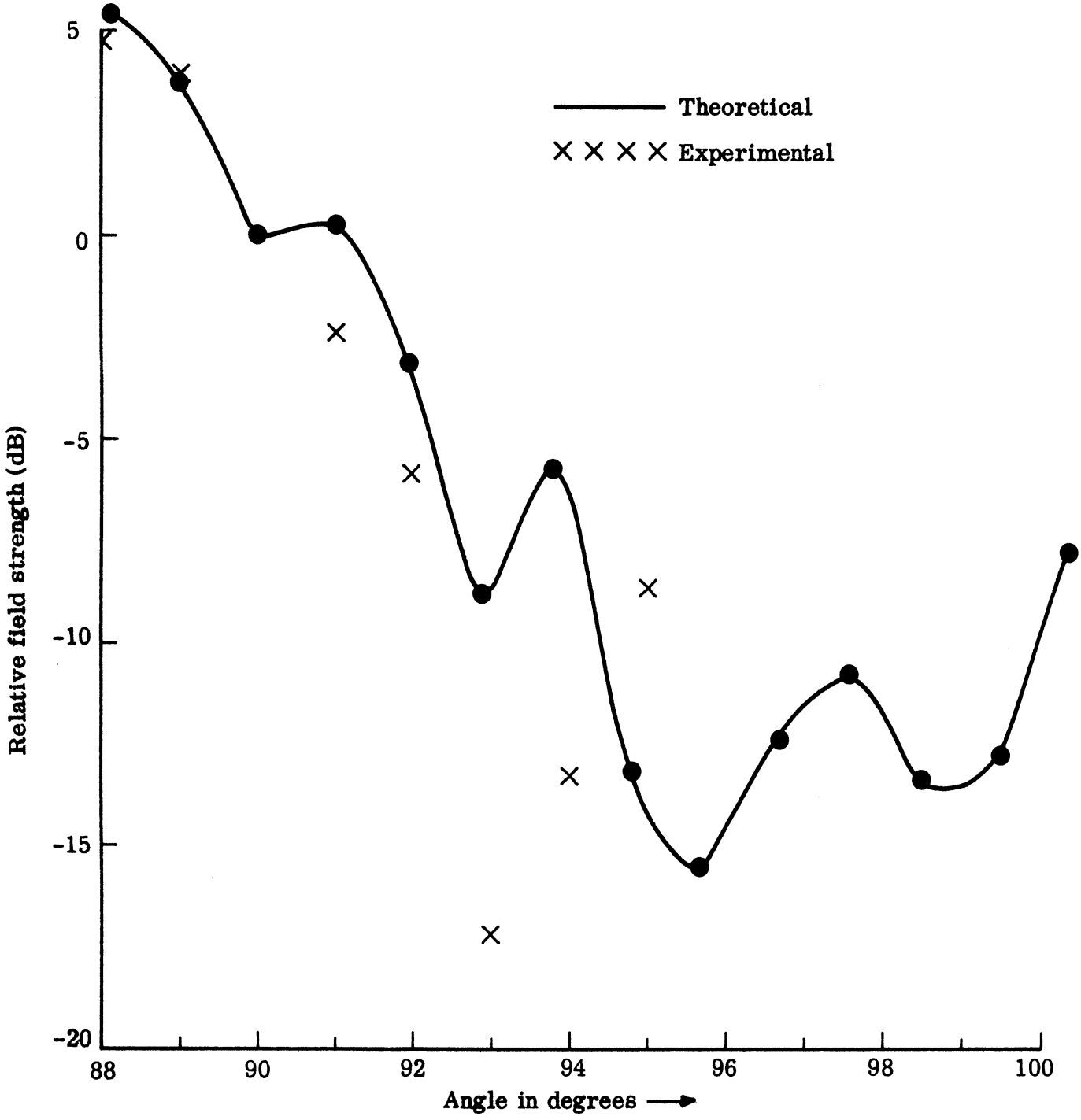

FIG. 7-4: Side band mode field strength variation as a function θ at a distance 300' away from the optimum double parasitic loop counterpoise VOR antenna (systems II) located 75' above ground, f = 109 MHz.

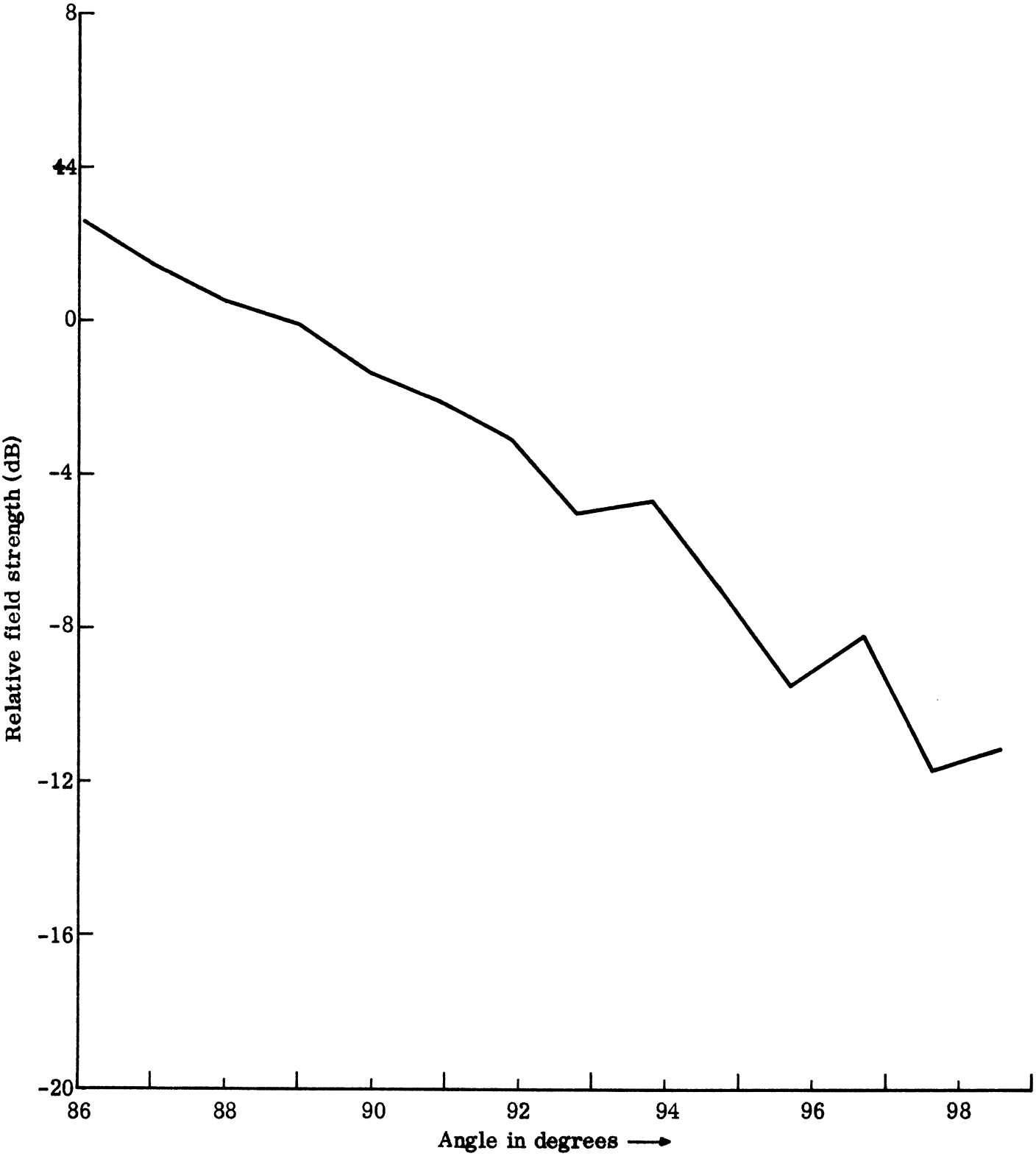

FIG. 7-5: Measured carrier mode field strength variation in a vertical plane located 300' away from a non-optimum double parasitic loop counterpoise VOR antenna (Systems I) f = 109 MHz.

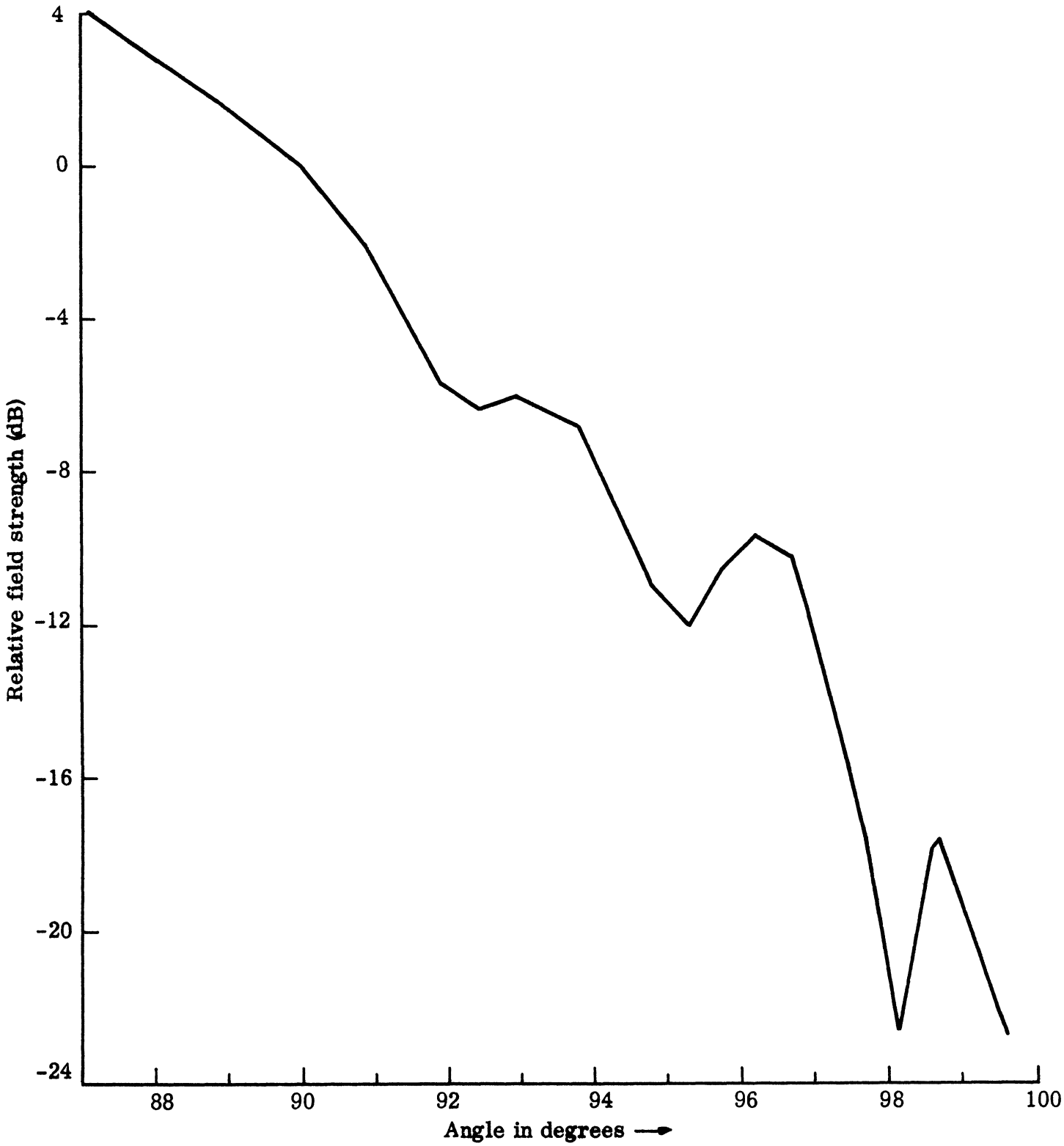

FIG. 7-6: Measured side band mode field strength variation in a vertical plane located 300' away from a non-optimum double parasitic loop counterpoise VOR antenna (Systems I). f = 109 MHz.

VIII

FLIGHT TESTS OF DOUBLE PARASITIC LOOP COUNTERPOISE AND STANDARD VOR ANTENNAS

8.1 Introduction

In this chapter we discuss the results of flight tests carried out on 109 MHz to determine the performance of a standard VOR system when the VOR ground station uses double parasitic loop counterpoise antennas and standard four Alford loop counterpoise antenna. The primary purpose of the flight tests has been to compare the observed scalloping errors in the VOR bearing indications in a flying aircraft produced by a known scattering object for the two cases. The secondary purpose has been to verify at the full scale frequency and for practical systems the horizontally polarized radiation field information obtained earlier for such antennas from theoretical and model measurements considerations. For this purpose the radiated fields produced by the test antenna were measured with the help of an aircraft flying at a constant altitude along chosen radial paths to and from the test antenna. The tests described here were performed at NAFEC.

8.2 Test Antennas

The standard VOR antenna consists of the four Alford loops located above a 150' diameter counterpoise elevated 75' above ground. The details of the antenna have been given in section 6.2 - 6-3.

The double parasitic loop counterpoise antenna system was obtained by installing two parasitic loops of proper dimensions at appropriate heights above the standard VOR Alford loop counterpoise antenna in the manner described in Chapters IV - VI. As mentioned in section 7.3, two double parasitic loop counterpoise antenna configurations have been chosen for the flight tests. These are referred to as antenna Systems I and II. The key design parameters of the two systems are:

System I (non-optimum)	$2B_1 = 46'10''$	$H_1 = 3'10''$
	$2B_2 = 32'6''$	$H_2 = 18'7''$
System II (optimum)	$2B_1 = 46'10''$	$H_1 = 4'9''$
	$2B_2 = 32'6''$	$H_2 = 19'2''$

Notice that the two systems differ with each other only in the heights of the parasitic loops above the counterpoise.

The free space side band mode horizon field gradient values produced by antenna systems I and II are about 15 and 23dB/6° respectively. These field gradient values are much larger than the corresponding value 5.54dB/6° obtainable from the conventional VOR antenna. On the basis of this criterion alone, it was anticipated that for a given scattering object located near the antenna, a standard VOR system using the antenna systems I and II would produce reduced amounts of scalloping effects in the VOR indicator of a flying aircraft. The main purpose of the flight tests discussed in the present chapter were to verify quantitatively the above statement.

8.3 Field Strength Results

In this section we describe the measured far fields produced by a standard VOR antenna and by the double parasitic loop counterpoise antenna system II. The field strength results presented here were obtained by employing an FAA aircraft flown at an altitude of 3220' along a specified radial toward the experimental VOR station operating on 109 MHz. Each selected inbound radial was flown three times and continuous recordings of test data were made beginning at a point 35 nautical miles from the station and ending after the aircraft had passed over the station. Similar tests were conducted while using each VOR antenna system. To ensure that the aircraft was flown along the same flight path each time, aircraft guidance was provided by an air traffic controller stationed at a precision tracking radar system station (EAIR at NAFEC).

All the results have been obtained only for the side band operation of the appropriate antenna. To operate the system in the side band mode, the omnidirectional radiation function (carrier mode) of the VOR was disconnected and after turning off the synchronous motor the goniometer was set at 45°. The aircraft was then flown along the prescribed course (see Fig. 6-2) and the horizontally polarized field was received by the horizontally polarized element of a crossed dipole mounted on the nose of the aircraft. The received data was then fed to a calibrated VOR receiver and strip chart recorder along with range marks. The results shown here are expressed in dB and have been obtained from the raw data after removing their dependence on the range.

Figures 8-1 and 8-2 show the reduced results obtained for the standard VOR and for double parasitic loop counterpoise system II antenna respectively when the aircraft was flying along the 90° radial (Fig. 6-2) of the station. The corresponding theoretical results are shown in Figs. 8-1 and 8-2 for comparison. Theoretical results have been obtained by assuming that the test antenna is located at a height Z_1 above a perfectly conducting infinite planar ground and the aircraft is in the far zone of the antenna. When the effects of the distance on the received field of the antenna are removed, the received field as a function of θ may be expressed as:

$$S_t(\theta) = e^{-ikZ_1 \cos\theta} S(\theta) - S'(\pi-\theta)\, e^{ikZ_1 \cos\theta},$$

where $S(\theta)$ is the free space elevation plane complex far field pattern of the test antenna. Explicit expressions for $S(\theta)$ for the test antenna have been given in earlier chapters. Notice that the results are shown only for $70^o \leq \theta < 90^o$. For $\theta < 70^o$ the aircraft was flying at a relatively high rate of change of θ. Consequently the raw data recorded in the aircraft was changing too fast. It has been found that for $\theta < 70^o$ the results were too erratic to be reduced. The agreement between theory and experiment is excellent in Figs. 8-1 and 8-2. In both cases the theory quite accurately predicts the positions of the pattern minima. The experimental results in Fig. 8-1 do not show the first few maxima and minima in the range $70^o \leq \theta \leq 80^o$. This is attributed to the fact that the amount of undulations of the field within this range is too small (as evidenced by the theoretical results) to be recorded. It is anticipated that the theory may be improved further by assuming a more realistic reflection coefficient for the ground. Observe that the minimum nearest to the horizon in Fig. 8-1 is about 10dB down locally whereas the corresponding minimum in Fig. 8-2 is about 3dB down locally. The smaller value of the theoretical minimum in Fig. 8-2 is due to the large value of the free space field gradient associated with the antenna system II. The experimental value of the local minimum in Fig. 8-2 is $\simeq$ 5.3dB which seems to indicate that system II does not have the gradient of theory.

In order to investigate the effects of trees on the fields produced by the double parasitic loop counterpoise antenna, the aircraft was flown above the woods along the $\phi = 220^o$ radial (Fig. 6-2). The results are shown in Fig. 8-3. As compared with the $\phi = 90^o$ radial case shown in Fig. 8-2, Fig. 8-3 indicates that the ground reflection effects are much reduced. This is attributed to the fact that the trees reduced considerably the scattered energy reaching the aircraft.

8.4 Scalloping Effects

It is known that a scattering object located in the vicinity of a VOR station produces scalloping effects in the VOR indications of a flying aircraft. The mechanism and approximate analysis of scalloping effects in some ideal situations have been discussed in the FAA Handbook (1968). In the present section we do not go into any theoretical results but only compare the scalloping effects observed with different antennas in the presence of known scattering objects located above ground.

In order to collect the scalloping data, the aircraft was flown in a 20 mile orbit around the VOR station and at an altitude of 6575 feet. This altitude corresponds to the minimum direction nearest to the horizon in the elevation plane pattern including the effects of ground of a conventional VOR antenna. It has been found

during orbital flights of conventional VOR systems that the scalloping effects become strongest at heights which correspond to these minimum directions. It should be noted here that for an optimum double parasitic loop counterpoise antenna above ground the depths of these pattern minima are considerably smaller than those of the standard VOR antenna (see Figs. 8-1 and 8-2). From this consideration we expected to see reduced scalloping effects with the parasitic antenna systems.

To produce the scalloping effects a wire grid reflector was installed 1000' from the test antenna in the manner described in section 6.4. The orientation of the scattering object with respect to the VOR station is shown in Fig. 8-4. A typical set of scalloping data obtained at a height of 6575' with a standard VOR antenna is shown in Fig. 8-5. The abscissa in Fig. 8-5 represents the azimuth of the aircraft with respect to the VOR station and the ordinate gives the amount of course scalloping amplitude due to the scattering object. The two sets of results shown in Fig. 8-5 correspond to the two receivers used in the aircraft. The full scale scalloping in Fig. 8-5 is 12.5^{o}. Thus we observe from this figure that with a conventional VOR system there appears 12.5^{o} scalloping at the azimuth of about 140^{o} when flying at 6575' altitude on a 20 mile orbit. Similar sets of data obtained with VOR systems using antenna systems I and II are shown in Figs. 8-6 and 8-7 for the same elevation of the scattering object and for similar orbital flights. As anticipated earlier, it is found that both the double parasitic loop counterpoise antennas produce reduced scalloping effects. The optimum antenna system II produces the least amount of scalloping. The scalloping observed in three cases are given below for comparison.

Standard Alford Loop Counterpoise Antenna	12.5^{o}
Double Parasitic Loop Counterpoise Antenna System I	2.5^{o}
Double Parasitic Loop counterpoise Antenna System II	2^{o}

It is clear from the results given above that the optimum double parasitic loop counterpoise antenna produces a 6 to 1 reduction in the scalloping effects observed in standard VOR indications of a flying aircraft. On comparing Figs. 8-6 and 8-7 with Figs. 8-5, it is found that the parasitic antenna systems produce strong bending of the course. This observed slow bending of the course is attributed to the vertically polarized radiation from the parasitic loop counterpoise antennas.

8.5 Distance Range

In order to determine the distance range of a VOR system using an optimum double parasitic loop counterpoise antenna, a radial flight was conducted at an altitude of 6575'. As the aircraft was flown radially away from the VOR system, it was observed that the signal did not reach the 5 microvolt level until a range of 65 miles had been reached. The distance from the antenna at which the signal level reached 5 microvolts is taken to be the distance range of the VOR station.

Perhaps we should make a comment here about the manner in which the above data were collected. Initially when efforts were made to collect aircraft data it was observed that the sawtooth amplitude (note the sawtooth nature of the scalloping data shown in Fig. 8-5) was not of the proper magnitude. Upon some consideration of this problem it was concluded that the cause for the reduced amplitude sawtooth was the improper space modulation of the VOR signal. A reason for the reduced space modulation is due to the fact that the parasitic rings create such a small signal near the horizon that the signal radiated in the side band mode was considerably less than that radiated in the carrier mode. We should also note here that the carrier mode intelligence is carried by frequency modulation, whereas in the side band mode the intelligence is carried by amplitude modulation in the form of space modulation of the rf characteristics of the VOR signal. In order to achieve the necessary amplitude required for the sawtooth associated with the scalloping data, it was necessary to make some adjustments in the side band carrier powers. To achieve the proper space modulation it was necessary to reduce the carrier power by approximately 50 percent. This was achieved by introducing a length of RG-8 cable in the carrier transmission line from the transmitter to the antenna. This is of importance because we have mentioned above that the distance range was approximately 65 miles. After taking into consideration the fact that the power radiated in the carrier mode was reduced by 3dB, we can say that one could achieve approximately a distance range of 84 miles by operating the station at full power assuming that the station employing the parasitic system radiates the same amount of power in the carrier mode as the conventional VOR without the parasitic rings. The distance range associated with the conventional VOR with a 150' counterpoise is in the neighborhood of 87 miles. Although we have noted above that it was necessary to juggle the power characteristics through the use of an attenuator, in an actual situation in which parasitic rings are to be installed on a station, one would construct a power divider to properly distribute the power between the carrier and the side band modes rather than using a lossy attenuator.

8.6 Discussion

The flight test results discussed above clearly indicate that conventional VOR antennas can be converted into double parasitic loop counterpoise VOR an-

tennas with some distinct advantages. The measured field strength results discussed above indicate that the theories developed for the radiation fields produced by double parasitic loop counterpoise and standard VOR antennas have sufficient accuracy for the practical design of such antennas. Detailed discussion of the radiation properties of double parasitic loop counterpoise and standard VOR antennas located above ground may be found elsewhere (Sengupta and Ferris, 1971). With an optimum parasitic system, the scalloping effects have been observed to be reduced by a factor of 6 to 1 over the conventional system. It appears that the parasitic system has a distance range comparable to that of a conventional system. During the flight tests of the double parasitic loop system, large polarization errors were observed in bearing indications. In the next chapter we discuss the experimental study of the polarization errors involved in a standard VOR system using such antennas.

In the above we have given only those flight test results which clearly demonstrate the application of parasitic loop counterpoise antennas to a VOR system. Detailed discussions of the flight test results will be given in a separate publication by FAA.

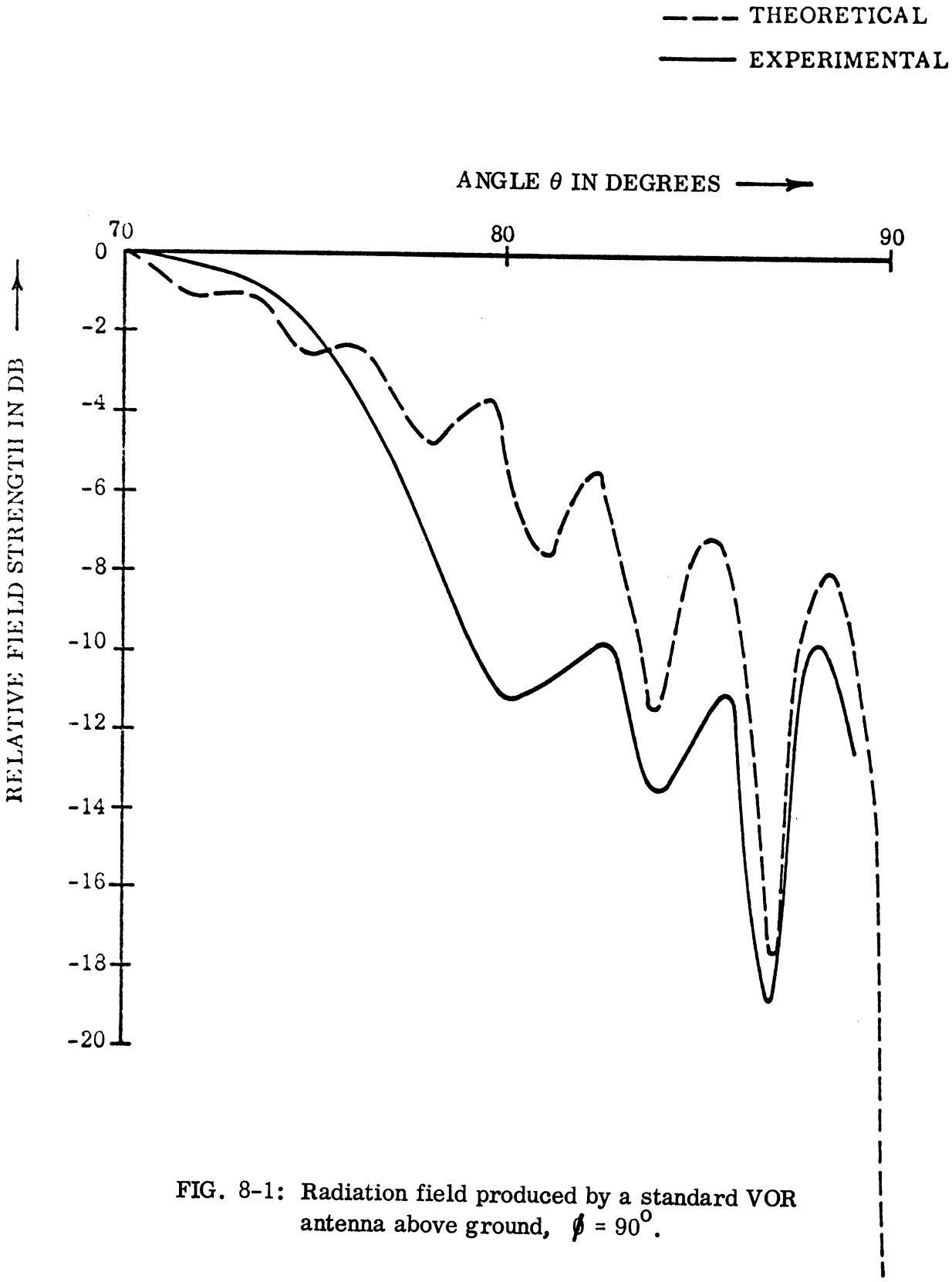

FIG. 8-1: Radiation field produced by a standard VOR antenna above ground, $\phi = 90^{o}$.

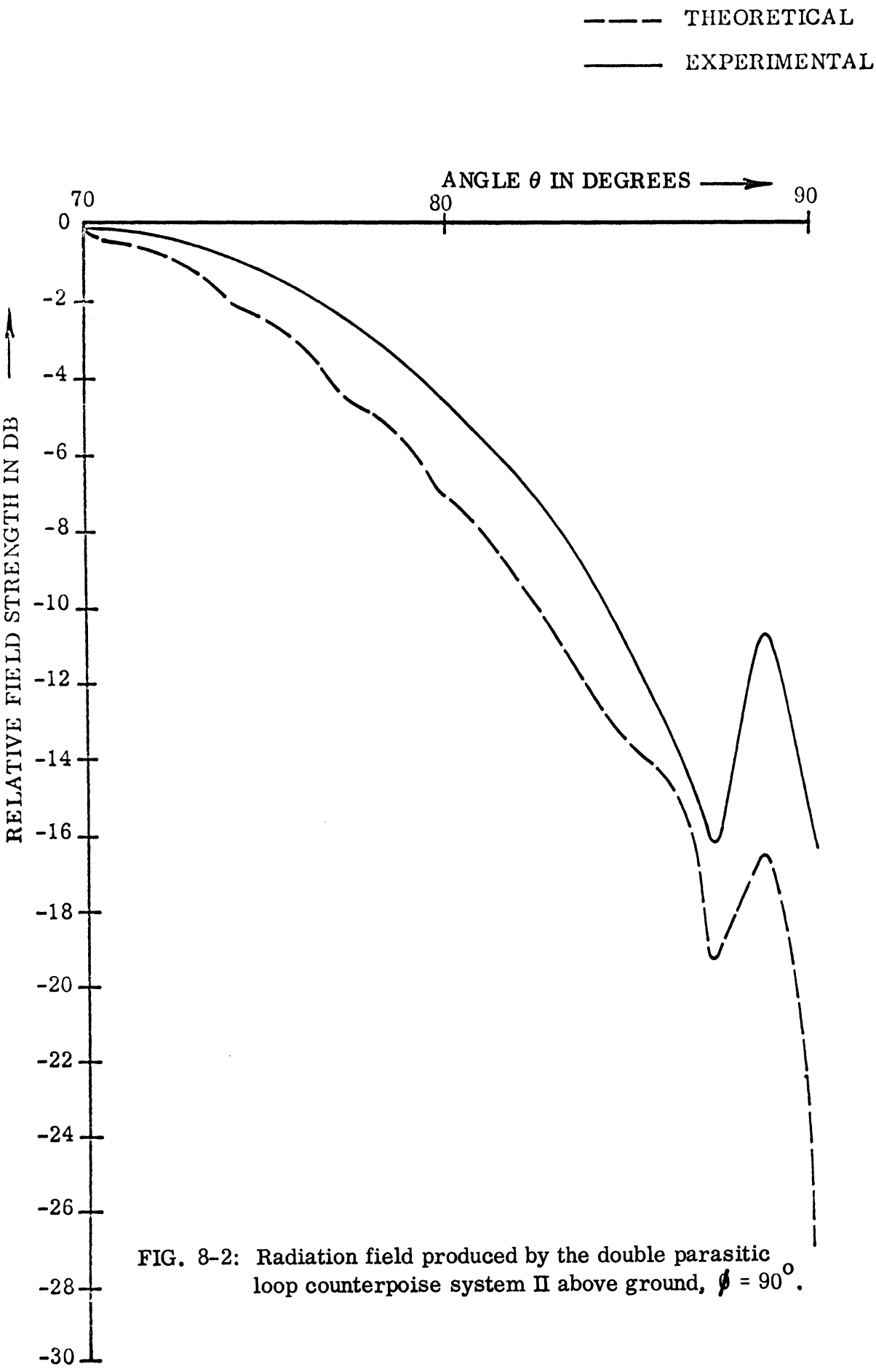

FIG. 8-2: Radiation field produced by the double parasitic loop counterpoise system II above ground, $\phi = 90^{o}$.

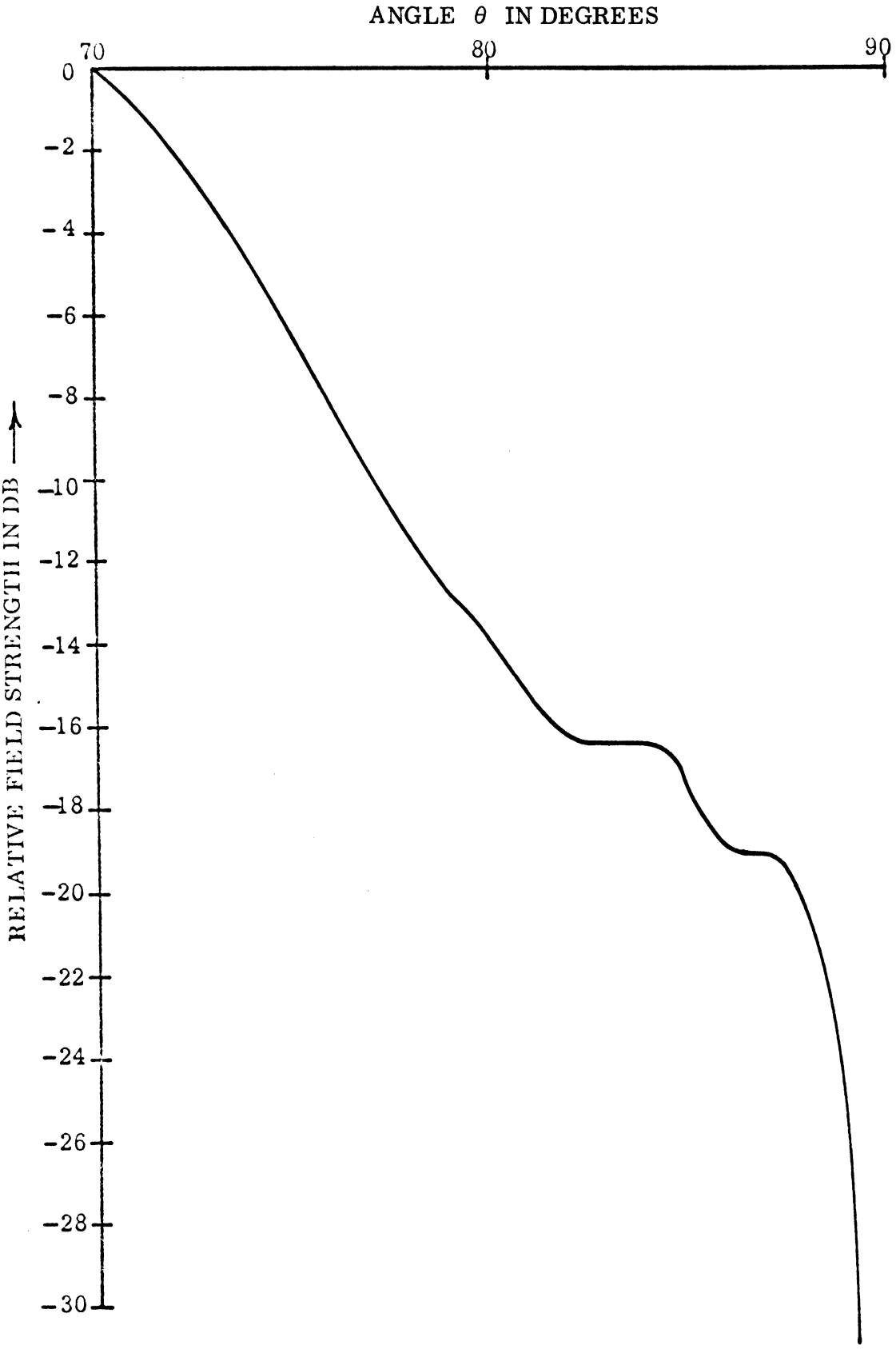

FIG. 8-3: Radiation field produced by a double parasitic loop counterpoise antenna systemII above ground, $\phi = 220^{o}$.

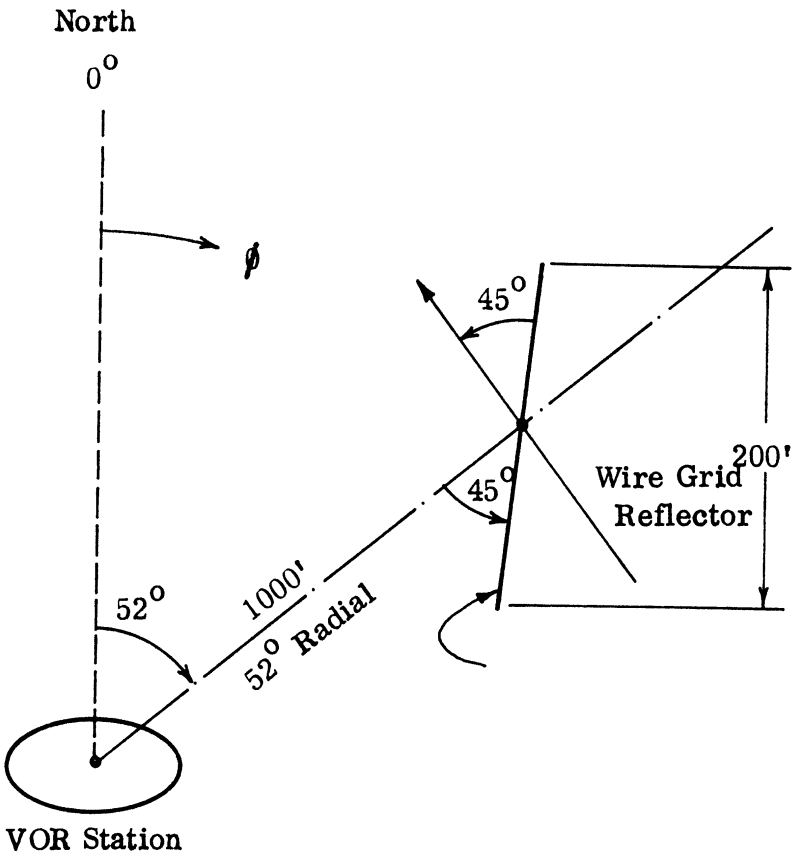

FIG. 8-4: Location of the wire grid reflector with respect to the VOR station.

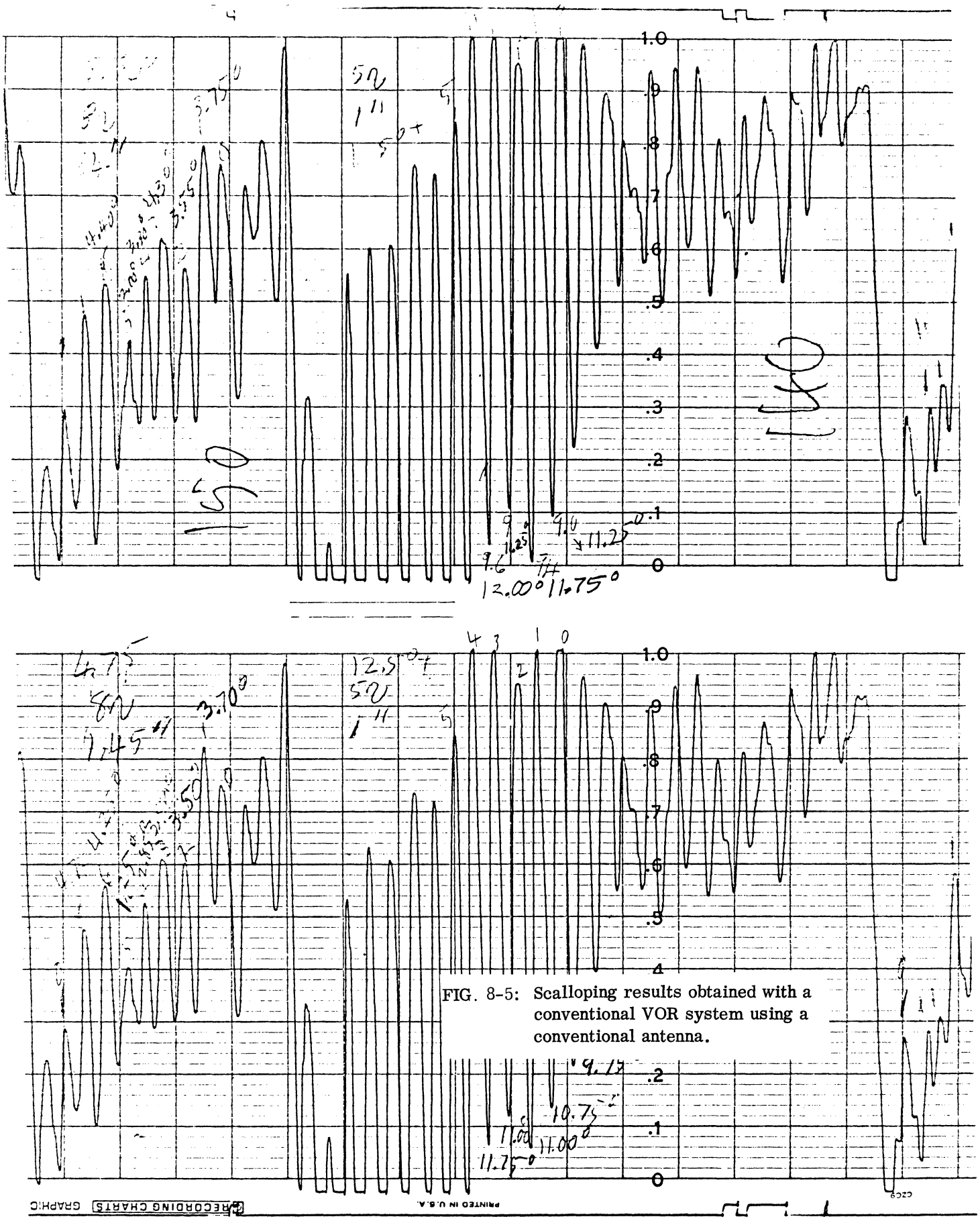

FIG. 8-5: Scalloping results obtained with a conventional VOR system using a conventional antenna.

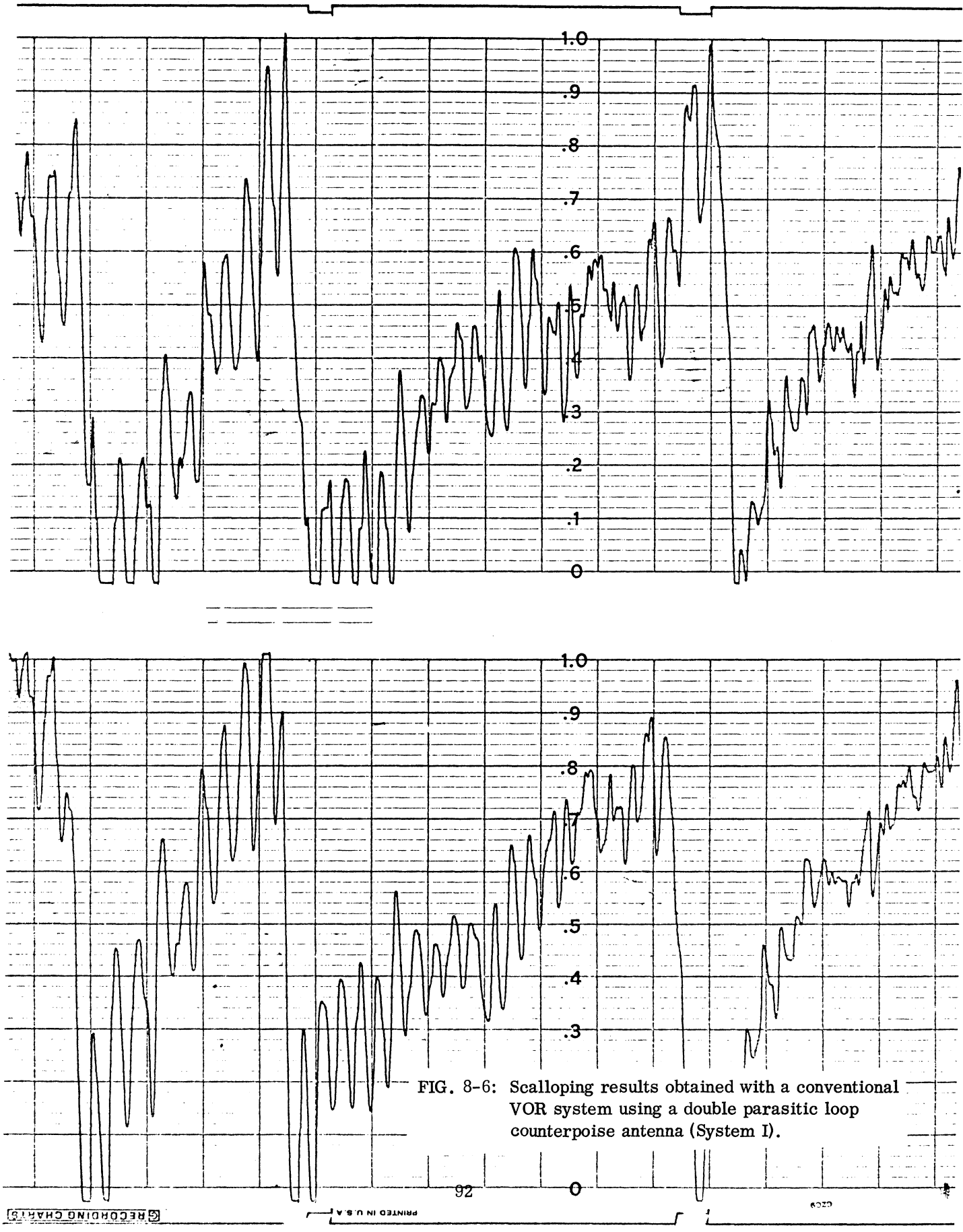

FIG. 8-6: Scalloping results obtained with a conventional VOR system using a double parasitic loop counterpoise antenna (System I).

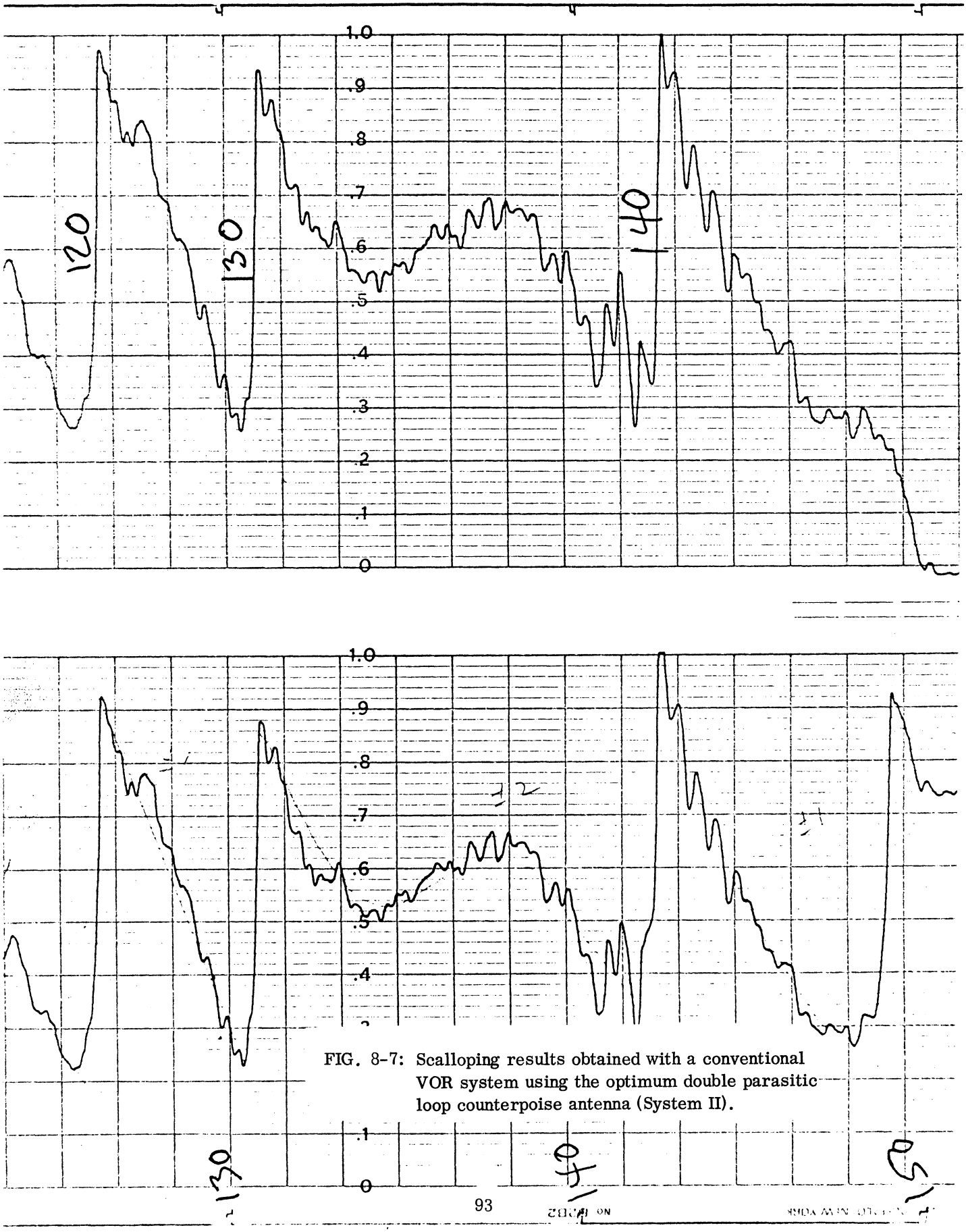

FIG. 8-7: Scalloping results obtained with a conventional VOR system using the optimum double parasitic loop counterpoise antenna (System II).

IX

EXPERIMENTAL STUDY OF THE POLARIZATION ERROR

9.1 Introduction

The results discussed in chapter VIII indicated that the use of a double parasitic loop counterpoise antenna in a standard VOR system reduced the scalloping errors in the bearing indications of a flying aircraft by a factor of 6 to 1. However, the polarization errors associated with the VOR station using the new antenna system have been found to be $\pm 6^{o}$ at certain distances from the station. As recommended by the FAA, the acceptable polarization error in a conventional VOR is $\pm 2^{o}$. Basically, the polarization errors are generated by the cross-polarized component (vertically polarized) of the field produced by the antenna (Anderson et al 1953; Anderson 1965). In addition to the polarization errors, the observed slow course bends in the scalloping data discussed in section 8.4 are believed to be due to the cross-polarized radiation from the antenna.

In the present chapter we discuss the results obtained from an experimental study of the cross-polarized radiation characteristics of double parasitic loop counterpoise and standard VOR antennas. During the course of this study we have developed an active polarizer configuration to reduce the polarization errors in a standard VOR system. Due to lack of time our polarization study remains incomplete. We report here the results obtained from only this limited investigation.

9.2 Polarization Errors in Standard VOR System

The standard 4-Alford loop VOR antenna produces appreciable amounts of undesirable vertically polarized radiation (Anderson, 1965). At the present time the FAA employs a parasitically excited element, called the polarizer, in the antenna system of a standard VOR ground station to bring down the polarization errors associated with the station within the acceptable limits. The design and performance of such a polarizer is discussed in a FAA report (Anderson et al, 1953). Basically, the polarizer produces a vertical component of field which is in phase opposition to the vertical component of the field produced at the far field point by the VOR antenna. The magnitude of the polarizer field is determined primarily by the element lengths of the polarizer and somewhat by its position relative to the 4-Alford loop array; the phase of the polarizer field is controlled mainly by the position of the polarizer with respect to the Alford loop system. It is clear that, for ideal operation, the vertical plane radiation pattern of the polarizer must be identical to the vertical plane cross-polarized radiation pattern of the VOR antenna and that the two fields must be equal

and out of phase at the far field point for all elevation angles. As reported by Anderson (1965), the use of a passive polarizer reduces the polarization errors associated with a standard VOR system to acceptable values.

9.3 Polarization Error Study with the Passive Polarizer

In this section we discuss the results obtained from an experimental investigation of the horizontal and vertical components of the fields and the associated polarization errors produced by a double parasitic loop counterpoise and standard VOR antennas. The passive polarizer, mentioned in the previous section, has been used to reduce the cross polarized fields in both cases. The investigation discussed here has been carried out at NAFEC at the full scale frequency of 109 MHz.

The test plan employed during this part of the investigation is as follows.

(i) The parasitic loops and the existing FAA polarizer were removed; the wooden parasitic loop supports were left in place. The antenna system thus consisted of 4-Alford loop array above a 150' diameter counterpoise located 75' above ground.

(ii) The polarization error, horizontally and vertically polarized field components were then measured employing an aircraft. The reduced results are shown in Fig. 9-1.

(iii) The FAA polarizer was reinstalled and the polarization error of the standard 4-Alford loop system minimized. Data were collected as noted in (ii) and the reduced results are shown in Fig. 9-2.

(iv) The parasitic loops were then reinstalled with the polarizer removed so that the antenna behaved as a double parasitic loop counterpoise system II, discussed in chapter VIII. Similar data were collected and the reduced results are shown in Fig. 9-3.

(v) The polarizer was then installed in the same location and it was adjusted for minimum polarization error for the antenna system II. The flying aircraft collected similar data and the reduced results are shown in Fig. 9-4.

The results shown in Figs. 9-1 to 9-4 were obtained employing an FAA aircraft flown at an altitude of 3220 feet along the 90^{o} radial (Fig. 6-2) of the Mannheim experimental VOR facility with the VOR operating at a frequency of 109 MHz.

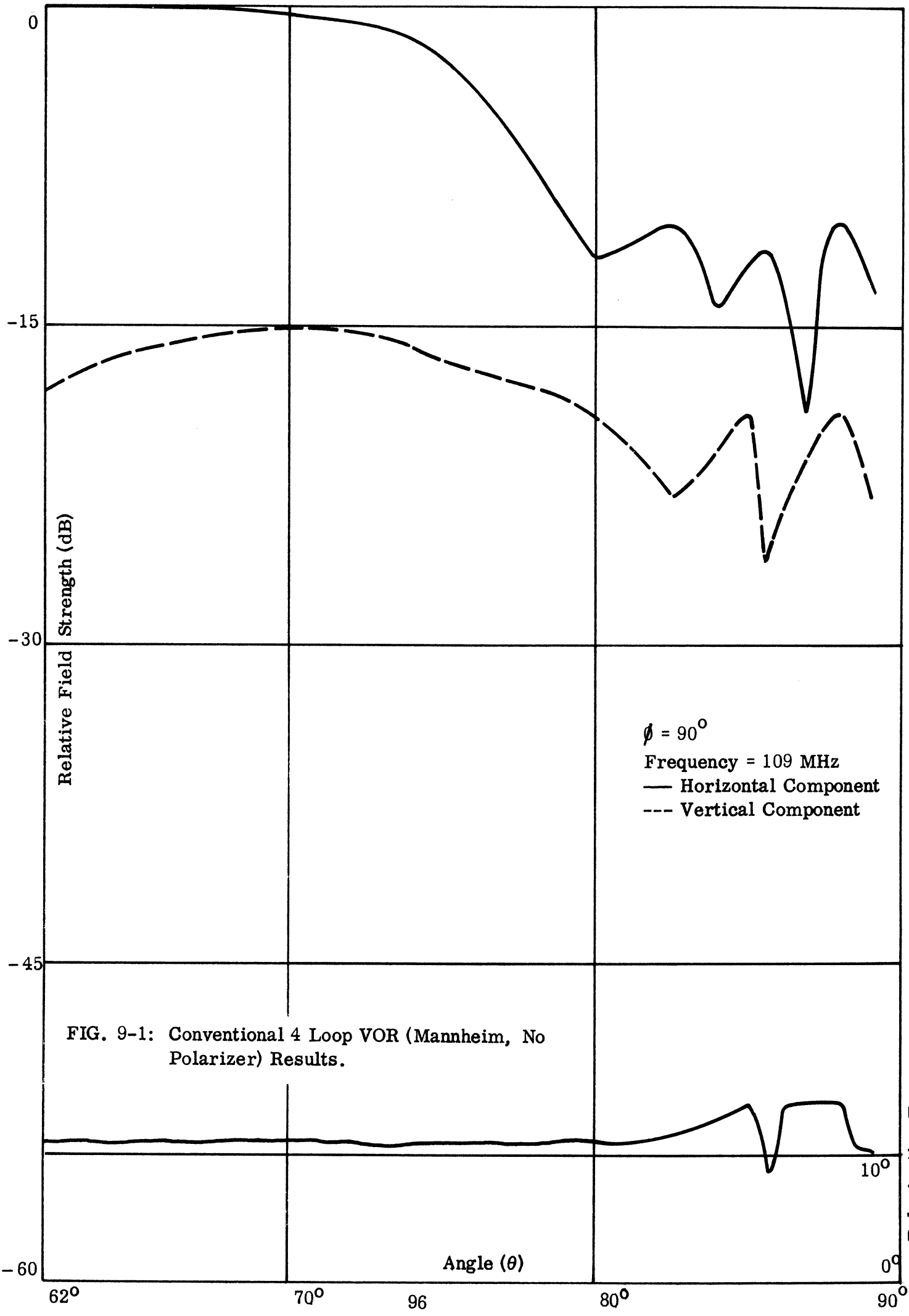

FIG. 9-1: Conventional 4 Loop VOR (Mannheim, No Polarizer) Results.

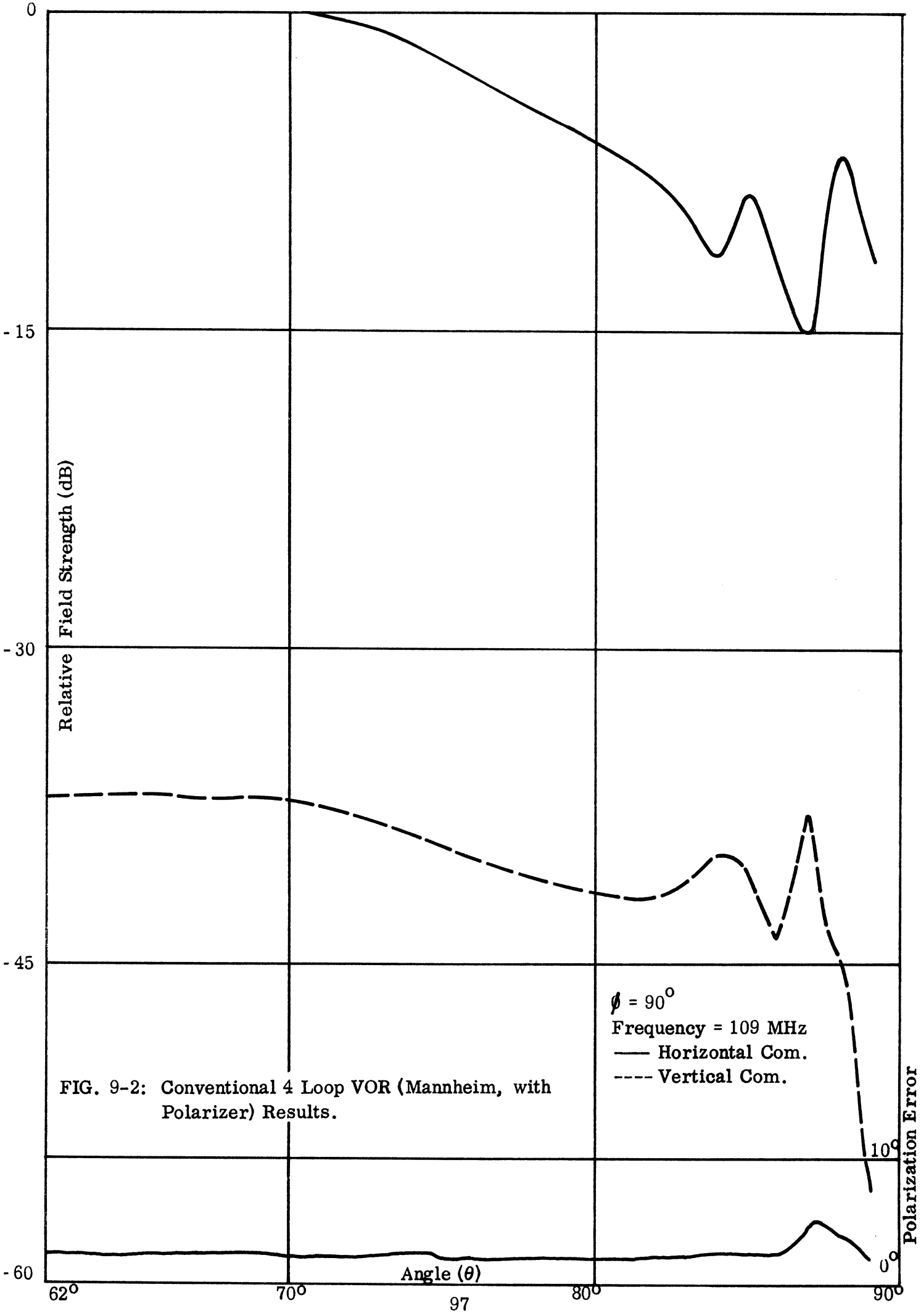

FIG. 9-2: Conventional 4 Loop VOR (Mannheim, with Polarizer) Results.

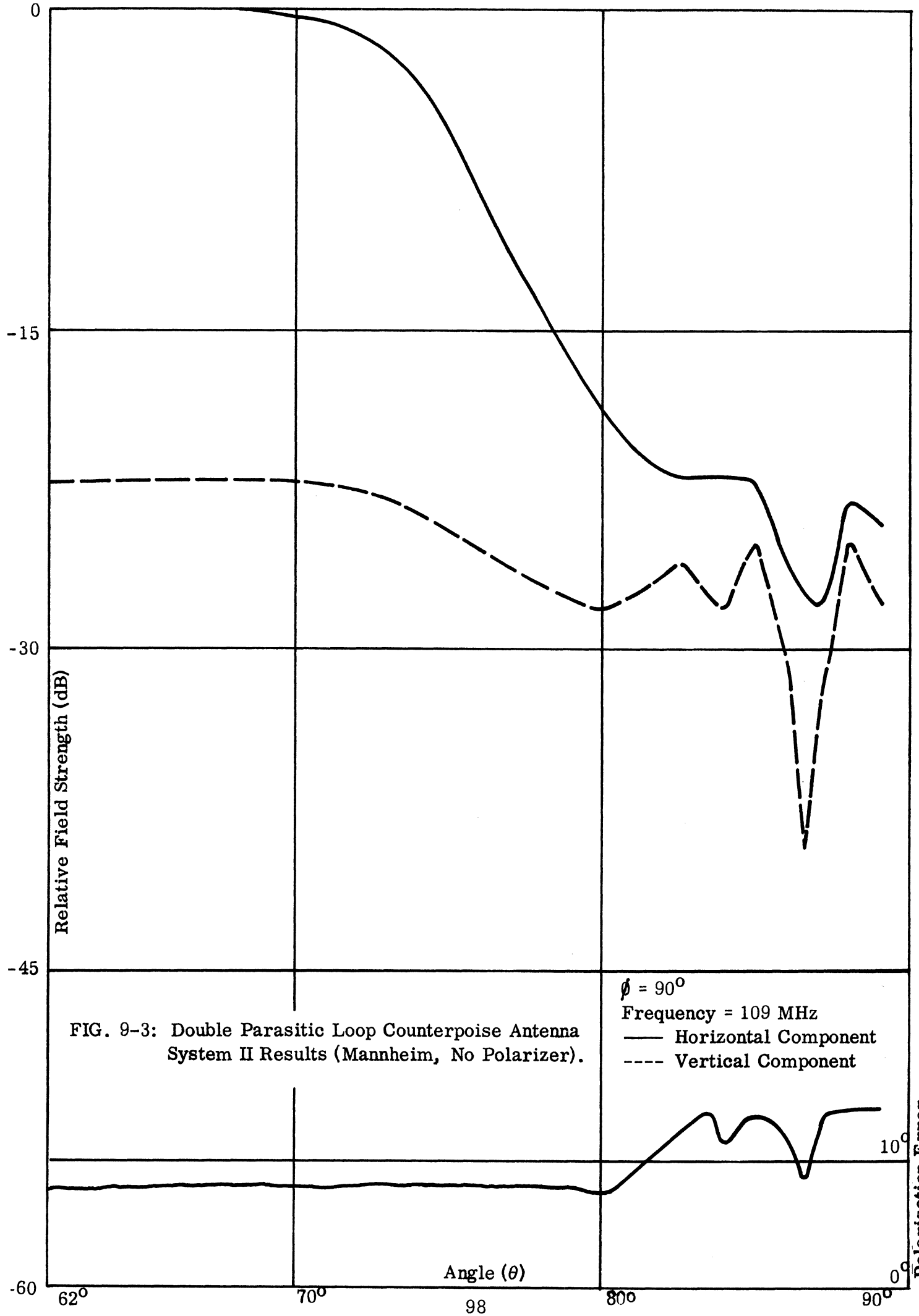

FIG. 9-3: Double Parasitic Loop Counterpoise Antenna System II Results (Mannheim, No Polarizer).

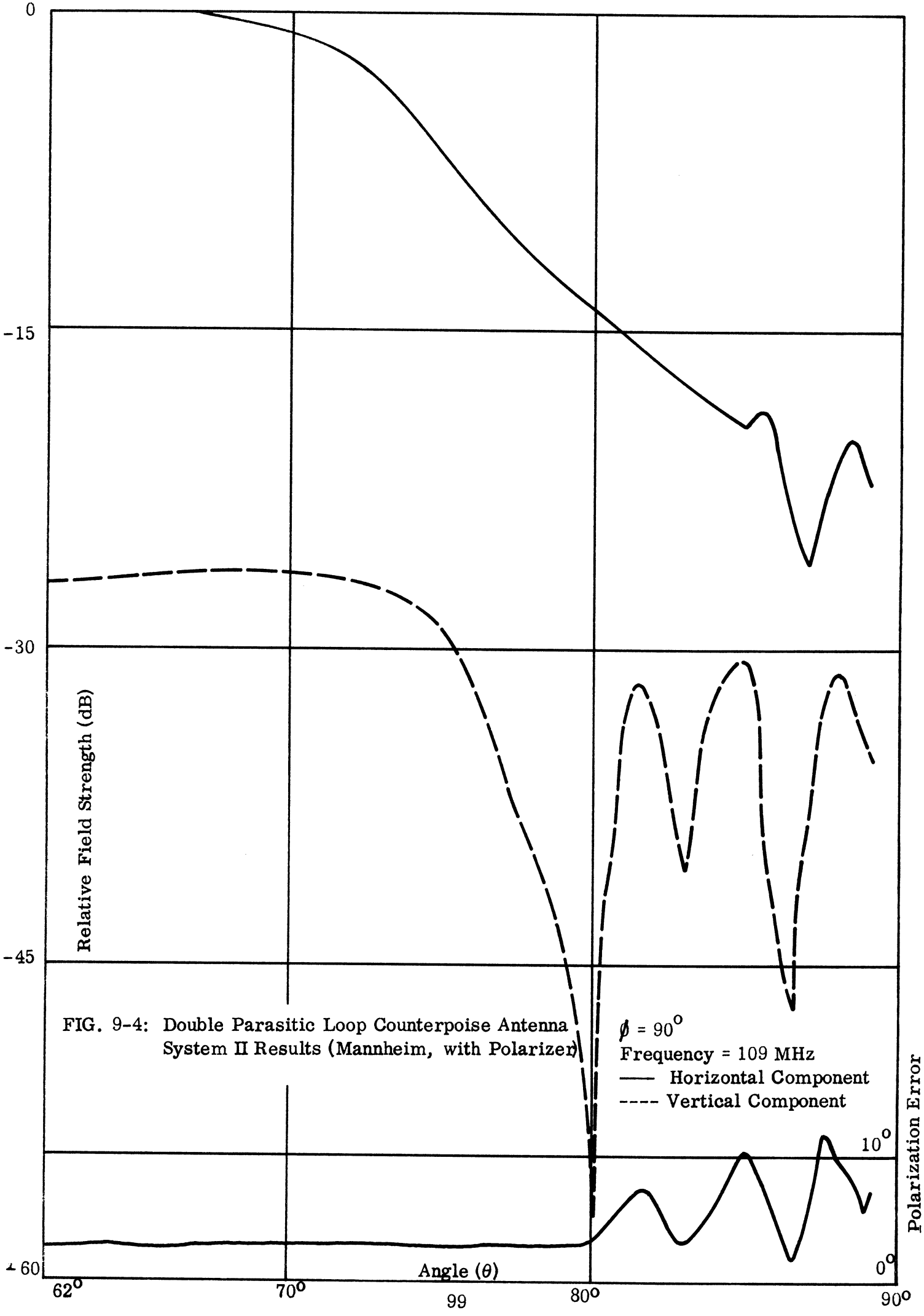

FIG. 9-4: Double Parasitic Loop Counterpoise Antenna System II Results (Mannheim, with Polarizer)

The aircraft flew along the same path three times and data were recorded during each flight starting at 35 nautical miles from the station and continuing until the aircraft passed over the station. No data were plotted for $0 \leq \theta < 62^{o}$ because the raw data recorded in the aircraft were difficult to reduce accurately into pattern form due to the relatively high rate of angular change while the aircraft was flying through this region. To provide assurance that the aircraft was flown along the same flight path each time, aircraft guidance was provided by an air traffic controller stationed at a precision tracking radar system (EAIR at NAFEC).

The horizontally polarized field strength was measured in the flying aircraft as described in section 8.3. The vertically polarized data for the VOR side band mode was obtained in a similar manner with the following changes. The VOR goniometer was set at 135^{o} and the signal was sensed by the vertical element of the crossed dipole mounted on the nose of the aircraft. The polarization error data was collected by having the VOR station operating in its normal mode and the data were sensed by the crossed dipole and reduced to polarization error data by means of a polariscope and recorded on a strip chart.

The field strength data shown in Figs. 9-1 to 9-4 are relative plots in dB with the range effects removed. However, the differences between the vertically and horizontally polarized components are factual for each case. Thus the difference between these two plots is an indication of the polarization error associated with the system. Notice that both the horizontally and vertically polarized data exhibit interference pattern structures in the region $80^{o} < \theta < 90^{o}$, i.e, from 10^{o} above the horizon to the horizon. The explanation for this is as discussed in section 8.3. It should be observed that the interference patterns differ for the horizontally and vertically polarized components recorded for each condition tested. This phenomenon results from the fact that the reflection coefficient of ground for horizontally and vertically polarized energy has a 180^{o} phase difference at shallow angles of incidence ($< 10^{o}$), (Westman, 1956).

Comparing the horizontally polarized data, for the conventional 4-loop system (Figs. 9-1 and 9-2) and the double parasitic loop system II (Figs. 9-3 and 9-4), it can be seen that their gradients (change of field strength versus angle) differ significantly. Further, it can be seen that the vertically and horizontally polarized field strengths associated with the parasitic system (Figs. 9-3 and 9-4) also differ and tend toward equal amplitudes, (in the 80 to 90 degree region), more rapidly than do the same components of the 4-loop system (Figs. 9-1 and 9-2). A comparison of the vertically polarized data of Figs. 9-1 and 9-3 shows that the parasitic loops have a slight effect on the absolute value of the vertically polarized component.

It can be seen from Figs. 9-1 and 9-2 that the passive polarizer reduces the vertically polarized component of the field relative to the horizontally polarized component by better than about 23dB for $82^{o} < \theta < 90^{o}$. Whereas for the parasitic system the corresponding reduction in the vertical component has been found to be about 10dB in the range $82^{o} < \theta < 90^{o}$.

To obtain a better understanding of the differences between the vertically and horizontally polarized energy, additional field strength and polarization data was collected by having the aircraft flown along the 220^{o} radial of the Mannheim facility. Radiation from the antenna was directed toward a densely wooded area (Fig.6-2) where the trees are approximately 60 feet tall and in full foliage. The effect of the trees is either to absorb or randomly scatter much of the energy radiated below the counterpoise for both senses of polarization. Horizontally and vertically polarized field strength and polarization data collected for the 220^{o} radial are shown in Fig. 9-5. From a review of this data it can be seen that both the field strength and polarization data are less erratic, as might be expected due to the reduction in the reflected component from the earth.

Referring now to the polarization data plotted at the bottom of each figure (Figs. 9-1 to 9-5), it can be seen that this data is well behaved from 62^{o} - 80^{o}; however, in the region of 80^{o} - 90^{o} the polarization error becomes erratic. Upon close examination of the field strength and polarization data, it can be seen that the polarization error increases when the difference between the vertically and horizontally polarized field components decreases and vice versa. Figure 9-2 indicates that the passive polarizer is capable of reducing the polarization errors to tolerable limits for the standard VOR antenna case. Comparing Figs 9-3 and 9-4, it can be seen that the passive polarizer is capable of reducing the polarization error for the parasitic system to tolerable levels in the range $62^{o} < \theta < 80^{o}$, however, for $\theta > 80^{o}$ the polarization error increases up to about 12^{o}. It appears from the results shown in Fig. 9-4 that the polarizer field is not strong enough to reduce the vertical component of the field produced by the parasitic antenna system such that the polarization error stays within acceptable limits in the range $80^{o} < \theta < 90^{o}$.

It can be noted also that in the parasitic loop counterpoise VOR antenna system there are at least two additional sources of vertically polarized energy, each at a different height above the counterpoise and above ground. Each source of vertical polarization has a field strength pattern with a distinctive number of lobes. It was stated in section 9.2 that the radiation pattern of the polarizer should be identical in shape and magnitude, but opposite in phase, to the vertically polarized signal that it is required to cancel. Inasmuch as more than one vertically polarized signal is being generated by the parasitic loop counterpoise system, and because the field strength patterns of these signals are different in shape, a separate vertically polarized cancelling signal is required for each vertically polarized signal generated.

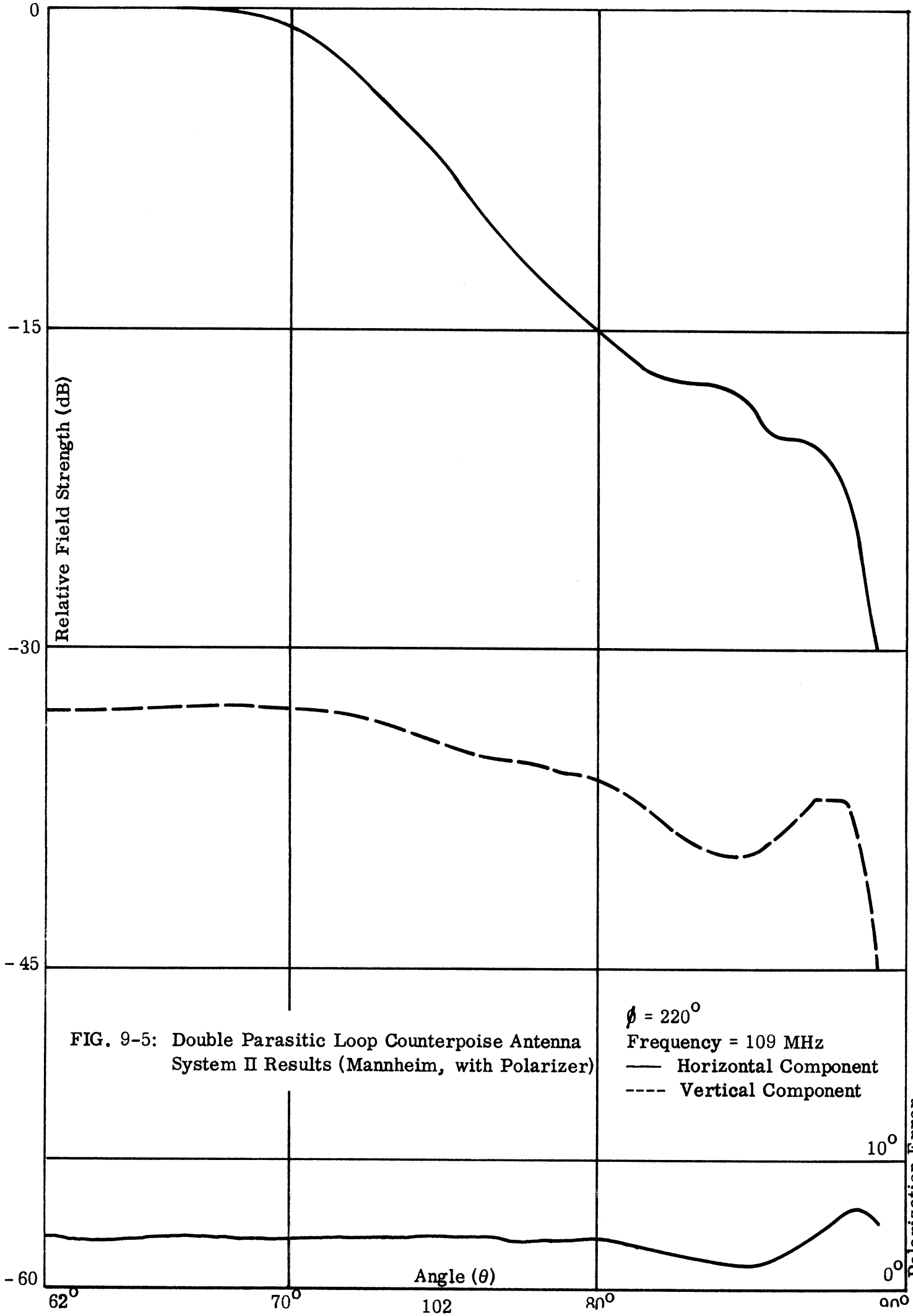

FIG. 9-5: Double Parasitic Loop Counterpoise Antenna System II Results (Mannheim, with Polarizer)

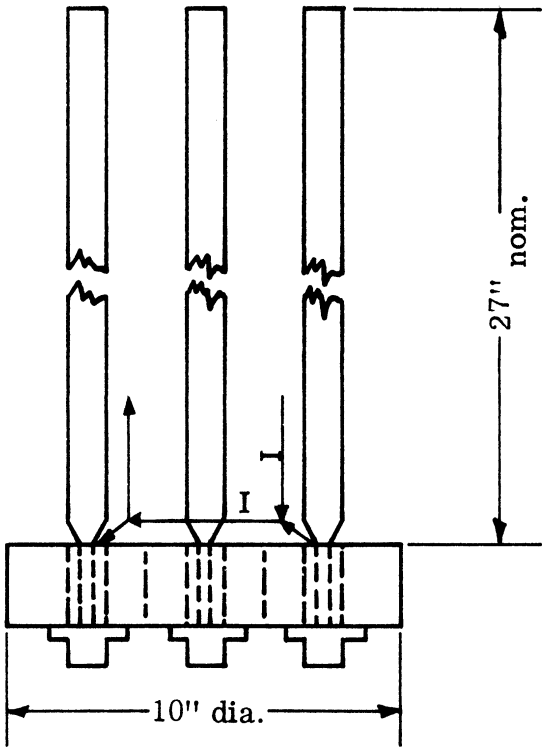

FIG. 9-6: Active Polarizer No. 1.

It is conceivable that the polarizer field may be increased further by increasing the number of parasitic elements in the passive polarizer and/or by using two passive polarizers in the system. Another alternative is to use an active polarizer which is described in the next sections.

9.4 The Active Polarizer

Two active polarizer designs were considered: the first choice was to convert the parasitic polarizer into an active polarizer as shown in Fig. 9-6, the second choice was to design a polarizer made of dipole elements as shown in Fig. 9-7. The second choice was to be a four-element dipole array, vertically polarized. Initially it was thought that the simplest approach would be to convert the existing parasitic polarizer to an active polarizer. The necessary design drawings were prepared and the conversion made at the NAFEC shop facilities. Preliminary tests were conducted at the NAFEC antenna range and the results of these tests showed that the active polarizer (No. 1) radiated equal amounts of energy polarized horizontally and vertically. This polarizer design was felt to be unacceptable because of the large horizontal component being radiated. Therefore, the second polarizer (No. 2) was designed and a full-scale model fabricated. This model consisted of a four-element vertically polarized dipole array as shown in Fig. 9-7. The antenna was then installed at the Mannheim facility and later adjustments were made to reduce the unwanted vertical component radiated by the VOR system.

The large horizontal component being radiated by polarizer No. 1 was believed to be caused by the horizontal current flowing in the hub of the polarizer (see Fig. 9-6). However, for polarizer No. 2 this horizontal current component has been eliminated by providing only vertical paths for the currents to flow (see Fig. 9-7).

Polarizer No. 2 consists of four dipoles arranged in dipole pairs (see Fig. 9-7). Excitation for each dipole is the same except as will be noted below. Therefore, the excitation for one dipole will be discussed. To excite a dipole properly two RF sources of equal magnitude and opposite phase are required. Because a coaxial transmission line is used in the VOR system it is necessary to provide a conversion (balun) from the unbalanced (coaxial system) to a balanced transmission line for the dipole. Since the dipoles are spaced close together ($> \lambda/10$) each balun was fabricated employing a type BNC coaxial Tee and two lengths of RG-58/U coaxial cable whose lengths differed by 180 electrical degrees at 109 MHz. Four coaxial baluns were fabricated (one for each dipole).

In Fig. 9-7 there are four dipole elements labeled 1-4. Each dipole has two elements labeled T (top) and B (bottom). To achieve the desired figure of eight pattern in the horizontal plane, it was necessary to excite a dipole pair 180^{o} out of phase. To obtain the proper phasing between dipole pairs two co-axial baluns were required and were attached to the dipoles such that the top element of one dipole was 180^{o} out of phase with the bottom element and vice versa for the second dipole element. The two balun tees were then interconnected by a third (BNC) Tee which functioned as the input for one of the dipole pairs and was fed by one of the VOR side band excitation sources as noted below. The second dipole pair was excited in a similar manner.

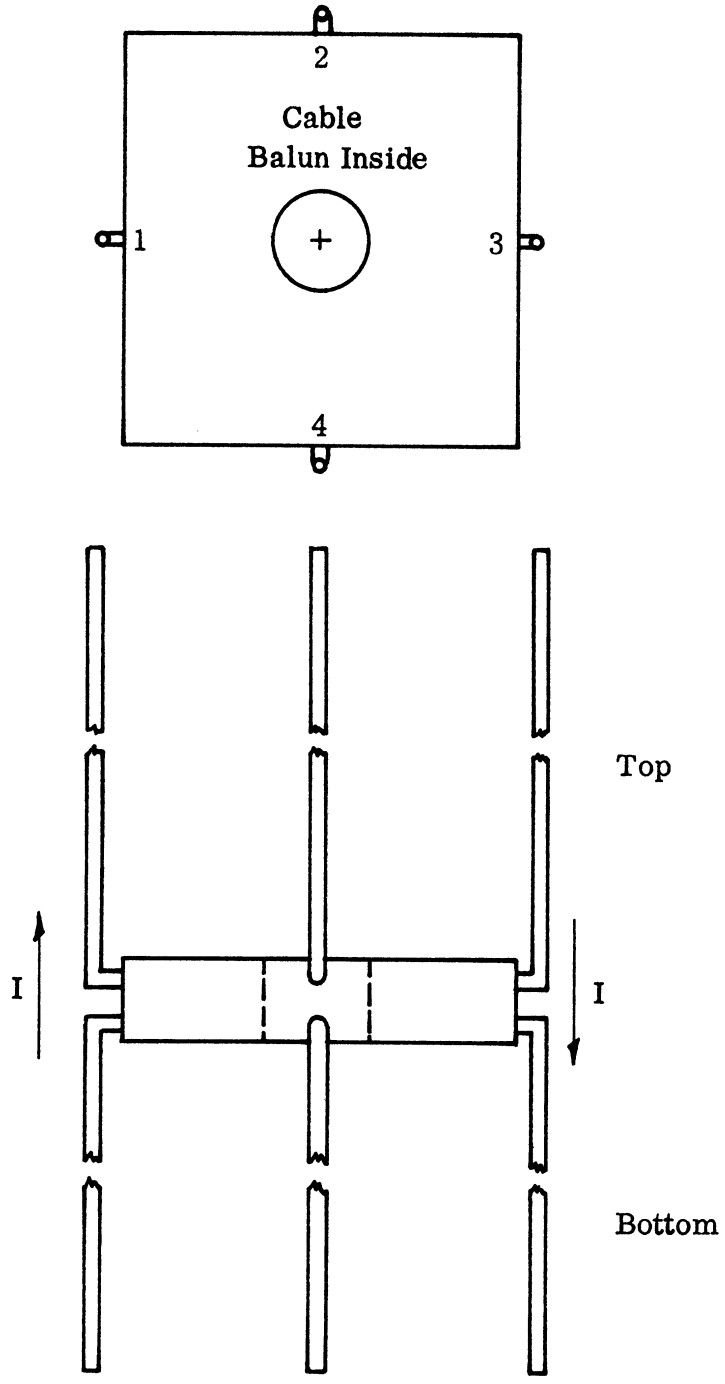

FIG. 9-7: Active Polarizer No. 2.

Basically polarizer No. 2 consists of two simple arrays each consisting of two dipoles that radiate two figure-of-eight patterns in the horizontal plane. The two figure-of-eight patterns are orthogonal to each other and are excited such that elements one and three are excited by a cosine wave and elements two and four are excited by a sine wave. These cosine and sine wave excitations are obtained from the VOR system as noted below. In this manner the figure-of-eight pattern is caused to rotate in the horizontal plane at the frequency of the sine and cosine patterns exciting the two dipole arrays.

Excitation for the active polarizer is obtained from the VOR side band excitation sources. The excitation from the VOR side-bands is connected to the polarizer such that the vertically polarized figure-of-eight pattern maximum occurs in space quadrature with the horizontally polarized pattern maximum associated with the VOR Alford loop system. The active polarizer excitation is fed through a variable attenuator and phase shifter to facilitate adjusting the amplitude and phase excitation of the polarizer antennas independently from the VOR side band excitation. This provides a means for adjusting the amplitude and phase of the signal being radiated by the polarizer to minimize the unwanted vertical component being radiated by the Alford loop system. The pattern shape of the active polarizer may be adjusted by varying the height of the polarizer above the counterpoise.

To completely cancel the unwanted vertical component it would be necessary for the active polarizer antenna to be located at the phase center of the unwanted vertical component being radiated by the system. There has not been a study conducted to determine either the source, or the phase center of the vertical component being radiated by the Alford loops. Therefore, it was not possible to know the precise location at which the polarizer should be located. As a consequence our initial effort was to place the polarizer at a convenient location above the Alford loop system and to adjust the amplitude and phase of the excitation to cancel out the unwanted vertical component at specific elevation angles.

9.5 Parasitic Loop Counterpoise Antenna System II with Active Polarizer

In this section flight tests and results using the active polarizer (polarizer No.2) with the parasitic loop counterpoise antenna (system II) are discussed. The active polarizer was positioned such that each of the four dipoles was mounted directly above and on the center line associated with each of the four Alford loops presently employed in the conventional four-loop VOR. The plane including the dipole centers was located 40" above the plane associated with the top of the Alford loops as shown in Fig. 9-8. This orientation was chosen partially out of convenience and also to insure that the active polarizer would not be influenced by the

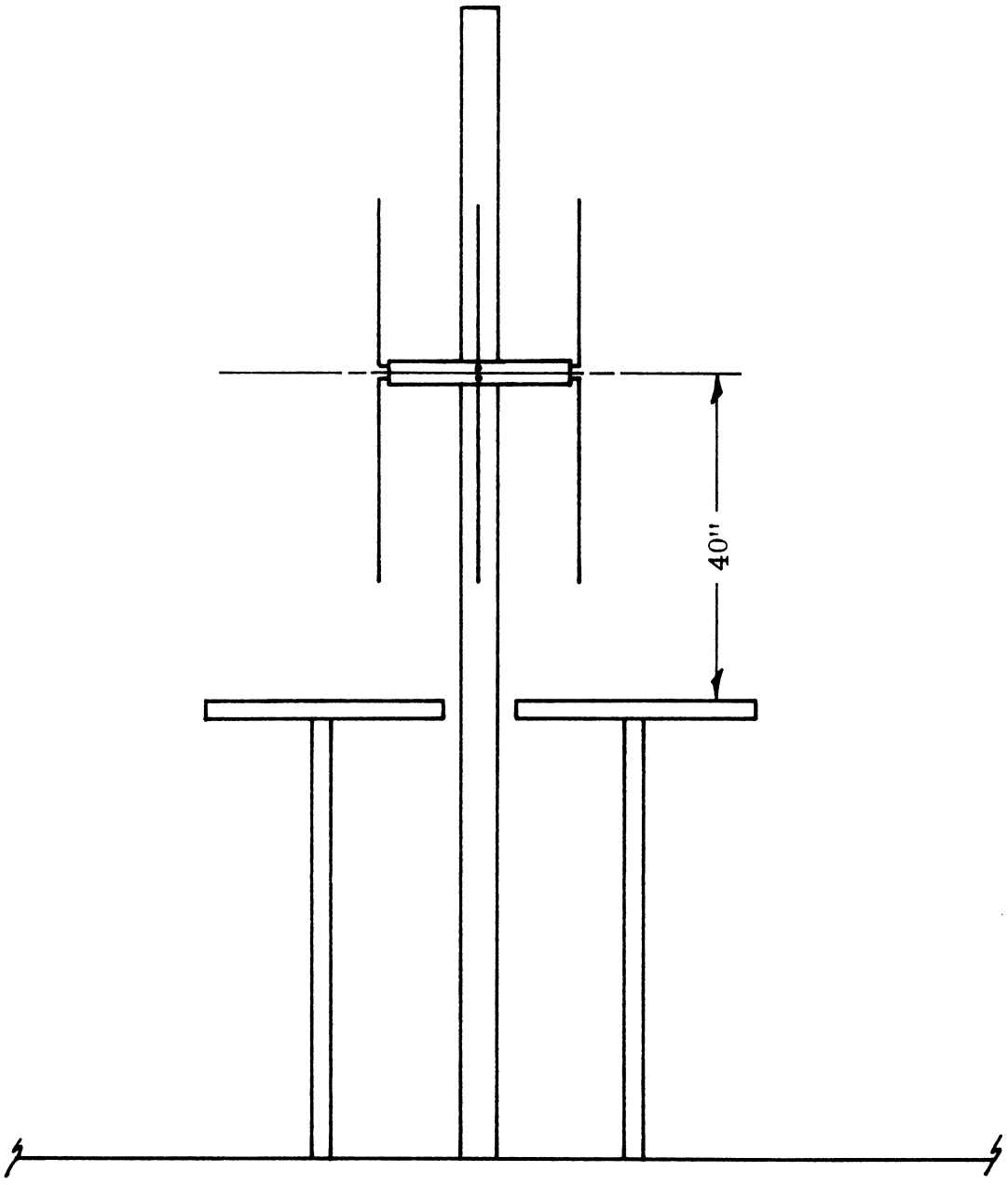

FIG. 9-8: Active Polarizer Installation.

vertical component radiated from the Alford loop system. Polarizer No. 2 consists of four dipoles that are arranged in dipole pairs (shown in Fig. 9-7) and its operation is discussed in the previous section. The two inputs associated with each of the dipole pairs are interconnected through a pair of phase shifters and attenuators to the side band outputs from the VOR transmitter. The power level sampled for the active polarizer is approximately 7dB below the power level fed to the Alford loop system in the side band mode. For example, the power available for the side band mode is approximately five watts and the power available to the active polarizer is approximately one watt.

After the polarizer was installed at the Mannheim facility as noted above, a radiation pattern was measured by having an aircraft flown at a constant altitude (3220 feet) and from a distance of 35 miles from the station along the 90^{o} radial over the station. The field strength was recorded and later the pattern was plotted and is shown in Fig. 9-9 with the range effect removed. In addition, patterns were also collected for the horizontally and vertically polarized components of the double parasitic loop counterpoise antenna system II. Figure 9-10 shows the horizontally and vertically polarized patterns for the 4-loop VOR with parasitic rings at Mannheim with the active polarizer unexcited. A comparison of the vertically polarized pattern for the double parasitic antenna system II and the active polarizer (Figs. 9-9 and 9-10) show that the two patterns do not agree. However, because of the time element it was decided that additional positioning of the active polarizer should not be attempted but instead efforts should be made to reduce the polarization error in a particular direction ($\phi = 90^{o}$) and at a particular elevation angle ($\theta = 86.9^{o}$) to determine the effectiveness of the active polarizer in controlling the polarization error.

Since much of the previous work had been performed along the azimuth angle of 90^{o} it was decided that the polarization error should be reduced to a minimum along this radial and at an angle of 3.1^{o} above the horizon ($\theta = 86.9^{o}$). The aircraft was flown along a 3.1^{o} depression angle starting approximately 35 miles from the station to within a mile of the station. During this flight radio communication was maintained between aircraft personnel and the ground personnel. Instructions were radioed from the aircraft to the ground as to the settings of the polarizer attenuators and phasors. The procedure used was first to adjust the attenuators in 1dB steps until a minimum polarization error was observed. Then the phasor was adjusted in 10^{o} steps for a similar indication. This procedure was repeated for two flights after which it was felt that the polarization error had been reduced to a minimum ($\pm 2.5^{o}$). The aircraft was then flown down the depression angle (third flight) with no adjustments being made and the polarization error recorded as a function of distance from the VOR station. A plot of these data is shown in Fig. 9-11. It is inter-

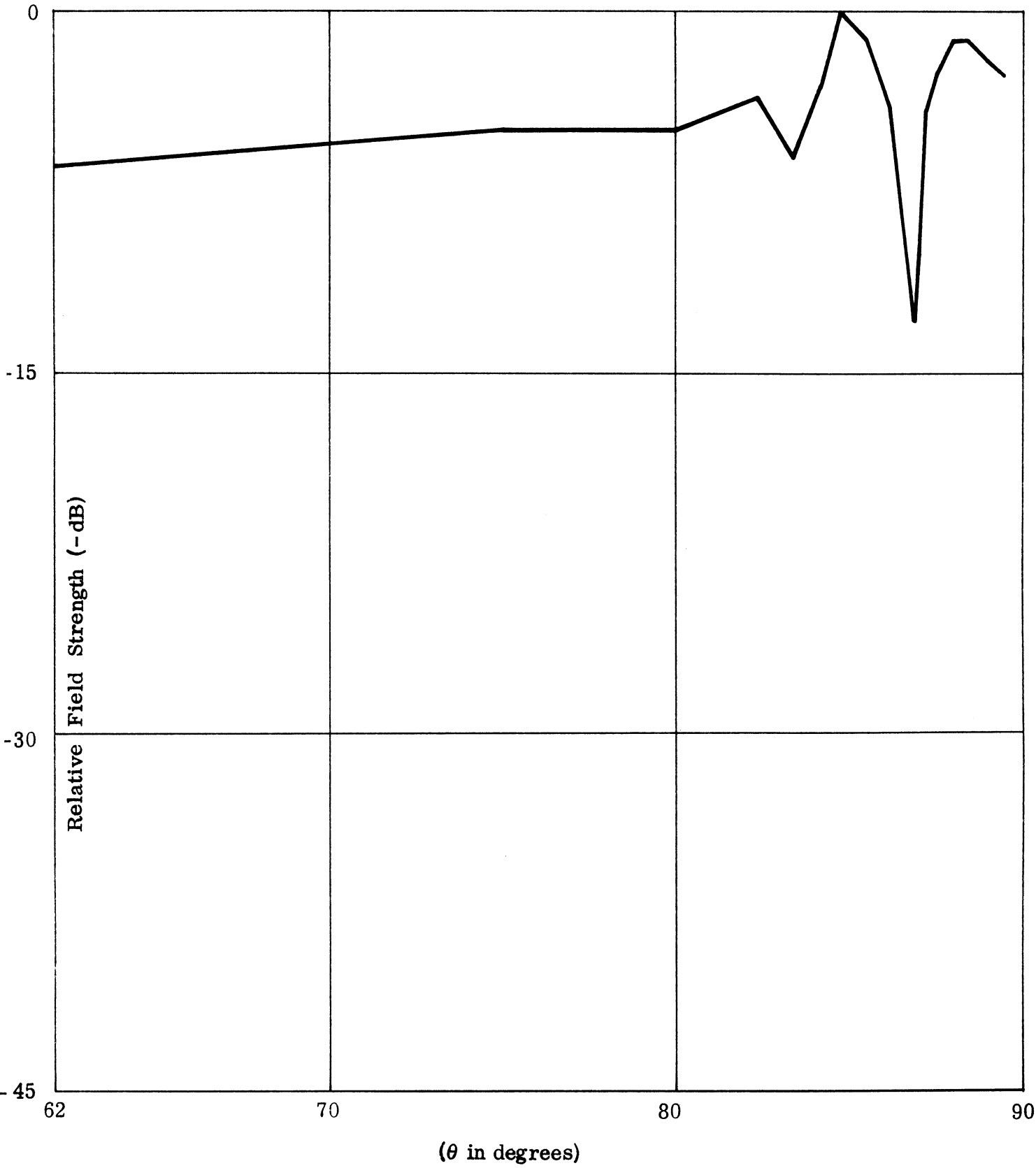

FIG. 9-9: Field Strength for Active Polarizer No. 2 (Mannheim).

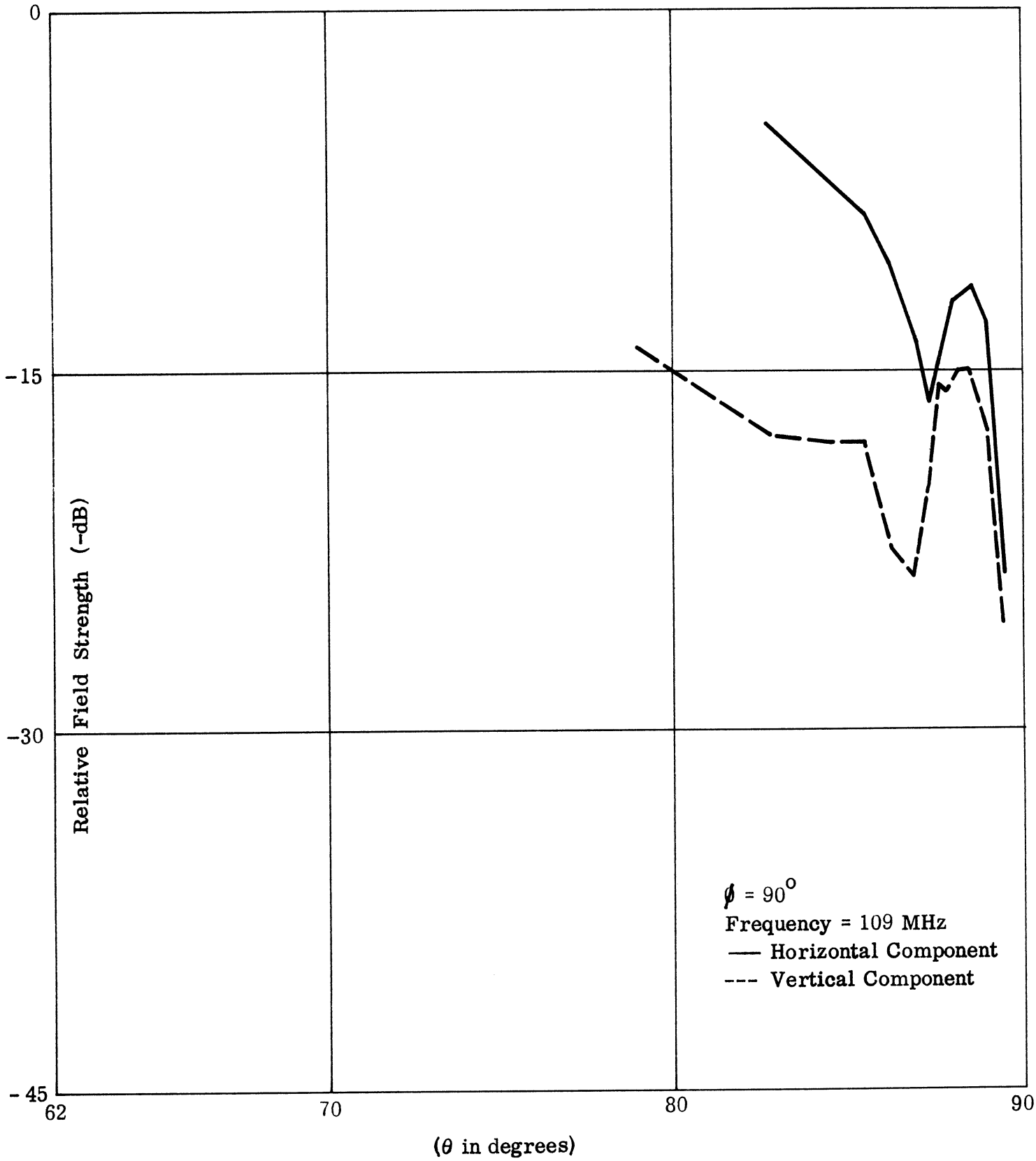

FIG. 9-10: Field Strength for Double Parasitic Loop Counterpoise Antenna System II, (Mannheim Active Polarizer Unexcited).

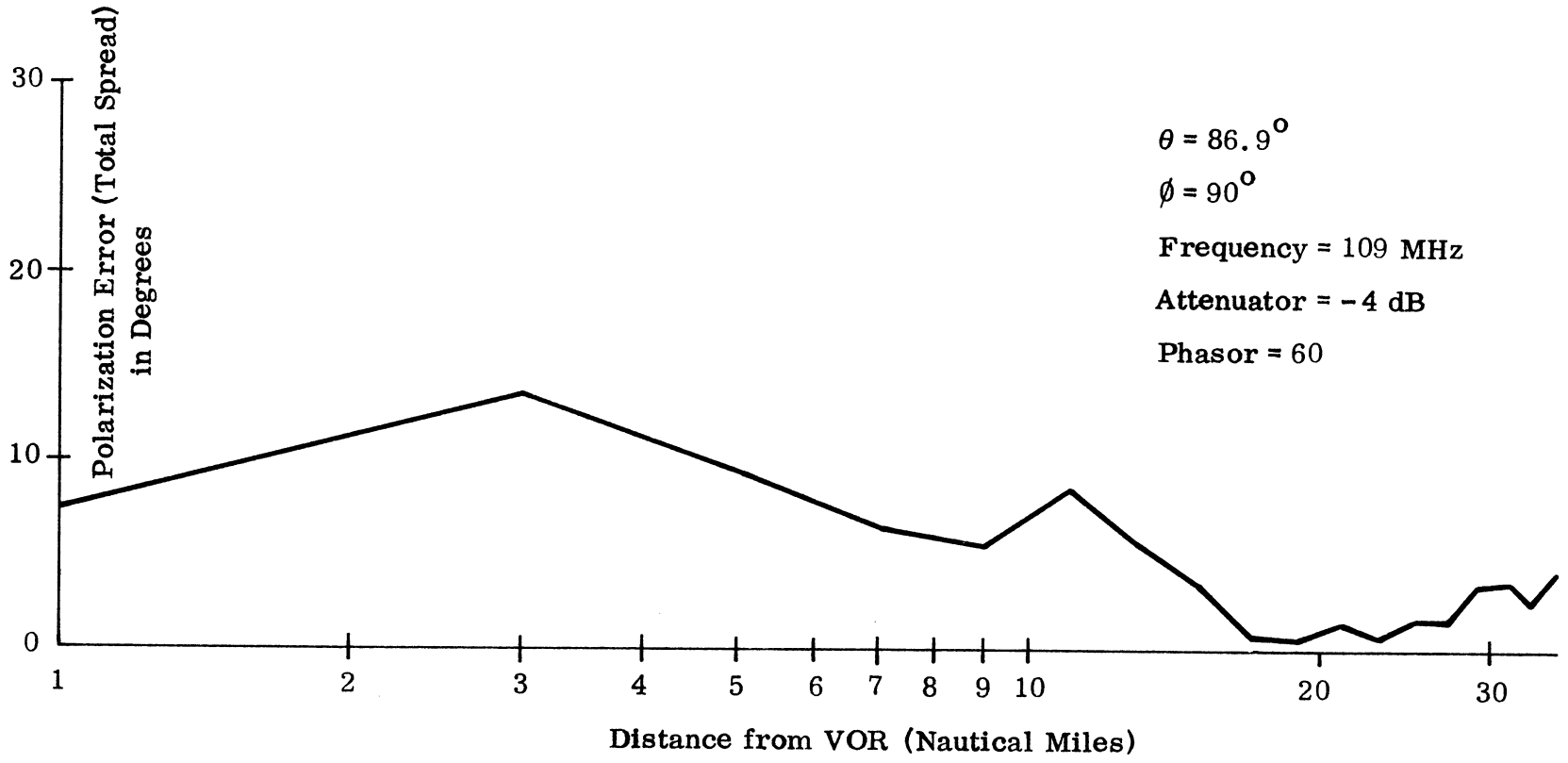

FIG. 9-11: Polarization Error for Double Parasitic Loop Counterpoise Antenna System II (Mannheim/Active Polarizer Excited).

esting to observe that the polarization error is relatively small at low elevation angles, however, as the aircraft approaches the station the polarization error builds up to a maximum of $\pm 6^{o}$, approximately 3 miles from the station. The cause for this buildup is unknown. A suggested cause may be that to fly along the 3.1^{o} depression angle it was necessary for the pilot to have before him the altitudes he should be at as he approached pre-specified mile markers from the Mannheim VOR. These mile markers were the measured horizontal distances of the aircraft from the Mannehim VOR. These data were radioed to the pilot from a precision ground-tracking radar (EAIR) that skin tracked the aircraft. Therefore, it was necessary for the pilot to keep the aircraft in a shallow dive towards the VOR station (by adjusting his altitude at the mile markers) and it is conceivable that as he approached the station he was not able to maintain the proper altitudes necessary to be on the 3.1^{o} slope. It should be noted here that the 3.1^{o} null associated with the horizontally polarized energy radiated by the Mannheim facility is approximately 0.5^{o} wide. As a consequence to ensure that the aircraft remains in the null, it would be necessary for the pilot to adjust his altitude to within $\pm$ 10 percent.

After the settings of the attenuators and phase shifters associated with the active polarizer were established as described in the previous paragraph, several radials were flown while the aircraft was held to a constant altitude of 6575 feet. The purpose of these flights was to determine the manner in which the polarization error varied as a function of the elevation angle. Figures 9-12 a-d show the polarization error as a function of elevation angle for the following radials: $\phi = 90^{o}$, 180^{o}, 220^{o}, and 335^{o}. It is interesting to note that along the 90^{o} radial a minimum in the polarization error does occur at approximately 3^{o} above the horizon. However, outside of this region the polarization error is found to be excessive.

9.6 Discussion

On the basis of the results given in this chapter, it is found that a single FAA passive polarizer is not capable of reducing satisfactorily the polarization errors associated with the double parasitic loop counterpoise antenna system II. A passive polarizer with more than four parasitic elements should be investigated for further reduction of polarization errors in parasitic loop antenna systems. It is also recommended that the parasitic loop system II, with passive polarizer adjusted as in Fig. 9-4, be flight tested for scalloping data. Careful considerations should be given to the use of two passive polarizers in the antenna system. As discussed before, a single polarizer whether active or passive is not likely to do a satisfactory job on the parasitic loop counterpoise VOR antenna system.

With regard to the active polarizer, it can be said that it is relatively easy to adjust the polarization error in the aircraft when the active polarizer is used in the VOR ground station antenna system. It has been shown that using this technique the polarization error can be reduced to a reasonably small value in a

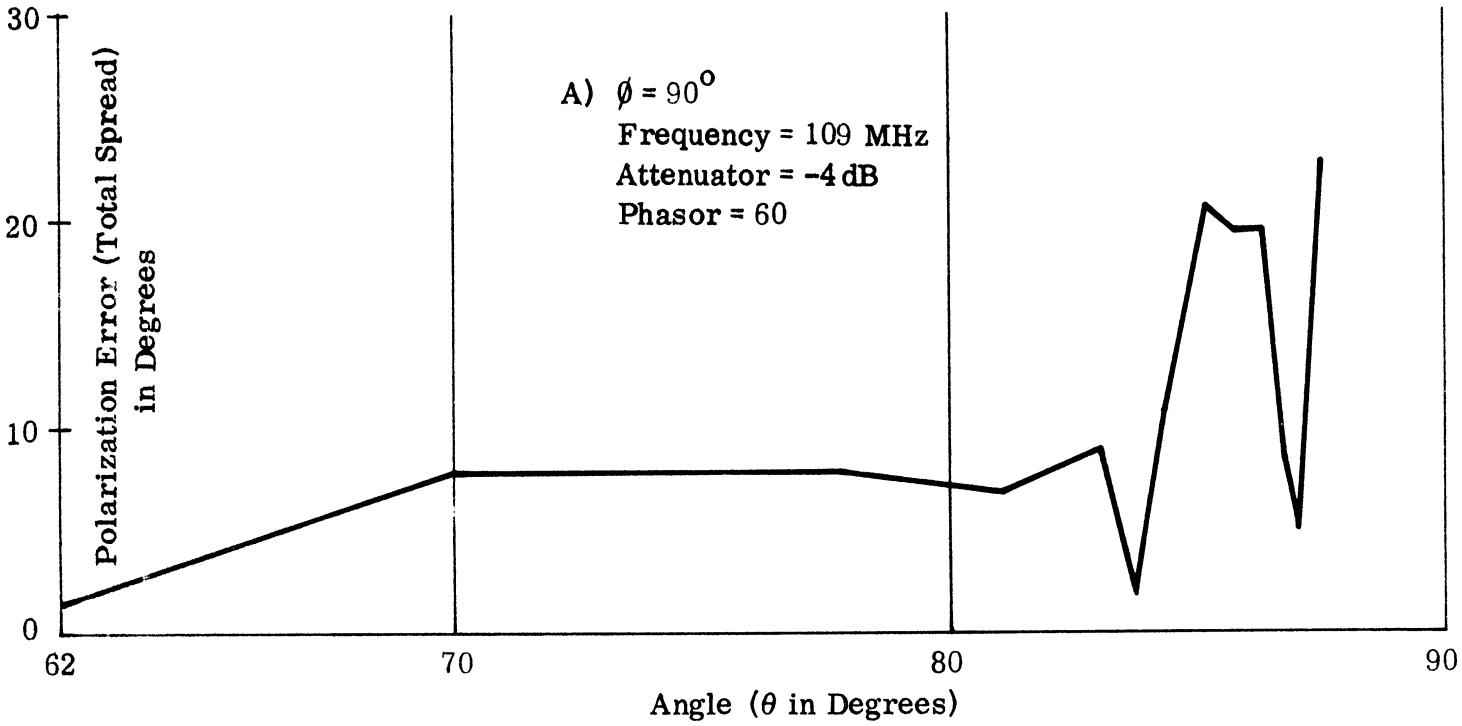

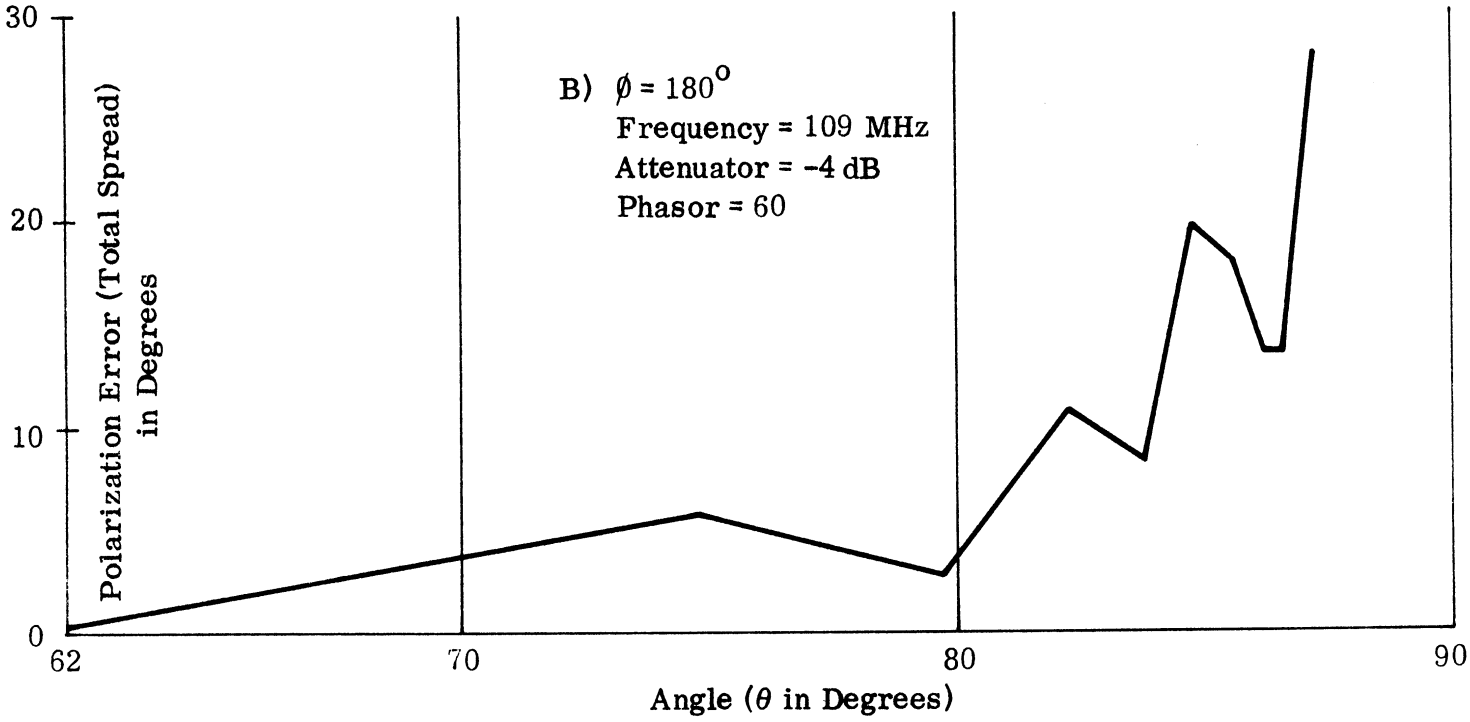

FIG. 9-12a, b: Polarization Error versus Elevation Angle for Double Parasitic Loop Counterpoise Antenna System II (Mannheim, Active Polarizer Excited).

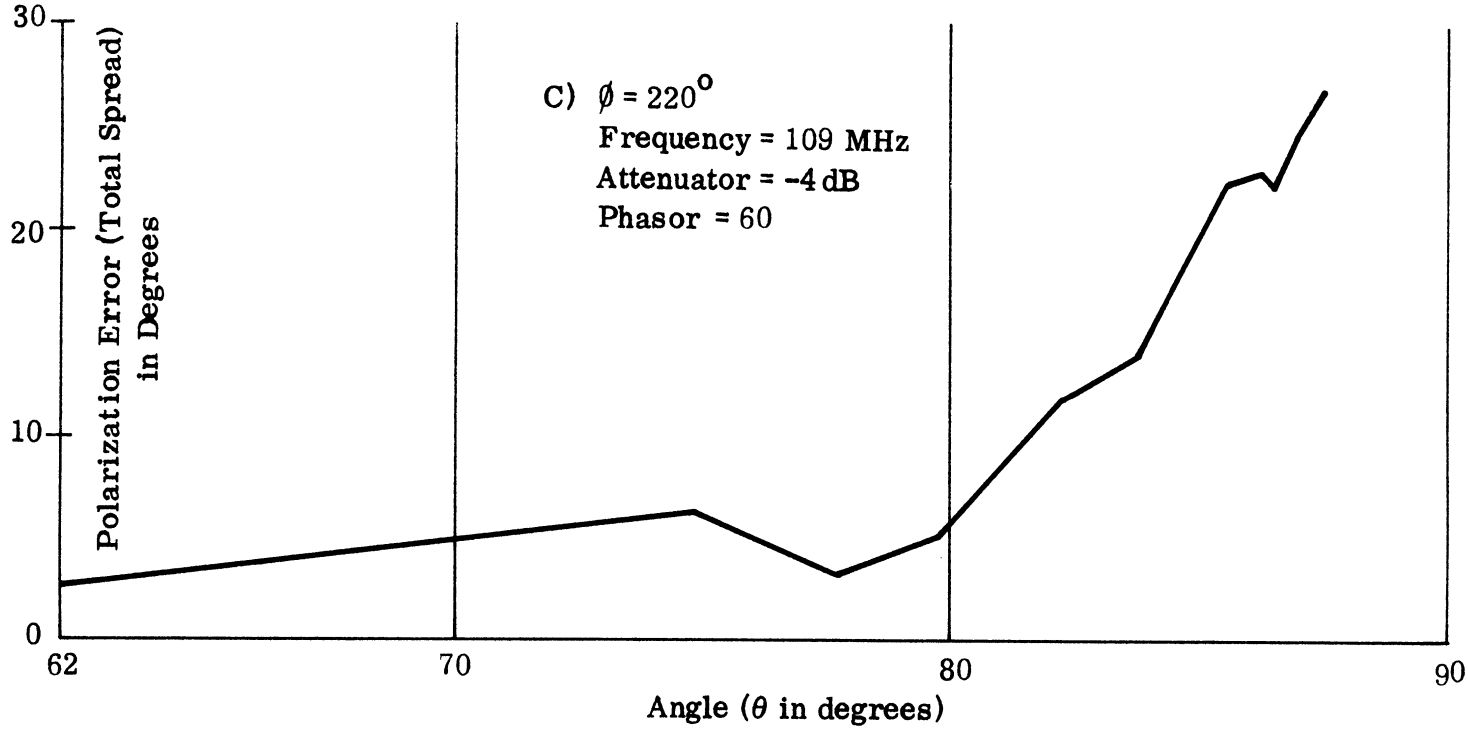

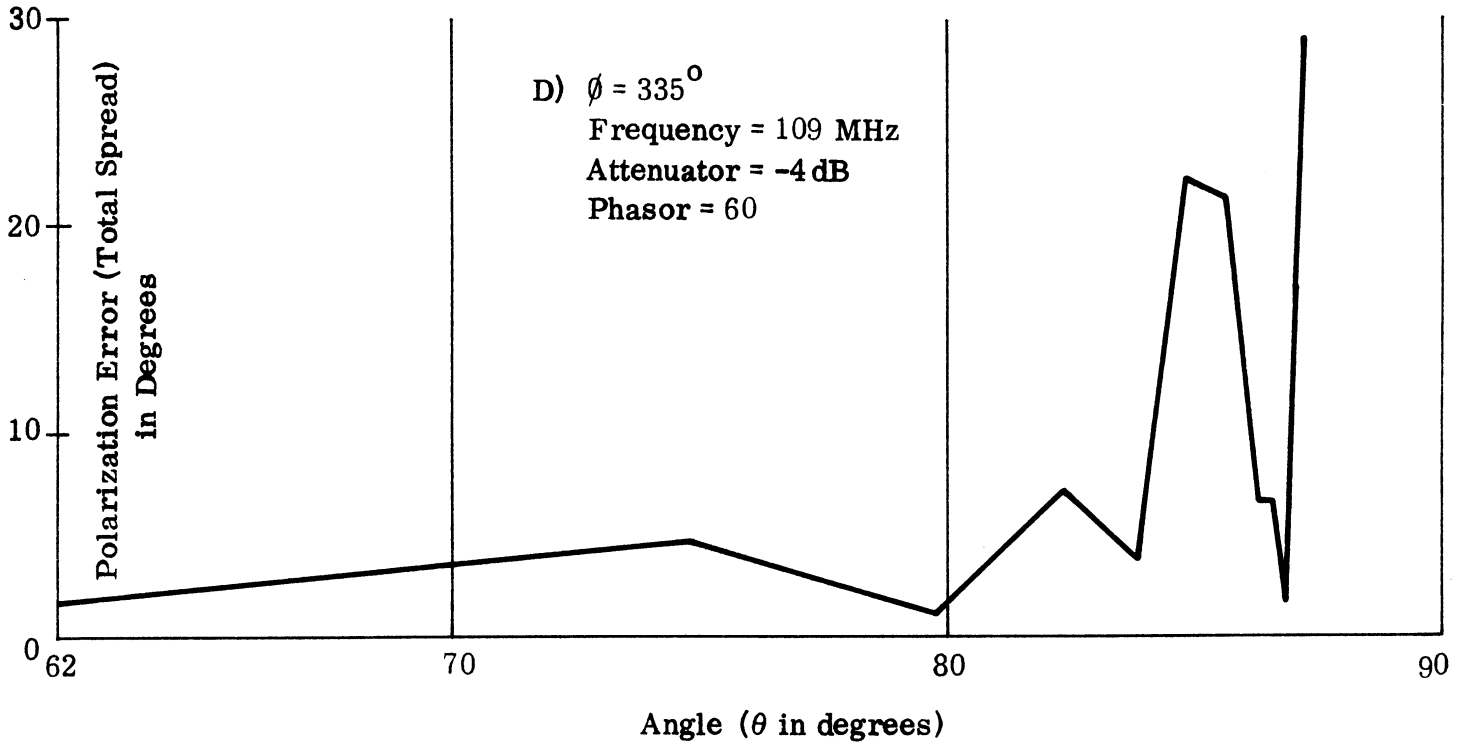

FIG. 9-12c, d: Polarization Error versus Elevation Angle for Double Parasitic Loop Counterpoise Antenna System II (Mannheim, Active Polarizer Excited).

minimum amount of time and with a minimum amount of effort. This was done for one specific vertical angle only. However, the results shown in section 9.5 indicate the existence of large polarization errors in certain directions. Time did not permit us to investigate this problem further. It is believed that insufficient time has been spent working with the polarization problems associated with the parasitic loop counterpoise antenna system. It is thus inappropriate to draw any definite conclusions as to the manner or to what degree the polarization errors could be reduced for a standard VOR system using double parasitic loop counterpoise antennas. It is recommended that tests be continued using the active polarizer. As mentioned in section 9.1, the dominant source of the polarization error is the cross-polarized radiation from the standard VOR antennas. We therefore feel that a theoretical investigation of the cross-polarized radiation fields from standard 4-loop VOR and double parasitic loop counterpoise antennas will be of fundamental importance here. The results of such investigation will be immensely helpful in the proper design and adjustments of a polarizer so that the vertical components of the field produced by the test antenna may be reduced to the desired value.

X

APPLICATION OF PARASITIC LOOP COUNTERPOISE ANTENNA TO VOR SYSTEM

10.1 Introduction

In the previous chapters we have discussed in detail the radiation characteristics of parasitic loop counterpoise antennas. Satisfactory theories have been developed for the radiation fields produced by such antennas operating in carrier and side band modes. These new antennas are compatible with the conventional VOR systems in the sense that a conventional VOR antenna can be converted into the new system by introducing parasitic loops of proper dimensions at the appropriate heights above the counterpoise (Sengupta and Ferris, 1972). We have already seen in Chapter VIII that such a conversion does have some distinct advantages.

In the present chapter we discuss in greater detail the application of parasitic loop counterpoise antennas to conventional VOR systems. It will be shown that such antennas are capable of bringing out superior performance from the existing conventional VOR systems.

10.2 Limitations of Conventional VOR Systems

The performance of a conventional VOR system located in ideal terrain has been discussed in section 1.2. In an actual situation the scattered and/or specular reflections from the ground and other nearby objects (in fact whenever there exists a multipath between the VOR station and the flying aircraft) combine with the desired signals at the aircraft. The overall effect of this is to disturb the direct relationship between the previously mentioned phase difference and the bearing of the aircraft and thereby produce omni-range course scalloping. This causes siting errors and scalloping in the bearing indications of a VOR. Detailed discussions on the scalloping amplitude and frequency under various situations are given by Anderson and Keary (1952).

In general it can be said that the phenomenon of scalloping and associated effects depend mainly on two factors: (i) the free space vertical plane pattern characteristics in the directions near and below the plane of the counterpoise, and (ii) the nature of the scattering properties of the disturbing objects and of the multipath sources. The second factor is more or less beyond the control of the

designer. There are a number of locations where the antenna must be installed at a considerable height above the ground in order to avoid interference from surrounding objects such as heavily wooded or built-up areas (Winnick and Brandewie, 1970). In such cases, the first factor, i.e. the vertical plane antenna pattern characteristics near the horizon become quite important in determining the accuracy of the existing conventional VOR bearing indications.

From the viewpoint of scalloping effects, the ideal requirement on the free space vertical plane pattern of a VOR antenna would be such that the response of the antenna goes abruptly to zero in all directions below the horizon, i.e. the field gradient at the horizon would be infinite. As mentioned before, the field gradient obtainable from existing conventional VOR antennas using 52' diameter counterpoises is about $3dB/6^{o}$ which may be considered to be rather low. This is the fundamental reason why an elevated conventional VOR stations located in non-ideal terrain tend to produce inaccurate results in the presence of multipath signals.

Another undesirable phenomenon that is encountered in a conventional VOR is the appearance of nulls in the vertical plane patterns of such antennas elevated above ground. Assuming a perfectly conducting infinite ground plane, it is easy to show that for the horizontal polarization due to reflection from the ground there will appear some minima and maxima in the vertical plane patterns. The number of these minima (or maxima) will depend on the height of the antenna above the ground. Depending on the free space elevation pattern of the antenna, some of these minima in the pattern may in some cases actually become nulls. It is quite straightforward to show that the radiation from the antenna in directions below the horizon are mainly responsible for such minima or nulls in the pattern. Usually the minimum in the pattern nearest the horizon is deepest. Siting errors and scalloping effects become most intense in these null directions. It is again obvious that such undesirable effects are produced by the conventional VOR system because of the unfavorable vertical plane characteristics of the antenna near the horizon.

10.3 Application of Parasitic Loop Counterpoise Antennas

It is evident from the discussions given in the previous section that an antenna having a large field gradient, if incorporated into the present-day conventional VOR system, would produce at least two-fold improvement in the overall system performance: (i) it would reduce the multipath signals caused by scattering objects in the vicinity of the VOR station, and (ii) it would reduce the depths of the minima that appear in the vertical plane patterns of a VOR antenna above a perfectly conducting ground plane and thereby improve the accuracy of the system.

As mentioned before, the field gradient of a conventional VOR antenna with a 52' diameter counterpoise is about 3dB/6°. A much larger field gradient is necessary if one desires to obtain better performance from the system. Theoretically it is possible to improve this gradient by increasing the diameter of the counterpoise (Sengupta and Ferris 1970). This increase is very slow, e.g. as discussed in Chapter II, the field gradient of a similar antenna with a 150' diameter counterpoise is about 5.5dB/6°. Such a technique of improving is thus considered to be unwieldy mechanically and expensive.

From the discussions of the radiation characteristics of parasitic loop counterpoise antennas given in Chapters III, IV and VII, we single out the following two properties of an optimum double parasitic loop counterpoise antenna:

1) the antenna is capable of producing a field gradient of about 23dB/6° at the horizon. This field gradient is much larger than that of a conventional VOR antenna.

2) the side band mode vertical plane pattern of a double parasitic loop counterpoise antenna above a perfectly conducting ground has a 3dB minimum near the horizon whereas for the conventional antenna the depth of the corresponding minimum is about 10dB for the given height of the antennas above ground.

Thus it can be said beyond any doubt that an optimum double parasitic loop counterpoise antenna when used in a conventional VOR system will greatly reduce the scalloping and other associated errors that appear in the bearing indications of a flying aircraft. This should be weighted against possible decrease in distance range at low altitudes. An additional advantage of the parasitic loop concept is that it provides a way for easy and inexpensive modifications of the existing VOR antennas to obtain a large gradient performance.

10.4 Discussion

In the above we have discussed briefly the performance of existing VOR systems and their limitations under unfavorable siting conditions. It has been clearly demonstrated that an optimum double parasitic loop counterpoise antenna would greatly improve the performance of the existing conventional VOR system located in environments where multipath propagation of some kind exists. On the basis of the results discussed in chapter VIII, it can be concluded that such an antenna located 75' above ground will reduce the scalloping errors of a conventional VOR system by a factor of 6 to 1. Thus, on a given site if it is

necessary to mount the VOR antenna on a tower, the use of parasitic loop counterpoise antennas will give superior performance. However, the polarization errors associated with the antenna has been found to be large. As mentioned in chapter IX, efforts should be devoted to reduce the polarization error so that the new antenna system may be brought into use in a practical standard VOR system.

XI

CONCLUSIONS AND RECOMMENDATIONS

11.1 Conclusions

The radiation fields produced by conventional VOR and parasitic loop counterpoise antennas have been investigated both theoretically and experimentally. Theoretical expressions for the side band mode radiation patterns produced by conventional Alford loop counterpoise VOR antennas and by single parasitic loop counterpoise antennas have been obtained by applying the concepts of geometrical theory of diffraction and the results of Sommerfeld's theory of half-plane diffraction. Within the range of approximation the agreement between theory and experiment has been found to be very good.

The theory of double parasitic loop counterpoise antennas has been developed by generalizing the above theory for single parasitic loop systems and by taking into account the effects of mutual interaction between the parasitic loops. It has been found that if the separation between the parasitic loops is larger than a wavelength, the mutual interaction effects may be neglected. The agreement between theory and experiment has been found satisfactory within the range of approximation.

On the basis of theoretical parametric studies of the double parasitic loop counterpoise antenna patterns, we have developed two optimum antennas using 150' and 52' diameter counterpoises. The antennas have been optimized in the sense that the free space side band mode elevation plane patterns possess maximum field gradient at the horizon. Theoretical optimum field gradients have been found to be about $23dB/6^{o}$ in both cases. These findings have been confirmed by results obtained from model measurements.

The design and the method of mechanical implementation of a full scale optimum double parasitic loop antenna with 150' diameter counterpoise have been carried out. The conventional VOR antenna at NAFEC has been transformed into the above optimum system by installing two parasitic loops at appropriate places. The performance of this new antenna has been tested by ground and flight measurements at 109 MHz. The results of the full scale measurements have verified the validity of the design procedure used and have confirmed the predictions arrived at from theoretical considerations.

Finally, this new VOR antenna system has been flight tested in order to compare its performance with that of a conventional VOR antenna. It has been found that the new antenna system reduces the scalloping errors in the bearing

indications of a flying aircraft by a factor of 6 to 1. The distance range of the VOR station with a new antenna has been found to be comparable to that of the same station using a conventional antenna.

Although the polarization errors associated with the parasitic loop system have been found to be large in directions of $\theta > 80^{o}$, we believe that this error can be reduced to acceptable limits by improving the existing passive polarizer and by adding an active polarizer.

We have discussed only the essential flight test results which are pertinent to the application of double parasitic loop counterpoise antennas to a standard VOR system. Further discussions of the flight test results will be given in a separate report by FAA.

It is concluded that a properly designed double parasitic loop counterpoise antenna will greatly improve the accuracy of conventional VOR systems. Where the terrain surrounding the VOR station is not ideal, the use of such an antenna mounted at a proper height will definitely bring out superior performance from the system.

The most significant contributions and findings of the present research are enumerated below.

1) Development of an accurate theory for conventional VOR antenna radiation patterns.

2) Development of satisfactory theory of double parasitic loop counterpoise antenna patterns and the optimization of such antennas with regard to the horizontal field gradient characteristics.

3) Demonstration of the fact that optimum double parasitic loop counterpoise antennas definitely reduce by a significant amount the scalloping errors associated with conventional VOR systems located in a non-ideal environment. In such situtations, therefore, we feel that the use of a double parasitic loop counterpoise antenna rather than the conventional antenna should be seriously considered.

We therefore conclude that the purpose of the present investigation as given in Chapter I has been fulfilled.

11.2 Recommendations for Further Work

Although we have discussed in detail the radiation characteristics of parasitic loop counterpoise antennas and the application of specific antenna configuration to a conventional VOR system, we feel that further work should be done to exploit the parasitic loop concept to the fullest extent. In particular we recommend the following.

1) Investigate the double (or multiple) parasitic loop counterpoise antennas when the parasitic loops are located in the same plane. In certain cases this configuration may be preferable mechanically.

2) It is conceivable that desirable performance may be obtained from a VOR antenna with smaller counterpoise by judiciously placing one or more parasitic loops above it. Reduced size counterpoise will provide definite advantages in many cases.

3) Investigate the radiation characteristics of an array of parasitic loops with VOR Alford loops (or loop) as the only excited element and having no counterpoise.

4) The polarization error associated with a conventional VOR system using double parasitic loop counterpoise antennas should be studied further.

5) The general application of large gradient antennas to VOR systems under various situations should be investigated in further detail.

Since our polarization error studies are incomplete, we strongly recommend that the item (4) above be investigated further before making a final evaluation and judgement on the application of double parasitic loop counterpoise antennas to a conventional VOR system.

ACKNOWLEDGMENT

We are pleased to acknowledge the benefit of several helpful discussions with Mr. Sterling R. Anderson and we acknowledge also the valuable counsel and suggestions by Professor Ralph E. Hiatt. Our thanks are due to Mr. E. Bublitz for his help in carrying out the model measurements and in the construction and assembly of the full scale antenna. We also wish to acknowledge the work of Dr. A. T. Lin who prepared the computer programming for this report. Finally, we are grateful to the Federal Aviation Administration for making available their experimental facilities at NAFEC and for providing assistance during the full scale measurements. The cooperation and help obtained from Mr. S. Taggart and Mr. E. Lind at NAFEC are gratefully acknowledged.

REFERENCES

Anderson, S.R., H.F.Keary and W.L.Wright (June 1953), The Four-Loop VOR Antenna, T.D.Report No.210, Civil Aeronautics Administration Technical Development and Evaluation Center, Indianapolis, Ind.

Anderson, S.R. (1965), "VHF Omnirange Accuracy Improvements," IEEE Trans., AME-12, No. 1, pp. 26-35.

Anderson, S.R. and H.F.Keary (1952), "VHF Omnirange Wave Reflections from Wires," Civil Aeronautics Administration Technical Development Report No. 121, Technical Development and Evaluation Center, Indianapolis, Ind.

Federal Aviation Administration, Department of Transportation (1968), Handbook: VOR/VORTAC Siting Criteria, No. 6700.11, Systems Research and Development Service, Washington, D.C.

Hurley, H.C., S.R.Anderson and H.F.Keary (1951), "The Civil Aeronautics Administration VHF Omnirange," Proc.IRE, 39, No. 12, pp. 1506-1520.

Keller, J.B. (1962), "Geometrical Theory of Diffraction," J.Opt.Soc.Amer., 52, No. 2, pp. 116-130.

Sengupta, D.L. and J.E.Ferris (1970), "On the Radiation Patterns of Parasitic Loop Counterpoise Antennas," IEEE Trans., AP-18, No. 1, pp. 34-41.

Sengupta, D.L. and J.E.Ferris (1970a), "VOR Parasitic Loop Counterpoise Systems-II," The University of Michigan Radiation Laboratory Report 3051-3-T, Interim Report.

Sengupta, D.L. and J.E.Ferris (1971), "VOR Parasitic Loop Counterpoise-II." Interim Report No. 6, Contract FA69-WA-2085, Project 330-001-03N, The University of Michigan Radiation Laboratory Report 3051-6-T.

Sengupta, D.L. and J.E.Ferris (1972), "A Double Parasitic Loop Counterpoise Antenna and its Application to Aircraft Navigation Systems", IEEE Trans. AP-20, No. 1, pp. 97-99.

Sengupta, D.L. (1971), "Theory of VOR Antenna Radiation Patterns," IEE London, Vol. 7, No. 15, pp. 418-420.

Sengupta, D.L., J.E. Ferris and V.H. Weston (1968), "Theoretical and Experimental Investigation of Parasitic Loop Counterpoise Antennas," The University of Michigan Radiation Laboratory Report 8905-1-F, FAA Report SRDS RD-68-50.

Sengupta, D.L. and V.H. Weston (1968), "A New VOR Antenna System," Proc. IEEE 56, No. 7, pp. 1284-1286.

Sengupta, D.L. and V.H. Weston (1969), "Investigation of the Parasitic Loop Counterpoise Antenna," IEEE Trans., AP-17, No. 2, pp. 180-191.

Sommerfeld, A. (1954), Optics, Academic Press, New York, pp. 247-265.

Westman, V. (1956), Reference Data for Radio Engineers, Fourth Edition, pp. 696-698.

Winick, A.B. and D.M. Brandwie (1970), "VOR/DME System Improvements," Proc. IEEE, 58, No. 3, pp. 430-437.

APPENDIX A

THE RADIATION FIELD OF A CIRCULAR LOOP CARRYING A NON-UNIFORM HARMONIC CURRENT

A. 1 Introduction

The radiation field produced by a circular loop carrying a non-uniform current is discussed theoretically in this appendix. The problem under investigation has direct bearing on the determination of the radiation field of a parasitic loop counterpoise antenna with a figure-of-eight type of excitation in the azimuthal plane. This type of excitation is used in the double parasitic loop counterpoise antenna operating in the side band mode. The non-uniform excitation causes the induced currents in the parasitic loops to be non-uniform. The performance of parasitic loop counterpoise antennas with non-uniform excitation cannot be explained by the theory developed for similar antennas with omnidirectional excitation.

A. 2 Nature of Excitation

In a practical VOR antenna system, the figure-of-eight pattern in azimuth is obtained by placing two Alford loops side by side and exciting them with equal but out of phase signals. Let us consider two small circular loops (i.e. radius of the loop $<<\lambda$) carrying the currents of the form

$$I_o e^{-i\omega t} \quad \text{and} \quad I_o e^{-i(\omega t+\psi)} \tag{A. 1}$$

be oriented along the x-axis as shown in Fig. A-1. The two loops lie in the x-y plane. The two loops are separated by a distance 2d and the phase difference ψ between their currents is kept arbitrary for the present. It can be shown that the far field produced by the system at the point $P(R_o, \theta, \phi)$ is polarized in the ϕ-direction and is given by:

$$E_\phi = \eta_o I_o \left(\frac{ka}{2}\right)^2 \frac{e^{i(kR_1 - \frac{\psi}{2})}}{R_o} 2 \sin\theta \cos\left[kd \sin\theta \cos\phi + \frac{\psi}{2}\right] \tag{A. 2}$$

where

η_o is the intrinsic impedance of free space,

$k = 2\pi/\lambda$ is the propagation constant in free space.

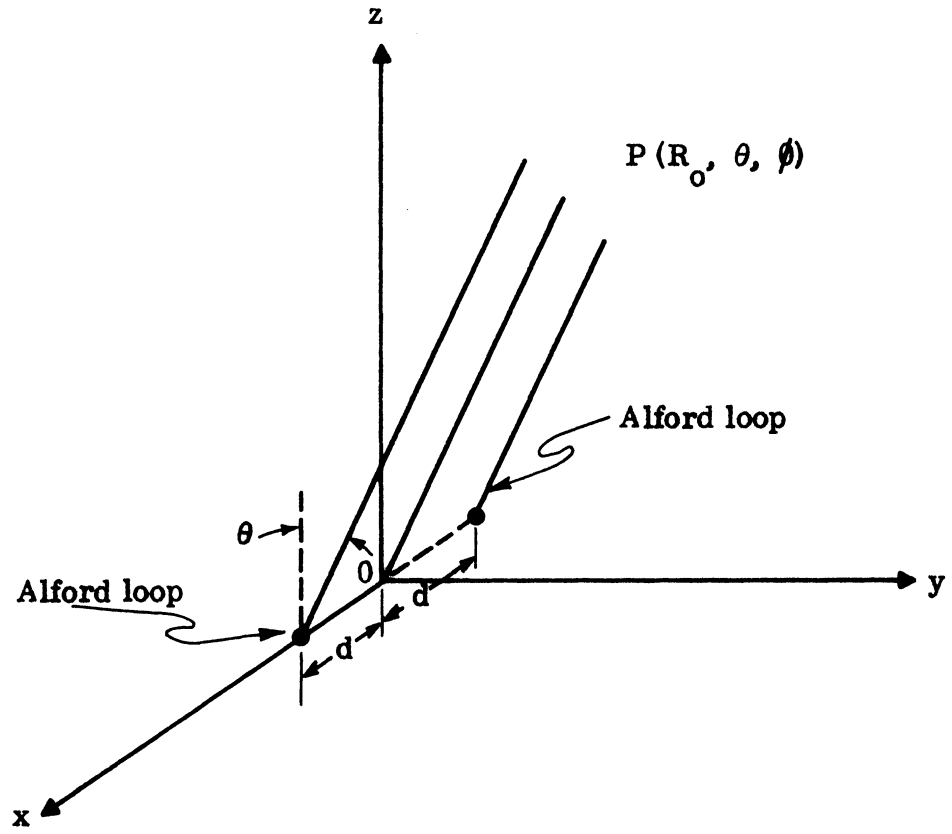

FIG. A-1: Coordinate System Used.

If $\psi = \pi$, then eq. (A. 2) reduces to

$$E_\phi = i2\eta_o I_o \left(\frac{ka}{2}\right)^2 \frac{e^{ikR_o}}{R_o} \sin\theta \sin\left[kd \sin\theta \cos\phi\right] . \qquad (A.3)$$

Equation (A. 3) indicates that in the azimuthal plane (θ=constant) the far field pattern is a figure-of-eight having maxima along ϕ=0 and π. Usually $kd \ll 1$ and under this assumption we can simplify (A. 3) as follows:

$$E_\phi = i2\eta_o \left(\frac{ka}{2}\right)^2 \frac{e^{ikR_o}}{R_o} (kd) \sin^2\theta \cos\phi . \qquad (A.4)$$

Any parasitic loop placed with its axis along the z-axis will carry an induced current proportional to the field given by (A. 4) or (A. 3) as the case may be. To simplify our analysis we assume that the parasitic current in the present case is of the form:

$$I = I_o \cos \phi \,, \tag{A.5}$$

where I_o is a constant and ϕ is measured around the loop, the origin being at the x-axis. Equation (A.5) physically means that $I(\phi)$ vanishes at $\phi = \pm \pi/2$, where it reverses direction, so that the currents in the range

$$-\frac{\pi}{2} \leq \phi \leq \frac{\pi}{2}$$

are always counterclockwise when the currents in the range

$$\frac{\pi}{2} \leq \phi \leq \frac{3\pi}{2}$$

are clockwise. This may be looked upon as a dipole mode such that the charge density on the loop is $q(\phi) \propto \sin\phi$. This means that the loop is oppositely charged at $\phi=\pi/2$ and $\phi = -\pi/2$ and the current oscillates in synchronism on the two halves much as in two parallel dipoles that are driven in phase. Notice that this is true regardless of the fact whether the parasitic loop is large or small.

A.3 Far Field Expressions

In this section we obtain the far field produced by a circular loop carrying a current of the form given by eq. (A.5). The loop is oriented in the x-y plane as shown in Fig. A-2. To obtain the far field it is convenient to determine the vector potential $\bar{A}$ produced by the current at the far field point $P(R_o, \theta, \phi)$ and then obtain the field from the potential. With time dependence $e^{-i\omega t}$ and using standard notation the following expressions define the relationships between the fields and the vector potential.

$$\bar{E} = -i\omega \hat{r}_o \times (\hat{r}_o \times \bar{A}) = i\omega \left[\hat{\theta} A_\theta + \hat{\phi} A_\phi\right] \,, \tag{A.6}$$

$$\bar{B} = ik\,(\hat{r}_1 \times \bar{A}) = ik\left[\hat{\phi} A_\theta - \hat{\theta} A_\phi\right], \tag{A.7}$$

where r_o, $\hat{\theta}$, $\hat{\phi}$ are the unit vectors in R_o, θ and ϕ directions respectively. The components A_θ and A_ϕ of the vector potential in terms of the rectangular components are:

$$A_\theta = \left[A_x \cos\phi + A_y \sin\phi\right] \cos\theta \,, \tag{A.8}$$

$$A_\phi = -A_x \sin\phi + A_y \cos\phi \,. \tag{A.9}$$

In the present configuration, as shown in Fig. A-2, A_x and A_y are given by the following:

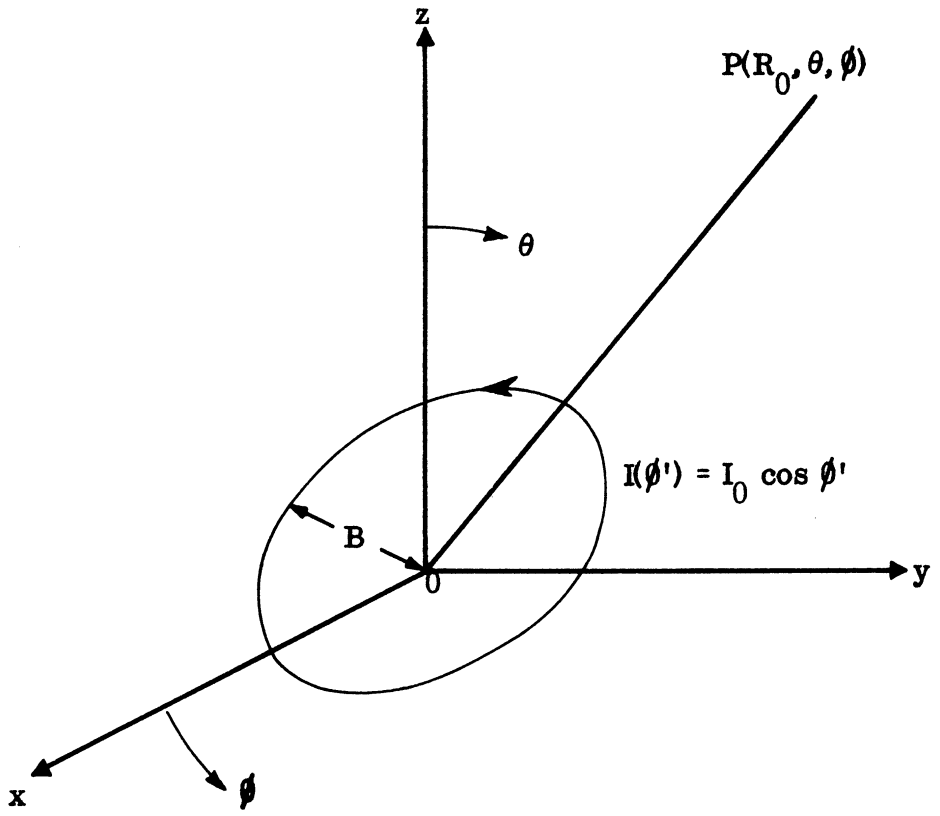

FIG. A-2: Orientation of the circular loop.

$$A_x = -\frac{\mu_o B}{4\pi}\frac{e^{ikR_o}}{R_o}\int_0^{2\pi} I(\phi')e^{-ik\,B\sin\theta\cos(\phi-\phi')}\sin\phi'\,d\phi' \qquad \text{(A. 10)}$$

$$A_y = \frac{\mu_o B}{4\pi}\frac{e^{ikR_o}}{R_o}\int_0^{2\pi} I(\phi')e^{-ik\,B\sin\theta\cos(\phi-\phi')}\cos\phi'\,d\phi' \qquad \text{(A. 11)}$$

where μ_o is the permeability of free space. After introducing (A. 5) into (A. 10) and (A. 11), the following two equations are obtained:

$$A_x = -\frac{\mu_o BI_o}{8\pi}\frac{e^{ikR_o}}{R_o}\int_0^{2\pi} e^{-ik\,B\sin\theta\cos(\phi-\phi')}\sin 2\phi'\,d\phi', \qquad \text{(A. 12)}$$

$$A_y = \frac{\mu_o B I_o}{8\pi} \frac{e^{ikR_o}}{R_o} \int_0^{2\pi} e^{-ikB\sin\theta\cos(\phi-\phi')} (1+\cos 2\phi')\, d\phi' \quad . \tag{A.13}$$

To evaluate the integrals in (A. 12) and (A. 13), we make use of the following result:

$$\int_0^{2\pi} e^{i(n\pm 1)\phi'} e^{ikB\sin\theta\cos(\phi-\phi')}\, d\phi' = 2\pi i^{n\pm 1} e^{i(n\pm 1)\phi} J_{n\pm 1}(kB\sin\theta) \quad , \tag{A.14}$$

where $J_{n\pm 1}$ is the standard notation for the Bessel function of the first kind. Using (A. 14), we obtain the following from (A. 12) and (A. 13).

$$A_x = \frac{\mu_o B I_o}{4} \frac{e^{ikR_o}}{R_o} J_2(kB\sin\theta)\sin 2\phi \quad , \tag{A.15}$$

$$A_y = \frac{\mu_o B I_o}{4} \frac{e^{ikR_o}}{R_o} \left[J_0(kB\sin\theta) - J_2(kB\sin\theta)\cos 2\phi\right] \quad . \tag{A.16}$$

After introducing (A. 15) and (A. 16) into (A. 8) and (A. 9) and with some algebraic manipulation, we obtain

$$A_\theta = \frac{\mu_o B I_o}{2} \frac{e^{ikR_o}}{R_o} \frac{J_1(kB\sin\theta)}{(kB\sin\theta)} \cos\theta \sin\phi \quad , \tag{A.17}$$

$$A_\phi = \frac{\mu_o B I_o}{2} \frac{e^{ikR_o}}{R_o} J_1'(kB\sin\theta)\cos\phi \quad , \tag{A.18}$$

where the prime in (A. 18) indicates differentiation with respect to the argument.

Using eq. (A. 6) along with (A. 17) and (A. 18), we obtain the two components of the electric field in the far zone as given by the following:

$$E_\theta = i\eta_o I_o \left(\frac{kB}{2}\right) \frac{e^{ikR_o}}{R_o} \frac{J_1(kB\sin\theta)}{(kB\sin\theta)} \cos\theta \sin\phi \quad , \tag{A.19}$$

$$E_\phi = i\eta_o I_o \left(\frac{kB}{2}\right) \frac{e^{ikR_o}}{R_o} J_1'(kB\sin\theta)\cos\phi \quad . \tag{A.20}$$

With uniform current, a circular loop does not produce any θ-component of the electric field. Thus, the existence of E_θ in the present case is attributed to

the non-uniform current carried by the loop. Equations (A. 19) and (A. 20) have been used in Section 3. 4 to derive the far field produced by a non-uniformly excited single parasitic loop counterpoise antenna.

A. 4 Discussion

On the basis of eqs. (A. 19) and (A. 20), we make the following comments with regard to the radiation field produced by a circular loop carrying a non-uniform current $I=I_o\cos\phi$.

(i) Near $\theta\sim 0^o$ the Bessel functions in (A. 19) and (A. 20) may be replaced by their small argument values, i.e. $J'(x) \simeq 1/2$ and $J_1(x) / x \sim 1/2$. Thus the total far field may be written as

$$\bar{E}=\hat{\theta}E_\theta+\hat{\phi}E_\phi \simeq i\eta_o I_o\left(\frac{kB}{2}\right)\frac{e^{ikR_o}}{R_o}\ \frac{1}{2}\left(\hat{\theta}\cos\theta\sin\phi+\hat{\phi}\cos\phi\right)$$

$$= i\eta_o I_o\left(\frac{kB}{2}\right)\frac{e^{ikR_o}}{R_o}\ \frac{1}{2}\hat{y}\ . \qquad (A.21)$$

Equation (A. 21) means that near the axial region of space ($\theta\sim 0^o$) the far electric field is not equal to zero and it is polarized along the y-direction.

(ii) In the $\phi=0^o$ plane, i.e. in the vertical plane containing the directions of maxima of the figure-of-eight excitation, the field is polarized in the ϕ-direction and is given by:

$$E_\theta \equiv 0\ , \qquad E_\phi = i\eta_o I_o\left(\frac{kB}{2}\right)\frac{e^{ikR_o}}{R_o}\ J_1'(kB\sin\theta)\ . \qquad (A.22)$$

(iii) In the $\phi = \pi/2$ plane, i.e. in the vertical plane containing the directions of minima of the figure-of-eight excitation, the horizontal (i.e. ϕ-component) component of the electric field is identically equal to zero and the electric field is given by

$$E_\phi \equiv 0\ , \qquad E_\theta = i\eta_o I_o\left(\frac{kB}{2}\right)\frac{e^{ikR_o}}{R_o}\ \frac{J_1(kB\sin\theta)}{(kB\sin\theta)}\cos\theta\ ,. \qquad (A.23)$$

(iv) In the $\phi = \pi/4$ plane

$$E_\theta = i\eta_o I_o\left(\frac{kB}{2}\right)\frac{e^{ikR_o}}{R_o}\ \frac{J_1(kB\sin\theta)}{(kB\sin\theta)}\ \frac{\cos\theta}{\sqrt{2}}\ , \qquad (A.24)$$

$$E_{\phi} = i\eta_o I_o \left(\frac{kB}{2}\right) \frac{e^{ikR_o}}{R_o} \frac{J_1'(kB \sin\theta)}{\sqrt{2}} \quad . \tag{A.25}$$

(v) In the horizontal plane ($\theta = \pi/2$),

$$E_{\theta} \equiv 0 \,, \qquad E_{\phi} = i\eta_o I_o \left(\frac{kB}{2}\right) \frac{e^{ikR_o}}{R_o} J_1' (kB)\cos\phi \quad . \tag{A.26}$$

The important findings of the present investigation are that the non-uniformity of the current in the circular loop produces the following two effects: (i) the field is non-zero in the axial direction, and (ii) there exists a cross-polarized component of the field. It is thus anticipated that a parasitic loop counterpoise antenna operating in the side band mode may give rise to appreciable amounts of cross-polarized components in certain directions of space. The results given here will be found useful in the analysis of the cross-polarization characteristics of parasitic loop counterpoise antenna systems.

APPENDIX B

MUTUAL COUPLING EFFECTS IN PARASITIC LOOP COUNTERPOISE ANTENNAS

B. 1 Introduction

This appendix deals with the theoretical investigation of mutual coupling effects in a double parasitic loop counterpoise antenna. In Chapter IV an approximate theory was developed for the double parasitic loop counterpoise antenna by neglecting the effects of mutual coupling. There, the far field radiation pattern produced by the antenna was obtained by simply superposing individual free space fields. This theory explains with a fair amount of accuracy the far field for the cases when the spacing between the parasitic elements is large compared to wavelength. In a situation where the loops are not widely spaced, the interaction between the parasitic currents may become quite important. It is the purpose of this appendix to develop theoretical expressions for the parasitic currents and also for the far field produced by a double parasitic loop counterpoise antenna by taking into account the effects of mutual coupling.

B. 2 Parasitic Currents

Consider a double parasitic loop counterpoise antenna as shown in Fig. B-2. It is assumed that the antenna is operating in the carrier mode.

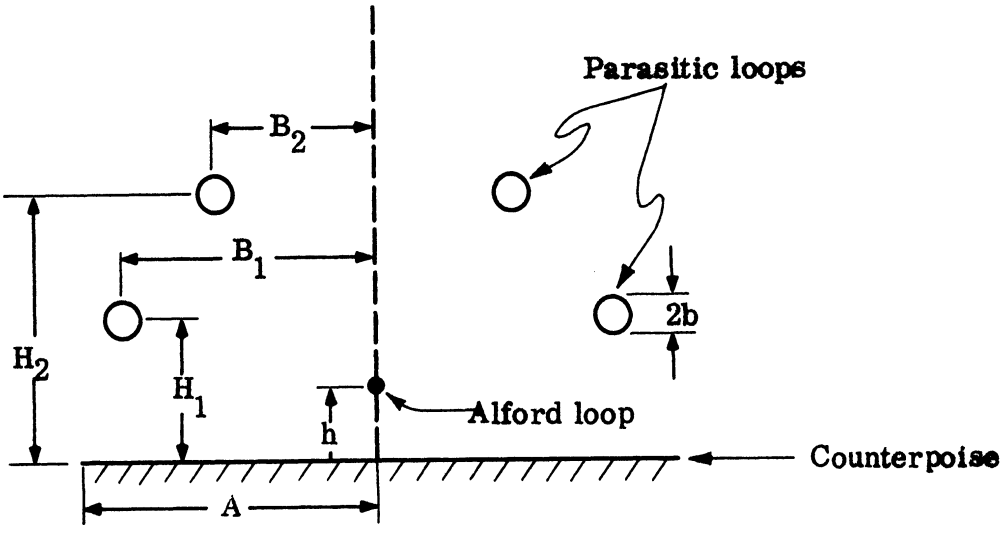

FIG. B-1: Double parasitic loop counterpoise antenna.

The Alford loop situated at a height h above the counterpoise is the only excited element. Let I_1^T and I_2^T be the total currents in the two parasitic loops maintained by the excited element. Symmetry of the system and the nature of the excitation dictate that the distribution of the current along each parasitic element will be constant. Let us assume that in the absence of mutual coupling between the parasitic loops, the induced parasitic currents will be represented by I_1^O and I_2^O respectively. The method of determining I_1^O and I_2^O for the above configuration has been discussed elsewhere (Sengupta et al, 1968). By taking the mutual interaction into account we can write

$$I_1^T = I_1^O + K_{21} I_2^T \tag{B.1}$$

$$I_2^T = I_2^O + K_{12} I_1^T \ , \tag{B.2}$$

where K_{12} and K_{21} may be defined as the coefficients of coupling for the mutually induced currents. Notice that these are not the conventional coefficients of mutual coupling and hence $K_{12} \neq K_{21}$. From (B. 1) and (B. 2) the following are obtained for the parasitic currents.

$$I_1^T = \frac{I_1^O + K_{21} I_2^O}{1-K_{21}K_{12}} \ , \tag{B.3}$$

$$I_2^T = \frac{I_2^O + K_{12} I_1^O}{1-K_{12}K_{21}} \ . \tag{B.4}$$

In general K_{12}, K_{21} are complex constants for a particular configuration of the antenna and $|K_{12}|$, $|K_{21}| < 1$. Thus the problem reduces to the determination of these two coefficients. We discuss this in the next section.

B. 2. 1 Determination of the Coupling Coefficients K_{12}, K_{21}

We outline here the basic mathematical steps involved in obtaining K_{12},. For this purpose we represent the configuration as shown in Fig. B-2. In this representation the first parasitic loop is replaced by a point source of suitable strength placed at a height H_1 above the counterpoise. The current in the first parasitic loop being I_1^T, the field produced by the current at the point P located on the second parasitic loop is given by

$$E_{\phi}^{inc}(P) \simeq \eta_o I_1^T \left(\frac{kB_1}{2}\right) \left[J_1(kB_1 \sin\theta_{12}) \frac{e^{ikr_{12}}}{r_{12}} - J_1(kB_1 \sin\theta'_{12}) \frac{e^{ikr'_{12}}}{r'_{12}} \right], \tag{B.5}$$

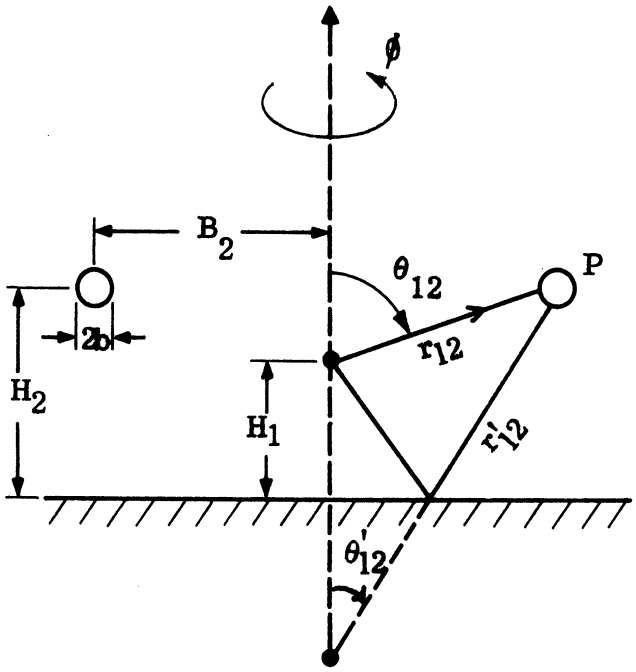

FIG. B-2: Rays contributing to K_{12}.

where

η_o is the intrinsic impedance of free space,
$k = 2\pi/\lambda$ is the propagation constant in free space,

$$r_{12}^2 = B_2^2 + (H_2 - H_1)^2 \; ; \qquad (r'_{12})^2 = B_2^2 + (H_2 + H_1)^2 \tag{B.6}$$

$$\sin\theta_{12} = \frac{B_2}{r_{12}} \; ; \qquad \sin\theta'_{12} = \frac{B_2}{r'_{12}} \; , \tag{B.7}$$

J_1 is the Bessel function of the first kind and first order.

In eq. (B.5) only the direct and reflected fields due to the parasitic current I_1^T are used to obtain the incident field at P produced by this current; the contribution to the field at P due to diffraction effects at the edges of the counterpoise are neglected for the present. If necessary, they will be taken into account later. The current induced on the second parasitic loop due to the field $E_\phi^{inc}(P)$ is obtained by using the following relation.

$$I_2^{T'} \simeq \frac{2\pi}{i\eta_o kM} E_\phi^{inc}(P) \; , \tag{B.8}$$

where

$$M = 0.577 + \ell n \left(\frac{kb}{2}\right) - \frac{i\pi}{2} \; . \tag{B.9}$$

After introducing (B. 5) into (B. 8) we obtain the following expression for K_{12}.

$$K_{12} = \frac{2\pi}{iM}\left(\frac{kB_1}{2}\right)\left[J_1(kB_1\sin\theta_{12})\frac{e^{ikr_{12}}}{kr_{12}} - J_1(kB_1\sin\theta'_{12})\frac{e^{ikr'_{12}}}{kr'_{12}}\right]. \qquad \text{(B. 10)}$$

Following a similar procedure it can be shown that the other coupling coefficient K_{21} is given by:

$$K_{21} = \frac{2\pi}{iM}\left(\frac{kB_2}{2}\right)\left[J_1(kB_2\sin\theta_{21})\frac{e^{ikr_{21}}}{kr_{21}} - J_1(kB_2\sin\theta'_{21})\frac{e^{ikr'_{21}}}{kr'_{21}}\right], \qquad \text{(B. 11)}$$

where

$$r_{21}^2 = B_1^2 + (H_2 - H_1)^2 \; ; \quad (r'_{21})^2 = B_1^2 + (H_2 + H_1)^2 , \qquad \text{(B. 12)}$$

$$\sin\theta_{21} = +\frac{B_1}{r_{21}} \; ; \quad \sin\theta'_{21} = \frac{B_1}{r'_{21}} . \qquad \text{(B. 13)}$$

This completes the derivation of expressions for the coupling coefffcients. In the next section we derive the explicit expressions for the parasitic currents due to the fields produced by the Alford loop carrying a current of magnitude I_o .

B. 2. 2 Expressions for the Parasitic Currents

It can be shown (Sengupta et al, 1968) that in the absence of mutual coupling the current induced in the first parasitic loop is given by

$$I_1^O = I_o\left(\frac{ka}{2}\right)^2\left[P_1 + Q_1\right] , \qquad \text{(B. 14)}$$

where a is the radius of the excited loop and,

$$P_1 = \frac{2\pi(kB_1)}{iM}\left[\frac{e^{ikr_1}}{(kr_1)^2} - \frac{e^{ikr_2}}{(kr_2)^2}\right] , \qquad \text{(B. 15)}$$

$$Q_1 = \frac{\pi^2(kB_1)}{M^2}\,\frac{e^{ikr_1}}{(kr_1)^2}\left[\left(\frac{1}{\pi kB_1}\right)^{1/2} e^{i(2kB_1+\frac{\pi}{4})} - \left(\frac{1}{\pi kH_1}\right)^{1/2} e^{i(2kH_1-\frac{\pi}{4})}\right], \quad \text{(B. 16)}$$

$$r_1^2 = B_1^2 + (H_1-h)^2 \; ; \; r_2^2 = B_1^2 + (H_1+h)^2 \quad . \quad \text{(B. 17)}$$

Similarly, the current induced in the second parasitic loop due to the field produced by the Alford loop only is given by

$$I_2^O = I_o\left(\frac{ka}{2}\right)^2 \left[P_2 + Q_2\right] , \quad \text{(B. 18)}$$

where

$$P_2 = \frac{2\pi(kB_2)}{iM}\left[\frac{e^{ikr_1'}}{(kr_1')^2} - \frac{e^{ikr_2'}}{(kr_2')^2}\right] , \quad \text{(B. 19)}$$

$$Q_2 = \frac{\pi^2(kB_2)}{M^2}\,\frac{e^{ikr_1'}}{(kr_1')^2}\left[\left(\frac{1}{\pi kB_2}\right)^{1/2} e^{i(2kB_2+\frac{\pi}{4})} - \left(\frac{1}{\pi kH_2}\right)^{1/2} e^{i(2kH_2-\frac{\pi}{4})}\right], \quad \text{(B. 20)}$$

$$(r_1')^2 = B_2^2 + (H_2-h)^2 \; ; \; (r_2')^2 = B_2^2 + (H_2+h)^2 \quad . \quad \text{(B. 21)}$$

After using (B. 3), (B. 4), (B. 10), (B. 11), (B. 14) and (B. 18), the parasitic currents I_1^T and I_2^T are obtained as follows:

$$I_1^T = I_o\left(\frac{ka}{2}\right)^2 \cdot \frac{1}{1-K_{12}K_{21}}\left[(P_1+Q_1)+K_{21}(P_2+Q_2)\right] \quad \text{(B. 22)}$$

$$I_2^T = I_o\left(\frac{ka}{2}\right)^2 \frac{1}{1-K_{12}K_{21}}\left[(P_2+Q_2)+K_{12}(P_1+Q_1)\right] \quad . \quad \text{(B. 23)}$$

Equations (B. 22) and (B. 23) are expressed so that they may be computed numerically. It should be noted that in the absence of mutual coupling, (B. 22) and (B. 23) reduce to (B. 14) and (B. 18) respectively.

B. 3 Far Field Expressions

In this section the far field produced by the double parasitic loop counterpoise antenna will be given. The method of obtaining the expressions is similar to that discussed in the case of a single parasitic loop counterpoise antenna (Sengupta and Weston, 1969) and hence will not be repeated here. All the expressions are arranged such that they may be programmed for numerical computation. The ___

far field is expressed formally as :

$$E_{\phi} \sim \eta_o I_o \left(\frac{ka}{2}\right)^2 \frac{e^{i(kR-\frac{\pi}{4})}}{R} S(\theta) \quad , \tag{B.24}$$

where

$$S(\theta) = S^A(\theta) + S_1^P(\theta) + S_2^P(\theta) \quad . \tag{B.25}$$

In the above equations $S(\theta)$ is identified with the complex far field pattern of the antenna; the three terms on the right hand side of (B.25) are the complex far field patterns produced by the Alford loop, the first and second parasitic loops above the counterpoise. Explicit expressions for the three terms in (B.25) are given below for future reference.

$$S^A(\theta) = \left\{ \frac{F^o(\theta)\sin\theta}{2} e^{-ikA\sin\theta} + \frac{|\cos\theta| \sin(\frac{\phi_o}{2})}{\sqrt{\pi k r_o \sin\theta}} e^{ikr_o} L^o(\theta) \right\} , \tag{B.26}$$

$$L^o(\theta) = \frac{e^{i(\frac{\pi}{2}-kA\sin\theta)}}{\sqrt{1-\sin\theta}} \left[\frac{\cos^{3/2}\phi_o - \sin^{3/2}\theta}{\cos\phi_o - \sin\theta} \right] - \frac{e^{ikA\sin\theta}}{\sqrt{1+\sin\theta}} \frac{\cos^{3/2}\phi_o}{\cos\phi_o + \sin\theta} , \tag{B.27}$$

$$F^o(\theta) = e^{ikr_o\sin(\theta-\phi_o)} \int_{-\infty}^{p_1} e^{i\pi\frac{t^2}{2}} dt - e^{ikr_o\sin(\theta+\phi_o)} \int_{-\infty}^{p_2} e^{i\pi\frac{t^2}{2}} dt \quad , \tag{B.28}$$

$$p_1 = 2\left(\frac{kr_o}{\pi}\right)^{1/2} \cos\left(\frac{\phi_o - \theta - \frac{\pi}{2}}{2}\right) , \tag{B.29}$$

$$p_2 = 2\left(\frac{kr_o}{\pi}\right)^{1/2} \cos\left(\frac{\phi_o - \theta + \frac{\pi}{2}}{2}\right) , \tag{B.30}$$

$$r_o^2 = A^2 + h^2 ; \qquad \tan\phi_o = \frac{h}{A} \quad , \tag{B.31}$$

$$S_1^P(\theta) = \frac{kB_1}{2(1-K_{12}K_{21})} \left[(P_1+Q_1) + K_{21}(P_2+Q_2) \right] F_1(\theta) , \tag{B.32}$$

where P_1, Q_1 are as given by eqs. (B.15) and (B.16) and

$$F_1(\theta)=\frac{J_1(kB_1\sin\theta)}{\sqrt{2}}\,F_1^P(\theta)e^{-ikA\sin\theta}+\frac{|\cos\theta|\sin(\frac{\phi_{p_1}}{2})}{\sqrt{\pi kr_{p_1}\sin\theta}}\,e^{ikr_{p_1}}\,L_1^P(\theta)\,, \tag{B.33}$$

$$L_1^P(\theta)=\frac{e^{i(\frac{\pi}{2}-kA\sin\theta)}}{\sqrt{1-\sin\theta}}\left[\frac{\cos^{1/2}(\phi_{p_1})J_1(kB_1\cos\phi_{p_1})-\sin^{1/2}\theta J_1(kB_1\sin\theta)}{\cos\phi_{p_1}-\sin\theta}\right]$$
$$-\frac{e^{ikA\sin\theta}}{\sqrt{1+\sin\theta}}\left[\frac{J_1(kB_1\cos\phi_{p_1})\cos^{1/2}(\phi_{p_1})}{\cos\phi_{p_1}+\sin\theta}\right]\,, \tag{B.34}$$

$$F_1^P(\theta)=e^{ikr_{p_1}\sin(\theta-\phi_{p_1})}\int_{-\infty}^{p_5}e^{i\pi\frac{t^2}{2}}dt-e^{ikr_{p_1}\sin(\theta+\phi_{p_1})}\int_{-\infty}^{p_6}e^{i\pi\frac{t^2}{2}}dt, \tag{B.35}$$

$$p_5=2(\frac{kr_{p_1}}{\pi})^{1/2}\cos(\frac{\phi_{p_1}-\theta-\frac{\pi}{2}}{2})\,, \tag{B.36}$$

$$p_6=2(\frac{kr_{p_1}}{\pi})^{1/2}\cos(\frac{\phi_{p_1}+\theta+\frac{\pi}{2}}{2})\,, \tag{B.37}$$

$$r_{p_1}^2=A^2+H_1^2\,, \tag{B.38}$$

$$\tan\phi_{p_1}=\frac{H_1}{A}\,, \tag{B.39}$$

$$S_2^P(\theta)=\frac{kB_2}{2(1-K_{12}K_{21})}\left[(P_2+Q_2)+K_{12}(P_1+Q_1)\right]F_2(\theta)\,, \tag{B.40}$$

where P_2, Q_2 are given by (B. 19) and (B. 20), $F_2(\theta)$ is given by (B. 33) - (B. 39) with the parameters H_1, B_1 replaced by H_2, B_2 and K_{12}, K_{21} are as given by (B.10) and (B. 11)

B.4 Numerical Results

Expressions for the complex far field pattern produced by a double parasititic loop counterpoise antenna in the presence of mutual effects as discussed above, are:

$$S(\theta) = S^{A}(\theta) + S_1^{P}(\theta) + S_2^{P}(\theta) \quad , \tag{B.25}$$

where

$$S_1^{P}(\theta) = \frac{kB_1}{2(1-K_{12}K_{21})} \left[P_1+Q_1+K_{21}(P_2+Q_2)\right] F_1(\theta) \ , \tag{B.32}$$

$$S_2^{P}(\theta) = \frac{kB_2}{2(1-K_{12}K_{21})} \left[P_2+Q_2+K_{12}(P_1+Q_1)\right] F_2(\theta) \ , \tag{B.40}$$

where all the other notations are as explained in the previous sections. In the absence of mutual effects, eqs. (B.32) and (B.40) reduce to ($K_{21}=K_{12}=0$):

$$S_1^{P}(\theta) = (P_1 + Q_1)\, F_1(\theta)\, kB_{1/2} \ , \tag{B.41}$$

$$S_2^{P}(\theta) = (P_2 + Q_2)\, F_2(\theta)\, kB_{2/2} \ . \tag{B.42}$$

It is instructive to study the orders of magnitudes of the various quantities $K_{12}, K_{21}, P_1, Q_1, P_2$ and Q_2 which are constants for a specific configuration of the antenna. Let us consider the case of a double parasitic loop counterpoise antenna operating in the carrier mode. The antenna has the following parameters:

kh = 2.75, kb = 0.287, kA = 17.69, kH_1= 4.02, kB_1= 7.759, kH_2= 12.06 and kB_2= 7.759.

Note that for this antenna $H_2-H_1 \sim 1.3\lambda$ and $2B_1=2B_2= 2.5\lambda$. The parameter kb is deliberately chosen to be large (usually we have considered kb=0.15) for the reason that large values of kb give rise to large values of parasitic currents which in turn should increase the mutual effects. The parameter H_2-H_1 is chosen to be larger than a wavelength because this is the case of interest to us and we intend to study the quantitative effects of mutual interaction for such values of the separation distance between the parasitic loops.

For the above parameters of the antenna, the following numerical values have been obtained for the quantities mentioned above:

K_{12} = 0.146036-i 0.001367

K_{21} = 0.012024-i 0.047119

P_1 = -0.254652+i 0.505098

P_2 = 0.140834+i 0.125070

Q_1 = -0.105669-i 0.085823

Q_2 = 0.0132312+i 0.010157

It can be seen from the above values, that the mutual interaction terms in eq. (B. 40) are not appreciably large in the present case. This can also be seen from Fig. B-3 which shows the computed theoretical far field patterns of the same antenna with and without mutual coupling effects. From Fig. B-3 it is found that over most of the regions, the two patterns are almost identical. Near the region $90^o < \theta < 110^o$ where the pattern has a minimum, the two currents are found to be sharply different. It is desirable to consider the mutual effects in such regions.

The comparison between the theoretical and experimental patterns of the same antenna is shown in Fig. B-4. It is found that over most of the region of the main beam of the antenna, the agreement between theory and experiment is excellent and also that mutual effects may be neglected in this region. Careful inspection of Fig. B-4 indicates that the pattern obtained by taking into account the mutual effects is in slightly better agreement with the experimental results. It is anticipated that if $H_2 - H_1 < \lambda$, the mutual effects need be considered to obtain accurate patterns theoretically. On the basis of the results given here we conclude that for $(H_2-H_1) > \lambda$, the mutual effects may be neglected for pattern computations.

B. 5 Discussion

Expressions for the parasitic currents and the far field produced by a double parasitic loop counterpoise antenna have been derived above by taking into account the dominant effects of mutual interaction between the parasitic elements. From a comparison between theoretical and experimental results it has been found that the mutual effects may be neglected for cases when the separation between the parasitic elements is longer than a wavelength.

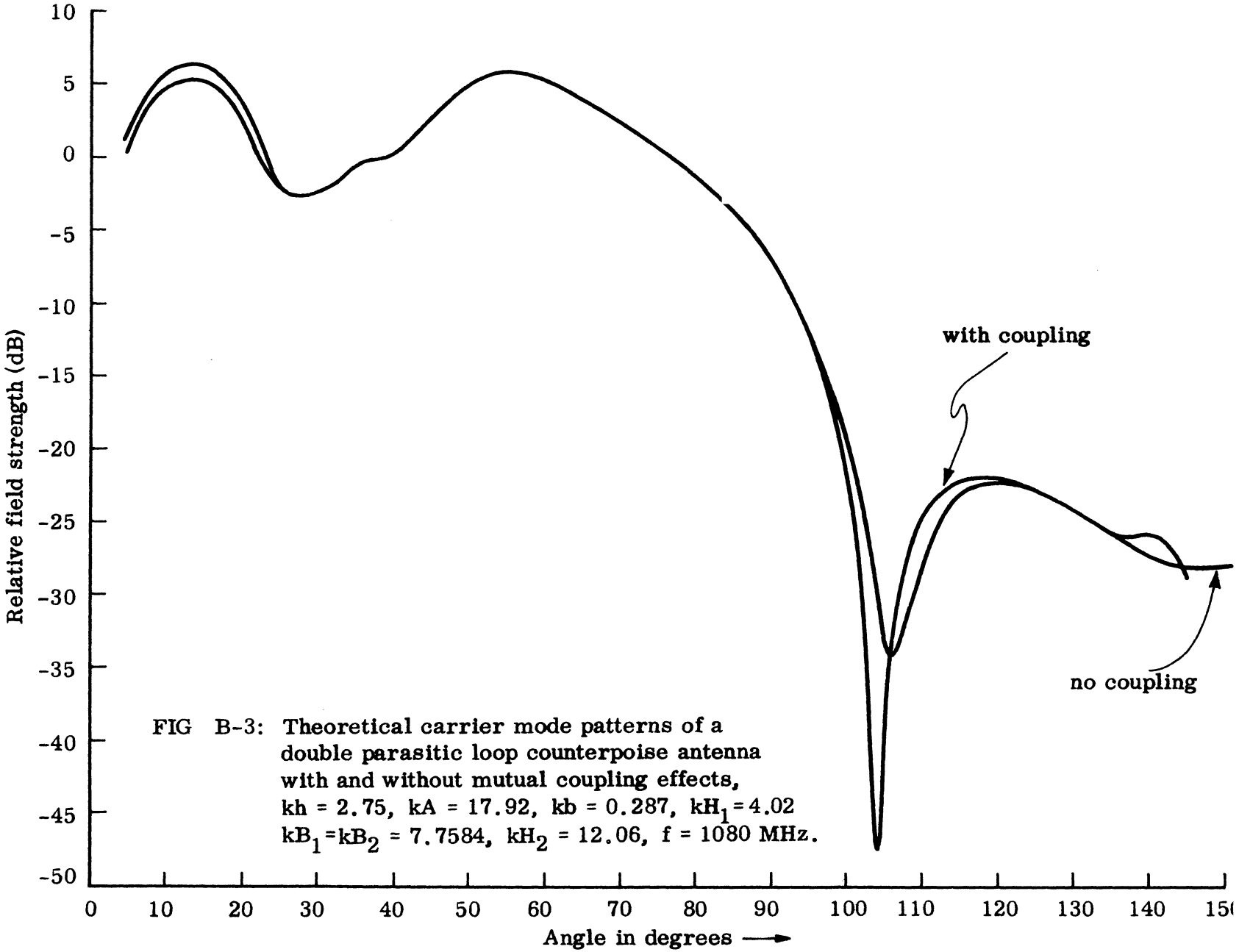

FIG B-3: Theoretical carrier mode patterns of a double parasitic loop counterpoise antenna with and without mutual coupling effects, kh = 2.75, kA = 17.92, kb = 0.287, $kH_1 = 4.02$ $kB_1 = kB_2 = 7.7584$, $kH_2 = 12.06$, f = 1080 MHz.

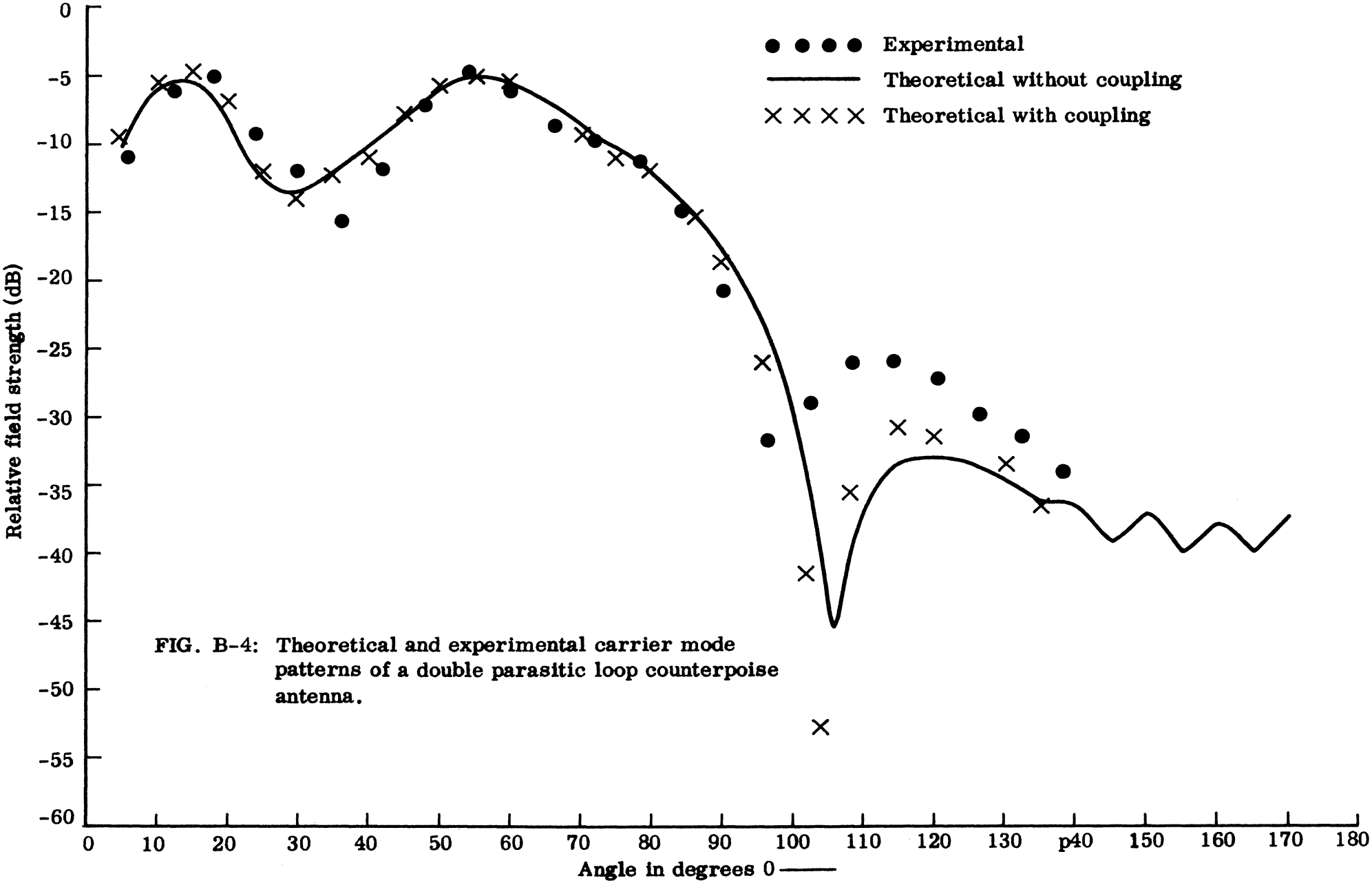

FIG. B-4: Theoretical and experimental carrier mode patterns of a double parasitic loop counterpoise antenna.

APPENDIX C

DOUBLE PARASITIC LOOP COUNTERPOISE ANTENNA PATTERNS

C.1 Introduction

In this section we summarize the results of a systematic experimental investigation of a double parasitic loop counterpoise antenna elevation patterns. The antenna operates in the side band mode and at the frequency f = 1080 MHz. The counterpoise size used is 5.2' so that the results will be applicable to a VOR antenna using 52' diameter counterpoise at the full scale frequency f = 108 MHz.

The excitation used has been a pair of Alford loops spaced 3.2" apart and located at a height 4.8" above the counterpoise. The two loops are excited out of phase so that the combined field produced by them has a figure-of-eight variation in the azimuthal plane. All the parasitic loops used have been fabricated from 1" wide conducting strips. All the measurements have been carried out in an indoor pattern range.

The basic purpose of the present investigation has been to develop an optimum configuration so that the antenna produces a maximum field gradient at the horizon for the side band mode of operation.

C.2 Preliminary Experiment

An initial radiation pattern investigation has been carried out for a double parasitic loop system with

$$H_2 = 22\,\tfrac{3}{8}\text{"}\ , \quad 2B_2 = 36\text{"} \quad \text{and} \quad H_1,\ B_1 \text{ variable.}$$

The purpose of this experiment has been to determine the effects of the parameters H_2, B_2 on the pattern and in particular to search for those values of H_1 and B_1 which may produce large field gradients at the horizon. The parameters H_2, B_2 where initially chosen on the basis of our previous investigation of single parasitic loop counterpoise antennas (Sengupta and Ferris, 1969).

The far field elevation patterns of the antenna have been measured at 1080 MHz with $2B_1$ varying in steps of 4" from 36" to 60" for each value of H_1. H_1 was varied from 4" to 7" in convenient steps. The main conclusion from this set of pattern results is that for low axial lobe and reasonably large field gradient $H_1 \simeq 6$" and $2B_1$ should lie between 48" - 60" . The important pattern characteristics obtained from this experiment are shown in Table C-I. The different notations used in the table are given below:

E_{max}	Amplitude of the far field in the direction of the principal maximum.
$E(\pi/2)$	Amplitude of the far field in the direction of the horizon (i.e. $\theta = \pi/2$).
$E(96^o)$	Amplitude of the far field in the direction $\theta=96^o$.
E_s	Amplitude of the first secondary lobe maximum below the horizon.
α_g	Field gradient/6^o at the horizon.
$E(0^o)$	Amplitude of the far field in the direction $\theta=0^o$.
$D_s=E(\pi/2)$	Level of the secondary lobe maximum field relative to the field at the horizon.

All the above results are expressed in dB.

TABLE C-I: PATTERN CHARACTERISTICS OF NON-UNIFORMLY EXCITED DOUBLE PARASITIC LOOP COUNTERPOISE ANTENNA
$H_2= 22\ 3/8"$, $2B_2= 36"$, $H_1=6"$, $2B_1$ variable.

$2B_1$	36"	40"	44"	48"	52"	56"	60"
E_{max}	- 3.0	- 5.5	- 3.0	- 3.0	- 5.0	- 5.0	- 6.0
$E(\pi/2)$	-28.5	-22.0	-19.0	-25.0	-22.0	-22.0	-32.0
$E(96^o)$	-35.0	-25.5	-28.0	-35.0	-29.0	-33.0	< -40.0
E_s	-27.0	---	-32.0	-28.0	---	-35.0	-33.0
$E(0^o)$	-22.0	-17.0	-16.0	-19.0	-19.0	-25.0	-23.0
α_g	6.5	3.5	9.0	10.0	7.0	11.0	> 8.0
$E_s-E(\pi/2)$	1.5	---	-13.0	- 3.0	---	-13.0	- 1.0

The values that are left out in the above table were found to be not applicable to the measured patterns. Three complete patterns are shown in Figs. C-1(a) - C-1(c) for three selected cases.

C.2 Optimization of the Lower Parasitic Loop Parameters

The next set of data have been taken for the purpose of obtaining the best values of the lower parasitic loop parameters H_1, B_1 for some fixed values H_2, B_2 of the upper parasitic loop parameters. During this experiment the upper loop parameters are fixed at $H_2 = 22\ 3/8"$, $2B_2= 36"$. The diameter of the lower parasitic loops were varied from 54" - 60" in steps of 2". For each value of $2B_1$, H_1 was varied from 5" - 7" in some convenient steps. The various pattern characteristics as obtained from the measured elevation patterns are shown in Tables C-II, C-III and C-IV.

TABLE C-II PATTERN CHARACTERISTICS OF NON-UNIFORMLY EXCITED DOUBLE PARASITIC LOOP COUNTERPOISE ANTENNA $2B_2$=36", H_2= 22 3/8", $2B_1$= 54", H_1 variable.

H_1	5 1/2"	5 3/4"	6"
E_{max}	- 7.0	- 7.0	- 7.0
$E(\pi/2)$	-22.0	-23.0	-23.0
$E(96^o)$	-28.0	-30.0	-32.0
E_s	---	---	---
$E(0^o)$	-27.0	-28.0	-22.0
α_g	6.0	7.0	9.0

TABLE C-III ------ $2B_1$ = 56" .

H_1	5"	5 1/2"	5 3/4"	6"	6 1/4"	7"
E_{max}	- 5.0	- 5.0	- 5.0	- 5.0	- 5.0	- 5.0
$E(\pi/2)$	-20.0	-21.0	-22.5	-23.0	-24.0	-26.0
$E(96^o)$	-26.5	-30.0	-32.0	-32.0	-33.0	-35.0
E_s	-37.0	---	---	-36.0	-33.5	-31.0
$E(0^o)$	-22.0	-30.0	-30.0	-24.0	-20.0	-15.0
α_g	6.5	9.0	9.5	9.0	9.0	10.0
E_s-$E(\pi/2)$	-17.0	---	---	-13.0	- 9.5	- 5.0

TABLE C-IV ----- $2B_1$ = 58" .

H_1	5 1/2"	5 3/4"	6"
E_{max}	- 6.0	- 6.0	- 6.0
$E(\pi/2)$	-24.0	-25.0	-26.0
$E(96^o)$	-35.0	-35.0	-35.0
E_s	-36.0	-36.0	-35.0
$E(0^o)$	-28.5	-29.0	-26.5
α_g	11.0	10.0	9.0
E_s-$E(\pi/2)$	-12.0	-11.0	- 9.0

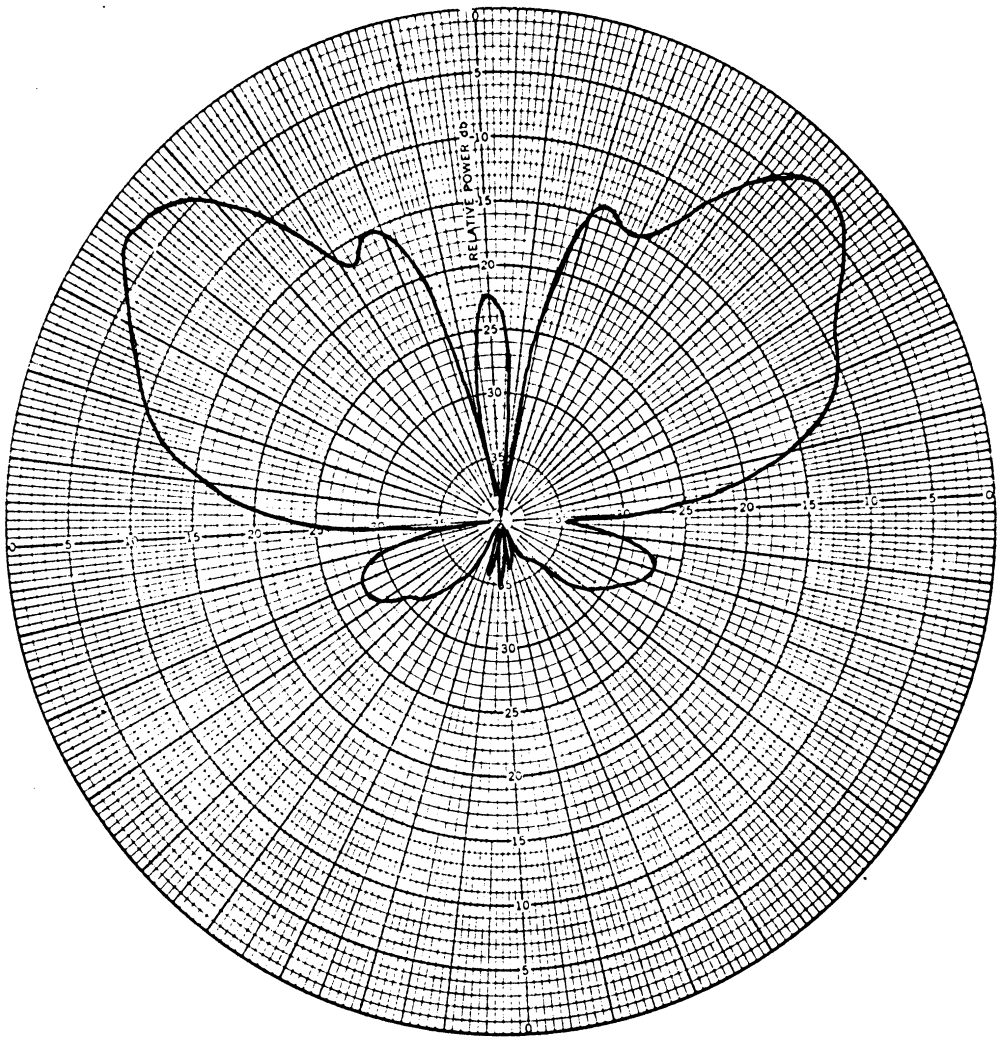

FIG. C-1a: Measured elevation plane side band mode pattern of a double parasitic loop counterpoise antenna.
2A=5.2', h=4.8" , f=1080 MHz, $2B_2$=36", H_2= 22 3/8",
H_1= 6" and $2B_1$= 36".

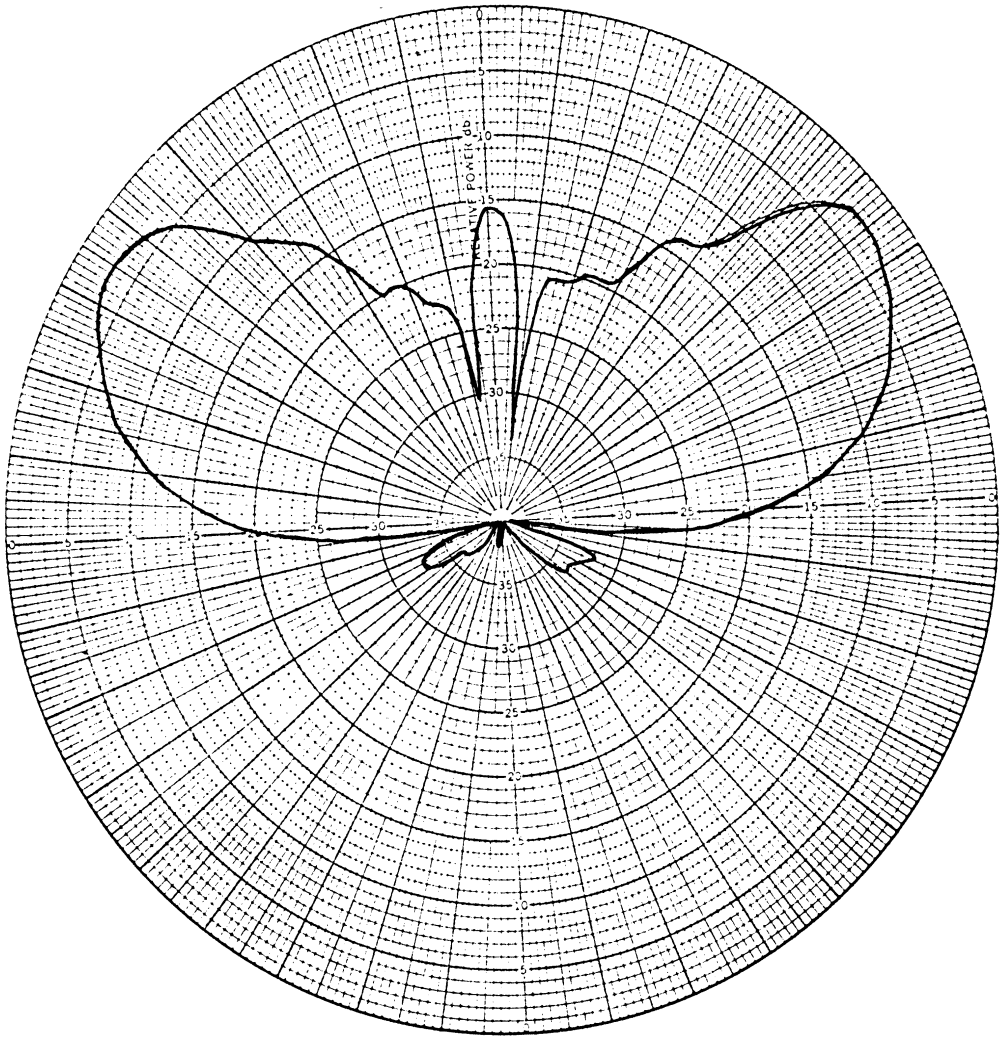

FIG. C-1b: Measured elevation plane side band mode pattern of a double parasitic loop counterpoise antenna.
2A=5.2', h=4.8", f=1080 MHz, $2B_2$=36", H_2=$22\frac{3}{8}$",
H_1=6" and $2B_1$=44".

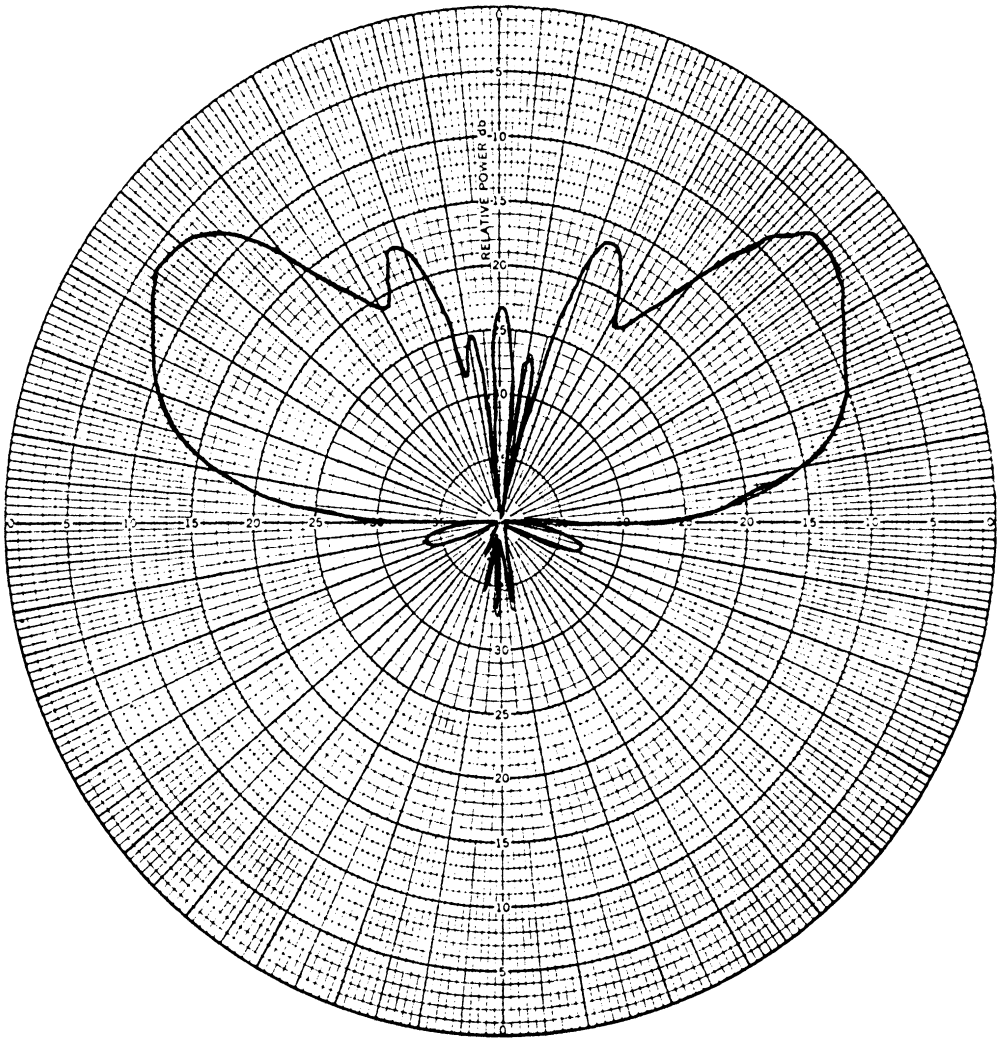

FIG. C-1c: Measured elevation plane side band mode pattern of a double parasitic loop counterpoise antenna.
2A=5.2', h=4.8", f=1080 MHz, $2B_2$=36", H_2= 22 3/8",
H_1=6" and $2B_1$=60" .

From the previous tables it is found that for values of the parameter H_1 between 5 1/2" and 5 3/4" the lobe maximum in the direction $\theta = 0^o$ is minimum. Notice that theoretically, for minimum axial lobe $H_1 = \lambda/2 = 5.465$" at f=1080 MHz.

From the results given in this section it appears that the best pattern for possible VOR application is obtained when $2B_2$=36" , H_2= 22 3/8", $2B_1$=56" and H_1=5 3/4" . The measured elevation pattern for this case is shown in Fig. C-2.

C.3 Optimization of the upper Parasitic Loop Parameters

In this set of experiments the lower parasitic loop parameters were fixed at $2B_1$=56" and H_1= 5 3/4" . The height of the upper loop was fixed at the value H_2= 22 3/8 " while the diameter $2B_2$ was varied from 34" - 40". The results are shown in Table C-V. Note that the field gradient values shown in Table C-V have been obtained from the measured polar plots and hence are approximate. More accurate values for α_g in some specific cases will be discussed in the next paragraph. A typical measured pattern having desirable characteristics is shown in Fig. C-3.

TABLE C-V: PATTERN CHARACTERISTICS OF NON-UNIFORMLY EXCITED DOUBLE PARASITIC LOOP COUNTERPOISE ANTENNA
$2B_1$=56" , H_1 5 3/4", H_2= 22 3/8" , $2B_2$ variable.

$2B_2$	34"	35"	36"	37"	38"	39"	40"
E_{max}	- 5.0	- 5.0	- 6.0	- 6.0	- 6.0	- 5.0	- 5.0
$E(\pi/2)$	-19.5	-20.5	-21.0	-22.5	-24.0	-25.5	-24.5
$E(96^o)$	-26.5	-28.0	-29.5	-32.0	-35.5	-36.0	-34.0
E_s	---	---	---	-36.0	-34.0	-32.0	-31.0
$E(0^o)$	-27.0	-28.0	-28.0	-29.0	-35.0	-35.0	-35.0
α_g	7.0	7.5	8.5	9.5	11.5	11.5	9.5
E_s-$E(\pi/2)$	---	---	---	-13.5	-10.0	-10.0	- 6.5

To obtain more accurate esimates for the field gradients, rectangular plots for the patterns have been obtained in ordinary and expanded scales for some selected cases. The patterns obtained in a few interesting cases are shown in Figs. C-4, C-5(a) - C-5(b), C-6(a) and C-6(b). As can be seen from these figures a field gradient value better than 12 dB can be obtained without appreciably increasing the field in the axial direction.

C.4 Maximum Obtainable Field Gradient

Two main criteria governed the basis of the investigations discussed in the preceding sections. These are: (i) the field gradient at the horizon be high, and

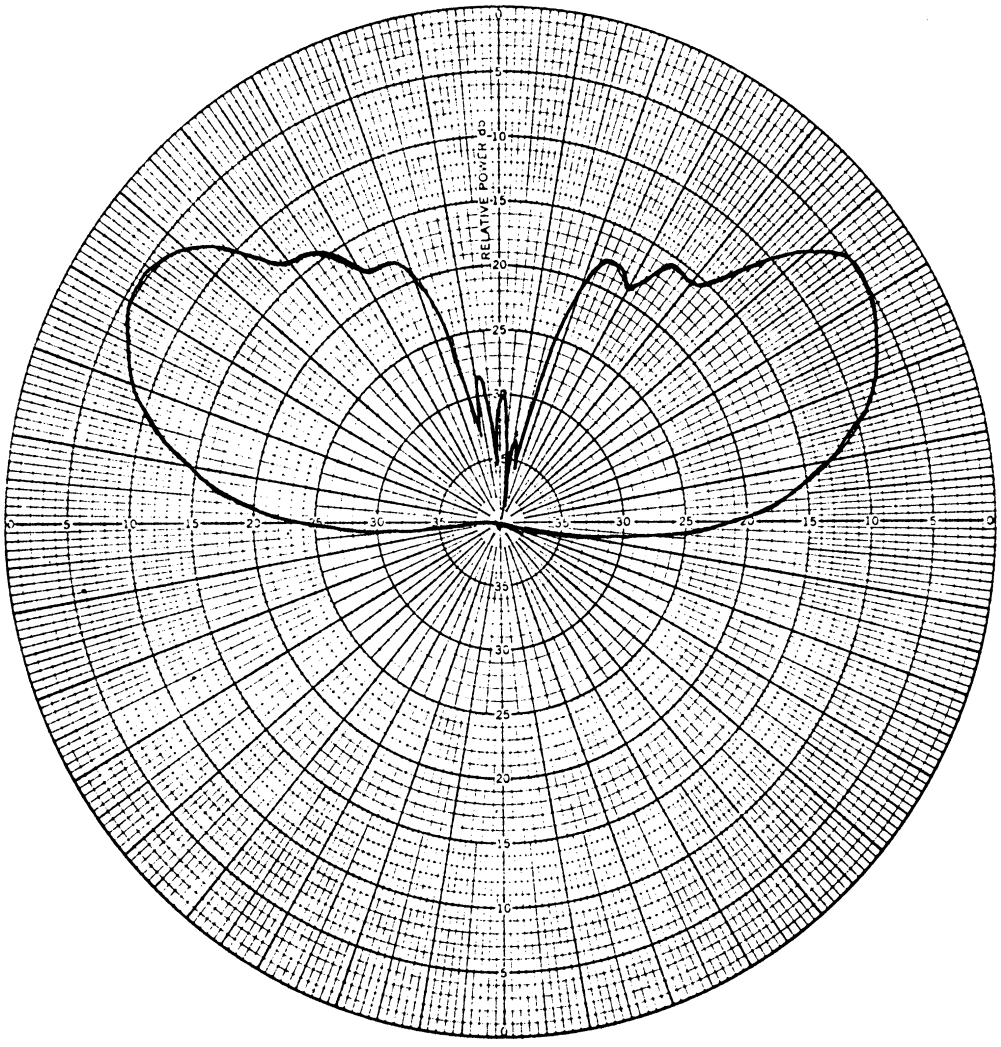

FIG. C-2: Measured elevation plane side band mode pattern of a double parasitic loop counterpoise antenna.
$2A=5.2'$, $h=4.8''$, $f=1080$ MHz, $2B_2=36''$, $H_2=22\ 3/8''$, $H_1=5\ 3/4''$, and $2B_1=56''$.

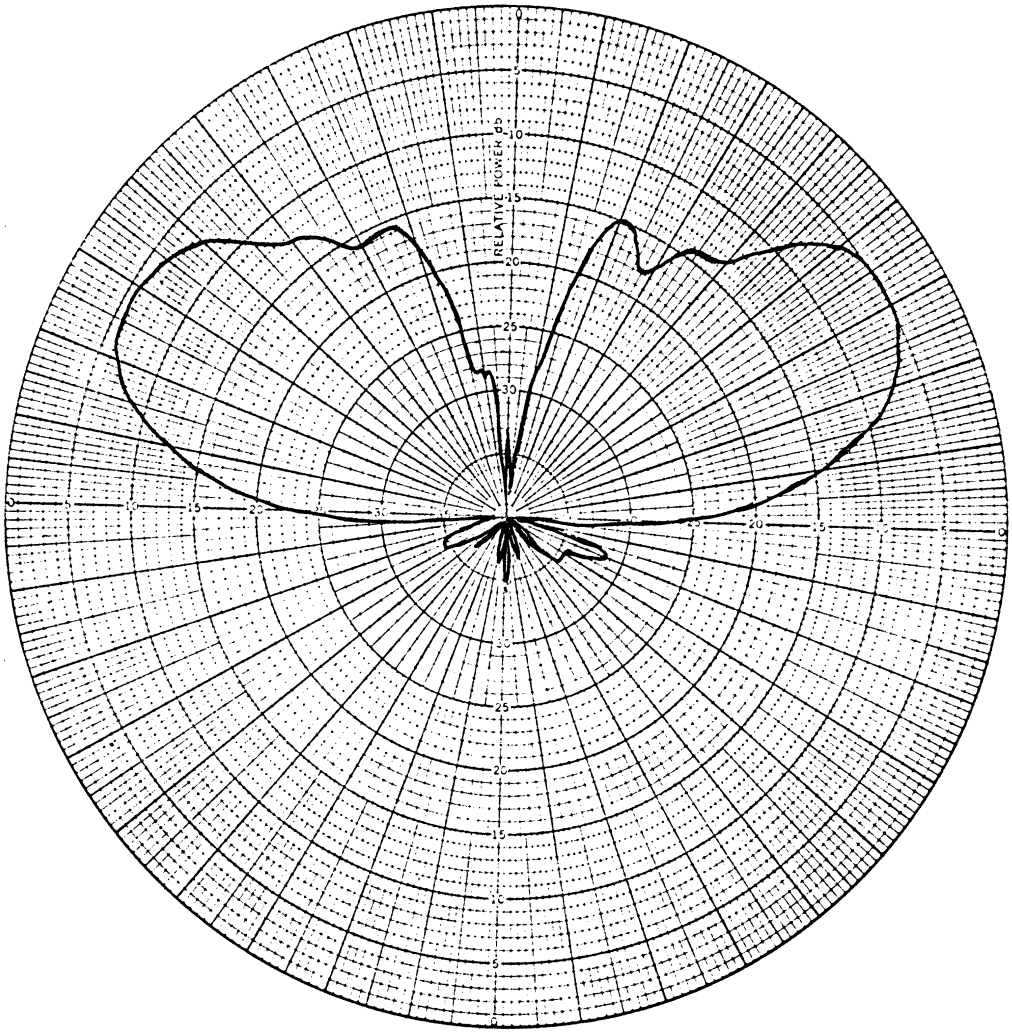

FIG. C-3: Measured elevation plane side band mode pattern of a double parasitic loop counterpoise antenna.
$2A = 5.2'$, $h = 4.8''$, $f = 1080$ MHz, $2B_2 = 40''$, $H_2 = 22\ 3/8''$, $H_1 = 5\ 3/4''$ and $2B_1 = 56''$.

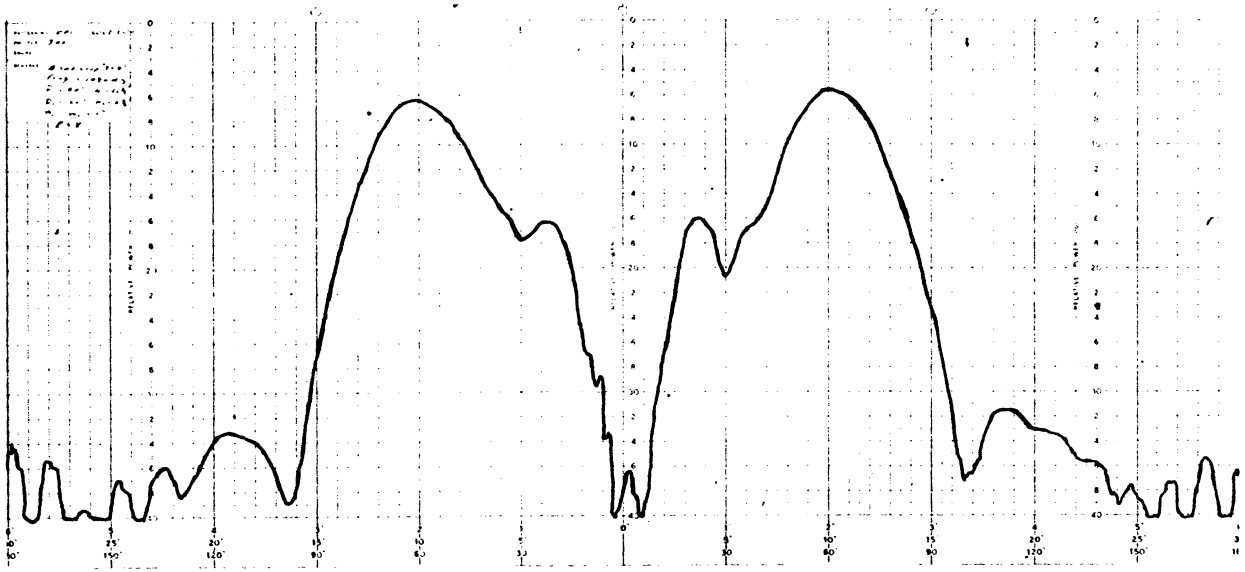

FIG. C-4: Measured elevation plane side band mode pattern of double parasitic loop counterpoise antenna, 2A = 5.2', h = 4.8", $2B_1$ = 56", H_1 = 5 3/4", $2B_2$ = 40", H_2 = 22 3/8", f = 1080 MHz.

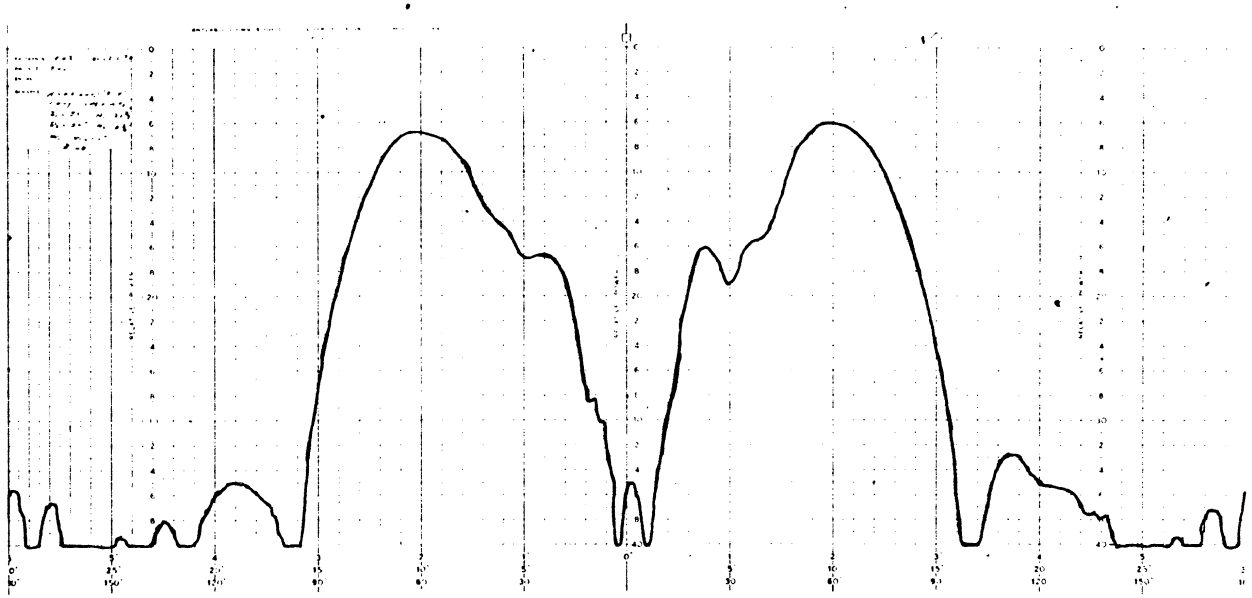

FIG. C-5a: Measured elevation plane side band mode pattern of double parasitic loop counterpoise antenna - complete pattern, 2A = 5.2', h = 4.8", $2B_1$ = 56", H_1 = 5 3/4", $2B_2$ = 39", H_2 = 22 3/8", f= 1080 MHz.

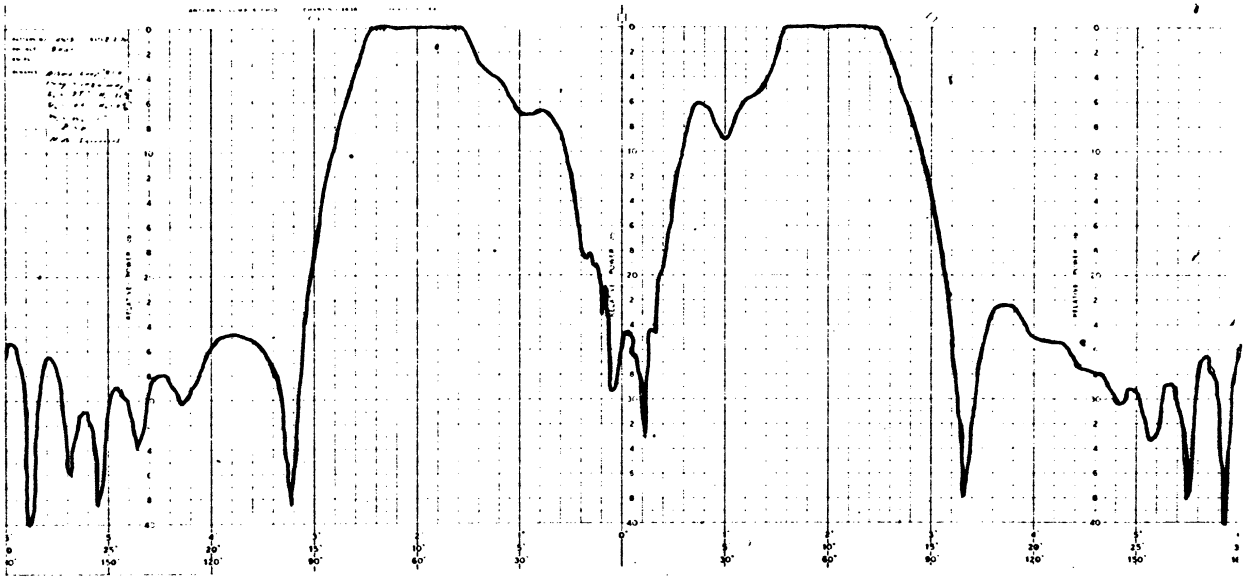

FIG. C-5b: Measured elevation plane side band mode pattern of double parasitic loop counterpoise antenna - details near and below the horizon, 2A = 5.2', h = 4.8", $2B_1$ = 56", H_1 = 5 3/4", $2B_2$ = 39", H_2 = 22 3/8", f = 1080 MHz.

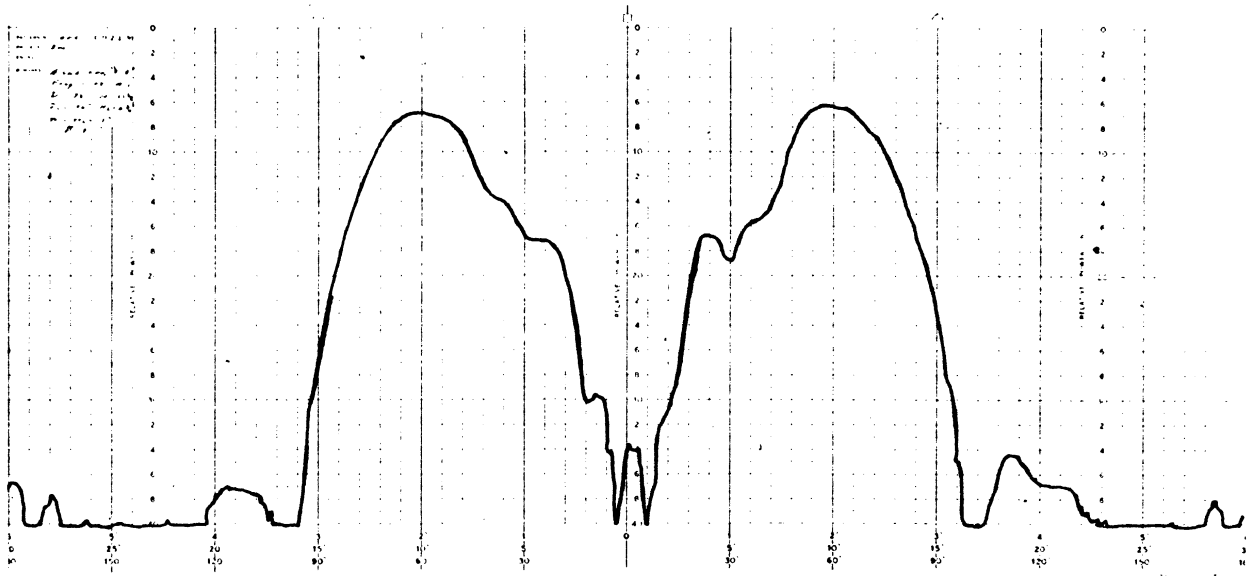

FIG. C-6a: Measured elevation plane side band mode pattern of double parasitic loop counterpoise antenna, complete pattern, 2A = 5.2', h = 4.8", $2B_1$ = 56", H_1 = 5 $^3/_4$", $2B_2$ = 38", H_2 = 22 $^3/_8$", f = 1080 MHz.

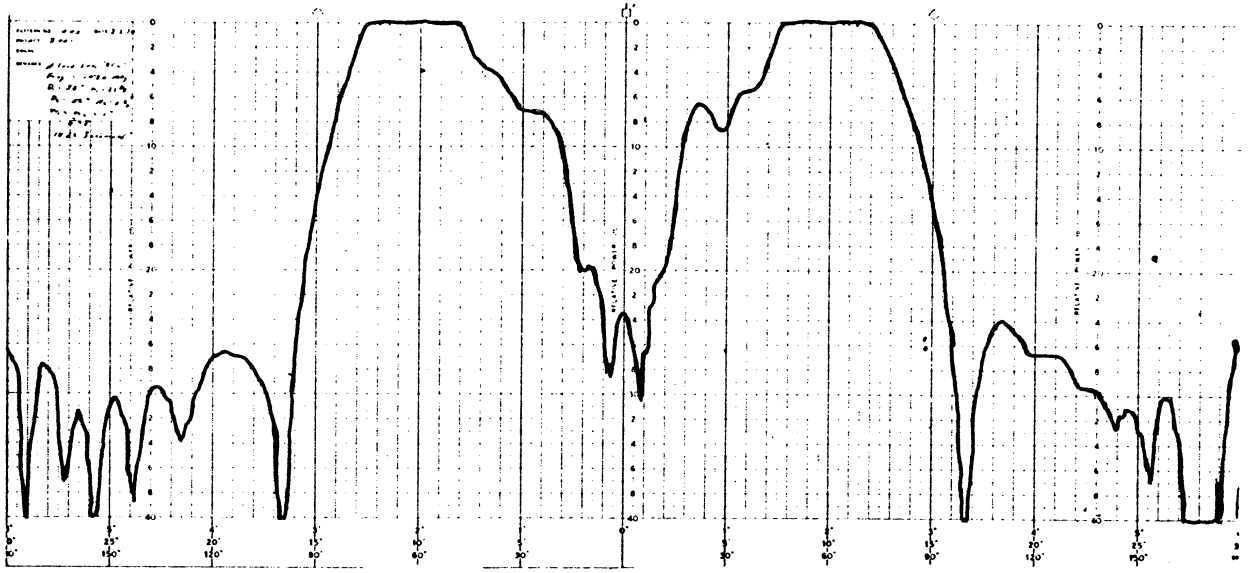

FIG. C-6B: Measured elevation plane side band mode pattern of double parasitic loop counterpoise antenna - details near and below the horizon, 2A = 5.2', h = 4.8", $2B_1$ = 56", H_1 = 5 3/4", $2B_2$ = 38", H_2 = 22 3/8", f = 1080 MHz.

(ii) the axial lobe amplitude be as small as possible. In this section we give the results obtained from an experiment where the second restriction on the pattern has been removed. The aim of this part of the investigation has been to determine the largest value of the field gradient that can be obtained from a double parasitic loop counterpoise antenna. The results are shown in Figs. C-7(a) and C-7(b). In this particular case the field gradient at the horizon is found to be better than 22dB/6° which may be considered to be a dramatic improvement.

C.5 Discussion

On the basis of the results given above it can be concluded that the parasitic loop concept has been found to be highly effective in improving the field gradient characteristics of a non-uniformly excited parasitic loop counterpoise antenna. From our investigation of the radiation characteristics of a double parasitic loop counterpoise antenna having figure-of-eight type of excitation we make the following two important observations.

(i) It is possible to obtain a field gradient at the horizon better than 12 dB/6° while maintaining the field in the axial direction to be less than 25 dB down from the field in the principal maximum direction.

(ii) It is possible to obtain a field gradient at the horizon better than 22 dB/6° while maintaining the axial field to be less than 16 dB down from the field in the principal maximum direction.

In all the above cases the secondary lobe maximum below the horizon has been found to be about 9 - 12 dB down from the field at the horizon.

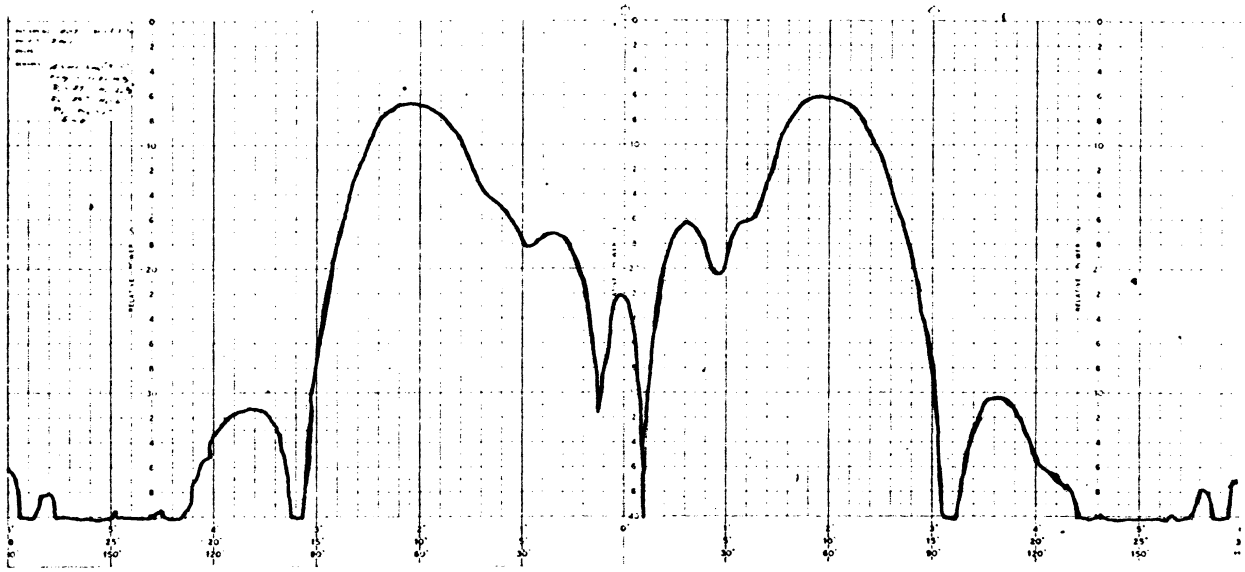

FIG. C-7a: Measured elevation plane side band mode pattern of very large gradient double parasitic loop counterpoise antenna - complete pattern, 2A = 5.2', h = 4.8", $2B_1$ = 56", H_1 = 6", $2B_2$ = 39", H_2 = 22 $^3/_8$", f = 1080 MHz.

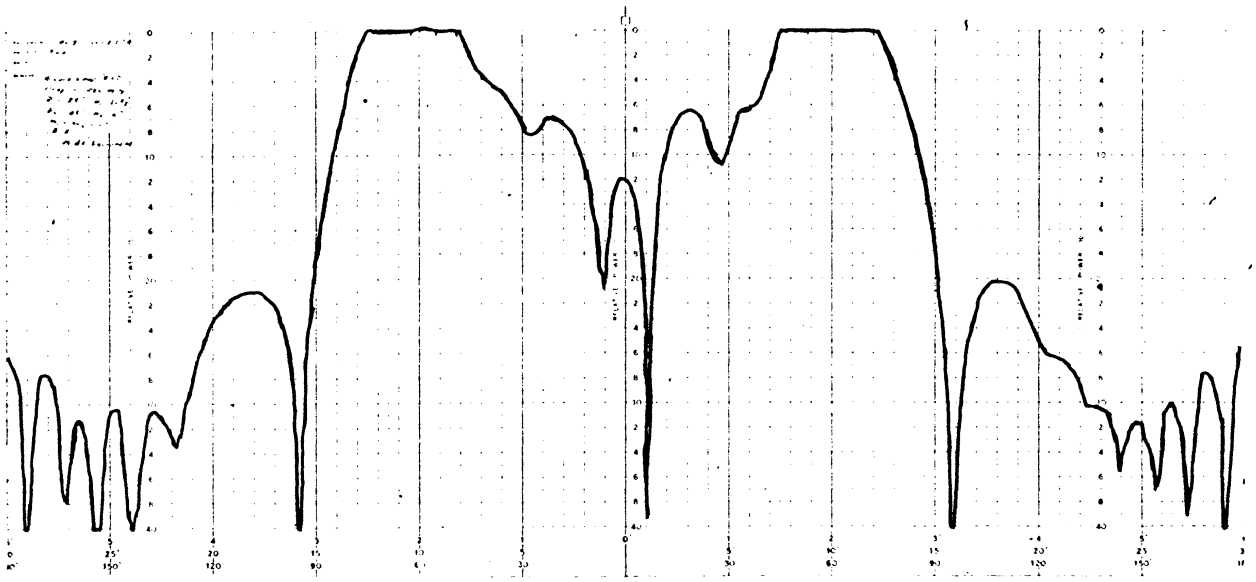

FIG. C-7b: Measured elevation plane side band mode pattern of very large gradient double parasitic loop counterpoise antenna - details near and below the horizon, 2A = 5.2', h = 4.8", $2B_1$ = 56", H_1 = 6", $2B_2$ = 39", H_2 = 22 3/8", f = 1080 MHz.

APPENDIX D

NUMERICAL VALUES FOR PARASITIC CURRENTS IN SINGLE PARASITIC LOOP COUNTERPOISE ANTENNAS

D. 1 Introduction

In this appendix the numerical values for the amplitude and phase of the different components of the parasitic currents are given for single parasitic loop counterpoise antennas operating in the carrier mode. The notations used are explained in Chapter III.

The basic parameters associated with the feed and the parasitic loop in all the antennas have the normalized dimensions kh=2.75, kb=0.15 at the frequency 1080 MHz.

TABLE D-I: PARASITIC CURRENT VALUES FOR kA = 17.92

	Real	Imaginary	Absolute	Argument (radians)
		kB = 4π	kH=3.7	
$I_{P_o}^{12}$	0.235203	0.060884	0.242955	0.253
$I_{P_o}^{34}$	0.000214	0.000635	0.000670	1.246
$I_{P_o}^{56}$	-0.003516	0.079530	0.019844	1.749
I_{P_o}/I_o	0.231900	0.081049	0.245656	0.336
		kB = 3θ	kH = 11.9	
$I_{P_o}^{12}$	-0.053762	0.171890	0.180102	1.874
$I_{P_o}^{34}$	-0.000723	0.000275	0.000774	2.778
$I_{P_o}^{56}$	+0.028226	0.004028	0.028512	0.142
I_{P_o}/I_o	-0.026258	0.176194	0.178140	1.819

TABLE D-II: PARASITIC CURRENT VALUES FOR kA = 51.69, kB=3π AS FUNCTIONS OF kH .

	Real	Imaginary	Absolute	Argument (radians)
		kH = 3.75		
$I_{P_o}^{12}$	-0.320886	-0.174901	0.365456	-2.643
$I_{P_o}^{34}$	-0.000005	0.000008	0.000009	2.150
$I_{P_o}^{56}$	0.005060	-0.020825	0.021431	-1.332
I_{P_o}/I_o	-0.315831	-0.195718	0.371557	-2.587
		kH = 4.00		
$I_{P_o}^{12}$	-0.312799	-0.203302	0.373062	-2.565
$I_{P_o}^{34}$	-0.000006	0.000008	0.000010	2.171
$I_{P_o}^{56}$	0.016357	-0.000828	0.016378	-0.051
I_{P_o}/I_o	-0.296447	-0.204122	0.359926	-2.539
		kH= 6.28		
$I_{P_o}^{12}$	-0.028638	-0.362861	0.363990	-1.650
$I_{P_o}^{34}$	-0.000012	0.000011	0.000016	2.425
$I_{P_o}^{56}$	-0.022557	-0.034135	0.040915	-2.155
I_{P_o}/I_o	-0.051207	-0.396986	0.400275	-1.699
		kH = 9.424		
$I_{P_o}^{12}$	0.253751	0.036038	0.256298	0.161
$I_{P_o}^{34}$	-0.000025	0.000005	0.000026	2.950
I_{P_o}/I_o	0.273649	0.016660	0.274155	0.061
		kH = 12.5664		
$I_{P_o}^{12}$	-0.118024	0.113270	0.163584	2.377
$I_{P_o}^{34}$	-0.000032	-0.000018	0.000036	-2.616
$I_{P_o}^{56}$	0.006505	0.077561	0.018727	1.216
I_{P_o}/I_o	-0.111550	0.130813	0.171917	2.277

(continued on next page)

kH = 13.00

$I_{P_o}^{12}$	-0.139680	0.064187	0.153722	2.711
$I_{P_o}^{34}$	-0.000031	-0.000023	0.000038	-2.502
$I_{P_o}^{56}$	-0.002196	0.008552	0.008829	1.822
I_{P_o}/I_o	-0.141906	0.072716	0.159452	2.668

kH = 13.5

$I_{P_o}^{12}$	-0.143060	0.005611	0.143170	3.102
$I_{P_o}^{34}$	-0.000028	-0.000028	0.000040	-2.367
$I_{P_o}^{56}$	0.003864	0.001230	0.004055	0.308
I_{P_o}/I_o	-0.139224	0.006813	0.139391	3.093

TABLE D-III: PARASITIC CURRENT VALUES FOR kA = 51.69, kH = 3.75 AS FUNCTIONS OF kB.

	Real	Imaginary	Absolute	Argument (radians)
		kB = 9.424778		
$I_{P_o}^{12}$	-0.320886	-0.174901	0.365456	-2.643
$I_{P_o}^{34}$	-0.000005	0.000008	0.000009	2.150
$I_{P_o}^{56}$	0.005060	-0.020825	0.021431	-1.332
I_{P_o}/I_o	-0.315831	-0.195718	0.371557	-2.587
		kB = 10.99557		
$I_{P_o}^{12}$	0.107100	-0.277345	0.297631	-1.199
$I_{P_o}^{34}$	0.000008	-0.000004	0.000009	-0.419
$I_{P_o}^{56}$	0.040861	0.046749	0.062089	0.853
I_{P_o}/I_o	0.148868	-0.230599	0.274477	-0.998
		kB = 4π		
$I_{P_o}^{12}$	0.236309	0.064329	0.244908	0.266
$I_{P_o}^{34}$	0.000004	-0.000008	0.000009	-1.057
$I_{P_o}^{56}$	-0.006193	0.017157	0.018240	1.917
I_{P_o}/I_o	0.230121	0.081478	0.244119	0.340
		kB = 14.13717		
$I_{P_o}^{12}$	-0.036089	0.200639	0.203859	1.749
$I_{P_o}^{34}$	-0.000008	0.000003	0.000008	2.812
$I_{P_o}^{56}$	-0.031215	-0.034283	0.046364	-2.309
I_{P_o}/I_o	-0.067311	0.166359	0.179461	1.955
		kB = 15.7096		
$I_{P_o}^{12}$	-0.170716	-0.017859	0.171647	-3.037
$I_{P_o}^{34}$	-0.000004	0.000008	0.000009	2.039
$I_{P_o}^{56}$	0.006265	-0.014580	0.015869	-1.165
I_{P_o}/I_o	-0.164455	-0.032431	0.167622	-2.947

TABLE D-IV: PARASITIC CURRENT VALUES FOR kA = 51.69, kH = 13.00 AS FUNCTIONS OF kB

	Real	Imaginary	Absolute	Argument (radians)
		kB = 8.168161		
$I^{12}_{P_o}$	-0.048299	0.128762	0.137522	1.930
$I^{34}_{P_o}$	-0.000020	-0.000028	0.000034	-2.178
$I^{56}_{P_o}$	-0.020082	-0.001074	0.020110	-3.088
I_{P_o}/I_o	-0.068003	0.127659	0.144829	2.063
		kB = 8.796459		
$I^{12}_{P_o}$	-0.098755	0.107530	0.146000	2.314
$I^{34}_{P_o}$	-0.000030	-0.000031	0.000040	-2.341
$I^{56}_{P_o}$	-0.001798	-0.007079	0.007303	-1.820
I_{P_o}/I_o	-0.100583	0.100420	0.142130	2.357
		kB = 10.05310		
$I^{12}_{P_o}$	-0.160590	0.003433	0.160627	3.120
$I^{34}_{P_o}$	-0.000021	-0.000006	0.000022	-2.856
$I^{56}_{P_o}$	-0.020466	0.017674	0.020522	3.055
I_{P_o}/I_o	-0.181057	0.005194	0.181131	3.113
		kB = 10.68142		
$I^{12}_{P_o}$	-0.153549	-0.064811	0.166667	-2.742
$I^{34}_{P_o}$	-0.000005	0.000012	0.000013	1.931
$I^{56}_{P_o}$	-0.012413	-0.020845	0.024261	-2.108
I_{P_o}/I_o	-0.165967	-0.085644	0.186762	-2.665
		kB = 11.30973		
$I^{12}_{P_o}$	-0.115851	-0.126891	0.171822	-2.311
$I^{34}_{P_o}$	0.000012	0.000026	0.000029	1.130
$I^{56}_{P_o}$	0.010212	-0.015715	0.018741	-0.995
I_{P_o}/I_o	-0.105626	-0.142580	0.177443	-2.208

APPENDIX E

COMPUTER PROGRAMS FOR IBM-360, MODEL-67

E.1 Program for evaluating the far field elevation plane side band mode pattern of a conventional VOR antenna ($S^A(\theta)$ versus θ). The subroutines given in this section are also used in all the subsequent programs.

The following flow diagram applies to the Main program for the VOR side band mode.

Flow Diagram for the Main Program

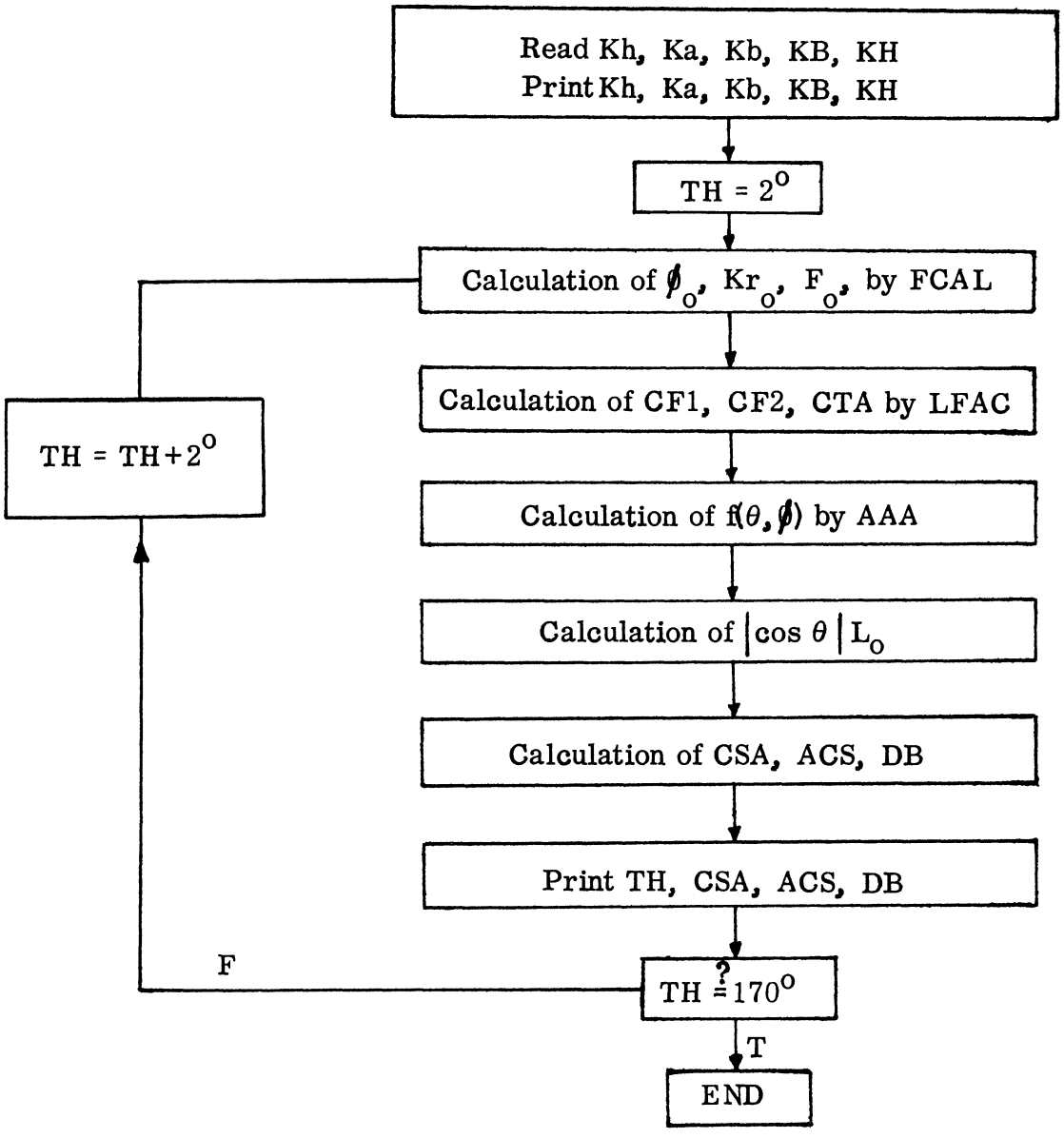

LIST OF SOME OF THE SYMBOLS USED

SQ2 = square root of two

PI = π

RCON = $\frac{\pi}{180}$

KH = kh

KB = kb

KA = ka

KCB = kB

KCH = kH

TH = θ

PHZ = ϕ_o

KRZ = kr_o

CFZ = F_o

TS = $\sin(\theta)$

TC = $\cos(\theta)$

CF1 = $\sqrt{2}\, e^{i(\pi/2 - ka \sin\theta)}$

CF1 = $e^{i(\frac{\pi}{2} - KA \sin\theta)} \frac{|\cos\theta|}{\sqrt{1 - \sin\theta}}$

CF2 = O

CXZ = e^{-ik_o}

CF2 = $e^{ika \sin\theta} \frac{|\cos\theta|}{\sqrt{1 + \sin\theta}}$

CSA = S_A

ACS = $|S_A|$

CLZ = $|\cos\theta| L_o$

DB = $20 \log_{10} |S_A|$

CTA = $e^{-Ka \sin\theta}$

AAA
FCAL
LFAC
} Subroutines

Main

```
0001            IMPLICIT REAL*8(A,B,D-H,P,Q-Z),COMPLEX*16(C)
0002            REAL*8 CDABS
0003            DIMENSION THV(140),CSAV(140),CSUMV(140)
0004            COMPLEX*16 DCMPLX,CFNEWP,CFNEWT
0005            CEIX(XX) = DCMPLX(DCOS(XX),DSIN(XX))
0006            LOGICAL TERM/.FALSE./
0007            DATA SQ2/1.41421356237331/, PI/3.14159265358979/
0008            DATA PCT/1.57079632679491/, EGAM/.57721566490153 3/
0009            DATA RCON/.01745329251992/, PCF/.78539816339744 8/
0010            DATA MTI/3/,ITS/1/
0011            REAL*8 TH1(10)/5.D0,82.D0,115.D0,7*0.D0/,TH2(10)/80.D0,110.D
               & 170.D0,7*0.D0/, THS(10)/5.D0,2.D0,5.D0,7*0.D0/
0012            NAMELIST /IN/KH,KA,KE,KCB,KCH
0013          111 READ(1,IN,END=100)
0014            WRITE (6,999)
0015          999   FORMAT ('1')
0016            WRITE(6,1000)KE,KA,KE,KCB,KCH
0017           1000 FORMAT(' KE = ',G15.7,' KA = ',G15.7,' KE = ',G15.7/
               1 ' KCE = ',G15.7,' KCF = ',G15.7//)
0018            CELKB=DCMPLX(PCT,EGAM+DLOG(KB*.5D0))
0019            CELPP=DCMPLX(EGAM+DLOG(KE*.5D0),-PCT)
0020            INDEX=1
0021            CFNEWA=DCMPLX(0.D0,1.E4D0)
0022            DO 100 I=2,170,2
0023            TH=I*RCON
0024            CALL FCAL(KH,KA,TH,PH2,KE2,CF2)
0025            CALL FCAL(KCH,KA,TH,PHP,KEP,CFP)
0026            TS = DSIN(TH)
0027            TC = DCOS(TH)
0028            CALL EFAC(TS,TC,KA,CF1,CF2,CTA)
0029            TS1 = DSQRT(TS)
0030            PC=DCOS(PHP)
0031            PC1=DSQRT(PC)
0032            BSL1=BJONE(KCB*PC)
0033            BSL2=BJONE(KCB*TS)
0034            T1=(PC1*BSL1-TS1*BSL2)/(PC-TS)
0035            T2=PC1*BSL1/(PC+TS)
```

```
0036                CLE=CF1*T1-CF2*T2
0037                EC = DCOS(ERZ)
0038                EC1 = DSQRT(EC*EC*EC)
0039                TS1 = TS1*TS1*TS1
0040                AEC=AAA(EC)
0041                ATS=AAA(TS)
0042                CFNEWE=DCMPLX(C.LC,AEC)
0043                CFNEWT=DCMPLX(0.D0,ATS)
0044                CT1=(CFNEWP*EC1-CFNEWT*TS1)/(EC-TS)
0045                CT2=CFNEWE*EC1/(EC+TS)
0046                CL2=CF1*CT1-CF2*CT2
0047                T1 = DSIN(PHZ*.5DC)/DSQRT(PI*KRZ*TS)
0048                CXZ = CEIX(KRZ)
0049                CSA=CF2*CTA*CFNEW1*TS/SQ2+CX2*CL2*T1
0050                ACS=CDABS(CSA)
0051                AE=2C.D0*DLOG10(ACS)
0052                IB=IB/RCCN
0053                WRITE(6,50)TH,CSA,ACS,AE

0054          50    FORMAT(F12.3,1P4D15.C)
0055           100  CONTINUE
0056                GO TO 111
0057                END

 TOTAL MEMORY REQUIREMENTS 002266 BYTES
```

```
FORTRAN IV G COMPILER          AAA

0001                FUNCTION AAA(TS)
0002                IMPLICIT REAL*8 (A-Z)
0003                DATA KD/0.92/
0004                AAA=2.D0*DSIN(KD*TS)
0005                RETURN
0006                END

 TOTAL MEMORY REQUIREMENTS 00015E BYTES
```

```
FORTRAN IV G COMPILER          LEAC

0001                SUBROUTINE LEAC(TS,TC,KA,CE1,CE2,CTA)
0002                IMPLICIT REAL*8(A,B,D-H,K,O-Z),COMPLEX*16(C)
0003                COMPLEX*16 DCMPLX
0004                DATA [illegible]/1.41421356237[illegible]/
0005                T2 = KA*TS
0006                T1 = DCOS(T2)
0007                T2 = DSIN(T2)
0008                CTA = DCMPLX(T1,-T2)
0009                ATC = DABS(TC)
0010                IF (ATC.LT.1.D-[illegible]) GO TO [illegible]
0011                T = [illegible]/DSQRT(1.D0-TS)
0012                CE1 = T*DCMPLX(T2,T1)
0013                T = [illegible]/DSQRT(1.D0+TS)
0014                CE2 = T*DCMPLX(T1,T2)
0015                RETURN
0016                CE1 = [illegible]*DCMPLX(T2,T1)
0017                CE2 = [illegible]
0018                RETURN
0019                END
```

```
FORTRAN IV G COMPILER                    FCAL

0001          SUBROUTINE FCAL(KH,KA,TH,PHI,KR,CFZZ)
0002          IMPLICIT REAL*8 (A,B,D-F,K,P-Z),COMPLEX*16(C)
0003          COMPLEX*16 DCMPLX
0004          CFIX(XX) = DCMPLX(DCOS(XX),DSIN(XX))
0005          DATA SQ2/1.41421356237309/, PI/3.14159265358979/
0006          DATA PQT/1.57079632679049/
0007          PHT = DATAN2(KH,KA)
0008          KR = DSQRT(KA*KA+KH*KH)
0009          P2 = 2.D0*DSQRT(KR/PI)
0010          P1 = P2*DCOS((PHI-TH-PQT)/2.D0)
0011          P2 = P2*DCOS((PHI+TH+PQT)/2.D0)
0012          CALL FRNL(A,B,P1)
0013          CF1 = DCMPLX(A,B)
0014          CALL FRNL(A,B,P2)
0015          CF2 = DCMPLX(A,B)
0016          CA = CFIX(KR*DSIN(TH-PHI))
0017          CB = CFIX(KR*DSIN(TH+PHI))
0018          CFZZ = CA-CB
0019          CFZZ = CFZZ*(.500,.500)
0020          CA = CA*CF1
0021          CB = CB*CF2
0022          CFZZ = CFZZ+CA-CB
0023          RETURN
0024          END

TOTAL MEMORY REQUIREMENTS 000518 BYTES
```

SUBROUTINE

```
0001          SUBROUTINE FRNL(C,S,XX)
0002          IMPLICIT REAL*8 (A-H,O-Z)
0003          ZZ = XX*1.2533141373155
0004          Z = ZZ*ZZ
0005          GO TO 3
0006          ENTRY CS(C,S,X)
0007          Z = DABS(X)
0008          ZZ = DSQRT(Z)
0009    3     IF (Z.GT.4.DO) GO TO 4
0010          C = ZZ
0011          S = Z*C
0012          Z = Z*Z
0013          C = C*((((((.50998348D-10*Z-.10140729D-7)*Z+.11605284D-5)*Z
              & -.85224622D-4)*Z+.36938586D-2)*Z-.079788405)*Z+.79788455)
0014          S = S*(((((-.66777447D-9*Z+.11225331D-6)*Z-.10525853D-4)*Z
              & +.60435371D-3)*Z-.18997110D-1)*Z+.26596149)
0015          RETURN
              C
0016    4     D = DCOS(Z)
0017          S = DSIN(Z)
0018          Z = 4.DO/Z
0019          A = (((((((.87682583D-3*Z-.41692894D-2)*Z+.79709430D-2)*Z
              & -.67928011D-2)*Z-.30953412D-3)*Z+.59721508D-2)*Z-.16064281D-4)*Z
              & -.02493321S)*Z-.44440909D-8
0020          B = ((((((-.66339256D-3*Z+.34014090D-2)*Z-.72716901D-2)*Z
              & +.74282459D-2)*Z-.40271450D-3)*Z-.93149105D-2)*Z-.12079984D-5)*Z
              & +.19947115
0021          Z = DSIGN(.5DO,ZZ)
0022          ZZ = 2.DO/ZZ
0023          C = Z + ZZ*(D*A+S*B)
0024          S = Z + ZZ*(S*A-D*B)
0025          RETURN
0026          END
```

SUBROUTINE

```
0001          FUNCTION DJONE(X)
0002          IMPLICIT REAL*8 (A-Z)
0003          REAL*8 CJ1(7)/.5D0,-.56249985,.21093573,-.3954289D-1,.443319D-2,
             & -.31761D-3,.1109D-4/
0004          REAL*8 CY1(7)/-.6366198D0,.2212091D0,2.1682709,-1.3164827,
             & .3123951D0,-.400976D-1,.27873D-2/
0005          REAL*8 CF1(7)/.79788456,.156D-5,.1659667D-1,.17105D-3,-.249511D-2,
             & .113653D-2,-.20033D-3/
0006          REAL*8 CT1(7)/-2.35619449,.12499612,.565D-4,-.637879D-2,.74348D-3,
             & .79824D-3,-.29166D-3/
0007          ENTRY JONE(X)
0008          IF (DABS(X) .LE. 3.D0) GO TO 600
0009          TOX = 3.D0 / X
0010          F1 = P(TOX,CF1,7)
0011          T1 = X + P(TOX,CT1,7)
0012          JONE = F1*DCOS(T1)/DSQRT(DABS(X))
0013    98    DJONE = JONE
0014    99     RETURN
0015    600   TOX = X*X/9.D0
0016    9     JONE = X*P(TOX,CJ1,7)
0017          GO TO 98
0018          ENTRY YONE(X)
0019          IF (X .LE. 3.D0) GO TO 700
0020          TOX = 3.D0 / X
0021          F1 = P(TOX,CF1,7)
0022          T1 = X + P(TOX,CT1,7)
0023          YONE = F1*DSIN(T1)/DSQRT(X)
0024          RETURN
0025    700   TOX = X*X/9.D0
0026          F1 = .6366197723676*X*DLOG(X/2.D0)*P(TOX,CJ1,7)
0027          YONE = F1 + P(TOX,CY1,7)/X
0028          RETURN
0029          END
```

E.2 Program for evaluating the far field elevation plane carrier mode patterns of conventional VOR and single parasitic loop counterpoise antennas $\left[S^A(\theta),\ S(\theta)\right]$.

Main

```
0001                  IMPLICIT REAL*8(A,B,D-H,K,O-Z),COMPLEX*16(C)
0002                  REAL*8 CDABS
0003                  COMPLEX*16 DCMPLX
0004                  CEIX(XX) = DCMPLX(DCOS(XX),DSIN(XX))
0005                  LOGICAL TERM/.FALSE./
0006                  DATA SQ2/1.41421356237331/, PI/3.14159265358979/
0007                  DATA PDT/1.5707963267949/, EGAM/.577215664901533/
0008                  DATA RCON/.01745329251992/, PDF/.7853981633974 48/
0009                  DATA NTL/3/,ITS/1/
0010                  REAL*8 TH1(10)/5.D0,82.D0,115.D0,7*0.D0/,TH2(10)/80.D0,110.D0,
                     & 170.D0,7*0.D0/, THS(10)/5.D0,2.D0,5.D0,7*0.D0/
0011            10    WRITE (6,999)
0012           999    FORMAT ('1')
0013                  NAMELIST /IN/KH,KA,KB,KCB,KCH
0014                  READ (1,IN,END=500)
0015                  KCB=KCB*3.1415927
0016                  WRITE(6,1000)KH,KB,KA,KCH,KCB
0017          1000    FORMAT(' KH = ',G15.7,'  KB = ',G15.7,'  KA = ',G15.7/
                     &' KCH = ',G15.7,' KCB = ',G15.7/1X)
0018                  IF (.NOT.TERM) WRITE (6,2000)
0019          2000    FORMAT('-',5X,'THETA',4X,'RE(SA)',9X,'IM(SA)',8X,'RE(SP+SP2)',5X,
                     &'IM(SP+SP2)',7X,'RE(S)',10X,'IM(S)',10X,'SQ|S|',10X,'|S| DB' /1X)
0020                  CPLKB = DCMPLX(PDT,EGAM+DLOG(KB*.5D0))
0021                  DO 100 IT=ITS,NTL
0022                  THSIT = THS(IT)
0023                  IF (THSIT) 75,76,75
0024           75     NRT = (TH2(IT)-TH1(IT))/THSIT + 1.5
0025                  GO TO 77
0026           76     NRT = 1
0027           77     THL = TH1(IT)-THSIT
0028                  DO 100 I=1,NRT
0029                  TH = (THL+I*THSIT)*RCON
0030                  CALL FCAL(KH,KA,TH,PHZ,KRZ,CFZ)
0031                  CALL FCAL(KCH,KA,TH,PHP,KRP,CFP)
0032                  TS = DSIN(TH)
0033                  TC = DCOS(TH)
0034                  CALL LEAC(TS,TC,KA,CF1,CF2,CTA)
0035                  TS1 = DSQRT(TS)
0036                  PC = DCOS(PHP)
0037                  PC1 = DSQRT(PC)
0038                  BSL1 = DJONE(KCB*PC)
0039                  BSL2 = DJONE(KCB*TS)
0040                  T1 = (PC1*BSL1-TS1*BSL2)/(PC-TS)
```

```
0041                T2 = PC1*BSL1/(PC+TS)
0042                CLP = CF1*T1 - CF2*T2
0043                PC = DCOS(PHZ)
0044                PC1 = DSQRT(PC*PC*PC)
0045                TS1 = TS1*TS1*TS1
0046                T1 = (PC1-TS1)/(PC-TS)
0047                T2 = PC1 / (PC+TS)
0048                CLZ = CF1*T1 - CF2*T2
0049                T1 = DSIN(PHZ*.5D0)/DSQRT(PI*KRZ*TS)
0050                CXZ = CEIX(KRZ)
0051                CSA = (TS/SQ2)*CFZ*CTA + T1*CXZ*CLZ
0052                T1 = KCP*KCB
0053                T2 = PI*T1
0054                KP1S = T1 + (KCH-KH)**2
0055                CX1 = CEIX(DSQRT(KP1S))/KP1S
0056                KP2S = T1 + (KCH+KH)**2
0057                CT3 = CEIX(DSQRT(KP2S))/KP2S
0058                CT1 = (T2/CPLKB)*(CX1-CT3)
0059                CT2 = (BSL2/SQ2)*CFP*CTA
0060                T1 = DSIN(PHP*.5D0)/DSQRT(PI*KRP*TS)
0061                CT2 = CF2 + T1*CLP*CEIX(KPP)
0062                CSP = CT1 * CT2
0063                T1 = PI*KCB
0064                T1 = DSQRT(T1*T1*T1)
0065                CT1 = CEIX(KCB+KCB+POF) - DSQRT(KCB/KCH)*CEIX(KCH+KCH-POF)
0066                CT1 = CT1 * CX1 * T1
0067                CT1 = CT1 / (-2.D0*CPLKB*CPLKB)
0068                CSP2 = CT1*CT2
0069                ASA = CDABS(CSA)**2
0070                DBCSA = 10.D0*DLOG10(ASA)
0071                CSUM = CSP+CSP2
0072                ASUM = CDABS(CSUM)**2
0073                ARGSUM = ARGC(CSUM)/PCON
0074                DASUM = 10.D0*DLOG10(ASUM)
0075                CS = CSA+CSP+CSP2
0076                ACS = CDABS(CS)**2
0077                DBSUM = 10.D0*DLOG10(ACS)
0078                TH = TH/PCON
0079                IF (TERM) GO TO 79
0080                WRITE(6,2001) TH,CSA,CSUM,CS,ACS,DBSUM
0081        2001    FORMAT(F12.3,1P8D15.6)
0082                GO TO 100
0083        79      WRITE (6,1001) TH,CSA,CSUM,CS,ACS,DBSUM
0084        1001    FORMAT('0TH = ',G15.7,' SA = ',2G15.7/' SP+SP2 = ',2G15.7/
                   &' S = ',2G15.7/' /S/ SQ = ',G15.7,' /S/ DB = ',G15.7)
0085        100     CONTINUE
0086                GO TO 10
0087        500     CALL SYSTEM
0088                END
```

E.3 Program for evaluating the far field elevation plane carrier mode pattern of a double parasitic loop counterpoise antenna. (Mutual effects neglected.)

Main

```
0001                  IMPLICIT COMPLEX*8(A,B,D-H,K,O-Z),COMPLEX*16(C)
0002                  REAL*8 CDABS
0003                  DIMENSION THV(90), CSAV(90), CSUMV1(90), CSUMV2(90)
0004                  NAMELIST /IN/KH,KA,KB,KCB,KCH
0005                111 READ(1,IN,END=100)
0006                  CALL TAB(KH,KA,KCB   ,KCH,THV,CSAV,CSUMV1,KB)
0007                  READ(1,IN,END=100)
0008                  CALL TAB(KH,KA,KCB   ,KCH,THV,CSAV,CSUMV2,KB)
0009                  WRITE(6,30)
0010               30 FORMAT(' ','TH,CS,ACS,DBSUM=')
0011                  DO 20 I=1,85
0012                  TH=THV(I)
0013                  CS=CSAV(I)+CSUMV1(I)+CSUMV2(I)
0014                  ACS=CDABS(CS)**2
0015                  DBSUM=10.D0*DLOG10(ACS)
0016                  WRITE(6,50)TH,CS,ACS,DBSUM
0017               50 FORMAT(F11.3,1P4D15.6)
0018               20 CONTINUE
0019                  GO TO 111
0020              100 CALL SYSTEM
0021                  END

 TOTAL MEMORY REQUIREMENTS 001722 BYTES
```

Tab

```
      SUBROUTINE TAB(KH,KA,KCB  ,KCH,THV,CSAV,CSUMV,KB)
      IMPLICIT REAL*8(A,B,D-H,K,O-Z),COMPLEX*16(C)
      REAL*8 CDABS
      DIMENSION THV(90), CSAV(90), CSUMV(90)
      COMPLEX*16 DCMPLX
      CEIX(XX) = DCMPLX(DCOS(XX),DSIN(XX))
      LOGICAL TERM/.FALSE./
      DATA SQ2/1.41421356237311/, PI/3.14159265358979/
      DATA POT/1.57079632679491/, EGAM/.577215664901533/
      DATA RCON/.01745329251992/, PQF/.785398163397448/
      DATA NTL/3/,ITS/1/
      REAL*8 TH1(10)/5.D0,82.D0,115.D0,7*0.D0/,TH2(10)/80.D0,110.D0,
     & 170.D0,7*0.D0/, THS(10)/5.D0,2.D0,5.D0,7*0.D0/
      WRITE (6,1000) KH,KB,KA,KCH,KCB
 1000 FORMAT(' KH = ',G15.7,'  KB = ',G15.7,'  KA = ',G15.7/
     &' KCH = ',G15.7,' KCB = ',G15.7/1X)
      CPLKB = DCMPLX(POT,EGAM+DLOG(KB*.5D0))
      INDEX=1
      DO 100 I=2,170,2
      TH=I*RCON
      CALL FCAL(KH,KA,TH,PHZ,KRZ,CFZ)
      CALL FCAL(KCH,KA,TH,PHP,KRP,CFP)
      TS = DSIN(TH)
      TC = DCOS(TH)
      CALL LFAC(TS,TC,KA,CF1,CF2,CTA)
      TS1 = DSQRT(TS)
      PC = DCOS(PHP)
      PC1 = DSQRT(PC)
      BSL1 = DJONE(KCB*PC)
      BSL2 = DJONE(KCB*TS)
      T1 = (PC1*BSL1-TS1*BSL2)/(PC-TS)
      T2 = PC1*PSL1/(PC+TS)
      CLP = CF1*T1 - CF2*T2
      PC = DCOS(PHZ)
      PC1 = DSQRT(PC*PC*PC)
      TS1 = TS1*TS1*TS1
      T1 = (PC1-TS1)/(PC-TS)
      T2 = PC1 / (PC+TS)
      CLZ = CF1*T1 - CF2*T2
      T1 = DSIN(PHZ*.5D0)/DSQRT(PI*KRZ*TS)
      CXZ = CEIX(KRZ)
      CSA = (TS/SQ2)*CFZ*CTA + T1*CXZ*CLZ
      T1 = KCB*KCB
      T2 = PI*T1
      KR1S = T1 + (KCH-KH)**2
      CX1 = CEIX(DSQRT(KR1S))/KR1S
      KR2S = T1 + (KCH+KH)**2
      CT3 = CEIX(DSQRT(KR2S))/KR2S
      CT1 = (T2/CPLKB)*(CX1-CT3)
      CT2 = (BSL2/SQ2)*CFP*CTA
      T1 = DSIN(PHP*.5D0)/DSQRT(PI*KRP*TS)
      CT2 = CT2 + T1*CLP*CEIX(KRP)
      CSP = CT1 * CT2
      T1 = PI*KCB
      T1 = DSQRT(T1*T1*T1)
```

```
                CT1 = CDEXP(KCB+KCB+POF) - DSQRT(KCB/KCH)*CDEXP(KCH+KCH-POF)
                CT1 = CT1 * CX1 * T1
                CT1 = CT1 / (-2.D0*CPLKB*CPLKB)
                CSP2 = CT1*CT2
                ASA = CDABS(CSA)**2
                DASA = 10.D0*DLOG10(ASA)
                CSUM = CSP+CSP2
                ASUM = CDABS(CSUM)**2
                ARGSUM = ARGC(CSUM)/RCON
                DASUM = 10.D0*DLOG10(ASUM)
                CS = CSA+CSP+CSP2
                ACS = CDABS(CS)**2
                DBSUM = 10.D0*DLOG10(ACS)
                TH=TH/RCON
                THV(INDEX)=TH
                CSAV(INDEX)=CSA
                CSUMV(INDEX)=CSUM
                INDEX=INDEX+1
                IF (TERM) GO TO 79
                GO TO 100
          79    WRITE (6,1001) TH,CSA,CSUM,CS,ACS,DBSUM
        1001    FORMAT('0TH = ',G15.7,' SA = ',2G15.7/' SP+SP2 = ',2G15.7/
               &' S = ',2G15.7/' /S/ SQ = ',G15.7,' /S/ DB = ',G15.7)
         100    CONTINUE
                RETURN
                END

 TOTAL MEMORY REQUIREMENTS 001038 BYTES
```

E.4 Program for evaluating the far field elevation plane side band mode pattern of a double parasitic loop counterpoise antenna (mutual effects neglected).

Main

```
0001            IMPLICIT REAL*8(A,B,D-H,K,O-Z),COMPLEX*16(C)
0002            REAL*8 CDABS
0003            DIMENSION THV(90), CSAV(90), CSUMV1(90), CSUMV2(90)
0004            NAMELIST /IN/KH,KA,KB,KCB,KCH
0005        111 READ(1,IN,END=100)
0006            WRITE (6,999)
0007        999 FORMAT ('1')
0008            WRITE(6,1000)KH,KA,KB,KCB,KCH
0009           1000 FORMAT(' KH = ',G15.7,' KA = ',G15.7,' KB = ',G15.7/
                   1 ' KCB = ',G15.7,' KCH = ',G15.7//)
0010            CALL TAB(KH,KA,KCB  ,KCH,THV,CSAV,CSUMV1,KB)
0011            READ(1,IN,END=100)
0012            WRITE(6,1000)KH,KA,KB,KCB,KCH
0013            CALL TAB(KH,KA,KCB  ,KCH,THV,CSAV,CSUMV2,KB)
0014            DO 20 I=1,85
0015            TH=THV(I)
0016            CS=CSAV(I)+CSUMV1(I)+CSUMV2(I)
0017            ACS=CDABS(CS)
0018            DBSUM=20.D0*DLOG10(ACS)
0019            WRITE(6,50)TH,CS,ACS,DBSUM
0020         50 FORMAT(F12.3,1P4D15.6)
0021         20 CONTINUE
0022            GO TO 111
0023        100 CALL SYSTEM
0024            END

 TOTAL MEMORY REQUIREMENTS 0017C6 BYTES
```

```
0001                  SUBROUTINE TAB(KH,KA,KCH  ,KCH,THV,CSAV,CSUMV,KB)
0002                  IMPLICIT REAL*8(A,B,D-H,K,O-Z),COMPLEX*16(C)
0003                  REAL*8 CDABS
0004                  DIMENSION THV(90), CSAV(90), CSUMV(90)
0005                  COMPLEX*16 DCMPLX,CFNEWP,CFNEWT
0006                  CFIX(XX) = DCMPLX(DCOS(XX),DSIN(XX))
0007                  LOGICAL TERM/.FALSE./
0008                  DATA SQ2/1.4142135623731/, PI/3.14159265358979/
0009                  DATA POT/1.57079632679349/, EGAM/.577215664901533/
0010                  DATA PCON/.017453292519922/, PUF/.785398163397448/
0011                  DATA NTL/3/,ITS/1/
0012                  REAL*8 TH1(10)/5.DO,82.DO,115.DO,7*0.DO/,TH2(10)/80.DO,110.DO
                     & 170.DO,7*0.DO/,THS(10)/5.DO,2.DO,5.DO,7*0.DO/
0013                  CPLKB=DCMPLX(POT,EGAM+DLOG(KB*.5DO))
0014                  CPLKM=DCMPLX(EGAM+DLOG(KB*.5DO),-POT)
0015                  INDEX=1
0016                  CFNEWA=DCMPLX(0.DO,1.84DO)
0017                  DO 100 I=2,170,2
0018                  TH=I*PCON
0019                  CALL FCAL(KH,KA,TH,PHZ,KRZ,CFZ)
0020                  CALL FCAL(KCH,KA,TH,PHP,KRP,CFP)
0021                  TS = DSIN(TH)
0022                  TC = DCOS(TH)
0023                  CALL LEAC(TS,TC,KA,CF1,CF2,CTA)
0024                  TS1 = DSQRT(TS)
0025                  PC=DCOS(PHP)
0026                  PC1=DSQRT(PC)
0027                  BSL1=DJCNE(KCB*PC)
0028                  BSL2=DJCNE(KCB*TS)
0029                  T1=(PC1*BSL1-TS1*BSL2)/(PC-TS)
0030                  T2=PC1*BSL1/(PC+TS)
0031                  CLP=CF1*T1-CF2*T2
0032                  PC = DCOS(PHZ)
0033                  PC1 = DSQRT(PC*PC*PC)
0034                  TS1 = TS1*TS1*TS1
0035                  APC=AAA(PC)
0036                  ATS=AAA(TS)
0037                  CFNEWP=DCMPLX(0.DO,APC)
0038                  CFNEWT=DCMPLX(0.DO,ATS)
0039                  CT1=(CFNEWP*PC1-CFNEWT*TS1)/(PC-TS)
0040                  CT2=CFNEWP*PC1/(PC+TS)
0041                  CLZ=CF1*CT1-CF2*CT2
0042                  T1 = DSIN(PHZ*.5DO)/DSQRT(PI*KRZ*TS)
0043                  CXZ = CFIX(KRZ)
0044                  CSA=CFZ*CTA*CFNEWT*TS/SQ2+CXZ*CLZ*T1
0045                  T1=KCB*KCB
0046                  T2=PI*T1
0047                  KR1S=T1+(KCH-KH)**2
0048                  CX1=CFIX(DSQRT(KR1S))/KR1S
0049                  KR2S=T1+(KCH+KH)**2
0050                  CT3=CFIX(DSQRT(KR2S))/KR2S
0051                  KCBR1=KCB/DSQRT(KR1S)
0052                  KCBR2=KCB/DSQRT(KR2S)
0053                  CT1=CX1*KCBR1-CT3*KCBR2
0054                  CT1=CT1*CFNEWA*T2/CPLKM
```

```
0055                CT2=CFP*CTA*BSL2/SQ2
0056                T1=DSIN(PHP*.5D0)/DSQRT(PI*KRP*TS)
0057                CT2=CT2+T1*CLP*CFIX(KRP)
0058                CSP12=CT1*CT2
0059                T1=PI*KCB
0060                T1=DSQRT(T1*T1*T1)
0061                CT1=CFIX(KCB+KCB+POF)-DSQRT(KCB/KCH)*CFIX(KCH+KCH-POF)
0062                CT1=CT1*CX1*T1
0063                CT1=-CT1*KCBR1/2.D0/CPLKB/CPLKM
0064                CSP56=CT1*CT2
0065                CSUM=CSP12+CSP56
0066                TH=TH/FCON
0067                THV(INDEX)=TH
0068                CSAV(INDEX)=CSA
0069                CSUMV(INDEX)=CSUM
0070                INDEX=INDEX+1
0071          100 CONTINUE
0072                RETURN
0073                END
```

TOTAL MEMORY REQUIREMENTS 001104 BYTES

FORTRAN IV G COMPILER AAA 04-13-71 20:59.24 PAGE 1

```
0001                FUNCTION AAA(TS)
0002                IMPLICIT REAL*8 (A-Z)
0003                DATA KD/0.9276/
0004                AAA=2.D0*DSIN(KD*TS)
0005                RETURN
0006                END
```

TOTAL MEMORY REQUIREMENTS 00015E BYTES

E.5 Program for evaluating the mutual coupling coefficients K_{12}, K_{21} and also the far field elevation plane carrier mode pattern of a double parasitic loop counterpoise antenna taking into account the effects of mutual coupling.

Main

```
0001                  IMPLICIT REAL*8(A,B,D-H,K,O-Z),COMPLEX*16(C)
0002                  REAL*8 CDABS
0003                  COMPLEX*16 DCMPLX
0004                  CEIX(XX) = DCMPLX(DCOS(XX),DSIN(XX))
0005                  LOGICAL TERM/.FALSE./
0006                  DATA SQ2/1.41421356237331/, PI/3.14159265358979/
0007                  DATA PQT/1.57079632679489/, EGAM/.577215664901533/
0008                  DATA RCON/.01745329251992/, PQF/.785398163397448/
0009                  DATA NTL/3/,ITS/1/
0010                  REAL*8 TH1(10)/5.D0,82.D0,115.D0,7*0.D0/,TH2(10)/80.D0,110.D0,
                     & 170.D0,7*0.D0/, THS(10)/5.D0,2.D0,5.D0,7*0.D0/
0011                  NAMELIST /IN/ KH,KB,KA,KCB1,KCH1,KCB2,KCH2
0012                1 READ(1,IN)
0013               10 WRITE (6,999)
0014              999 FORMAT ('1')
0015                  WRITE(6,1000)KH,KB,KA,KCH1,KCB1,KCH2,KCB2
0016             1000 FORMAT(' KH = ',G15.7,'  KB = ',G15.7,'  KA = ',G15.7/
                     &' KCH1= ',G15.7,' KCB1= ',G15.7/
                     &' KCH2= ',G15.7,' KCB2= ',G15.7/1X)
0017                  IF (.NOT.TERM) WRITE (6,2000)
0018             2000 FORMAT('-',5X,'THETA',4X,'RE(SA)',9X,'IM(SA)',8X,'RE(SP+SP2)',5X,
                     &'IM(SP+SP2)',7X,'RE(S)',10X,'IM(S)',10X,'SQ|S|',10X,'|S| DB' /1X)
0019                  CPLKB = DCMPLX(PQT,EGAM+DLOG(KB*.5D0))
0020                  CPLKM=DCMPLX(EGAM+DLOG(KB*0.5D0),-PQT)
0021                  KR0=(KCH1-KH)*(KCH1-KH)
0022                  KR1=KCB1*KCB1+KR0
0023                  KR0P=(KCH2-KH)**2
0024                  KR1P=KCB2*KCB2+KR0P
0025                  KD0=(KCH2-KCH1)*(KCH2-KCH1)
0026                  KD12=(KCB1-KCB2)*(KCB1-KCB2)+KD0
0027                  KD12P=(KCB1+KCB2)*(KCB1+KCB2)+KD0
0028                  KR=DSQRT(KR1)
0029                  KRP=DSQRT(KR1P)
0030                  KD=DSQRT(KD12)
0031                  KDP=DSQRT(KD12P)
0032                  PKD=DSQRT(2.D0/PI/KD)
0033                  PKDP=DSQRT(2.D0/PI/KDP)
0034                  CT1=CEIX(KD+PQF)
0035                  CT2=CEIX(KDP-PQF)
0036                  CT3=PKD*CT1-PKDP*CT2
0037                  KB1B2=DSQRT(KCB1/KCB2)
0038                  KB2B1=DSQRT(KCB2/KCB1)
0039                  CT4=CEIX(KR)/KR
0040                  CT5=CEIX(KRP)/KRP
```

```
0041                CK2=2I*PI/CPLK2/CPLKM
0042                CK12P=   CK1*KCB1/KB*KB132*CT4*CT3
0043                CK21P=   CK2*KCB2/KBP*KB231*CT5*CT3
0044                KB2=(KCH1+KH)**2
0045                KB=KCB1*KCB1+KB2
0046                KBPP=(KCH2+KH)**2
0047                KB2P=KCB2*KCB2+KB2PP
0048                KB=DSQRT(KB2)
0049                KBP=DSQRT(KB2P)
0050                CT6=CEIX(KB)/KB
0051                CT7=CEIX(KBP)/KBP
0052                CK12PP=-CK2*KCB1/KB*KB132*CT6*CT3
0053                CK21PP=-CK2*KCB2/KBP*KB231*CT7*CT3
0054                CK12=CK12P+CK12PP
0055                CK21=CK21P+CK21PP
0056                WRITE(6,8000)CK12,CK21
0057          8000  FORMAT(4D15.6)
0058                DO 100 IT=ITS,NTH
0059                THSIT = THS(IT)
0060                IF (THSIT) 75,77,75
0061          75    NBT = (TH2(IT)-TH1(IT))/THSIT + 1.5
0062                GO TO 77
0063          76    NBT = 1
0064          77    THL = TH1(IT)-THSIT
0065                DO 100 I=1,NBT
0066                TH = (THL+I*THSIT)*PCON
0067                CALL FCAL(KH,KA,TH,PHZ,KBZ,CFZ)
0068                TS = DSIN(TH)
0069                TC = DCOS(TH)
0070                CALL LEAC(TS,TC,KA,CF1,CF2,CTA)
0071                TS1 = DSQRT(TS)
0072                PC = DCOS(PHZ)
0073                PC1 = DSQRT(PC*PC*PC)
0074                TS1 = TS1*TS1*TS1
0075                T1 = (PC1-TS1)/(PC-TS)
0076                T2 = PC1 / (PC+TS)
0077                CLZ = CF1*T1 - CF2*T2
0078                T1 = DSIN(PHZ*.5D0)/DSQRT(PI*KBZ*TS)
0079                CXZ = CEIX(KBZ)
0080                CSA = (TS/SQ2)*CFZ*CTA + T1*CXZ*CLZ
0081                CALL FOF(TH,KA,KH,KCH1,KB,KCB1,CP1,CQ1,CF1)
0082                CALL FOF(TH,KA,KH,KCH2,KB,KCB2,CP2,CQ2,CF2)
0083                WRITE(6,8000)CP1,CP2
0084                WRITE(6,8000)CQ1,CQ2
0085                WRITE(6,8000)CF1,CF2
0086                CT=KCB1/(2.0D0*(1.0D0-CK12*CK21))
0087                CS1=(CP1+CQ1+CK21*(CP2+CQ2))*CF1*CT
0088                CT=CT*KCB2/KCB1
0089                CS2=((CP2+CQ2+CK12*(CP1+CQ1))*CF2*CT
0090                CS=CSA+CS1+CS2
0091                ACS=CDABS(CS)
0092                DB=20.0D0*DLOG10(ACS)
0093                TH=TH/PCON
0094                WRITE(6,8001)TH,CSA,CS1,CS2,CS,ACS,DB
0095          8001  FORMAT(1X,F7.3,1P10D12.4)
0096            100 CONTINUE
0097                GO TO 1
0098                END
```

TOTAL MEMORY REQUIREMENTS 01162 BYTES

```
FORTRAN IV G COMPILER                    DATE

      SUBROUTINE PSD(TS,AA,KE,KM,KC,KCH,CP,CO,CF)
      IMPLICIT REAL*8(A,B,D-H,K,O-Z),COMPLEX*16(C)
      COMPLEX*16 CEXP,CY
      CEXP(XX) = CDEXP(DCMPLX(0.D0,XX))
      DATA PI/3.14159265358979/, PI2/6.28318530717959/
      DATA PHP/1.570796326794897/, EGAM/.5772156649015329/
      DATA EPS/.01745329251994330/, PHI/.7853981633974483/
      CF = DCMPLX(PHP,-(AM+DLOG(KB*.5D0)))
      TS = DSIN(TH)
      TC = DCOS(TH)
      CALL PCAL(KCH,KA,KB,PHP,KPP,CFP)
      CALL PCAC(TS,TC,KA,CF1,CF2,CTA)
      T1=2.D0*PI*KCP
      KP1S=KCP*KCP+(KCH-KH)**2
      CY1 = CDEXP(DCMPLX(0.D0,KP1S))/KP1S
      KP2S=KCP*KCP+(KCH+KH)**2
      CT2 = CDEXP(DCMPLX(0.D0,KP2S))/KP2S
      CP = (CF1/CDLOG(T1))*(CTA-CT2)
      PC = DSQRT(TS)
      PHP = DSQRT(PHP)
      PC1 = DSQRT(PC)
      SC11 = DCOS(KCP*PC)
      SC12 = DSIN(KCP*TS)
      T1 = (PC1*SC11-TC1*SC12)/(PC-TS)
      T2 = (PC1*SC11/(PC+TS)
      CTP = CF1*T1 - CF2*T2
      SC22 = (SC12/SC22)*PHP*CTA
      T1 = DSQRT(PHP*.5D0*PI/DCOSH(PI*KCP*TS)
      CP = CT2 + T1*CDEXP(CMPLX(KCP)
      T1=DCOS(PI*KCP*TS)
      CT1 = CDEXP(KCP*(CH+PHP)) - DSQRT(KCH/KCH)*CDEXP(KCH+KCH-PHP)
      CT1 = CT1 * CX1 * T1
      CO=CT1/(-1.D0*CDEXP(CMPLX(0.D0*CPLX*8)
      RETURN
      END

 TOTAL MEMORY REQUIREMENTS 000048 BYTES

FORTRAN IV G COMPILER                    DATE

      FUNCTION ARSC(CS)
      IMPLICIT REAL*8(A-Z)
      DIMENSION CS(2)
      ARSC = DATAN2(CS(2),CS(1))
      RETURN
      END

 TOTAL MEMORY REQUIREMENTS 000140 BYTES
EXECUTION TERMINATED
```

E.6 Program for evaluating the far field elevation plane side band mode pattern of a conventional VOR antenna above ground.

Main

```
0001            IMPLICIT REAL*8(A,B,D-H,K,O-Z),COMPLEX*16(C)
0002            REAL*8 CDABS
0003            DIMENSION THV(90), CSAV(90), CSUMV(90)
0004            COMPLEX*16 DCMPLX,CFNEWP,CFNEWT
0005            CEIX(XX) = DCMPLX(DCOS(XX),DSIN(XX))
0006            LOGICAL TERM/.FALSE./
0007            DATA SQ2/1.4142135623731/, PI/3.141592653589793/
0008            DATA POT/1.5707963267949/, EGAM/.5772156649015328/
0009            DATA RCON/.01745329251992/, POF/.7853981633974483/
0010            DATA NIL/3/,ITS/1/
0011            REAL*8 TH1(10)/5.D0,82.D0,115.D0,7*0.D0/,TH2(10)/80.D0,110.D0,
               & 170.D0,7*0.D0/, THS(10)/5.D0,2.D0,5.D0,7*0.D0/
0012            NAMELIST /IN/KH,KA,KB,KCB,KCH
0013            RAT=1.09/1.08
0014          111 READ(1,IN,END=100)
0015            KH=KH*RAT
0016            KA=KA*RAT
0017            KB=KB*RAT
0018            KCB=KCB*3.1415927
0019            WRITE (6,999)
0020          999   FORMAT ('1')
0021            WRITE(6,1000)KH,KA,KB,KCB,KCH
0022           1000 FORMAT(' KH = ',G15.7,' KA = ',G15.7,' KB = ',G15.7/
               1 ' KCB = ',G15.7,' KCH = ',G15.7//)
0023            CPLKB=DCMPLX(POT,EGAM+DLOG(KB*.5D0))
0024            CPLKM=DCMPLX(EGAM+DLOG(KB*.5D0),-POT)
0025            INDEX=1
0026            CFNEWA=DCMPLX(0.D0,1.84D0)
0027            DO 100 J=1,90
0028            IF((J/2)*2.NE.J) TH=(J+1)*RCON
0029            IF((J/2)*2.EQ.J) TH=PI-J*RCON
0030            CALL FCAL(KH,KA,TH,PHZ,KRZ,CFZ)
0031            CALL FCAL(KCH,KA,TH,PHP,KRP,CFP)
0032            TS = DSIN(TH)
0033            TC = DCOS(TH)
0034            CALL LFAC(TS,TC,KA,CF1,CF2,CTA)
0035            TS1 = DSQRT(TS)
```

```
0036                PC=DCOS(PHP)
0037                PC1=DSQRT(PC)
0038                BSL1=BJONE(KCB*PC)
0039                BSL2=BJONE(KCB*TS)
0040                T1=(PC1*BSL1-TS1*BSL2)/(PC-TS)
0041                T2=PC1*BSL1/(PC+TS)
0042                CLP=CF1*T1-CF2*T2
0043                PC = DCOS(PHZ)
0044                PC1 = DSQRT(PC*PC*PC)
0045                TS1 = TS1*TS1*TS1
0046                APC=AAA(PC)
0047                ATS=AAA(TS)
0048                CFNEWP=DCMPLX(0.D0,APC)
0049                CFNEWT=DCMPLX(0.D0,ATS)
0050                CT1=(CFNEWP*PC1-CFNEWT*TS1)/(PC-TS)
0051                CT2=CFNEWP*PC1/(PC+TS)
0052                CLZ=CF1*CT1-CF2*CT2
0053                T1 = DSIN(PHZ*.5D0)/DSQRT(PI*KRZ*TS)
0054                CXZ = CEIX(KRZ)
0055                CSA=CFZ*CTA*CFNEWT*TS/SQ2+CXZ*CLZ*T1
0056                CSAV(INDEX)=CSA
0057                THV(INDEX)=TH
0058                INDEX=INDEX+1
0059          100 CONTINUE
0060                WRITE(6,51)
0061           51   FORMAT(' ','TH,CSA,ACS,DB=')
0062                DO 20 I=1,90,2
0063                THA=THV(I)
0064                ZI=6.89*7.5*RAT*DCOS(THA)
0065                TH=THV(I)/RCON
0066                CSA=CEIX(-ZI)*CSAV(I)-CEIX(ZI)*CSAV(I+1)
0067                ACS=CDABS(CSA)
0068                IF(ACS.LT.1.D-4) ACS=1.D-4
0069                DB=20.D0*DLOG10(ACS)
0070                WRITE(6,50)TH,CSA,ACS,DB
0071             50 FORMAT(F12.3,1P4D15.6)
0072           20   CONTINUE
0073                GO TO 111
0074                END

 TOTAL MEMORY REQUIREMENTS 001CFE BYTES
```

```
$RUN -LOAD#+SUB+RLIB 1=*SOURCE*
EXECUTION BEGINS




 FORTRAN IV G COMPILER        AAA              04-07-71        10:11.14        PAGE

  0001                  FUNCTION AAA(TS)
  0002                  IMPLICIT REAL*8 (A-Z)
  0003                  DATA KD/0.9276/
  0004                  AAA=2.D0*DSIN(KD*TS)
  0005                  RETURN
  0006                  END

   TOTAL MEMORY REQUIREMENTS 00015E BYTES
EXECUTION TERMINATED
```

E.7 Program for evaluating the far field elevation plane carrier mode pattern of a double parasitic loop counterpoise antenna above ground.

```
FORTRAN IV G COMPILER        MAIN

0001                 IMPLICIT REAL*8(A,B,D-H,K,O-Z),COMPLEX*16(C)
0002                 REAL*8 CDABS
0003                 DIMENSION THV(90), CSAV(90), CSUMV1(90), CSUMV2(90)
0004                 NAMELIST /IN/KH,KA,KB,KCB,KCH
0005                 CPIX(ZZ)=DCMPLX(DCOS(ZZ),DSIN(ZZ))
0006                 RCON=0.01745329251992
0007                 RAT=1.09/1.08
0008              111 READ(1,IN,END=100)
0009                 KH=KH*RAT
0010                 KA=KA*RAT
0011                 KB=KB*RAT
0012                 CALL TAB(KH,KA,KCB  ,KCH,THV,CSAV,CSUMV1,KB)
0013                 READ(1,IN,END=100)
0014                 KH=KH*RAT
0015                 KA=KA*RAT
0016                 KB=KB*RAT
0017                 CALL TAB(KH,KA,KCB  ,KCH,THV,CSAV,CSUMV2,KB)
0018                 WRITE(6,30)
0019              30 FORMAT(' ','TH,CS,ACS,DBSUM=')
0020                 DO 20 I=1,90,2
0021                 THA=THV(I)
0022                 ZI=6.89*7.5*RAT*DCOS(THA)
0023                 TH=THV(I)/RCON
0024                 CS=CPIX(-ZI)*(CSAV(I)+CSUMV1(I)+CSUMV2(I))-CPIX(ZI)*(CSAV(I+1)+
                    1CSUMV1(I+1)+CSUMV2(I+1))
0025                 ACS=CDABS(CS)**2
0026                 IF(ACS.LT.1.D-4) ACS=1.D-4
0027                 DBSUM=10.D0*DLOG10(ACS)
0028                 WRITE(6,50)TH,CS,ACS,DBSUM
0029              50 FORMAT(F11.3,1P4D15.6)
0030              20 CONTINUE
0031                 GO TO 111
0032             100 CALL SYSTEM
0033                 END

 TOTAL MEMORY REQUIREMENTS 0019C6 BYTES
```

```
FORTRAN IV G COMPILER        TAB

0001                SUBROUTINE TAB(KH,KA,KCB  ,KCH,THV,CSAV,CSUMV,KB)
0002                IMPLICIT REAL*8(A,B,D-H,K,O-Z),COMPLEX*16(C)
0003                REAL*8 CDABS
0004                DIMENSION THV(90), CSAV(90), CSUMV(90)
0005                COMPLEX*16 DCMPLX
0006                CEIX(XX) = DCMPLX(DCOS(XX),DSIN(XX))
0007                LOGICAL TERM/.FALSE./
0008                DATA SQ2/1.41421356237312/, PI/3.14159265358979/
0009                DATA POT/1.57079632679491/, EGAM/.577215664901533/
0010                DATA PCON/.01745329251992/, POF/.785398163397448/
0011                DATA NTL/3/,ITS/1/
0012                REAL*8 TH1(10)/5.D0,82.D0,115.D0,7*0.D0/,TH2(10)/80.D0,110.D0,
                   & 170.D0,7*0.D0/, THS(10)/5.D0,2.D0,5.D0,7*0.D0/
0013                WRITE (6,1000) KH,KB,KA,KCH,KCB
0014          1000  FORMAT(' KH = ',G15.7,'  KB = ',G15.7,'  KA = ',G15.7/
                   &' KCH = ',G15.7,' KCB = ',G15.7/1X)
0015                CPLKB = DCMPLX(POT,EGAM+DLOG(KB*.5D0))
0016                INDEX=1
0017                DO 100 I=1,90
0018                IF((I/2)*2.NE.I) TH=(I+1)*RCON
0019                IF((I/2)*2.EQ.I) TH=PI-I*RCON
0020                CALL FCAL(KH,KA,TH,PHZ,KRZ,CFZ)
0021                CALL FCAL(KCH,KA,TH,PHP,KRP,CFP)
0022                TS = DSIN(TH)
0023                TC = DCOS(TH)
0024                CALL LFAC(TS,TC,KA,CF1,CF2,CTA)
0025                TS1 = DSQRT(TS)
0026                PC = DCOS(PHP)
0027                PC1 = DSQRT(PC)
0028                BSL1 = DJONE(KCB*PC)
0029                BSL2 = DJONE(KCB*TS)
0030                T1 = (PC1*BSL1-TS1*BSL2)/(PC-TS)
0031                T2 = PC1*BSL1/(PC+TS)
0032                CLP = CF1*T1 - CF2*T2
0033                PC = DCOS(PHZ)
0034                PC1 = DSQRT(PC*PC*PC)
0035                TS1 = TS1*TS1*TS1
0036                T1 = (PC1-TS1)/(PC-TS)
0037                T2 = PC1 / (PC+TS)
0038                CLZ = CF1*T1 - CF2*T2
0039                T1 = DSIN(PHZ*.5D0)/DSQRT(PI*KRZ*TS)
0040                CXZ = CEIX(KRZ)
0041                CSA = (TS/SQ2)*CFZ*CTA + T1*CXZ*CLZ
0042                T1 = KCB*KCB
0043                T2 = PI*T1
0044                KR1S = T1 + (KCH-KH)**2
0045                CX1 = CEIX(DSQRT(KR1S))/KR1S
0046                KR2S = T1 + (KCH+KH)**2
0047                CT3 = CEIX(DSQRT(KR2S))/KR2S
0048                CT1 = (T2/CPLKB)*(CX1-CT3)
0049                CT2 = (BSL2/SQ2)*CFP*CTA
0050                T1 = DSIN(PHP*.5D0)/DSQRT(PI*KRP*TS)
0051                CT2 = CT2 + T1*CLP*CEIX(KRP)
0052                CSP = CT1 * CT2
0053                T1 = PI*KCB
```

```
FORTRAN IV G LEVEL 21                                    MAIN
0054                  T1 = 1.0/((T1*T1)*T1)
0055                  CT1 = C1*(RC*T*(C1+PLF) - 1.5*T1*(RC1/RCH)*CEIX(RCP+RCH-PCF)
0056                  CT1 = CT1 * CT1 * T1
0057                  CT1 = CT1 / (-2.*C1*LN*(PLAS)
0058                  CSA = 2.*CT2
0059                  ASA = 1.0/SIN(CSA)**2
0060                  ACS = 1.0-1.0/(ASA)
0061                  CSU = CSP+CSP2
0062                  CSUM = COS(CSU)**2
0063                  ASUM = ACOS(CSUM)/CSU
0064                  DSUM = (1.0)*ALOG(ZSUM)
0065                  CS = CSP+CSP2
0066                  ACS = COS(CS)**2
0067                  DSUM = 1.0*ALOG(ACS)
0068                  WRITE(1,60)T
0069                  WRITE(1,70)CSP
0070                  WRITE(1,80)CSUM
0071                  IF(T-1.0) 30,30,20
0072                  DO 10 I=1,2
0073                  WRITE(1,90) (T,CSP,CSU,CSUM,CS,ACS,DSUM
0074            90    FORMAT(' T = ',G15.7,' CSP = ',G15.7,' CSU = ',G15.7,' CSUM = ',G15.7/
0075           1' CS = ',G15.7,' ACS = ',G15.7,' DSUM = ',G15.7)
0076           10     CONTINUE
0077                  GO TO 40
0078           30     CONTINUE

TOTAL MEMORY REQUIREMENTS ...
```

E.8 Program for evaluating the far field elevation plane side band mode pattern of a double parasitic loop counterpoise antenna.

Main

```
0001              IMPLICIT REAL*8(A,B,D-H,K,O-Z),COMPLEX*16(C)
0002              REAL*8 CDABS
0003              DIMENSION THV(90), CSAV(90), CSUMV1(90), CSUMV2(90)
0004              NAMELIST /IN/KH,KA,KB,KCB,KCH
0005              CPIX(ZZ)=DCMPLX(DCOS(ZZ),DSIN(ZZ))
0006              RCON=0.01745329251992
0007              RAT=1.09/1.08
0008           111  READ(1,IN,END=100)
0009              WRITE (6,999)
0010           999  FORMAT ('1')
0011              KH=KH*RAT
0012              KA=KA*RAT
0013              KB=KB*RAT
0014              WRITE(6,1000)KH,KA,KB,KCB,KCH
0015          1000 FORMAT(' KH = ',G15.7,' KA = ',G15.7,' KB = ',G15.7/
                 1 ' KCB = ',G15.7,' KCH = ',G15.7//)
0016              CALL TAB(KH,KA,KCB  ,KCH,THV,CSAV,CSUMV1,KB)
0017              READ(1,IN,END=100)
0018              KH=KH*RAT
0019              KA=KA*RAT
0020              KB=KB*RAT
0021              WRITE(6,1000)KH,KA,KB,KCB,KCH
0022              CALL TAB(KH,KA,KCB  ,KCH,THV,CSAV,CSUMV2,KB)
0023              WRITE(6,30)
0024           30 FORMAT(' ','Z2,TH,THR,CS,ACS,DBSUM=')
0025              DO 20 I=1,90,2
0026              THA=THV(I)
0027              ZI=6.89*7.5*RAT*DCOS(THA)
0028              TH=THV(I)/RCON
0029              CS=CPIX(-ZI)*(CSAV(I)+CSUMV1(I)+CSUMV2(I))-CPIX(ZI)*(CSAV(I+1)+
                 1CSUMV1(I+1)+CSUMV2(I+1))
0030              ACS=CDABS(CS)
0031              IF(ACS.LT.1.D-4) ACS=1.D-4
0032              DBSUM=20.D0*DLOG10(ACS)
0033              WRITE(6,50)TH,CS,ACS,DBSUM
0034           50 FORMAT(F12.3,1P4D15.6)
0035           20 CONTINUE
0036              GO TO 111
0037          100 CALL SYSTEM
0038              END

 TOTAL MEMORY REQUIREMENTS 001AA2 BYTES
```

```
0001                SUBROUTINE TAB(KH,KA,KCB  ,KCH,THV,CSAV,CSUMV,KB)
0002                IMPLICIT REAL*8(A-H,K,O-Z),COMPLEX*16(C)
0003                REAL*8 DSIN
0004                DIMENSION THV(90), CSAV(90), CSUMV(90)
0005                COMPLEX*16 DCMPLX,CFNEWP,CFNEWT
0006                CEXA(XX) = DCMPLX(DCOS(XX),DSIN(XX))
0007                LOGICAL TEST/.FALSE./
0008                DATA SQ2/1.4142135623731/, PI/3.14159265358979/
0009                DATA PHT/1.57079632679491/, EGAM/.577215664901533/
0010                DATA EGMN/.017453292519922/, PQF/.78539816339744831/
0011                DATA NTE/5/,ITS/1/
0012                REAL*8 TH1(10)/5.00,82.00,115.00,7*0.00/,TH2(10)/80.00,110.0
                   & 170.00,7*0.00/,THS(10)/5.00,2.00,5.00,7*0.00/
0013                CPLKB=DCMPLX(PHT,EGAM+DLOG(KB*.500))
0014                CPLKM=DCMPLX(EGAM+DLOG(KB*.500),-PHT)
0015                INDEX=1
0016                CFNEWA=DCMPLX(0.00,1.8400)
0017                DO 100 I=1,90
0018                IF((I/2)*2.NE.I) TH=(I+1)*RCON
0019                IF((I/2)*2.EQ.I) TH=PI-I*RCON
0020                CALL FCAL(KH,KA,TH,PHZ,KRZ,CFZ)
0021                CALL FCAL(KCH,KA,TH,PHP,KRP,CFP)
0022                TS = DSIN(TH)
0023                TC = DCOS(TH)
0024                CALL LFAC(TS,TC,KA,CF1,CF2,CTA)
0025                TS1 = DSQRT(TS)
0026                PC=DCOS(PHP)
0027                PC1=DSQRT(PC)
0028                BSL1=DBESJ1(KCB*PC)
0029                BSL2=DBESJ1(KCB*TS)
0030                T1=(PC1*BSL1-TS1*BSL2)/(PC-TS)
0031                T2=PC1*BSL1/(PC+TS)
0032                CLP=CF1*T1-CF2*T2
0033                PC = DCOS(PHZ)
0034                PC1 = DSQRT(PC*PC*PC)
0035                TS1 = TS1*TS1*TS1
0036                APC=AAA(PC)
0037                ATS=AAA(TS)
0038                CFNEWP=DCMPLX(0.00,APC)
0039                CFNEWT=DCMPLX(0.00,ATS)
0040                CT1=(CFNEWP*PC1-CFNEWT*TS1)/(PC-TS)
0041                CT2=CFNEWP*PC1/(PC+TS)
0042                CLZ=CF1*CT1-CF2*CT2
0043                T1 = DSIN(PHZ*.500)/DSQRT(PI*KRZ*TS)
0044                CX7 = CEXP(KRZ)
0045                CSA=CF7*CTA*CFNEWT*TS/SQ2+CX7*CLZ*T1
0046                T1=KCB*KCB
0047                T2=PI*T1
0048                KR1S=T1+(KCH-KH)**2
0049                CX1=CEXP(DSQRT(KR1S))/KR1S
0050                KR2S=T1+(KCH+KH)**2
0051                CT3=CEXP(DSQRT(KR2S))/KR2S
0052                KCBR1=KCB/DSQRT(KR1S)
0053                KCBR2=KCB/DSQRT(KR2S)
0054                CT1=CX1*KCBR1-CT3*KCBR2
```

```
FORTRAN IV G COMPILER        TAB              02-16-71        08:31.58        PAGE 000

0055                CT1=CT1*CFNEWA*T2/CPLKM
0056                CT2=CFP*CTA*BSL2/SQ2
0057                T1=DSIN(PHP*.5D0)/DSQRT(PI*KRP*TS)
0058                CT2=CT2+T1*CLP*CEIX(KRP)
0059                CSP12=CT1*CT2
0060                T1=PI*KCB
0061                T1=DSQRT(T1*T1*T1)
0062                CT1=CEIX(KCB+KCB+POF)-DSQRT(KCB/KCH)*CEIX(KCH+KCH-POF)
0063                CT1=CT1*CX1*T1
0064                CT1=-CT1*KCBR1/2.D0/CPLKB/CPLKM
0065                CSP56=CT1*CT2
0066                CSUM=CSP12+CSP56
0067                THV(INDEX)=TH
0068                CSAV(INDEX)=CSA
0069                CSUMV(INDEX)=CSUM
0070                INDEX=INDEX+1
0071            100 CONTINUE
0072                RETURN
0073                END

 TOTAL MEMORY REQUIREMENTS 001162 BYTES


FORTRAN IV G COMPILER        AAA              02-16-71        08:32.03        PAGE 00

0001                FUNCTION AAA(TS)
0002                IMPLICIT REAL*8 (A-Z)
0003                DATA KD/0.92/
0004                AAA=2.D0*DSIN(KD*TS)
0005                RETURN
0006                END

 TOTAL MEMORY REQUIREMENTS 00015E BYTES
```

E.9 Program for evaluating the quasi far zone elevation plane side band mode field of conventional VOR antenna above ground.

Main

```
      IMPLICIT COMPLEX*8(A,B,D-H,K,O-Z),COMPLEX*16(C)
      REAL*8 CONST
      DIMENSION THV(90), CSAV(90), CSDMV(90)
      COMPLEX*16 DCMPLX,CFN,KP,CFNPT
      CFIX(XX) = DCMPLX(DCOS(XX),DSIN(XX))
      LOGICAL ITS/.FALSE./
      DATA S32/1.414213562373L/, PI/3.14159265358979/
      DATA PPI/1.570796326794L/, EGAM/.577215664901533/
      DATA RCON/.0174532925199L/, PHF/.7853981633974L/
      DATA NTL/3/,ITS/1/
      REAL*8 TH1(10)/5.00,82.00,115.00,7*0.00/,TH2(10)/80.00,110.
     & 170.00,7*0.00/, THS(10)/5.00,2.00,5.00,7*0.00/
      NAMELIST /IN/KH,KA,KB,KCB,KCH
      RAT=1.09/1.00
  111 READ(1,IN,END=100)
      KH=KH*RAT
      KA=KA*RAT
      KB=KB*RAT
      KCB=KCH*3.1415927
      WRITE (6,999)
  999 FORMAT ('1')
      WRITE(6,1000)KH,KA,KB,KCB,KCH
 1000 FORMAT(' KH = ',G15.7,' KA = ',G15.7,' KB = ',G15.7/
     1 ' KCB = ',G15.7,' KCH = ',G15.7//)
      CPLKB=DCMPLX(PGT,EGAM+DLOG(KB*.500))
      CPLKH=DCMPLX(EGAM+DLOG(KB*.500),-PGT)
      INDEX=1
      CFNEGA=DCMPLX(0.00,1.8400)
      DO 10 I=1,32
      I1=(I+1)/2
      DEG=2.5*I1
      Z2=8.0-DEG
      IF((I/2)*2.NE.I) TH=DATAN2((7.5-Z2),30.000)+PGT
      IF((I/2)*2.EQ.I) TH=DATAN2((7.5+Z2),30.000)+PGT
      CALL FCAL(KH,KA,TH,PHZ,KRZ,CFZ)
      CALL FCAL(KCH,KA,TH,PHP,KRP,CFP)
      TS = DSIN(TH)
      TC = DCOS(TH)
      CALL LFAC(TS,TC,KA,CF1,CF2,CTA)
      TS1 = DSQRT(TS)
      PC=DCOS(PHP)
      PC1=DSQRT(PC)
```

```
0041                BSL1=DJONE(KCB*PC)
0042                BSL2=DJONE(KCB*TS)
0043                T1=(PC1*BSL1-TS1*BSL2)/(PC-TS)
0044                T2=PC1*BSL1/(PC+TS)
0045                CLP=CF1*T1-CF2*T2
0046                PC = DCOS(PHZ)
0047                PC1 = DSQRT(PC*PC*PC)
0048                TS1 = TS1*TS1*TS1
0049                APC=AAA(PC)
0050                ATS=AAA(TS)
0051                CFNEWP=DCMPLX(0.D0,APC)
0052                CFNEWT=DCMPLX(0.D0,ATS)
0053                CT1=(CFNEWP*PC1-CFNEWT*TS1)/(PC-TS)
0054               CT2=CFNEWP*PC1/(PC+TS)
0055                CLZ=CF1*CT1-CF2*CT2
0056                T1 = DSIN(PHZ*.5D0)/DSQRT(PI*KRZ*TS)
0057                CXZ = CEIX(KRZ)
0058                CSA=CFZ*CTA*CFNEWT*TS/SQ2+CXZ*CLZ*T1
0059                CSAV(INDEX)=CSA
0060                THV(INDEX)=TH
0061                INDEX=INDEX+1
0062             100 CONTINUE
0063                WRITE(6,51)
0064              51  FORMAT(' ','Z2,TH,THR,CSA,ACS,DB=')
0065                DO 20 I=1,32,2
0066                TH=THV(I)/RCON
0067                THR=THV(I+1)/RCON
0068                Z2=8.0-((I+1)/2)*0.5
0069                CSA=CSAV(I)-CEIX(Z2*6.89*RAT/2.)*CSAV(I+1)
0070                ACS=CDABS(CSA)
0071                IF(ACS.LT.1.D-4) ACS=1.D-4
0072                DB=20.D0*DLOG10(ACS)
0073                WRITE(6,50)Z2,TH,THR,CSA,ACS,DB
0074              50  FORMAT(F11.3,1P6D15.6)
0075              20  CONTINUE
0076                GO TO 111
0077                END

  TOTAL MEMORY REQUIREMENTS 001D6A BYTES
```

AAA

```
0001                FUNCTION AAA(TS)
0002                IMPLICIT REAL*8 (A-Z)
0003                DATA KD/0.9276/
0004                AAA=2.D0*DSIN(KD*TS)
0005                RETURN
0006                END

   TOTAL MEMORY REQUIREMENTS 00015E BYTES
EXECUTION TERMINATED
```

E.10 **Program for evaluating the quasi far zone elevation plane carrier mode field of a double parasitic loop counterpoise antenna above ground.**

Main

```
0001              IMPLICIT REAL*8(A,B,D-H,K,O-Z),COMPLEX*16(C)
0002              REAL*8 CDABS
0003              DIMENSION THV(90), CSAV(90), CSUMV1(90), CSUMV2(90)
0004              NAMELIST /IN/KH,KA,KB,KCB,KCH
0005              CPIX(ZZ)=DCMPLX(DCOS(ZZ),DSIN(ZZ))
0006              RCON=0.01745329251992
0007              RAT=1.09/1.08
0008            111 READ(1,IN,END=100)
0009                KH=KH*RAT
0010                KA=KA*RAT
0011                KB=KB*RAT
0012                CALL TAB(KH,KA,KCB  ,KCH,THV,CSAV,CSUMV1,KB)
0013                READ(1,IN,END=100)
0014                KH=KH*RAT
0015                KA=KA*RAT
0016                KB=KB*RAT
0017                CALL TAB(KH,KA,KCB  ,KCH,THV,CSAV,CSUMV2,KB)
0018                WRITE(6,30)
0019             30 FORMAT(' ','Z2,TH,THR,CS,ACS,DBSUM=')
0020                DO 20 I=1,32,2
0021                TH=THV(I)
0022                THR=THV(I+1)
0023                Z2=8.0-((I+1)/2)*0.5
0024                CS=CSAV(I)+CSUMV1(I)+CSUMV2(I)-CPIX(Z2*6.89*RAT/2.)*(CSAV(I+1)+
                   1CSUMV1(I+1)+CSUMV2(I+1))
0025                ACS=CDABS(CS)**2
0026                IF(ACS.LT.1.D-4) ACS=1.D-4
0027                DBSUM=10.D0*DLOG10(ACS)
0028                WRITE(6,50)Z2,TH,THR,CS,ACS,DBSUM
0029             50 FORMAT(F11.3,1P6D15.6)
0030             20 CONTINUE
0031                GO TO 111
0032            100 CALL SYSTEM
0033                END

 TOTAL MEMORY REQUIREMENTS 0019BE BYTES
```

```
0001              SUBROUTINE TAB(KH,KA,KCB  ,KCH,THV,CSAV,CSUMV,KB)
0002              IMPLICIT REAL*8(A,B,D-H,K,O-Z),COMPLEX*16(C)
0003              REAL*8 CDABS
0004              DIMENSION THV(90), CSAV(90), CSUMV(90)
0005              COMPLEX*16 DCMPLX
0006              CEIX(XX) = DCMPLX(DCOS(XX),DSIN(XX))
0007              LOGICAL TERM/.FALSE./
0008              DATA SQ2/1.41421356237311/, PI/3.14159265358979/
0009              DATA POT/1.57079632679491/, EGAM/.577215664901533/
0010              DATA RCON/.01745329251992/, POF/.785398163397448/
0011              DATA NTL/3/,ITS/1/
0012              REAL*8 TH1(10)/5.D0,82.D0,115.D0,7*0.D0/,TH2(10)/80.D0,110.D0,
                 & 170.D0,7*0.D0/, THS(10)/5.D0,2.D0,5.D0,7*0.D0/
0013              WRITE (6,1000) KH,KB,KA,KCH,KCB
0014          1000  FORMAT(' KH = ',G15.7,'  KB = ',G15.7,'  KA = ',G15.7/
                 &' KCH = ',G15.7,' KCB = ',G15.7/1X)
0015              CPLKB = DCMPLX(POT,EGAM+DLOG(KB*.5D0))
0016              INDEX=1
0017              DO 100 I=1,32
0018              I1=(I+1)/2
0019              DEC=0.5*I1
0020              Z2=8.0-DEC
0021              IF((I/2)*2.NE.I) TH=DATAN2((7.5-Z2),30.0D0)+POT
0022              IF((I/2)*2.EQ.I) TH=DATAN2((7.5+Z2),30.0D0)+POT
0023              CALL FCAL(KH,KA,TH,PHZ,KRZ,CFZ)
0024              CALL FCAL(KCH,KA,TH,PHP,KRP,CFP)
0025              TS = DSIN(TH)
0026              TC = DCOS(TH)
0027              CALL LFAC(TS,TC,KA,CF1,CF2,CTA)
0028              TS1 = DSQRT(TS)
0029              PC = DCOS(PHP)
0030              PC1 = DSQRT(PC)
0031              BSL1 = DJONE(KCB*PC)
0032              BSL2 = DJONE(KCB*TS)
0033              T1 = (PC1*BSL1-TS1*BSL2)/(PC-TS)
0034              T2 = PC1*BSL1/(PC+TS)
0035              CLP = CF1*T1 - CF2*T2
0036              PC = DCOS(PHZ)
0037              PC1 = DSQRT(PC*PC*PC)
0038              TS1 = TS1*TS1*TS1
0039              T1 = (PC1-TS1)/(PC-TS)
0040              T2 = PC1 / (PC+TS)
0041              CLZ = CF1*T1 - CF2*T2
0042              T1 = DSIN(PHZ*.5D0)/DSQRT(PI*KRZ*TS)
0043              CXZ = CEIX(KRZ)
0044              CSA = (TS/SQ2)*CFZ*CTA + T1*CXZ*CLZ
0045              T1 = KCB*KCB
0046              T2 = PI*T1
0047              KR1S = T1 + (KCH-KH)**2
0048              CX1 = CEIX(DSQRT(KR1S))/KR1S
0049              KR2S = T1 + (KCH+KH)**2
0050              CT3 = CEIX(DSQRT(KR2S))/KR2S
0051              CT1 = (T2/CPLKB)*(CX1-CT3)
0052              CT2 = (BSL2/SQ2)*CFP*CTA
0053              T1 = DSIN(PHP*.5D0)/DSQRT(PI*KRP*TS)
```

```
0054                CT2 = CT2 + T1*CLP*CEIX(KRP)
0055                CSP = CT1 * CT2
0056                T1 = PI*KCB
0057                T1 = DSQRT(T1*T1*T1)
0058                CT1 = CEIX(KCB+KCB+POF) - DSQRT(KCB/KCH)*CEIX(KCH+KCH-POF)
0059                CT1 = CT1 * CX1 * T1
0060                CT1 = CT1 / (-2.D0*CPLKB*CPLKB)
0061                CSP2 = CT1*CT2
0062                ASA = CDABS(CSA)**2
0063                DBCSA = 10.D0*DLOG10(ASA)
0064                CSUM = CSP+CSP2
0065                ASUM = CDABS(CSUM)**2
0066                ARCSUM = ARGC(CSUM)/RCON
0067                DASUM = 10.D0*DLOG10(ASUM)
0068                CS = CSA+CSP+CSP2
0069                ACS = CDABS(CS)**2
0070                DBSUM = 10.D0*DLOG10(ACS)
0071                TH=TH/RCON
0072                THV(INDEX)=TH
0073                CSAV(INDEX)=CSA
0074                CSUMV(INDEX)=CSUM
0075                INDEX=INDEX+1
0076                IF (TERM) GO TO 79
0077                GO TO 100
0078          79    WRITE (6,1001) TH,CSA,CSUM,CS,ACS,DBSUM
0079          1001  FORMAT('0TH = ',G15.7,' SA = ',2G15.7/' SP+SP2 = ',2G15.7/
                    &' S = ',2G15.7/' /S/ SQ = ',G15.7,' /S/ DB = ',G15.7)
0080          100   CONTINUE
0081                RETURN
0082                END
```

TOTAL MEMORY REQUIREMENTS 001114 BYTES

E.11 Program for evaluating the quasi far zone elevation plane side band mode field of a double parasitic loop counterpoise antenna above ground.

Main

```
0001            IMPLICIT REAL*8(A,B,D-H,K,O-Z),COMPLEX*16(C)
0002            REAL*8 CDABS
0003            DIMENSION THV(90), CSAV(90), CSUMV1(90), CSUMV2(90)
0004            NAMELIST /IN/KH,KA,KB,KCB,KCH
0005            CPIX(ZZ)=DCMPLX(DCOS(ZZ),DSIN(ZZ))
0006            RAT=1.09/1.08
0007        111 READ(1,IN,END=100)
0008            WRITE (6,999)
0009        999 FORMAT ('1')
0010            KH=KH*RAT
0011            KA=KA*RAT
0012            KB=KB*RAT
0013            WRITE(6,1000)KH,KA,KB,KCB,KCH
0014       1000 FORMAT(' KH = ',G15.7,' KA = ',G15.7,' KB = ',G15.7/
                1 ' KCB = ',G15.7,' KCH = ',G15.7//)
0015            CALL TAB(KH,KA,KCB  ,KCH,THV,CSAV,CSUMV1,KB)
0016            READ(1,IN,END=100)
0017            KH=KH*RAT
0018            KA=KA*RAT
0019            KB=KB*RAT
0020            WRITE(6,1000)KH,KA,KB,KCB,KCH
0021            CALL TAB(KH,KA,KCB  ,KCH,THV,CSAV,CSUMV2,KB)
0022            WRITE(6,30)
0023         30 FORMAT(' ','Z2,TH,THR,CS,ACS,DBSUM=')
0024            DO 20 I=1,32,2
0025            TH=THV(I)
0026            THR=THV(I+1)
0027            Z2=8.0-((I+1)/2)*0.5
0028            CS=CSAV(I)+CSUMV1(I)+CSUMV2(I)-CPIX(Z2*6.89*RAT/2.)*(CSAV(I+1)+
                1CSUMV1(I+1)+CSUMV2(I+1))
0029            ACS=CDABS(CS)
0030            IF(ACS.LT.1.D-4) ACS=1.D-4
0031            DBSUM=20.D0*DLOG10(ACS)
0032            WRITE(6,50)Z2,TH,THR,CS,ACS,DBSUM
0033         50 FORMAT(F11.3,1P6D15.6)
0034         20 CONTINUE
0035            GO TO 111
0036        100 CALL SYSTEM
0037            END

 TOTAL MEMORY REQUIREMENTS 001A76 BYTES
```

```
0001                SUBROUTINE TAB(KH,KA,KCB  ,KCH,THV,CSAV,CSUMV,KB)
0002                IMPLICIT REAL*8(A,B,D-H,K,O-Z),COMPLEX*16(C)
0003                REAL*8 CDABS
0004                DIMENSION THV(90), CSAV(90), CSUMV(90)
0005                COMPLEX*16 DCMPLX,CFNEWP,CFNEWT
0006                CEIX(XX) = DCMPLX(DCOS(XX),DSIN(XX))
0007                LOGICAL TERM/.FALSE./
0008                DATA SQ2/1.41421356237311/, PI/3.14159265358979/
0009                DATA POT/1.5707963267949/, EGAM/.577215664901533/
0010                DATA RCON/.01745329251992/, POF/.785398163397448/
0011                DATA NTL/3/,ITS/1/
0012                REAL*8 TH1(10)/5.D0,82.D0,115.D0,7*0.D0/,TH2(10)/80.D0,110.D0,
                   & 170.D0,7*0.D0/,THS(10)/5.D0,2.D0,5.D0,7*0.D0/
0013                CPLKB=DCMPLX(POT,EGAM+DLOG(KB*.5D0))
0014                CPLKM=DCMPLX(EGAM+DLOG(KB*.5D0),-POT)
0015                INDEX=1
0016                CFNEWA=DCMPLX(0.D0,1.84D0)
0017                DO 100 I=1,32
0018                I1=(I+1)/2
0019                DEC=0.5*I1
0020                Z2=8.0-DEC
0021                IF((I/2)*2.NE.I) TH=DATAN2((7.5-Z2),30.0D0)+POT
0022                IF((I/2)*2.EQ.I) TH=DATAN2((7.5+Z2),30.0D0)+POT
0023                CALL FCAL(KH,KA,TH,PHZ,KRZ,CFZ)
0024                CALL FCAL(KCH,KA,TH,PHP,KRP,CFP)
0025                TS = DSIN(TH)
0026                TC = DCOS(TH)
0027                CALL LFAC(TS,TC,KA,CF1,CF2,CTA)
0028                TS1 = DSQRT(TS)
0029                PC=DCOS(PHP)
0030                PC1=DSQRT(PC)
0031                BSL1=DJONE(KCB*PC)
0032                BSL2=DJONE(KCB*TS)
0033                T1=(PC1*BSL1-TS1*BSL2)/(PC-TS)
0034                T2=PC1*BSL1/(PC+TS)
0035                CLP=CF1*T1-CF2*T2
0036                PC = DCOS(PHZ)
0037                PC1 = DSQRT(PC*PC*PC)
0038                TS1 = TS1*TS1*TS1
0039                APC=AAA(PC)
0040                ATS=AAA(TS)
0041                CFNEWP=DCMPLX(0.D0,APC)
0042                CFNEWT=DCMPLX(0.D0,ATS)
0043                CT1=(CFNEWP*PC1-CFNEWT*TS1)/(PC-TS)
0044                CT2=CFNEWP*PC1/(PC+TS)
0045                CLZ=CF1*CT1-CF2*CT2
0046                T1 = DSIN(PHZ*.5D0)/DSQRT(PI*KRZ*TS)
0047                CXZ = CEIX(KRZ)
0048                CSA=CFZ*CTA*CFNEWT*TS/SQ2+CXZ*CLZ*T1
0049                T1=KCB*KCB
0050                T2=PI*T1
0051                KR1S=T1+(KCH-KH)**2
0052                CX1=CEIX(DSQRT(KR1S))/KR1S
0053                KR2S=T1+(KCH+KH)**2
0054                CT3=CEIX(DSQRT(KR2S))/KR2S
```

```
                KCBR1=KCB/DSQRT(KR1S)
                KCBR2=KCB/DSQRT(KR2S)
                CT1=CX1*KCBR1-CT3*KCBP2
                CT1=CT1*CPNEA*T2/CPLKM
                CT2=CPP*CTA*BSL2/SO2
                T1=DSIN(PHP*.500)/DSQRT(PI*KRP*TS)
                CT2=CT2+T1*CLP*CEIX(KPP)
                CSP12=CT1*CT2
                T1=PI*KCB
                T1=DSQRT(T1*T1*T1)
                CT1=CEIX(KCB+KCB+POF)-DSQRT(KCB/KCH)*CEIX(KCH+KCH-POF)
                CT1=CT1*CX1*T1
                CT1=-CT1*KCBR1/2.DC/CPLKB/CPLKM
                CSP56=CT1*CT2
                CSUM=CSP12+CSP56
                TH=TH/RCON
                THV(INDEX)=TH
                CSAV(INDEX)=CSA
                CSUMV(INDEX)=CSUM
                INDEX=INDEX+1
          100 CONTINUE
                RETURN
                END

TOTAL MEMORY REQUIREMENTS 0011E0 BYTES
```

AAA

```
0001            FUNCTION AAA(TS)
0002            IMPLICIT REAL*8 (A-Z)
0003            DATA KD/0.92/
0004            AAA=2.DO*DSIN(KD*TS)
0005            RETURN
0006            END

 TOTAL MEMORY REQUIREMENTS 00015E BYTES
```

APPENDIX F

THEORETICAL ELEVATION PATTERNS OF CONVENTIONAL VOR AND DOUBLE PARASITIC LOOP COUNTERPOISE ANTENNAS

The complex far electric field pattern functions are expressed as:

$$S(\theta) = \mathrm{Re}S(\theta) + i\ \mathrm{Im}\ S(\theta) \ ,$$

where $\mathrm{Re}S(\theta)$, $\mathrm{Im}\ S(\theta)$ represent the real and imaginary parts respectively of $S(\theta)$. In all the tables the different columns represent the following:

Column 1 gives the angle θ measured from the vertical axis,

Column 2 gives the real part of $S(\theta)$,

Column 3 gives the imaginary part of $S(\theta)$,

Column 4 gives $|S(\theta)|^2$ which is the power pattern,

Column 5 gives $20 \log_{10} |S(\theta)|$ i.e, gives the pattern in dB.

The phase of the far field can be easily obtained from Columns 2 and 3.

TABLE F-1a: FREE SPACE ELEVATION PLANE SIDE BAND MODE FAR FIELD PATTERN OF A CONVENTIONAL VOR ANTENNA. kh=2.75, kA=51.69, kd=0.92, kb=0.15, f=1080 MHz.

θ	Re $S(\theta)$	Im $S(\theta)$	$\lvert S(\theta)\rvert^2$	$20 \log_{10} \lvert S(\theta)\rvert$
[illegible]	[illegible]	2.345122D-02	3.035485D-02	-3.035544D 01
[illegible]	[illegible]	1.257412D-02	1.267484D-02	-3.794115D 01
[illegible]	[illegible]	-4.236151D-03	2.534100D-02	-3.192352D 01
[illegible]	[illegible]	1.969665D-02	2.543493D-02	-3.189139D 01
10.000	2.366071D-02	4.556921D-02	5.134571D-02	-2.578992D 01
12.000	5.703001D-02	4.547607D-02	7.294172D-02	-2.274048D 01
14.000	7.339045D-02	5.831615D-02	9.373864D-02	-2.056163D 01
16.000	8.362508D-02	9.946447D-02	1.299474D-01	-1.772465D 01
18.000	1.227108D-01	1.316994D-01	1.800074D-01	-1.489419D 01
20.000	1.683409D-01	1.505698D-01	2.258538D-01	-1.292345D 01
22.000	1.966654D-01	1.926155D-01	2.754210D-01	-1.120006D 01
24.000	2.380264D-01	2.565188D-01	3.499406D-01	-9.120113D 00
26.000	3.072572D-01	3.085064D-01	4.354115D-01	-7.222001D 00
28.000	3.730010D-01	3.540381D-01	5.142691D-01	-5.776191D 00
30.000	4.261031D-01	4.258366D-01	6.024174D-01	-4.402049D 00
32.000	4.958549D-01	5.183122D-01	7.191657D-01	-2.863421D 00
34.000	5.973578D-01	5.991118D-01	8.460327D-01	-1.452257D 00
36.000	6.960805D-01	6.698990D-01	9.621872D-01	-3.348084D-01
38.000	7.679706D-01	7.615188D-01	1.081522D 00	6.807070D-01
40.000	8.573186D-01	8.779463D-01	1.227104D 00	1.776630D 00
42.000	9.737227D-01	9.886427D-01	1.387642D 00	2.845549D 00
44.000	1.092431D 00	1.070568D 00	1.533769D 00	3.715197D 00
46.000	1.186954D 00	1.161515D 00	1.660716D 00	4.405907D 00
48.000	1.260807D 00	1.267452D 00	1.791471D 00	5.064193D 00
50.000	1.357257D 00	1.367177D 00	1.940723D 00	5.759272D 00
52.000	1.466963D 00	1.490401D 00	2.091238D 00	6.406067D 00
54.000	1.571300D 00	1.558549D 00	2.213156D 00	6.900240D 00
56.000	1.642489D 00	1.601940D 00	2.294337D 00	7.213143D 00
58.000	1.675569D 00	1.644795D 00	2.347953D 00	7.413786D 00
60.000	1.666977D 00	1.699541D 00	2.396056D 00	7.589936D 00
62.000	1.704670D 00	1.755802D 00	2.447190D 00	7.773355D 00
64.000	1.729456D 00	1.789331D 00	2.486520D 00	7.918822D 00
66.000	1.751183D 00	1.778923D 00	2.496239D 00	7.945723D 00
68.000	1.747933D 00	1.717760D 00	2.450708D 00	7.785831D 00
70.000	1.700556D 00	1.614207D 00	2.344688D 00	7.401702D 00
72.000	1.600573D 00	1.465275D 00	2.183546D 00	6.783248D 00
74.000	1.451312D 00	1.348574D 00	1.981150D 00	5.938349D 00
76.000	1.264406D 00	1.216857D 00	1.754883D 00	4.884965D 00
78.000	1.065261D 00	1.096226D 00	1.521606D 00	3.646046D 00
80.000	8.385709D-01	9.870618D-01	1.295180D 00	2.246605D 00

θ	Re S(θ)	Im S(θ)	$\lvert S(\theta)\rvert^2$	$20 \log_{10}\lvert S(\theta)\rvert$
82.000	6.267852D-01	8.861857D-01	1.0c5442D 00	7.121341D-01
84.000	4.292111D-01	7.890497L-01	8.982327D-01	-9.322225D-01
86.000	2.524166L-01	6.913924L-01	7.360290D-01	-2.662102D 00
88.000	1.009305D-01	5.902402E-01	5.988135D-01	-4.454169D 00
90.000	-2.210c76L-02	4.844343L-01	4.849385D-01	-6.286266D 00
92.000	-1.144643D-01	3.748315E-01	3.919251D-01	-8.135939D 00
94.000	-1.748381D-01	2.641357L-01	3.167586D-01	-9.985431D 00
96.000	-2.026353L-01	1.570027E-01	2.564996D-01	-1.181827D 01
98.000	-1.997053D-01	5.969471D-02	2.084368D-01	-1.362051D 01
100.000	-1.c69921D-01	-2.050110E-02	1.702311D-01	-1.537922D 01
102.000	-1.173194D-01	-7.635437E-02	1.399780D-01	-1.707881D 01
104.000	-5.479936L-02	-1.024085E-01	1.161487D-01	-1.869971D 01
106.000	5.513085E-03	-9.722471D-02	9.736089D-02	-2.023052D 01
108.000	4.972c86D-02	-8.557117L-02	8.229423D-02	-2.169201D 01
110.000	8.697629D-02	-1.937458E-02	6.972229D-02	-2.313257D 01

112.000	[illegible]	2.467[illegible]-02	5.934543D-02	-2.453225D 01
114.000	[illegible]	4.757869L-02	5.154890D-02	-2.575501D 01
116.000	-1.[illegible]	6.213796L-02	4.571805D-02	-2.679825D 01
118.000	-3.[illegible]	1.349760L-02	3.998154D-02	-2.796281D 01
120.000	-2.[illegible]	-1.c58c03D-02	3.456419D-02	-2.922747D 01
122.000	-8.[illegible]	-3.160938L-02	3.162033D-02	-3.000067D 01
124.000	2.[illegible]	-1.721769L-02	2.899625D-02	-3.075310D 01
126.000	2.[illegible]	9.980072L-03	2.482630D-02	-3.210176D 01
128.000	9.[illegible]	2.346c78L-02	2.346886D-02	-3.259018D 01
130.000	-1.[illegible]	1.059082L-02	2.204091D-02	-3.313541D 01
132.000	-1.[illegible]	-1.239656L-02	1.853409D-02	-3.464058D 01
134.000	8.[illegible]	-1.743883L-02	1.918637D-02	-3.434015D 01
136.000	1.[illegible]	5.7c7751D-04	1.642987D-02	-3.568732D 01
138.000	7.[illegible]	1.5c3844L-02	1.570725D-02	-3.607800D 01
140.000	-1.[illegible]	6.432434L-03	1.558451D-02	-3.614614L 01
142.000	-9.[illegible]	-1.167226E-02	1.278655D-02	-3.786493D 01
144.000	1.[illegible]	-9.345466D-03	1.476886D-02	-3.661306D 01
146.000	8.[illegible]	8.427874L-03	1.075034D-02	-3.937156D 01
148.000	-9.[illegible]	1.003875L-02	1.397c04D-02	-3.709231D 01
150.000	-8.[illegible]	-8.702223L-03	9.289935D-03	-4.063975D 01
152.000	9.[illegible]	-9.756214D-03	1.341439D-02	-3.744858D 01
154.000	5.[illegible]	6.364446E-03	8.165329D-03	-4.176053D 01
156.000	-9.[illegible]	9.c08864D-03	1.3c8067D-02	-3.766740D 01
158.000	-2.[illegible]	-7.093c63E-03	7.642436D-03	-4.233536D 01
160.000	9.[illegible]	-7.814699E-03	1.265700D-02	-3.795338D 01
162.000	-4.[illegible]	8.575426D-03	8.585376D-03	-4.132481D 01
164.000	-9.[illegible]	6.c1c4e4D-03	1.151901D-02	-3.877170D 01
166.000	4.[illegible]	-1.052899E-02	1.146819D-02	-3.881010D 01
168.000	8.[illegible]	-3.322510D-03	8.876682D-03	-4.103499D 01
170.000	-9.[illegible]	1.275936D-02	1.570057D-02	-3.6c8169D 01

GLOBAL TIME LIMIT EXCEEDED AT 4C5CA322

TABLE F-1b: FREE SPACE ELEVATION PLANE SIDE BAND MODE FAR FIELD PATTERN OF A CONVENTIONAL VOR ANTENNA. kh = 2.75, kA = 17.92, kb = 0.15, kd=0.92 f = 1080 MHz.

θ	Re $S(\theta)$	Im $S(\theta)$	$\lvert S(\theta)\rvert^2$	$20 \log_{10}\lvert S(\theta)\rvert$
2.000	-2.e32310D-02	8.25213eE-03	2.75e629D-02	-3.118614D 01
4.000	5.8C8500D-02	1.97e449E-02	6.135417D-02	-2.424312D 01
6.000	9.854e99D-02	2.421919E-02	1.C14814D-01	-1.987227D 01
8.000	1.0ee95eD-01	2.354551E-02	1.C92625D-01	-1.923058D 01
10.000	9.1212e5E-02	2.2493e5D-02	9.3945z6D-02	-2.C5425CD 01
12.000	e.48e711E-02	2.749374E-02	7.044395D-02	-2.3C4313D 01
14.000	4.249222E-02	4.425973D-02	6.1355e3D-02	-2.424291D 01
16.000	3.739542D-02	7.55953eE-02	8.4339C5D-02	-2.147943D 01
18.000	5.793340E-02	1.203516D-01	1.335694D-01	-1.748586D 01
20.000	1.357819D-01	1.739388E-01	2.035793D-01	-1.3E2533D 01
22.000	1.7e1526E-01	2.301559D-01	2.8983C1D-01	-1.C75713D 01
24.000	2.5ee0eeD-01	2.e359e2E-01	3.e46134D-01	-e.299513D 00
26.000	3.4e1053E-01	3.317302E-01	4.794098D-01	-6.385862D 00
28.000	4.2e136eD-01	3.7589C8E-01	5.682264D-01	-4.9C9572D 00
30.000	4.949958D-01	4.209344D-01	6.497742D-01	-3.744750D 00
32.000	5.52e075D-01	4.73e996E-01	7.280024D-01	-2.757343D 00
34.000	6.041se7D-01	5.4C8738E-01	8.1C9168D-01	-1.820474D 00
36.000	e.5ee512D-01	6.269466E-01	9.078838D-01	-8.393944D-01
38.000	7.184196E-01	7.328435E-01	1.C26249D 00	2.250529D-01
40.000	7.9e2489D-01	8.555470E-01	1.168748D 00	1.354421D 00
42.000	8.938058D-01	9.e87CC2E-01	1.332823D 00	2.495449D 00
44.000	1.C10e62D 00	1.123913E 00	1.511629D 00	3.5e89C6D 00
46.000	1.143353E 00	1.252366D 00	1.695782D 00	4.587401D 00
48.000	1.284140D 00	1.366304E 00	1.875047D 00	5.46C245D 00
50.000	1.424219E 00	1.4e0113D 00	2.C39688D 00	6.191276D 00
52.000	1.554052E 00	1.53084CE 00	2.181410D 00	6.774745D 00
54.000	1.6e4782E 00	1.57e168D 00	2.293930D 00	7.211603D 00
56.000	1.749148D 00	1.603952E 00	2.373222D 00	7.5C6768D 00
58.000	1.8024e2E 00	1.611510D 00	2.417496D 00	7.667314D 00
60.000	1.82e0e8D 00	1.604841E 00	2.426981D 00	7.7C1327D 00
62.000	1.8043e4E 00	1.587915E 00	2.403596D 00	7.617230D 00
64.000	1.7545e4D 00	1.564138E 00	2.350552D 00	7.423396D 00
66.000	1.e74038D 00	1.536C17D 00	2.271948D 00	7.127969D 00
68.000	1.5ee583D 00	1.505029E 00	2.172394D 00	6.738772D 00
70.000	1.43e701E 00	1.471663D 00	2.C56673D 00	6.263304D 00

θ	Re $S(\theta)$	Im $S(\theta)$	$\lvert S(\theta)\rvert^2$	$20 \log_{10} \lvert S(\theta)\rvert$
72.000	1.2[illegible]E 00	1.455571E 00	1.929468D 00	5.706752D 00
74.000	1.1[illegible]E 00	1.396793E 00	1.795152D 00	5.082024D 00
76.000	9.[illegible]E-01	1.351013E 00	1.657635D 00	4.389778D 00
78.000	7.[illegible]E-01	1.299798E 00	1.520278D 00	3.638459D 00
80.000	6.[illegible]E-01	1.240816E 00	1.385648D 00	2.834311D 00
82.000	4.504176E-01	1.173017E 00	1.256521D 00	1.983397D 00
84.000	2.917019D-01	1.095750E 00	1.133913D 00	1.091591D 00
86.000	1.442576E-01	1.008866E 00	1.019128D 00	1.645749D-01
88.000	1.091068E-02	9.127656E-01	9.128311D-01	-7.921912D-01
90.000	-1.058791E-01	8.[illegible]E-01	8.153148D-01	-1.773494D 00
92.000	-2.044[illegible]E-01	6.973511E-01	7.267172D-01	-2.772691D 00
94.000	-2.829[illegible]E-01	5.816098E-01	6.468062D-01	-3.784516D 00
96.000	-3.[illegible]E-01	4.[illegible]E-01	5.752001D-01	-4.[illegible]D 00
98.000	-3.76[illegible]E-01	3.465263E-01	5.113821D-01	-5.825089D 00
100.000	-3.9[illegible]E-01	2.332550E-01	4.547365D-01	-6.844[illegible]D 00
102.000	-3.[illegible]E-01	1.272182E-01	4.045789D-01	-7.859936D 00
104.000	-3.[illegible]E-01	3.174[illegible]E-02	3.601894D-01	-8.[illegible]D 00
106.000	-3.1[illegible]E-01	-5.[illegible]E-02	3.208559D-01	-9.873798D 00
108.000	-2.[illegible]E-01	-1.152753E-01	2.859328D-01	-1.0[illegible]D 01
110.000	-1.[illegible]E-01	-1.619184D-01	2.549109D-01	-1.187223D 01
112.000	-1.[illegible]E-01	-1.[illegible]E-01	2.274825D-01	-1.2[illegible]D 01
114.000	-5.73[illegible]E-02	-1.953279E-01	2.035610D-01	-1.3[illegible]D 01
116.000	7.[illegible]E-03	-1.[illegible]E-01	1.[illegible]D-01	-1.474128D 01
118.000	6.[illegible]E-02	-1.543893E-01	1.664029D-01	-1.557678D 01
120.000	1.[illegible]E-01	-1.132[illegible]E-01	1.527815D-01	-1.631859D 01
122.000	1.[illegible]E-01	-6.[illegible]E-02	1.413965D-01	-1.699110D 01
124.000	1.[illegible]E-01	-1.[illegible]E-02	1.308770D-01	-1.766274D 01
126.000	1.[illegible]E-01	2.[illegible]E-02	1.199240D-01	-1.842188D 01
128.000	8.712[illegible]E-02	6.[illegible]E-02	1.080469D-01	-1.932775D 01
130.000	4.[illegible]E-02	8.[illegible]E-02	9.[illegible]D-02	-2.034071D 01
132.000	4.[illegible]E-03	8.[illegible]E-02	8.[illegible]D-02	-2.125340D 01
134.000	-3.[illegible]E-02	7.341234E-02	8.158930D-02	-2.176734D 01
136.000	-6.[illegible]E-02	4.790202D-02	8.[illegible]D-02	-2.184492D 01
138.000	-7.[illegible]E-02	1.[illegible]E-02	8.[illegible]D-02	-2.186258D 01
140.000	-7.[illegible]E-02	-1.[illegible]E-02	7.[illegible]D-02	-2.227696D 01
142.000	-5.[illegible]	-4.[illegible]E-02	6.[illegible]D-02	-2.334622D 01
144.000	-2.[illegible]	-5.[illegible]E-02	5.[illegible]D-02	-2.488717D 01
146.000	1.[illegible]E-02	-4.[illegible]E-02	5.[illegible]D-02	-2.574569D 01
148.000	4.[illegible]	-3.[illegible]E-02	5.[illegible]D-02	-2.497759D 01
150.000	6.[illegible]	-1.[illegible]E-02	6.[illegible]D-02	-2.394123D 01
152.000	6.[illegible]	1.[illegible]E-02	6.[illegible]D-02	-2.394464D 01
154.000	4.[illegible]	2.[illegible]E-02	5.[illegible]D-02	-2.[illegible]D 01
156.000	1.[illegible]	3.[illegible]E-02	3.[illegible]D-02	-2.837793D 01
158.000	-2.[illegible]	3.[illegible]E-02	3.[illegible]D-02	-2.829176D 01
160.000	-5.[illegible]	1.[illegible]E-02	5.[illegible]D-02	-2.521581D 01
162.000	-6.[illegible]	-2.[illegible]E-03	6.[illegible]D-02	-2.[illegible]D 01
164.000	-5.[illegible]	-1.[illegible]E-02	5.[illegible]D-02	-2.[illegible]D 01
166.000	-2.[illegible]	-2.[illegible]E-02	3.[illegible]D-02	-2.[illegible]D 01
168.000	1.[illegible]	-2.[illegible]E-02	2.[illegible]D-02	-3.[illegible]D 01
170.000	3.[illegible]	-1.[illegible]E-02	5.[illegible]D-02	-2.[illegible]D 01

TABLE F-II: FREE SPACE ELEVATION PLANE CARRIER MODE FAR FIELD PATTERN OF AN OPTIMUM DOUBLE PARASITIC LOOP COUNTERPOISE ANTENNA

kh = 2.7755, kb = 0.1514, kA = 52.1686, kd = 0.9276, kH_1 = 3.4819, kB_1 = 16,3363, kH_2 = 12.7671, kB_2 = 11.3097, f = 1090 MHz.

θ	Re $S(\theta)$	Im $S(\theta)$	$\|S(\theta)\|^2$	$20 \log_{10}\|S(\theta)\|$
2.000	1.752402D-01	2.152913D-02	3.117264D-02	-1.506226D 01
4.000	3.257295D-01	1.339664D-02	1.069316D-01	-9.708938D 00
6.000	4.139432D-01	-1.135939D-02	1.714772D-01	-7.657936D 00
8.000	4.216881D-01	-2.957206D-02	1.786996D-01	-7.478765D 00
10.000	3.667943D-01	-6.269841D-02	1.535409D-01	-8.137760D 00
12.000	2.877435D-01	-1.175743D-01	1.274200D-01	-8.947624D 00
14.000	2.776902D-01	-1.647028D-01	1.042392D-01	-9.819639D 00
16.000	2.259829D-01	-1.948183D-01	8.812250D-02	-1.054913D 01
18.000	1.802499D-01	-2.271856D-01	8.410335D-02	-1.075187D 01
20.000	1.171404D-01	-2.610536D-01	8.187085D-02	-1.086871D 01
22.000	1.571947D-02	-2.812803D-01	7.936563D-02	-1.100367D 01
24.000	-1.044376D-01	-3.000088D-01	1.009125D-01	-9.960549D 00
26.000	-2.162369D-01	-3.398445D-01	1.622527D-01	-7.898082D 00
28.000	-2.945491D-01	-3.946210D-01	2.424849D-01	-6.153152D 00
30.000	-2.949041D-01	-4.478270D-01	2.875174D-01	-5.413356D 00
32.000	-1.750508D-01	-5.260532D-01	2.867326D-01	-5.425229D 00
34.000	5.832739D-02	-5.802197D-01	3.400570D-01	-4.684483D 00
36.000	3.540236D-01	-5.567152D-01	5.566074D-01	-2.544510D 00
38.000	6.562571D-01	-7.158322D-01	9.430891D-01	-2.544728D-01
40.000	9.170375D-01	-7.609364D-01	1.419982D 00	1.522828D 00
42.000	1.089514D 00	-8.079506D-01	1.839825D 00	2.647706D 00
44.000	1.143433D 00	-8.597676D-01	2.046639D 00	3.110412D 00
46.000	1.090029D 00	-9.075580D-01	2.011824D 00	3.033906D 00
48.000	9.760328D-01	-9.489199D-01	1.858758D 00	2.692229D 00
50.000	8.680234D-01	-9.924443D-01	1.738410D 00	2.401523D 00
52.000	7.952187D-01	-1.046740D 00	1.728037D 00	2.375530D 00
54.000	7.836052D-01	-1.110946D 00	1.824956D 00	2.612524D 00
56.000	7.719840D-01	-1.174713D 00	1.975910D 00	2.957671D 00
58.000	7.780640D-01	-1.224055D 00	2.103694D 00	3.229825D 00
60.000	7.629465D-01	-1.248298D 00	2.140334D 00	3.304816D 00

θ	Re $S(\theta)$	Im $S(\theta)$	$\lvert S(\theta)\rvert^2$	$20 \log_{10} \lvert S(\theta)\rvert$
62.000	7.1622280D-01	-1.2451640D 00	2.0634960D 00	3.1460370D 00
64.000	6.4376030D-01	-1.2215520D 00	1.9066170D 00	2.8020340D 00
66.000	5.6274500D-01	-1.1491510D 00	1.7307610D 00	2.3823720D 00
68.000	4.9473870D-01	-1.1572560D 00	1.5841030D 00	1.9975730D 00
70.000	4.5303540D-01	-1.1270060D 00	1.4799420D 00	1.7024460D 00
72.000	4.6244720D-01	-1.0901100D 00	1.4021970D 00	1.4680900D 00
74.000	5.0606320D-01	-1.0522900D 00	1.3223390D 00	1.2153980D 00
76.000	5.7050320D-01	-9.9937770D-01	1.2170960D 00	8.5325000D-01
78.000	6.5777240D-01	-9.0330230D-01	1.0779590D 00	3.2602250D-01
80.000	7.2130690D-01	-6.2598240D-01	9.1164420D-01	-4.0174640D-01
82.000	7.4732490D-01	-4.1935530D-01	7.3435340D-01	-1.3406490D 00
84.000	7.3226690D-01	-2.8424900D-01	5.6401260D-01	-2.4871100D 00
86.000	6.8336040D-01	-4.8214270D-03	4.1435930D-01	-3.8262300D 00
88.000	6.1786460D-01	1.5599850D-01	2.9248960D-01	-5.3368950D 00
90.000	5.4223320D-01	2.6138090D-01	1.9938800D-01	-7.0036100D 00
92.000	4.7884260D-01	3.0401430D-01	1.3198610D-01	-8.7947170D 00
94.000	5.2647250D-02	2.6737330D-01	8.5292310D-02	-1.0690900D 01
96.000	-5.8849110D-02	2.2498690D-01	5.4082330D-02	-1.2669450D 01
98.000	-1.2212220D-01	1.8744240D-01	3.3804230D-02	-1.4710290D 01
100.000	-1.3647830D-01	4.7846310D-02	2.0915580D-02	-1.6795300D 01
102.000	-1.1[illegible]D-01	-2.2396030D-02	1.2866460D-02	-1.8905410D 01
104.000	-8.2[illegible]D-02	-6.3286200D-02	7.9143590D-03	-2.1015840D 01
106.000	-4.[illegible]	-8.9122080D-02	4.8084340D-03	-2.3099430D 01
108.000	2.[illegible]	-9.8510850D-02	3.0544650D-03	-2.5150650D 01
110.000	[illegible]	-1.0126170D-02	1.9040370D-03	-2.7203310D 01
112.000	[illegible]	1.2051580D-02	1.1845530D-03	-2.9264450D 01
114.000	[illegible]	2.9235930D-02	7.5747730D-04	-3.1206830D 01
116.000	-1.42[illegible]	2.0919120D-02	5.0855570D-04	-3.2930930D 01
118.000	-1.71[illegible]	9.5380570D-03	3.3713330D-04	-3.4721790D 01
120.000	-1.2726770D-02	-7.3800070D-03	2.1569970D-04	-3.6661900D 01
122.000	-1.1768870D-03	-1.2491490D-02	1.5742230D-04	-3.8029340D 01
124.000	8.1544710D-03	-7.6211760D-03	1.2457770D-04	-3.9045000D 01
126.000	8.9813390D-03	1.9479820D-03	8.4100170D-05	-4.0752300D 01
128.000	1.3273680D-03	8.1897870D-03	7.0788440D-05	-4.1500440D 01
130.000	-5.8847690D-03	5.9599460D-03	7.0210360D-05	-4.1535990D 01
132.000	-8.5375520D-03	-2.3496750D-03	4.9043560D-05	-4.3093730D 01
134.000	5.5927310D-04	-7.4974050D-03	5.6523970D-05	-4.2477030D 01
136.000	6.6391530D-03	-2.7324030D-03	5.1807170D-05	-4.2856100D 01
138.000	3.7662360D-03	5.8144840D-03	4.3203700D-05	-4.3644770D 01
140.000	-5.3894070D-03	5.5216670D-03	5.6399870D-05	-4.2487910D 01
142.000	-4.7333320D-03	-3.6515340D-03	3.5738610D-05	-4.4468620D 01
144.000	3.5726090D-03	-6.5139690D-03	5.5985010D-05	-4.2519280D 01
146.000	5.1432250D-03	2.1252390D-03	3.0950360D-05	-4.5092010D 01
148.000	-2.9249590D-03	6.6239710D-03	5.2432390D-05	-4.2804000D 01
150.000	-6.8285780D-03	-1.4032940D-03	2.5413500D-05	-4.5946000D 01
152.000	2.8456120D-03	-6.3460690D-03	4.8370100D-05	-4.3154230D 01
154.000	4.[illegible]3740D-03	1.5383240D-03	1.8642610D-05	-4.7294930D 01

θ	Re $S(\theta)$	Im $S(\theta)$	$\lvert S(\theta)\rvert^2$	$20 \log_{10} \lvert S(\theta)\rvert$
156.000	-3.2292150-03	5.6883410-03	4.5100390-05	-4.3458260 01
158.000	-2.8030680-03	-2.2466470-03	1.2932670-05	-4.8803120 01
160.000	3.7616170-03	-5.2436420-03	4.1646540-05	-4.3804510 01
162.000	1.1338470-03	3.4274000-03	1.3032680-05	-4.8849560 01
164.000	-4.0357790-03	4.2768460-03	3.4578930-05	-4.4611880 01
166.000	9.1843860-04	-4.9233840-03	2.5064160-05	-4.6006000 01
168.000	5.6194270-03	-2.7914380-03	2.0892380-05	-4.6800120 01
170.000	-3.1126310-03	6.6189540-03	5.3499020-05	-4.2716540 01

TABLE F-III: FREE SPACE ELEVATION PLANE SIDE BAND MODE FAR FIELD PATTERN OF AN OPTIMUM DOUBLE PARASITIC LOOP COUNTERPOISE ANTENNA

kh = 2.7755, kb = 0.1514, kA = 52.1686, kd = 0.9276, kH_1 = 3.4819, kB_1 = 16.3363, kH_2 = 12.7671, kB_2 = 11.3097, f = 1090 MHz.

θ	Re $S(\theta)$	Im $S(\theta)$	$\lvert S(\theta)\rvert^2$	20 $\log_{10} \lvert S(\theta)\rvert$
2.000	-3.711336D-01	4.473580D-02	3.738251D-01	-8.546631D 00
4.000	-6.306896D-01	5.992726D-02	6.335303D-01	-3.964653D 00
6.000	-7.395394D-01	6.337945D-02	7.423001D-01	-2.583409D 00
8.000	-7.032273D-01	8.505561D-02	7.073601D-01	-3.007183D 00
10.000	-5.320305D-01	9.792023D-02	5.410157D-01	-5.335302D 00
12.000	-2.955216D-01	9.068049D-02	3.091213D-01	-1.019742D 01
14.000	-7.603380D-02	9.512080D-02	1.218060D-01	-1.828662D 01
16.000	1.016872D-01	1.155412D-01	1.539158D-01	-1.625434D 01
18.000	2.544991D-01	1.231929D-01	2.827477D-01	-1.097202D 01
20.000	3.979167D-01	1.184365D-01	4.151685D-01	-7.635512D 00
22.000	5.618896D-01	1.232012D-01	5.752377D-01	-4.803053D 00
24.000	7.822306D-01	1.332735D-01	7.935027D-01	-2.009032D 00
26.000	1.044606D 00	1.381358D-01	1.053699D 00	-4.543338D-01
28.000	1.282815D 00	1.594997D-01	1.292692D 00	2.229904D 00
30.000	1.484920D 00	2.243197D-01	1.452348D 00	3.241413D 00
32.000	1.465724D 00	3.271613D-01	1.501792D 00	3.532197D 00
34.000	1.356756D 00	4.494526D-01	1.429263D 00	3.102245D 00
36.000	1.123160D 00	5.893333D-01	1.268385D 00	2.065023D 00
38.000	8.378439D-01	7.476324D-01	1.122914D 00	1.006932D 00
40.000	6.056485D-01	9.025624D-01	1.086936D 00	7.240760D-01
42.000	5.031711D-01	1.023021D 00	1.140067D 00	1.133611D 00
44.000	5.509472D-01	1.103770D 00	1.233633D 00	1.823721D 00
46.000	7.344021D-01	1.169603D 00	1.381057D 00	2.804233D 00
48.000	1.025918D 00	1.242132D 00	1.611024D 00	4.142042D 00
50.000	1.379495D 00	1.317015D 00	1.907232D 00	5.608072D 00
52.000	1.727659D 00	1.380283D 00	2.211332D 00	6.893077D 00
54.000	2.009747D 00	1.434630D 00	2.469260D 00	7.851337D 00
56.000	2.209038D 00	1.497236D 00	2.668667D 00	8.525889D 00
58.000	2.357133D 00	1.574348D 00	2.834591D 00	9.049809D 00
60.000	2.499403D 00	1.646985D 00	2.993259D 00	9.522887D 00

θ	Re $S(\theta)$	Im $S(\theta)$	$\|S(\theta)\|^2$	$20 \log_{10} \|S(\theta)\|$
62.000	2.655125D 00	1.684207D 00	3.144240D 00	9.950313D 00
64.000	2.303602D 00	1.668176D 00	3.262361D 00	1.027064D 01
66.000	2.898519D 00	1.606974D 00	3.314178D 00	1.040752D 01
68.000	2.893594D 00	1.527080D 00	3.271829D 00	1.029581D 01
70.000	2.761923D 00	1.455045D 00	3.121758D 00	9.887984D 00
72.000	2.502779D 00	1.402477D 00	2.868944D 00	9.154442D 00
74.000	2.133631D 00	1.362023D 00	2.535517D 00	8.081332D 00
76.000	1.707589D 00	1.313537D 00	2.154361D 00	6.666371D 00
78.000	1.254991D 00	1.234933D 00	1.760699D 00	4.913703D 00
80.000	8.255137D-01	1.112030D 00	1.384949D 00	2.828675D 00
82.000	4.566720D-01	9.439868D-01	1.048647D 00	4.125863D-01
84.000	1.738162D-01	7.434930D-01	7.635404D-01	-2.343359D 00
86.000	-1.266548D-02	5.327631D-01	5.329137D-01	-5.466863D 00
88.000	-1.075963D-01	3.372245D-01	3.539736D-01	-9.020582D 00
90.000	-1.286573D-01	1.788920D-01	2.203521D-01	-1.313766D 01
92.000	-1.018351D-01	7.112899D-02	1.242164D-01	-1.811642D 01
94.000	-5.546332D-02	1.568607D-02	5.763882D-02	-2.478570D 01
96.000	-1.404184D-02	3.043054D-03	1.436779D-02	-3.685220D 01
98.000	6.925389D-03	1.554945D-02	1.702194D-02	-3.537982D 01
00.000	3.752232D-03	3.292354D-02	3.313667D-02	-2.959382D 01
02.000	-1.595015D-02	3.871120D-02	4.186842D-02	-2.756227D 01
04.000	-3.744570D-02	2.576506D-02	4.545348D-02	-2.684866D 01
06.000	-4.596033D-02	-1.424009D-03	4.588243D-02	-2.676707D 01
110.000	-5.644978D-03	-4.188303D-02	4.226173D-02	-2.748105D 01
112.000	2.810702D-02	-3.145163D-02	3.902742D-02	-2.817260D 01
114.000	3.516864D-02	-3.868471D-03	3.538077D-02	-2.902466D 01
116.000	2.304432D-02	2.268032D-02	3.233358D-02	-2.980692D 01
118.000	-3.612868D-03	2.952749D-02	2.974769D-02	-3.053093D 01
120.000	-2.332468D-02	1.255393D-02	2.648852D-02	-3.153884D 01
122.000	-2.005599D-02	-1.233746D-02	2.354688D-02	-3.256133D 01
124.000	1.132770D-03	-2.191972D-02	2.194897D-02	-3.317172D 01
126.000	1.750987D-02	-8.295272D-03	1.937453D-02	-3.425538D 01
128.000	1.336069D-02	1.176176D-02	1.699155D-02	-3.539534D 01
130.000	-5.972004D-03	1.506668D-02	1.620709D-02	-3.580590D 01
132.000	-1.352363D-02	-1.613156D-04	1.352464D-02	-3.737748D 01
134.000	-2.377370D-03	-1.238469D-02	1.261080D-02	-3.798515D 01
136.000	9.694559D-03	-6.045106D-03	1.142488D-02	-3.884297D 01
138.000	5.694179D-03	7.420672D-03	9.353611D-03	-4.058041D 01
140.000	-5.833898D-03	7.742724D-03	9.694531D-03	-4.026946D 01
142.000	-6.038993D-03	-3.647054D-03	7.054817D-03	-4.303028D 01
144.000	3.566525D-03	-7.438505D-03	8.249330D-03	-4.167163D 01
146.000	5.386015D-03	1.689846D-03	5.644886D-03	-4.496690D 01
148.000	-2.797968D-03	6.800710D-03	7.353793D-03	-4.266977D 01
150.000	-4.650459D-03	-1.150202D-03	4.790588D-03	-4.639222D 01
152.000	3.023199D-03	-6.426670D-03	7.102241D-03	-4.297209D 01
154.000	3.923515D-03	1.566301D-03	4.224603D-03	-4.748428D 01
156.000	-3.773752D-03	6.258240D-03	7.307994D-03	-4.272404D 01
158.000	-2.934382D-03	2.639695D-03	3.946972D-03	-4.807472D 01
160.000	4.621776D-03	5.990313D-03	7.566021D-03	-4.242265D 01
162.000	1.418581D-03	4.198077D-03	4.431278D-03	-4.706942D 01
164.000	-5.131574D-03	5.274048D-03	7.358576D-03	-4.266412D 01
166.000	7.109189D-04	6.126476D-03	6.167585D-03	-4.419770D 01
168.000	4.833254D-03	3.718943D-03	6.098432D-03	-4.429564D 01
170.000	-3.322334D-03	8.261237D-03	8.904265D-03	-4.100304D 01